

# Development of Guidelines for Bearing Resistance of Large Diameter Open-End Steel Piles

PUBLICATION NO. FHWA-HRT-20-011

MARCH 2020



U.S. Department of Transportation  
**Federal Highway Administration**

Research, Development, and Technology  
Turner-Fairbank Highway Research Center  
6300 Georgetown Pike  
McLean, VA 22101-2296

## FOREWORD

This report describes the development of guidelines for large diameter open-end piles (LDOEPs) made from steel. LDOEPs are a type of deep foundation element available for the support of transportation structures (e.g., bridges). In certain projects, for example, those with a need to support larger lateral, seismic, and axial loads, these foundations are preferred over similar size drilled shafts and/or pile groups because they provide a cost-effective solution while also addressing constructability and/or environmental concerns. However, current design guidance and codes are based on load tests for open-end piles with diameters less than 24 inches, casting doubt as to the reliability of static analysis methods to estimate the bearing resistance of LDOEPs in design. This report will be useful for geotechnical and bridge engineers, consultants, and contractors.

Cheryl A. Richter, PhD, PE  
Director, Office of Infrastructure  
Research and Development

### Notice

This document is disseminated under the sponsorship of the U.S. Department of Transportation (USDOT) in the interest of information exchange. The U.S. Government assumes no liability for the use of the information contained in this document.

The U.S. Government does not endorse products or manufacturers. Trademarks or manufacturers' names appear in this report only because they are considered essential to the objective of the document.

### Quality Assurance Statement

The Federal Highway Administration (FHWA) provides high-quality information to serve Government, industry, and the public in a manner that promotes public understanding. Standards and policies are used to ensure and maximize the quality, objectivity, utility, and integrity of its information. FHWA periodically reviews quality issues and adjusts its programs and processes to ensure continuous quality improvement.

Cover photo sources (from left to right): © Washington State Department of Transportation;  
© Shannon & Wilson, Inc.; © Shannon & Wilson, Inc.

## TECHNICAL REPORT DOCUMENTATION PAGE

1. Report No. FHWA-HRT-20-011	2. Government Accession No.	3. Recipient's Catalog No.	
4. Title and Subtitle Development of Guidelines for Bearing Resistance of Large Diameter Open-End Steel Piles		5. Report Date March 2020	
		6. Performing Organization Code:	
7. Author(s) Kathryn Petek, PhD, PE Michael McVay, PhD*, and Robert Mitchell, PE		8. Performing Organization Report No. 21-1-22024-007 R1	
9. Performing Organization Name and Address Shannon & Wilson, Inc. 400 North 34th Street, Suite 100 Seattle, WA 98103  *University of Florida, Gainesville, Florida 32611-6580		10. Work Unit No.	
		11. Contract or Grant No. DTFH61-14-C-00036	
12. Sponsoring Agency Name and Address U.S. Department of Transportation Federal Highway Administration 6300 Georgetown Pike McLean, VA 22101-2296		13. Type of Report and Period Covered Technical Report; September 2014–May 2019	
		14. Sponsoring Agency Code HRDI-40	
15. Supplementary Notes The Contracting Officer's Representative was Dr. Jennifer Nicks (HRDI-40). Technical Reviewers included Naser Abu-Hejleh, Michael Adams, and Silas Nichols.			
16. Abstract This FHWA project seeks to research bearing resistance of large diameter open-end piles (LDOEPs) using the load and resistance factor design framework. The research evaluates existing static design methods using a new load test data set of steel LDOEPs in cohesive, cohesionless, and mixed soil conditions. The analysis includes development of steel LDOEP-specific resistance factors for each of the design methods considering multiple load test failure criteria, combinations of design methods, and combinations of side and base conditions. Statistical analysis and resistance factor calibration is performed using First Order Second Moment, First Order Reliability Method, and Monte Carlo simulations. The numerous combinations of methods and considerations result in over 6,000 resistance factor values. Resistance factor trends and considerations are discussed. The report concludes with a recommended design approach for LDOEPs and recommended resistance factors for LDOEP design.			
17. Key Words Large diameter open-end pile, LDOEP, driven piles, bearing resistance, bridge foundations		18. Distribution Statement No restrictions. This document is available to the public through the National Technical Information Service, Springfield, VA 22161. <a href="http://www.ntis.gov">http://www.ntis.gov</a>	
19. Security Classif. (of this report) Unclassified	20. Security Classif. (of this page) Unclassified	21. No. of Pages 162	22. Price N/A

## SI\* (MODERN METRIC) CONVERSION FACTORS

### APPROXIMATE CONVERSIONS TO SI UNITS

Symbol	When You Know	Multiply By	To Find	Symbol
<b>LENGTH</b>				
in	inches	25.4	millimeters	mm
ft	feet	0.305	meters	m
yd	yards	0.914	meters	m
mi	miles	1.61	kilometers	km
<b>AREA</b>				
in <sup>2</sup>	square inches	645.2	square millimeters	mm <sup>2</sup>
ft <sup>2</sup>	square feet	0.093	square meters	m <sup>2</sup>
yd <sup>2</sup>	square yard	0.836	square meters	m <sup>2</sup>
ac	acres	0.405	hectares	ha
mi <sup>2</sup>	square miles	2.59	square kilometers	km <sup>2</sup>
<b>VOLUME</b>				
fl oz	fluid ounces	29.57	milliliters	mL
gal	gallons	3.785	liters	L
ft <sup>3</sup>	cubic feet	0.028	cubic meters	m <sup>3</sup>
yd <sup>3</sup>	cubic yards	0.765	cubic meters	m <sup>3</sup>
NOTE: volumes greater than 1,000 L shall be shown in m <sup>3</sup>				
<b>MASS</b>				
oz	ounces	28.35	grams	g
lb	pounds	0.454	kilograms	kg
T	short tons (2,000 lb)	0.907	megagrams (or "metric ton")	Mg (or "t")
<b>TEMPERATURE (exact degrees)</b>				
°F	Fahrenheit	5 (F-32)/9 or (F-32)/1.8	Celsius	°C
<b>ILLUMINATION</b>				
fc	foot-candles	10.76	lux	lx
fl	foot-Lamberts	3.426	candela/m <sup>2</sup>	cd/m <sup>2</sup>
<b>FORCE and PRESSURE or STRESS</b>				
lbf	poundforce	4.45	newtons	N
lbf/in <sup>2</sup>	poundforce per square inch	6.89	kilopascals	kPa
<b>APPROXIMATE CONVERSIONS FROM SI UNITS</b>				
Symbol	When You Know	Multiply By	To Find	Symbol
<b>LENGTH</b>				
mm	millimeters	0.039	inches	in
m	meters	3.28	feet	ft
m	meters	1.09	yards	yd
km	kilometers	0.621	miles	mi
<b>AREA</b>				
mm <sup>2</sup>	square millimeters	0.0016	square inches	in <sup>2</sup>
m <sup>2</sup>	square meters	10.764	square feet	ft <sup>2</sup>
m <sup>2</sup>	square meters	1.195	square yards	yd <sup>2</sup>
ha	hectares	2.47	acres	ac
km <sup>2</sup>	square kilometers	0.386	square miles	mi <sup>2</sup>
<b>VOLUME</b>				
mL	milliliters	0.034	fluid ounces	fl oz
L	liters	0.264	gallons	gal
m <sup>3</sup>	cubic meters	35.314	cubic feet	ft <sup>3</sup>
m <sup>3</sup>	cubic meters	1.307	cubic yards	yd <sup>3</sup>
<b>MASS</b>				
g	grams	0.035	ounces	oz
kg	kilograms	2.202	pounds	lb
Mg (or "t")	megagrams (or "metric ton")	1.103	short tons (2,000 lb)	T
<b>TEMPERATURE (exact degrees)</b>				
°C	Celsius	1.8C+32	Fahrenheit	°F
<b>ILLUMINATION</b>				
lx	lux	0.0929	foot-candles	fc
cd/m <sup>2</sup>	candela/m <sup>2</sup>	0.2919	foot-Lamberts	fl
<b>FORCE and PRESSURE or STRESS</b>				
N	newtons	2.225	poundforce	lbf
kPa	kilopascals	0.145	poundforce per square inch	lbf/in <sup>2</sup>

\*SI is the symbol for International System of Units. Appropriate rounding should be made to comply with Section 4 of ASTM E380. (Revised March 2003)

## TABLE OF CONTENTS

<b>CHAPTER 1. INTRODUCTION</b> .....	<b>1</b>
<b>CHAPTER 2. OVERVIEW OF LARGE DIAMETER OPEN-END PILES</b> .....	<b>3</b>
<b>DESCRIPTION OF LDOEPS</b> .....	<b>3</b>
<b>SELECTION OF LDOEPS</b> .....	<b>4</b>
<b>LDOEP BEHAVIOR</b> .....	<b>5</b>
Plug Development.....	5
Load Testing.....	7
Installation Considerations.....	8
<b>DESIGN COMMENTARY FOR LDOEPS</b> .....	<b>9</b>
Interior Pile Side Resistance.....	10
Open-End Pile Base Resistance.....	11
<b>CHAPTER 3. LOAD TEST DATA, MEASURED AND PREDICTED NOMINAL RESISTANCE, AND LRFD RESISTANCE FACTOR CALIBRATION</b> .....	<b>15</b>
<b>INTRODUCTION</b> .....	<b>15</b>
<b>LOAD TEST DATA SET</b> .....	<b>15</b>
<b>LOAD TEST FAILURE CRITERIA</b> .....	<b>22</b>
<b>SOIL PROPERTY EVALUATION</b> .....	<b>23</b>
<b>ESTIMATED PILE NOMINAL RESISTANCE</b> .....	<b>26</b>
Static Axial Resistance Design Methods.....	26
Static Axial Resistance Design Method Combinations.....	29
Side and Base Resistance Design Conditions.....	30
Calculation Approach.....	31
<b>RESISTANCE FACTOR CALIBRATION</b> .....	<b>31</b>
Calibration Input.....	31
FOSM.....	32
FORM.....	32
Monte Carlo.....	32
Data Filtering.....	34
<b>CHAPTER 4. LDOEP RESISTANCE FACTOR CALIBRATION RESULTS</b> .....	<b>35</b>
<b>NOMINAL PILE RESISTANCE</b> .....	<b>35</b>
<b>RESISTANCE FACTOR COMBINATIONS</b> .....	<b>35</b>
<b>FOSM AND FORM RESISTANCE FACTORS</b> .....	<b>35</b>
<b>MONTE CARLO RESISTANCE FACTORS</b> .....	<b>55</b>
<b>DISCUSSION</b> .....	<b>58</b>
Resistance Factor Calibration Method.....	58
Failure Criterion Method.....	58
Trends by Site Condition.....	59
Consideration of Minimum of Plugged and Unplugged with Interior Side Resistance.....	61

<b>CHAPTER 5. LDOEP DESIGN RECOMMENDATIONS .....</b>	<b>67</b>
<b>RECOMMENDED STATIC DESIGN METHODS.....</b>	<b>67</b>
<b>RECOMMENDED CALCULATION APPROACH.....</b>	<b>67</b>
<b>RECOMMENDED RESISTANCE FACTORS.....</b>	<b>68</b>
<b>RECOMMENDED FAILURE CRITERIA .....</b>	<b>70</b>
<b>FUTURE RESEARCH.....</b>	<b>71</b>
<b>APPENDIX A. RESISTANCE FACTOR CALIBRATION LOAD TEST DATA SET .....</b>	<b>73</b>
<b>APPENDIX B. MEASURED AND PREDICTED NOMINAL RESISTANCE SCATTER PLOTS.....</b>	<b>143</b>
<b>REFERENCES.....</b>	<b>145</b>

## LIST OF FIGURES

Figure 1. Photos. Examples of steel LDOEPs. ....	3
Figure 2. Photos. Examples of concrete LDOEPs. ....	4
Figure 3. Illustration. Schematic of a soil plug inside a pipe pile (Brown and Thompson 2015). ....	6
Figure 4. Illustration. Schematic diagram of pile plug development with terms PLR, IFR, and FFR. ....	13
Figure 5. Charts. Load test data set: histograms of pile diameter. ....	19
Figure 6. Chart. Load test data set: cumulative distribution function of pile diameter by soil type. ....	20
Figure 7. Graphs. Load test data set: plots of pile dimensions and maximum test loads. ....	21
Figure 8. Graph. Cumulative distribution function of resistance bias values for sample results (Cohesionless site, Max Load failure criterion, Gudavalli side and base resistance, Plugged condition). ....	33
Figure 9. Graphs. Comparison of FORM and FOSM resistance factors for filtered data with target reliability $\beta = 2.33$ . ....	52
Figure 10. Graphs. Comparison of FORM mean bias, COV, and resistance factors for Cohesive sites, filtered and unfiltered data sets with target reliability $\beta = 2.33$ . ....	53
Figure 11. Graphs. Comparison of FORM mean bias, COV, and resistance factors for Cohesionless sites, filtered and unfiltered data sets with target reliability $\beta = 2.33$ . ....	54
Figure 12. Graphs. Comparison of FORM resistance factors for target reliabilities of $\beta = 2.33$ and $\beta = 3.0$ . ....	55
Figure 13. Graphs. Comparison of FORM and Monte Carlo mean bias, COV, and resistance factors for Cohesionless sites, unfiltered data set, and target reliability $\beta =$ $2.33$ . ....	56
Figure 14. Graphs. Comparison of FORM and Monte Carlo mean bias, COV, and resistance factors for Mixed sites, unfiltered data set, and target reliability $\beta = 2.33$ . ....	57
Figure 15. Graph. Force displacement curve. Project: I-880 Port of Oakland Connector Viaduct (Caltrans Bridge No. 33-0612E). Pile designation: TP-9. ....	76
Figure 16. Graph. Force displacement curve. Project: I-880 Oakland Bridge Replacement. Pile designation: Pile 3-H. ....	77
Figure 17. Graph. Force displacement curve. Project: Noto Peninsula New Highway Route Bridges (Japan). Pile designation: TP-1. ....	78
Figure 18. Graph. Force displacement curve. Project: Noto Peninsula New Highway Route Bridges (Japan). Pile designation: TP-2. ....	79
Figure 19. Graph. Force displacement curve. Project: Pentre Site. Pile designation: TP-NC. ....	80
Figure 20. Graph. Force displacement curve. Project: Annacis Throughway Bridge Project – Highway 91. Pile designation: TP-D67m. ....	81
Figure 21. Graph. Force displacement curve. Project: Gulf Intracoastal Waterway West Closure Complex Test Site 1. Pile designation: TP-3. ....	82
Figure 22. Graph. Force displacement curve. Project: Gulf Intracoastal Waterway West Closure Complex Test Site 1. Pile designation: TP-4. ....	83
Figure 23. Graph. Force displacement curve. Project: Gulf Intracoastal Waterway West Closure Complex Test Site 1. Pile designation: TP-5. ....	84

Figure 24. Graph. Force displacement curve. Project: Gulf Intracoastal Waterway West Closure Complex Test Site 1. Pile designation: TP-6.....	85
Figure 25. Graph. Force displacement curve. Project: Gulf Intracoastal Waterway West Closure Complex Test Site 3. Pile designation: TP-11.....	86
Figure 26. Graph. Force displacement curve. Project: Port of Oakland Connector Viaduct Maritime On/Off-Ramps (Caltrans Bridge No. 33-612E). Pile designation: TP3-10NCI. ....	87
Figure 27. Graph. Force displacement curve. Project: Port of Oakland Connector Viaduct Maritime On/Off-Ramps (Caltrans Bridge No. 33-612E). Pile designation: TP6-17NCI. ....	88
Figure 28. Graph. Force displacement curve. Project: Tilbrook Grange Site. Pile designation: TP-OC. ....	89
Figure 29. Graph. Force displacement curve. Project: Red Sea Coast, Saudi Arabia. Pile designation: TP-A1.....	90
Figure 30. Graph. Force displacement curve. Project: Red Sea Coast, Saudi Arabia. Pile designation: TP-A2.....	91
Figure 31. Graph. Force displacement curve. Project: Santa Clara River Bridge (Caltrans Bridge No. 52-0449). Pile designation: Test-1. ....	92
Figure 32. Graph. Force displacement curve. Project: Santa Clara River Bridge (Caltrans Bridge No. 52-0449). Pile designation: Test-2. ....	93
Figure 33. Graph. Force displacement curve. Project: Hokkaido, Japan. Pile designation: TP-1.....	94
Figure 34. Graph. Force displacement curve. Project: Chiba, Japan. Pile designation: TP-2. ....	95
Figure 35. Graph. Force displacement curve. Project: EURIPIDES Joint Industry Project – offshore test piles. Pile designation: TP-1.1. ....	96
Figure 36. Graph. Force displacement curve. Project: EURIPIDES Joint Industry Project – offshore test piles. Pile designation: TP-1.3. ....	97
Figure 37. Graph. Force displacement curve. Project: EURIPIDES Joint Industry Project – offshore test piles. Pile designation: TP-2. ....	98
Figure 38. Graph. Force displacement curve. Project: EURIPIDES Joint Industry Project – offshore test piles. Pile designation: TP-2. ....	99
Figure 39. Graph. Force displacement curve. Project: Sakonnet River Bridge (Route 138). Pile designation: TestPile.....	100
Figure 40. Graph. Force displacement curve. Project: Berenda Slough Bridge (Caltrans Bridge No. 41-0009R). Pile designation: TestPile.....	101
Figure 41. Graph. Force displacement curve. Project: Seal Beach Blvd OC (Caltrans Bridge No. 55-1099). Pile designation: TP-2A2.....	102
Figure 42. Graph. Force displacement curve. Project: Mad River Bridge (Caltrans Bridge No. 04-0025L). Pile designation: TestPile.....	103
Figure 43. Graph. Force displacement curve. Project: Russian River Bridge (Caltrans Bridge No. 10-0301). Pile designation: TestPile.....	104
Figure 44. Graph. Force displacement curve. Project: San Joaquin River Bridge (Caltrans Bridge No. 41-90). Pile designation: TestPile.....	105
Figure 45. Graph. Force displacement curve. Project: Colorado River Bridge (Caltrans Bridge No. 54-1272). Pile designation: TestPile.....	106
Figure 46. Graph. Force displacement curve. Project: Russian River Bridge (Caltrans Bridge No. 20-38). Pile designation: TestPile.....	107

Figure 47. Graph. Force displacement curve. Project: Feather River Bridge (Caltrans Bridge No. 18-0026R). Pile designation: TP-1.....	108
Figure 48. Graph. Force displacement curve. Project: Feather River Bridge (Caltrans Bridge No. 18-0026R). Pile designation: TP-2.....	109
Figure 49. Graph. Force displacement curve. Project: Santa Clara River Bridge (Caltrans Bridge No. 53-2925). Pile designation: TestPile.....	110
Figure 50. Graph. Force displacement curve. Project: Port of Toamasina Offshore Jetty. Pile designation: 12A.....	111
Figure 51. Graph. Force displacement curve. Project: Port of Toamasina Offshore Jetty. Pile designation: 4B.....	112
Figure 52. Graph. Force displacement curve. Project: Trans-Tokyo Bay Highway. Pile designation: TP-1.....	113
Figure 53. Graph. Force displacement curve. Project: Legislative Route 795 Section B-6 Philadelphia, PA. Pile designation: TP-C.....	114
Figure 54. Graph. Force displacement curve. Project: Legislative Route 795 Section B-6 Philadelphia, PA. Pile designation: TP-E.....	115
Figure 55. Graph. Force displacement curve. Project: Louisiana Highway 1 Improvements Load Test Data Phase 1B. Pile designation: T-3-1.....	116
Figure 56. Graph. Force displacement curve. Project: I-880 5th Street Overhead Bridge (Caltrans Bridge No. 33-27). Pile designation: TestPile.....	117
Figure 57. Graph. Force displacement curve. Project: Port of Oakland Connector Viaduct Maritime On/Off-Ramps (Caltrans Bridge No. 33-612E). Pile designation: TP9-27NCI. ..	118
Figure 58. Graph. Force displacement curve. Project: Port Said. Pile designation: TP-22.....	119
Figure 59. Graph. Force displacement curve. Project: Port Said. Pile designation: TP-136.....	120
Figure 60. Graph. Force displacement curve. Project: Woodrow Wilson Bridge over Potomac River, VA and MD, USA. Pile designation: PL-3.....	121
Figure 61. Graph. Force displacement curve. Project: Feather River Bridge (Caltrans Bridge No. 18-0009). Pile designation: Pile-3.....	122
Figure 62. Graph. Force displacement curve. Project: Nippon Steel Corporation/Blast Furnace Foundations in Japan. Pile designation: BF-61.....	123
Figure 63. Graph. Force displacement curve. Project: Nippon Steel Corporation/Blast Furnace Foundations in Japan. Pile designation: H-27.....	124
Figure 64. Graph. Force displacement curve. Project: Nippon Steel Corporation/Blast Furnace Foundations in Japan. Pile designation: HS-40.....	125
Figure 65. Graph. Force displacement curve. Project: Nippon Steel Corporation/Blast Furnace Foundations in Japan. Pile designation: HS-41.....	126
Figure 66. Graph. Force displacement curve. Project: Port Mann Bridge. Pile designation: TestPile.....	127
Figure 67. Graph. Force displacement curve. Project: Woodrow Wilson Bridge over Potomac River, VA and MD, USA. Pile designation: PL-1.....	128
Figure 68. Graph. Force displacement curve. Project: Nippon Steel Corporation/Blast Furnace Foundations in Japan. Pile designation: HS-97.....	129
Figure 69. Graph. Force displacement curve. Project: Tokyo Port Bay Bridge. Pile designation: TP-4.....	130
Figure 70. Graph. Force displacement curve. Project: Tokyo Port Bay Bridge. Pile designation: TP-5.....	131

Figure 71. Graph. Force displacement curve. Project: Salinas River Bridge (Caltrans Bridge No. 44-216R/L). Pile designation: TestPile. ....	132
Figure 72. Graph. Force displacement curve. Project: Woodrow Wilson Bridge over Potomac River, VA and MD, USA. Pile designation: PL-2. ....	133
Figure 73. Graph. Force displacement curve. Project: Jin Mao Building. Pile designation: ST-1. ....	134
Figure 74. Graph. Force displacement curve. Project: Jin Mao Building. Pile designation: ST-2. ....	135
Figure 75. Graph. Force displacement curve. Project: Pitt River Bridge. Pile designation: Pile-P5. ....	136
Figure 76. Graph. Force displacement curve. Project: I-405 and SR-22 HOV Connector Separation Bridge (Caltrans Bridge No. 55-1103E). Pile designation: TP-9. ....	137
Figure 77. Graph. Force displacement curve. Project: I-405 and SR-22 HOV Connector Separation Bridge (Caltrans Bridge No. 55-1103E). Pile designation: TP-10. ....	138
Figure 78. Graph. Force displacement curve. Project: Highway 32 Stony Creek Bridge (Caltrans Bridge No. 11-0029). Pile designation: TP-6. ....	139
Figure 79. Graph. Force displacement curve. Project: Legislative Route 795 Section B-6 Philadelphia, PA. Pile designation: TP-D. ....	140
Figure 80. Graph. Force displacement curve. Project: Nippon Steel Corporation/Blast Furnace Foundations in Japan. Pile designation: BF-47. ....	141

## LIST OF TABLES

Table 1. Resistance factor calibration load test data set. Summary of static compression load tests.....	17
Table 2. Number of test piles by site condition. ....	19
Table 3. Number of test piles for alternate Variable Side site conditions. ....	22
Table 4. Number of test piles by site condition considered applicable to failure criteria.....	23
Table 5. Soil property correlations.....	25
Table 6. Static design methods considered in LDOEP evaluation. ....	26
Table 7. Selected side resistance design methods.....	28
Table 8. Selected base resistance design methods.....	29
Table 9. Side resistance static design method combinations for cohesive and cohesionless sites. ....	30
Table 10. Summary of analysis components considered in resistance factor calibration.....	36
Table 11. FORM resistance factors for Cohesive sites—Modified Davisson failure criterion with Filtered data and target reliability $\beta = 2.33$ .....	37
Table 12. FORM resistance factors for Cohesive sites—5 Percent Diameter failure criterion with Filtered data and target reliability $\beta = 2.33$ .....	38
Table 13. FORM resistance factors for Cohesive sites—Max Load failure criterion with Filtered data and target reliability $\beta = 2.33$ .....	39
Table 14. FORM resistance factors for Cohesionless sites—Modified Davisson failure criterion with Filtered data and target reliability $\beta = 2.33$ .....	40
Table 15. FORM resistance factors for Cohesionless sites—5 Percent Diameter failure criterion with Filtered data and target reliability $\beta = 2.33$ .....	41
Table 16. FORM resistance factors for Cohesionless sites—Max Load failure criterion with Filtered data and target reliability $\beta = 2.33$ .....	42
Table 17. FORM resistance factors for Mixed sites—Modified Davisson failure criterion with Filtered data and target reliability $\beta = 2.33$ .....	43
Table 18. FORM resistance factors for Mixed sites—5 Percent Diameter failure criterion with Filtered data and target reliability $\beta = 2.33$ .....	44
Table 19. FORM resistance factors for Mixed sites—Max Load failure criterion with Filtered data and target reliability $\beta = 2.33$ .....	45
Table 20. FORM resistance factors for Variable Side with Cohesive Base sites—Modified Davisson failure criterion with Filtered data and target reliability $\beta = 2.33$ .....	46
Table 21. FORM resistance factors for Variable Side with Cohesive Base sites—5 Percent Diameter failure criterion with Filtered data and target reliability $\beta = 2.33$ .....	47
Table 22. FORM resistance factors for Variable Side with Cohesive Base sites—Max Load failure criterion with Filtered data and target reliability $\beta = 2.33$ .....	48
Table 23. FORM resistance factors for Variable Side with Cohesionless Base sites—Modified Davisson failure criterion with Filtered data and target reliability $\beta = 2.33$ .....	49
Table 24. FORM resistance factors for Variable Side with Cohesionless Base sites—5 Percent Diameter failure criterion with Filtered data and target reliability $\beta = 2.33$ .....	50
Table 25. FORM resistance factors for Variable Side with Cohesionless Base sites—Max Load failure criterion with Filtered data and target reliability $\beta = 2.33$ . ....	51

Table 26. Resistance factors and efficiency values for Cohesive sites with the Minimum of Plugged and Unplugged with Interior Side Resistance calculation approach and the AASHTO/API base resistance method.....	62
Table 27. Resistance factors and efficiency values for Cohesive sites with the Minimum of Plugged and Unplugged with Interior Side Resistance calculation approach and the Brown base resistance method. ....	63
Table 28. Resistance factors and efficiency values for Variable Side with Cohesive Base sites with the Minimum of Plugged and Unplugged with Interior Side Resistance calculation approach and the Total Stress AASHTO/API base resistance method. ....	63
Table 29. Resistance factors and efficiency values for Variable Side with Cohesive Base sites with the Minimum of Plugged and Unplugged with Interior Side Resistance calculation approach and the Total Stress Brown base resistance method. ....	63
Table 30. Resistance factors and efficiency values for Cohesionless sites with the Minimum of Plugged and Unplugged with Interior Side Resistance calculation approach and the bearing capacity API base resistance method.....	64
Table 31. Resistance factors and efficiency values for Cohesionless sites with the Minimum of Plugged and Unplugged with Interior Side Resistance calculation approach and the Nordlund base resistance method. ....	65
Table 32. Resistance factors and efficiency values for Cohesionless sites with the Minimum of Plugged and Unplugged with Interior Side Resistance calculation approach and the Gudavalli base resistance method.....	65
Table 33. Resistance factors and efficiency values for Cohesionless sites with the Minimum of Plugged and Unplugged with Interior Side Resistance calculation approach and the Brown base resistance method. ....	65
Table 34. Recommended static design methods for the design of steel LDOEPs.....	67
Table 35. Recommended resistance factors for piles in Cohesive sites using Minimum of Plugged and Unplugged with Interior Side Resistance calculation approach. ....	68
Table 36. Recommended resistance factors for piles in Cohesionless sites using Minimum of Plugged and Unplugged with Interior Side Resistance calculation approach. ....	69
Table 37. Recommended resistance factors for side resistance of piles in Mixed sites using Minimum of Plugged and Unplugged with Interior Side Resistance calculation approach. ....	70
Table 38. Recommended resistance factors for base resistance of piles in Mixed sites using Minimum of Plugged and Unplugged with Interior Side Resistance calculation approach. ....	70
Table 39. Resistance factor calibration load test data set: load test nominal resistance. ....	74

## LIST OF ABBREVIATIONS

### Acronyms

AASHTO	American Association of State Highway and Transportation Officials
API	American Petroleum Institute
CAPWAP	Case Pile Wave Analysis Program
CDF	cumulative distribution function
COV	coefficient of variation
CPT	cone penetration test
DFLTD	Deep Foundation Load Test Database
DOT	department of transportation
FFR	final filling ratio
FHWA	Federal Highway Administration
FORM	First Order Reliability Method
FOSM	First Order Second Moment
ICP	Imperial College Pile
IFR	incremental filling ratio
LDOEP	large diameter open-end pile
LRFD	load and resistance factor design
NAVFAC	Naval Facilities Engineering Command
NCHRP	National Cooperative Highway Research Program
NGI	Norwegian Geotechnical Institute
OCR	over-consolidation ratio
PLR	plug length ratio
SPT	standard penetration test

### Symbols

$A$	pile cross- sectional area
$A_b$	Brown Method regression factor
$A_t$	plug area at pile base
$A_{tp}$	annular area of pile base
$B$	pile diameter
$B_b$	Brown Method regression factor
$b_i$	interior pile diameter
$C_F$	Correction factor for $K_\delta$
$COV_D$	dead load coefficient of variation
$COV_L$	live load coefficient of variation
$COV_Q$	coefficient of variation of the load

$COV_R$	resistance bias coefficient of variation
$D_b$	embedded depth in a stiff layer
$D_r$	relative density
$E$	pile modulus
$F_{vs}$	reduction factor for vibratory installation
$g$	limit state function
$G_s$	specific gravity
$K_a$	Rankine active earth pressure coefficient
$K_o$	lateral stress index
$K_\delta$	coefficient of lateral earth pressure at mid-point of soil layer
$L$	pile length
$l$	pile penetration depth
$N$	standard penetration
$N_c$	bearing capacity factor
$N_k$	cone factor
$N_q$	bearing capacity factor
$p_a$	atmospheric pressure
$pf$	probability of failure
$Q$	test load
$Q_D/Q_L$	dead load to live load ratio
$q_L$	limiting unit base resistance
$q_p$	unit base resistance
$q_s$	unit side resistance
$q_t$	cone tip resistance
$R_f$	friction ratio
$R_p$	total base resistance
$s_f$	pile top settlement
$S_u$	undrained shear strength
$\alpha$	adhesion factor
$\alpha_t$	dimensionless factor
$\beta$	friction coefficient
$\beta$	reliability index
$\gamma$	unit weight
$\gamma_D$	dead load factor
$\gamma_L$	live load factor
$\gamma_w$	weight of water
$\delta$	interface friction angle
$\delta$	interface friction angle between pile and soil

$\lambda_D$	mean dead load bias
$\lambda_L$	mean live load bias
$\lambda_R$	mean resistance bias
$\sigma_v$	total vertical stress
$\sigma'_v$	vertical effective stress
$\phi'$	internal friction angle
$\phi$	resistance factor
$\Phi$	standard normal cumulative distribution function
$\phi/\lambda$	efficiency
$\Psi$	psi
$\omega$	angle of pile taper from vertical

### **Schematic Abbreviations**

cos	cosine
exp	exponent
$L_i$	height of soil column
sin	sine
tan	tangent
$Z_i$	pile penetration



## CHAPTER 1. INTRODUCTION

This Federal Highway Administration (FHWA) project seeks to research bearing resistance of large diameter open-end piles (LDOEPs) using the load and resistance factor design (LRFD) framework. For this study, LDOEPs are considered as open-end steel pipe and concrete cylinder piles with diameters greater than 30 inches (762 mm).

Large diameter open-end steel pipe and concrete cylinder piles are increasingly used in transportation infrastructure projects. However, existing state and federal design guidelines, as well other standards such as the American Association of State Highway and Transportation Officials (AASHTO) *LRFD Bridge Design Specifications*, were generally developed for piles with diameters less than 24 inches (610 mm) (AASHTO 2017). Considering the increased pile dimensions and potential difference in open-end pile behavior, there is resulting uncertainty regarding the applicability of existing guidelines to LDOEPs. This potential uncertainty is reflected in AASHTO commentary that states that “experience has shown that the static analysis methods ... tend to significantly overestimate the available nominal resistance of large diameter pipes.” Based on this known issue, the AASHTO code recommends a static or dynamic load test should be considered for piles with diameters greater than 24 inches (610 mm).

Recognizing the uncertainty associated with LDOEPs, the Transportation Research Board of the National Academies launched National Cooperative Highway Research Program (NCHRP) Synthesis 478, which summarized the current practice for the design, testing, and use of LDOEPs in highway applications (Brown and Thompson 2015). NCHRP Synthesis 478 provides an in-depth review of the key issues for design and construction of LDOEPs. In addition, the study performed a survey of state transportation agencies and summarized reported practice regarding LDOEPs.

This research builds upon and expands NCHRP Synthesis 478 to develop specific recommendations for bearing resistance of LDOEPs. The project objectives of this research include:

- Assemble a comprehensive, searchable database of available load tests and performance data.
- Calibrate resistance factors for existing static analysis methods for the bearing resistance of LDOEPs using collected load test data.
- Develop practice-ready guidelines for LDOEPs with recommended procedures to predict and verify bearing resistance.

In fulfillment of these objectives, the research team collected over 150 load tests on steel and concrete LDOEPs. The load tests were incorporated into the new Deep Foundation Load Test Database (DFLTD) version 2.0 developed for the project. In addition to LDOEP data, the new database also incorporated over 1,600 load tests on other deep foundation types imported from the previous version of the database. DFLTD version 2.0 is available for distribution from FHWA.

The collected LDOEP load test was used for evaluation of existing static analysis methods and development of LDOEP-specific resistance factors. Preliminary studies included both steel and concrete LDOEPs in the existing static analysis design method evaluation. However, the preliminary analyses indicated insufficient available static load test data for evaluation of concrete cylinder LDOEPs. Therefore, only steel LDOEPs were considered in the resistance factor calibration.

Preliminary analyses also included evaluation of dynamic load testing with signal matching (e.g., Case Pile Wave Analysis Program (CAPWAP)) in comparison to the static load test data for verification of pile resistance. The preliminary analyses indicated the tendency for the signal matching analysis to underpredict static pile resistance. However, in several cases there was insufficient resistance mobilization due to refusal driving conditions. In addition, the signal matching analysis results were generally not available at the same time intervals as the static load test results, which potentially affects pile setup and corresponding pile resistance. Due to these limitations, verification of LDOEP bearing resistance was not considered as part of the research, and dynamic testing with signal matching test results were not included in the resistance factor calibration.

This report provides an overview of LDOEP applications and considerations and describes the static analysis method evaluation and resistance factor calibration performed for steel LDOEPs. The report includes resistance factor results for numerous design combinations considering various soil types, static design method combinations, pile plug conditions, failure criteria, and target reliabilities. Chapter 5 includes recommended resistance factor values and practice-ready design guidelines for bearing resistance of steel LDOEPs.

## CHAPTER 2. OVERVIEW OF LARGE DIAMETER OPEN-END PILES

### DESCRIPTION OF LDOEPs

This study considers LDOEPs to be open-end steel pipe and concrete cylinder piles with diameters greater than 30 inches (762 mm). The piles considered in this study are circular and voided along their whole length. The study does not include steel piles with constrictor plates or prestressed concrete piles with solid sections at the top.

Steel LDOEPs consist of either rolled straight seam or spiral welded pipes, as shown in figure 1-A and figure 1-B, respectively. Spiral weld pipe can be manufactured in various diameters with wall thicknesses up to 1 inch (25 mm). Spiral weld pipe is generally considered the most economical for fabricating LDOEPs. Rolled steel plate straight seam LDOEPs can be manufactured in various diameters and may have a wall thicknesses that exceeds 1 inch (25 mm). Individual sections with varying wall thickness may be welded together so that greater wall thickness can be provided where needed. Increased wall thickness may be used at the top of the pile to provide increased flexure stiffness and strength. Similarly, increased wall thickness may be used at the bottom of the pile to provide increased buckling resistance in the case of driving into dense and hard bearing stratum (Brown and Thompson 2015).



© Applied Foundation Testing.

A. Rolled plate straight seam weld.



© Applied Foundation Testing.

B. Spiral weld pipe.

**Figure 1. Photos. Examples of steel LDOEPs.**

In the United States, concrete LDOEPs generally range in diameter between 36 and 66 inches (914 and 1,676 mm) with wall thicknesses ranging between 5 and 6 inches (127 and 152 mm). Concrete LDOEPs are typically spun cast in 8-, 12-, or 16-foot (2.4-, 3.7-, or 4.9-m) sections that are joined and post-tensioned to the design pile length. Concrete LDOEPs may also be bed cast in cylindrical forms and prestressed in a manner similar to conventional concrete piling

(Brown and Thompson 2015). Figure 2-A shows the cross section of a concrete cylinder LDOEP, and figure 2-B depicts a rapid load test conducted over water.



© Applied Foundation Testing.

A. Pile cross section.



© Applied Foundation Testing.

B. Rapid load test over water.

### **Figure 2. Photos. Examples of concrete LDOEPs.**

Both steel and concrete LDOEPs may be installed using vibratory, impact driving, or a combination of vibratory and impact driving methods. Hydraulic impact driving hammers are frequently used in lieu of diesel impact hammers due to their increased efficiency and resulting ability to achieve higher loads.

### **SELECTION OF LDOEPs**

LDOEPs are increasingly used for deep foundation support of bridges on large infrastructure projects. LDOEPs can be effectively used to decrease project costs, shorten project schedules, and reduce environmental concerns. Specifically, LDOEPs can be effectively utilized to:

- Resist large lateral loads from an extreme event, such as a vessel impact or earthquake.
- Allow a significant unsupported length in the foundation due to scour, liquefaction, or other marine conditions.
- Provide deep foundation axial resistance when relatively loose or soft soil extends to significant depth.
- Resist large axial resistance to support large axial foundation loads.
- Eliminate the need for pile cap.
- Expedite and reduce marine complications of pile delivery, handling, and installation.

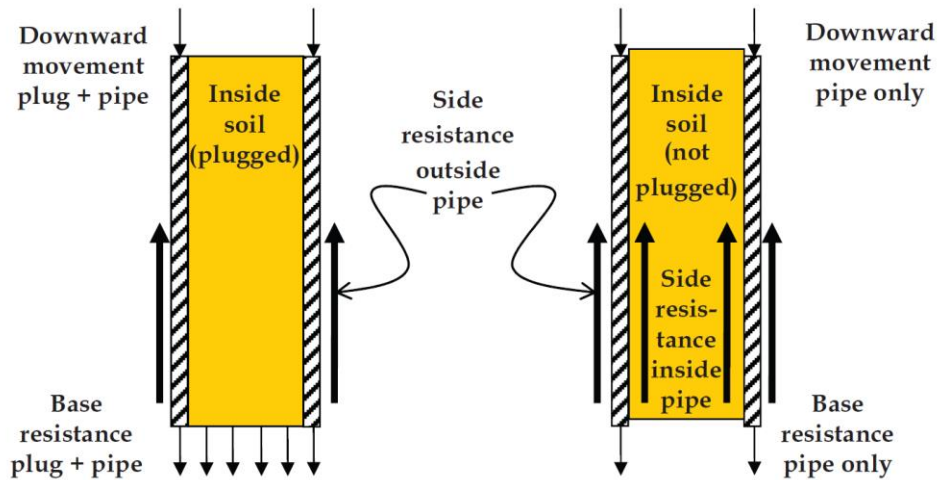
The survey of state agencies performed in 2014 for NCHRP Synthesis 478 identified LDOEP practice across the United States. Results of the survey indicated that over 40 percent of states have experience with LDOEPs. The majority of states reported limited experience with LDOEPs; however, the Alaska and California transportation agencies both indicated LDOEPs have been used on more than 50 projects in the last 10 yr. Survey results also indicated that static bearing resistance of LDOEPs is commonly evaluated using design methods provided in AASHTO, specifically the Nordlund method and the Tomlinson  $\alpha$ -method for cohesionless and cohesive deposits, respectively. Most state agencies reported using resistance factors provided in the AASHTO specifications. Some states reported using a combination of AASHTO and state agency resistance factors or only state agency resistance factors. The majority of states use high-strain dynamic testing to measure or demonstrate pile resistance, as well as to monitor driving stresses to reduce pile damage.

## **LDOEP BEHAVIOR**

Given their larger dimensions, the behavior of LDOEPs may differ from smaller diameter open-end piles. Diameter effects may impact pile plug development, load testing, and other installation-related considerations.

### **Plug Development**

During pile driving, side resistance develops on both the exterior and interior of an open-end pile as the pile penetrates through the soil. As side resistance builds up on the pile interior, especially if compaction and arching of the soil occurs, then a soil plug may form within the pile. Once plugged, the pile drives as a displacement pile and the base resistance acts over the entire end area. Figure 3 presents a schematic of plugged and unplugged pile conditions. In general, the likelihood of pile plugging decreases with increasing pile diameter (Ko and Jeong 2015). If a pile does not plug during driving, base resistance acts only on the pile annulus, and interior pile side resistance may be considered in the design. Additionally, the soil on the pile interior may be disturbed during the driving process, and the disturbance should be accounted for in the axial resistance calculation.



© 2015 National Academy of Sciences.

**Figure 3. Illustration. Schematic of a soil plug inside a pipe pile (Brown and Thompson 2015).**

Plug development is complicated by potentially different behavior during pile driving and under static loading. During pile driving and high-strain dynamic testing, soil on the pile interior may exhibit inertial resistance to downward pile acceleration, and thereby prevent formation of a pile plug. In such conditions, the pile driving behavior and dynamic test results will reflect an unplugged pile condition. However, under static loading conditions when the pile is not rapidly moving, the soil may indeed act as a plug within the pile interior (Lehane and Randolph 2002). Conversely, others have found that the inertia resistance of the soil plug in long LDOEPs may result in higher estimated side resistance during driving compared to base resistance of a long, plugged pile under static loading (Brown and Thompson 2015).

In general, plug development in LDOEPs is complex and requires careful consideration during pile design and installation. Analytical models, model tests, full-scale load tests, and production pile-driving observations have been used to evaluate potential pile plugging. Commentary and recommendations based on these observations include:

- Paikowsky and Whitman (1990) considered plugging of open-end piles using the pile penetration-to-diameter ratio. Based on small-diameter model tests, the authors suggest that plugging of open-end piles in medium dense to dense sands begins when the pile penetration-to-diameter ratio reaches 20 to 35. Paikowsky and Whitman (1990) further suggest that plugging may occur in soft to stiff clays for pile penetration-to-diameter ratios of 10 to 20, but that the clay plug may not contribute significantly to the total pile resistance.
- Paikowsky et al. (1989) suggested that pile plugging is more common for offshore piles due to the significantly longer lengths compared to onshore piles. Paikowsky et al. (1989) evaluated 48-inch (1,219-mm) diameter offshore piles in clay and identified pile plugging occurred at a critical depth of 75 times the pile diameter.

- Paik and Salgado (2003) stated that pile plugging typically does not occur for the pile diameters and lengths typically used in onshore applications. The authors suggest that the majority of piles in onshore applications have a partially plugged condition.
- Kindel (1977) reported on 30- to 48-inch (762- to 1,219-mm) diameter offshore piles in clay. In general, plugging did not occur during driving for pile penetrations ranging from 120 to 400 ft (37 to 122 m).
- Lehane and Randolph (2002) discussed that piles that do not plug during driving will behave in a fully plugged manner under static loading.
- Randolph et al. (1991) developed an analytical model to show that piles will typically behave plugged under static, drained loading conditions because arching action within the pile leads to high frictional capacity of the plug.
- Lee et al. (2003) evaluated pile plugging of open-end piles in sand using calibration chamber tests and one full-scale field load test. The base resistance values of the open-end piles were compared to those of closed-end piles in the same stratum. The comparison showed that the base resistance of the open-end pile was equal to that of the closed-end pile at pile penetrations greater than 17 diameters.

## **Load Testing**

Load testing may address uncertainties in the LDOEP design, including those related to plug development and interior pile side resistance discussed herein. However, total resistance of an LDOEP may also be difficult to measure.

Static load testing represents the gold standard to evaluate LDOEP resistance. However, static load testing generally requires large load frames and multiple reaction piles in order to achieve the high loads required to mobilize LDOEP resistance. Such systems typically result in significant project cost, which may be economically unfeasible in many cases. Static load testing of LDOEPs is further complicated by instrumentation challenges. Instrumentation can be installed along the pile length for evaluation of the force distribution along the pile side and base. However, such instrumentation, and the associated cabling, is generally installed prior to pile installation. The instrumentation may be directly cast into concrete LDOEPs or installed on the exterior of steel LDOEPs with some type of protective housing. The instrumentation, cabling, and protection system needs to be able to withstand the acceleration and resulting forces during the pile driving to avoid damage during the installation.

In lieu of static load testing, high-strain dynamic testing, such as pile-driving analyzer measurements and CAPWAP analyses, is frequently performed on LDOEPs. Dynamic testing may be used to estimate pile nominal resistance, develop pile driving criteria, and evaluate pile integrity. However, dynamic testing of LDOEPs presents unique challenges compared to the use and interpretation of conventional dynamic measurements (Brown and Thompson 2015). Mobilization of LDOEP nominal resistance may be difficult due to considerations of pile setup and the required size of pile driving hammers. In many cases, production pile driving hammers

may not be large enough to mobilize the total nominal resistance during restrike after setup has occurred.

Due to challenges mobilizing pile resistance with production pile driving hammers, superposition of end-of-drive and beginning-of-restrike dynamic testing results has also been used to evaluate nominal pile resistance of LDOEPs (Hussein et al. 2002 and Petek et al. 2012). This approach assumes that base resistance is mobilized at the end-of-drive condition and that side resistance can be fully mobilized during pile restrike. The superposition of resistances evaluated from different hammer blows allows for estimation of the total pile resistance when both components of the pile resistance cannot be mobilized during restrike.

Due to their increased diameter and wall thicknesses compared to smaller diameter piles, a number of recommendations and issues have been identified for the execution and analysis of LDOEP dynamic testing. For instance, some practitioners recommend two sets of strain gages and accelerometers be placed 90 degrees from one another at the top of a pile to monitor stress over the whole perimeter of the LDOEP (Brown and Thompson 2015). In addition, for the case of long, slender steel LDOEPs (lengths greater than 130 ft (40 m)), Rausche et al. (2010) showed a 2 to 10 percent difference in capacity, stresses, and blow counts if a residual stress analysis is performed. They recommend that, in general, residual stress analyses should be performed when a wave equation analyses is performed on long, slender LDOEPs.

Rapid load testing, such as Statnamic testing, is performed by some states as an alternative to static and high-strain dynamic testing. The test method can provide time and cost savings where high loads are required or access is difficult (Hannigan et al. 2016). In addition, the rate of loading in a rapid test may result in soil plug response more similar to static loading compared to dynamic testing.

### **Installation Considerations**

NCHRP Synthesis 478 identifies several installation-related factors that affect the design and performance of LDOEPs (Brown and Thompson 2015). These installation-related factors include:

- Consideration of pile length. During the pile-driving process, progressive failure, soil shearing, remolding, and other weakening effects may occur as a pile increasingly penetrates through a soil layer (Lehane and Jardine 1994). These weakening effects may result in a decrease of the unit side resistance as the pile length increases (Randolph and Puzrin 2003).
- Time dependency of axial resistance. The time required for pile setup increases with diameter due to increased soil disturbance and pore pressure generation in the soil surrounding the pile (Axelsson 2000). However, the amount of disturbance is related to the volume of soil displacement and therefore may be less for LDOEPs driven in an unplugged condition. For static and dynamic testing purposes, the evaluation of pile side resistance for an LDOEP may require a longer setup duration as compared to smaller diameter piles.

- Use of a vibratory hammer. To expedite construction, contractors will often install the initial pile section using a vibratory hammer and will use an impact hammer only for the final pile section. Some studies on smaller diameter open-end piles suggest that vibratory pile installation may result in lower axial resistance (Carnivan and Camp 2002, Mosher 1990, and Briaud et al. 1990). The reduced resistance may be due to extensive remolding of cohesive soils near the pile wall or liquefaction of cohesionless soils at the pile/soil interface.
- Use of constrictor plate within the pile. A constrictor plate may be welded within the interior of an LDOEP to facilitate formation of a plug during driving. The constrictor plate must allow water to pass to avoid buildup of stress in the pile and needs to be located at a sufficient depth to engage the soil and subsequently drive as a displacement pile (HCN 2014).
- Use of a driving shoe. A driving shoe, consisting of a ring of steel with greater thickness at the pile toe, may be required to allow pile penetration into a dense bearing stratum or rock. Driving shoes are typically installed within the pile interior, which results in a reduced interior pile diameter at the pile tip. This reduced interior diameter may subsequently result in reduced interior side friction and prohibit the development of a pile plug.
- Pile plugging in concrete LDOEPs. Due to the thicker pile wall, concrete LDOEPs will displace a greater volume of soil compared to steel LDOEPs. This greater volume displacement may affect the plug development and interior pile side resistance of concrete LDOEPs. Studies have shown that the plugging of concrete LDOEPs is relatively unlikely during driving (McVay et al. 2004 and Rausche and Webster 2007). However, soil and water buildup within the pile may result in excessive hoop stress, leading to longitudinal cracking.

## **DESIGN COMMENTARY FOR LDOEPs**

Numerous design methods are available in the literature developed for pile design. The *AASHTO LRFD Bridge Design Specifications* and the *FHWA Design and Construction of Pile Foundations* manual describe commonly used methods for the design of piles in cohesive and cohesionless soils (AASHTO 2017 and Hannigan et al. 2016). In general, the design methods are intended to be applicable to multiple pile types and include limited guidance for application to open-end piles. The limited available guidance, along with uncertainty in open-end pile behavior, has resulted in variable practices related to open-end pile design, including considerations related to interior pile side resistance, pile plug evaluation, and open-end pile base resistance. Relevant commentaries from various sources are summarized in the following sections.

## Interior Pile Side Resistance

During the driving process, open-end piles develop side resistance on both the pile interior and exterior. For piles that remain unplugged at the end of driving, the interior pile side resistance may be accounted for in design. There are varying recommendations in the literature about how to evaluate the interior pile side resistance. Commentary on the evaluation of interior pile side resistance includes:

- Hannigan et al. (2016) suggest the interior unit side resistance is about one-third to one-half of the exterior unit side resistance, depending on the soil, pile diameter, and pile shoe.
- Stevens et al. (1982) consider the range of lower to upper bound interior pile side resistance to be 50 to 100 percent, respectively, of the exterior pile side resistance.
- Design guidance from the American Petroleum Institute (API) generally recommends that the interior pile side resistance should be considered equal to that of the pile exterior (API 2011). However, API also recommends that the internal side resistance contribution should be limited to a maximum value equal to the base resistance acting on the soil plug.
- The Norwegian Geotechnical Institute (NGI) design method recommends interior pile side resistance acting on the soil plug be considered equal to three times the external value due to soil arching near the pile base (Clausen et al. 2005).
- Randolph et al. (1991) discuss that values of internal side resistance have historically been assumed to be comparable to values of external side resistance. However, the authors present examples where internal side resistance under dynamic loading is similar to residual skin friction on the pile exterior. The authors also describe other cases where arching action within the pile results in very high values of internal skin friction.
- Lehane and Randolph (2002) discuss the dependence of internal side friction on the dilatant capacity of the sand plug and the interface friction angle. The authors provide a range of typical friction coefficient  $\beta$  values from 0.1 to 0.6.
- Lehane and Gavin (2001) recommend the interior pile minimum friction coefficient  $\beta$  be calculated as  $\beta_{\min} = K_a \cdot \tan \delta$ , where  $K_a$  is the Rankine active earth pressure coefficient and  $\delta$  is the interface friction angle.

## Open-End Pile Base Resistance

Open-end pile base resistance is a function of the pile plug development. In the unplugged condition, base resistance acts over the pile annulus only, while base resistance will develop over the total cross-sectional area for plugged piles. It is common practice, as recommended in the API guidance and other sources, to compute base resistance as the lesser of the plugged resistance acting over the total cross section and the sum of the unplugged annular resistance and the internal pile side resistance (API 2011 and Clausen et al. 2005). Alternative newer methods compute base resistance as a function of partial plug development and consider resistance acting on the internal soil column.

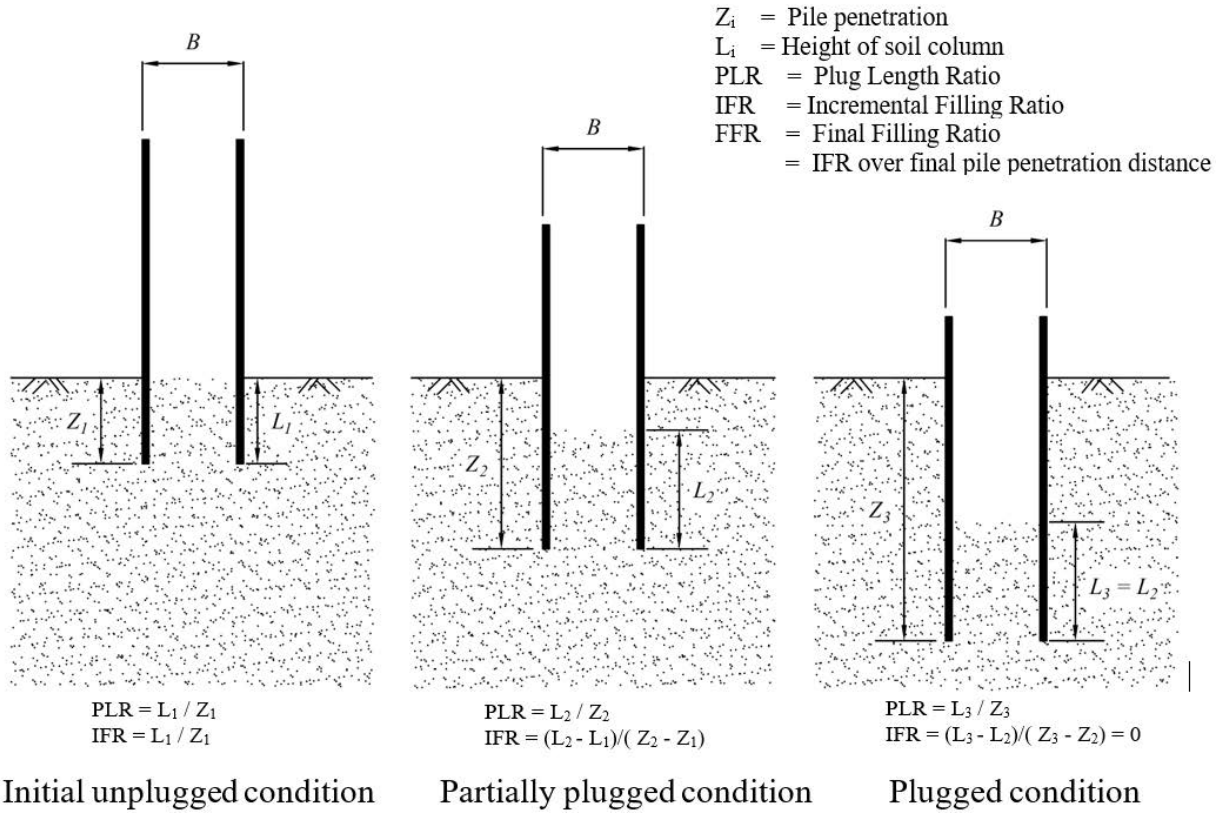
Several publications include guidance and specific recommendations for open-end pile base resistance. A summary of key points discussed with the individual methods and identified in the literature are summarized as follows:

- Lehane and Randolph (2002) describe that most piles will drive unplugged during installation but will behave in a fully plugged manner under static loading. The associated base resistance that develops below the pile plug is related to the amount of displacement during driving. The authors propose that base resistance for a pile that drives unplugged is approximately equivalent to that of a bored pile.
- Jardine et al. (2005) developed the Imperial College Pile (ICP) method that computes plugged base resistance to be approximately half of that available for closed-end piles. Unplugged open-end pile resistance is considered to act on the pile annulus only, and the internal side resistance acting on the pile plug is neglected.
- Mizutani et al. (2003) report that the Japanese recommendation for design of building foundations design code recommends open-end pile base resistance be computed as a factor  $\eta$  times the bearing resistance of a closed-end pile. The  $\eta$  factor is directly related to the ratio of the embedded depth in a stiff layer ( $D_b$ ) to the pile diameter ( $B$ ). For  $D_b/B$  values less than 5.0,  $\eta$  is equal to 0.16. For  $D_b/B$  values greater than 5.0,  $\eta$  is equal to 0.8.
- A design method developed for the State of Alaska recommends the use of “equivalent unit toe resistance” based on the reported CAPWAP values (Dickenson 2012). The CAPWAP resistance is considered to capture the state of plug development and reflect base resistance values that are intermediate between the fully plugged and unplugged condition. The “equivalent unit toe resistance” is applied over the full pile end area.
- Pile design methods by Yu and Yang (2012), Liu et al. (2012), and Doherty et al. (2010) decompose base resistance into components acting on the pile annulus and acting on the soil column within the pile. Yu and Yang (2012) relate the resistance acting on the pile annulus to the pile embedment and the length-to-diameter ratio, while the resistance acting on the soil column is related to the plug length ratio measured during driving.

- Recently developed pile design methods, including those by Lehane et al. (2005), Gudavalli et al. (2013), Lee et al. (2003), and Pail and Salgado (2003) quantify base resistance to the degree of pile plugging. The degree of pile plugging is quantified in these methods using the terms PLR, IFR, and FFR. These terms reflect the plug development during pile driving and are illustrated in figure 4. They are described as follows:
  - PLR is calculated as the height of the soil column within the pile divided by the pile embedment length. A value of 1.0 indicates that the pile is unplugged or “fully coring” with the soil column rising to the top of the pile. A PLR value closer to 0 implies that the soil column is low in the pile and the pile may be plugged. Gudavalli et al. (2013) discuss that unit side and base resistance generally decrease with increasing PLR.
  - The IFR is the *incremental* change in the height of the soil column divided by the *incremental* pile penetration length. An IFR value equal to 0 indicates the pile is plugged, and a value closer to 1.0 indicates the pile is unplugged. As described by Yu and Yang (2012), IFR tends to increase as the inner diameter of the pile increases. IFR generally varies inversely with pile length or penetration depth, as longer pipe piles are more likely to be fully plugged.
  - The FFR is the same as the IFR except that it is computed over the final pile penetration distance.

In general, the PLR, IFR, and FFR are difficult to measure during pile installation and to estimate during design. Correlations have been developed to quantify these terms for design purposes.

- The University of Western Australia method incorporates observations of Lehane and Randolph (2005) relating base resistance to the degree of displacement during driving as a function of FFR (equal to IFR at the end of driving). For an FFR value equal to zero corresponding to a plugged condition, the unit base resistance is equal to that for a closed-end pile. For an FFR value equal to 1.0, corresponding to an unplugged condition, the unit base resistance is equal to values reported for bored piles.



Source: FHWA.

**Figure 4. Illustration. Schematic diagram of pile plug development with terms PLR, IFR, and FFR.**



## **CHAPTER 3. LOAD TEST DATA, MEASURED AND PREDICTED NOMINAL RESISTANCE, AND LRFD RESISTANCE FACTOR CALIBRATION**

### **INTRODUCTION**

The LDOEP resistance factor calibration is performed in multiple steps using a new load test data set. The process is summarized in five steps as follows:

1. Select load test data set.
2. Evaluate measured nominal resistance of load test data set using load test failure criteria.
3. Characterize subsurface conditions and soil properties of each load test site.
4. Estimate predicted pile nominal resistance using static analysis resistance methods, incorporating results of subsurface characterization.
5. Compare predicted static analysis resistance with measured load test nominal resistance and compute resistance factors.

The following sections provide additional details and assumptions of the resistance factor calibration analysis steps.

### **LOAD TEST DATA SET**

The load test data set used in the resistance factor calibration was selected from the body of over 150 LDOEP load tests collected as part of the project. The data set was limited to include:

- Steel LDOEPs. Concrete LDOEPs are not included due to the limited available load test data.
- Static load tests. Static load testing is considered the “gold standard” for determining pile nominal resistance. Statnamic testing is a dynamic method that involves assessment of dynamic forces along the pile length with different levels of instrumentation to predict static LODEP nominal resistance. The Statnamic test dynamic force assessment adds variability to the load test interpretation. To avoid the incorporation of additional uncertainty into the analysis, only static load tests are considered.
- Compression loading. Due to potential differences in side resistance mobilization in compression and tension loading, and the lack of base resistance information from tension loading tests, only compression load tests are considered.
- Open-end piles. Test piles with artificial plugs, constrictor plates, or other means to induce pile plugging are excluded from the analysis to allow for evaluation of open-end pile response.

- Impact driven piles. Installation methods can have a significant effect on the pile behavior and response under static loading conditions. Most existing static design methods do not directly account for pile installation methods. In order to limit uncertainty in the load test data set, only piles installed using impact driving or combined vibratory and impact driving are considered. Piles installed using jetting, predrill, or entirely vibratory driving are not included due to potential impact of installation method on pile resistance.
- Sites with available information for subsurface characterization. Static design methods considered in the analysis require either in-situ strength and density properties or in-situ test results consisting of standard penetration test N-values and/or cone penetration test (CPT) results. Load tests are excluded when subsurface information is not available, or not available for the entire pile length.

Considering the above criteria, the load test data set includes 66 static, compression pile load tests at Cohesive, Cohesionless, and Mixed sites. Cohesive and Cohesionless sites are defined for the project as sites including 70 percent or greater of cohesive or cohesionless material along the pile length. Mixed sites have variable composition of cohesive and cohesionless material with neither type composing more the 70 percent of the material along the pile length. Table 1 provides a summary of the test piles used in the resistance factor calibration. Plots of the load test force displacement curves for each test are provided in appendix A. The load tests are available in the DFLTD version 2.0 (Petek et al. 2016).

**Table 1. Resistance factor calibration load test data set. Summary of static compression load tests.**

Subsurface Conditions	Project	Project Name	State	Country	Pile Designation	Diameter (inch)	Length (ft)	Max Force (kips)	Max Displ. (inch)	Construction Method	No. Borings	No. CPTs
Cohesive	1006	I-880 Port of Oakland Connector Viaduct (Caltrans Bridge No. 33-0612E)	CA	USA	TP-9	42.0	88.3	1,245	-1.38	Impact drive	2	6
	1007	I-880 Oakland Bridge Replacement	CA	USA	Pile3-H	42.0	105.5	1,209	-1.24	Impact drive	2	—
	1009	Noto Peninsula New Highway Route Bridges (Japan)	—	Japan	TP-1	31.5	36.1	1,057	-7.79	Impact drive	2	3
	1009	Noto Peninsula New Highway Route Bridges (Japan)	—	Japan	TP-2	31.5	36.1	832	-1.30	Impact drive	2	3
	1010	Pentre Site	—	Great Britain	TP-NC	30.0	191.9	1,349	-4.22	Impact drive	1	—
	1021	Annacis Throughway Bridge Project – Highway 91	—	Canada	TP-D67m	36.0	220.8	1,693	-3.72	Impact drive	—	1
	1031	Gulf Intracoastal Waterway West Closure Complex Test Site 1	LA	USA	TP-3	30.0	160.5	830	-4.50	Vibratory and impact drive	3	2
	1031	Gulf Intracoastal Waterway West Closure Complex Test Site 1	LA	USA	TP-4	30.0	170.3	1,060	-4.50	Impact drive	3	2
	1031	Gulf Intracoastal Waterway West Closure Complex Test Site 1	LA	USA	TP-5	30.0	161.0	900	-4.59	Impact drive	3	2
	1031	Gulf Intracoastal Waterway West Closure Complex Test Site 1	LA	USA	TP-6	30.0	150.0	830	-4.48	Impact drive	3	2
	1024	Gulf Intracoastal Waterway West Closure Complex Test Site 3	LA	USA	TP-11	30.0	190.0	1,215	-4.60	Vibratory and impact drive	3	3
	1063	Port of Oakland Connector Viaduct Maritime On/Off-Ramps (Caltrans Bridge No. 33-612E)	CA	USA	TP3-10NCI	42.0	98.0	845	-3.50	Impact drive	12	—
	1063	Port of Oakland Connector Viaduct Maritime On/Off-Ramps (Caltrans Bridge No. 33-612E)	CA	USA	TP6-17NCI	42.0	103.0	1,037	-0.83	Impact drive	12	—
1072	Tilbrook Grange Site	—	Great Britain	TP-OC	30.0	109.9	3,619	-4.02	Impact drive	1	—	
Cohesionless	1002	Red Sea Coast, Saudi Arabia	—	Saudi Arabia	TP-A1	56.0	216.5	1,397	-3.94	Impact drive	2	—
	1002	Red Sea Coast, Saudi Arabia	—	Saudi Arabia	TP-A2	56.0	239.5	1,454	-3.94	Impact drive	2	—
	1008	Santa Clara River Bridge (Caltrans Bridge No. 52-0449)	CA	USA	Test-1	84.0	68.7	1,995	-8.10	Vibratory and impact drive	1	—
	1008	Santa Clara River Bridge (Caltrans Bridge No. 52-0449)	CA	USA	Test-2	84.0	134.0	8,000	-4.10	Vibratory and impact drive	1	—
	1013	Hokkaido, Japan	—	Japan	TP-1	40.0	134.5	3,552	-3.84	Impact drive	1	—
	1014	Chiba, Japan	—	Japan	TP-2	31.5	157.5	1,888	-2.78	Impact drive	1	—
	1019	EURIPIDES Joint Industry Project – offshore test piles	—	Netherlands	TP-1.1	29.9	100.9	2,653	-10.27	Impact drive	1	3
	1019	EURIPIDES Joint Industry Project – offshore test piles	—	Netherlands	TP-1.3	29.9	155.0	5,202	-15.33	Impact drive	1	3
	1019	EURIPIDES Joint Industry Project – offshore test piles	—	Netherlands	TP-2	29.9	154.0	5,195	-13.57	Impact drive	1	3
	1019	EURIPIDES Joint Industry Project – offshore test piles	—	Netherlands	TP-2	29.9	154.0	6,708	-2.59	Impact drive	1	3
	1020	Sakonnet River Bridge (Route 138)	RI	USA	TestPile	72.0	136.2	2,990	-2.85	Vibratory and impact drive	1	—
	1023	Berenda Slough Bridge (Caltrans Bridge No. 41-0009R)	CA	USA	TestPile	42.0	106.0	1,618	-1.85	Impact drive	1	—
	1027	Seal Beach Blvd OC (Caltrans Bridge No. 55-1099)	CA	USA	TP-2A2	48.0	112.5	3,003	-0.88	Impact drive	5	2
	1056	Mad River Bridge (Caltrans Bridge No. 04-0025L)	CA	USA	TestPile	87.0	136.4	7,191	-11.02	Impact drive	1	—
	1057	Russian River Bridge (Caltrans Bridge No. 10-0301)	CA	USA	TestPile	66.0	120.7	3,200	-1.30	Impact drive	1	—
	1058	San Joaquin River Bridge (Caltrans Bridge No. 41-90)	CA	USA	TestPile	74.5	188.5	8,012	-2.15	Impact drive	2	—
	1059	Colorado River Bridge (Caltrans Bridge No. 54-1272)	CA	USA	TestPile	108.0	127.0	8,000	-0.97	Impact drive	1	—
	1060	Russian River Bridge (Caltrans Bridge No. 20-38)	CA	USA	TestPile	48.0	143.3	3,975	-5.20	Impact drive	1	—
	1061	Feather River Bridge (Caltrans Bridge No. 18-0026R)	CA	USA	TP-1	90.0	136.0	4,090	-8.00	Impact drive	1	—
	1061	Feather River Bridge (Caltrans Bridge No. 18-0026R)	CA	USA	TP-2	90.0	202.0	8,000	-3.00	Impact drive	1	—
	1062	Santa Clara River Bridge (Caltrans Bridge No. 53-2925)	CA	USA	TestPile	72.0	128.7	8,045	-6.17	Vibratory and impact drive	2	—
	1068	Port of Toamasina Offshore Jetty	—	Madagascar	12A	40.0	213.3	2,029	-2.60	Vibratory and impact drive	4	—
	1068	Port of Toamasina Offshore Jetty	—	Madagascar	4B	40.0	213.3	2,205	-1.38	Vibratory and impact drive	4	—
1069	Trans-Tokyo Bay Highway	—	Japan	TP-1	78.7	203.4	7,945	-8.20	Impact drive	1	1	
1070	Legislative Route 795 Section B-6 Philadelphia, PA	PA	USA	TP-C	30.0	64.2	1,499	-1.31	Impact drive	4	—	
1070	Legislative Route 795 Section B-6 Philadelphia, PA	PA	USA	TP-E	30.0	96.0	1,436	-4.15	Impact drive	4	—	

Subsurface Conditions		Project	Project Name	State	Country	Pile Designation	Diameter (inch)	Length (ft)	Max Force (kips)	Max Displ. (inch)	Construction Method	No. Borings	No. CPTs
Mixed	Side: Cohesive Base: Cohesionless	1003	Louisiana Highway 1 Improvements Load Test Data Phase 1B	LA	USA	T-3-1	30.0	195.0	1,597	-3.23	Impact drive	11	5
		1025	I-880 5th Street Overhead Bridge (Caltrans Bridge No. 33-27)	CA	USA	TestPile	96.0	136.6	6,742	-8.86	Impact drive	1	—
		1063	Port of Oakland Connector Viaduct Maritime On/Off-Ramps (Caltrans Bridge No. 33-612E)	CA	USA	TP9-27NCI	42.0	97.0	1,288	-1.21	Impact drive	12	—
		1067	Port Said	—	Egypt	TP-22	28.0	167.3	899	-1.25	Impact drive	1	—
		1067	Port Said	—	Egypt	TP-136	28.0	167.3	899	-1.19	Impact drive	1	—
	Side: Cohesionless Base: Cohesive	1011	Woodrow Wilson Bridge over Potomac River, VA and MD, USA	MD	USA	PL-3	36.0	96.3	1,764	-0.75	Impact drive	3	—
		1055	Feather River Bridge (Caltrans Bridge No. 18-0009)	CA	USA	Pile-3	48.0	173.1	2,500	-3.60	Impact drive	1	—
		1071	Nippon Steel Corporation/Blast Furnace Foundations in Japan	—	Japan	BF-61	47.2	75.6	1,834	-0.78	Impact drive	2	—
		1071	Nippon Steel Corporation/Blast Furnace Foundations in Japan	—	Japan	H-27	47.2	69.7	2,518	-0.92	Impact drive	2	—
		1071	Nippon Steel Corporation/Blast Furnace Foundations in Japan	—	Japan	HS-40	47.2	63.2	1,469	-1.68	Impact drive	2	—
	Side: Mixed Base: Cohesive	1001	Port Mann Bridge	—	Canada	TestPile	72.0	245.7	12,061	-6.59	Vibratory and impact drive	3	—
		1011	Woodrow Wilson Bridge over Potomac River, VA and MD, USA	MD	USA	PL-1	54.0	165.2	2,925	-2.68	Impact drive	3	—
		1071	Nippon Steel Corporation/Blast Furnace Foundations in Japan	—	Japan	HS-97	47.2	82.0	1,822	-0.94	Impact drive	2	—
	Side: Mixed Base: Cohesionless	1004	Tokyo Port Bay Bridge	—	Japan	TP-4	59.1	260.8	7,194	-10.08	Impact drive	1	1
		1004	Tokyo Port Bay Bridge	—	Japan	TP-5	59.1	301.8	8,093	-9.24	Impact drive	1	1
		1005	Salinas River Bridge (Caltrans Bridge No. 44-216R/L)	CA	USA	TestPile	72.0	118.0	1,513	-0.96	Impact drive	1	—
		1011	Woodrow Wilson Bridge over Potomac River, VA and MD, USA	MD	USA	PL-2	42.0	125.5	2,920	-2.68	Impact drive	3	—
		1012	Jin Mao Building	—	China	ST-1	36.0	262.5	3,698	-9.98	Impact drive	1	—
		1012	Jin Mao Building	—	China	ST-2	36.0	262.5	4,073	-7.63	Impact drive	1	—
		1022	Pitt River Bridge	—	Canada	Pile-P5	71.8	333.0	10,029	-3.26	Vibratory and impact drive	1	1
1026		I-405 and SR-22 HOV Connector Separation Bridge (Caltrans Bridge No. 55-1103E)	CA	USA	TP-9	48.0	75.0	1,772	-4.08	Vibratory and impact drive	4	5	
1026		I-405 and SR-22 HOV Connector Separation Bridge (Caltrans Bridge No. 55-1103E)	CA	USA	TP-10	48.0	100.0	2,600	-5.31	Vibratory and impact drive	4	5	
1035		Highway 32 Stony Creek Bridge (Caltrans Bridge No. 11-0029)	CA	USA	TP-6	99.6	169.9	7,859	-10.51	Impact drive	1	—	
1070		Legislative Route 795 Section B-6 Philadelphia, PA	PA	USA	TP-D	30.0	86.2	896	-2.74	Impact drive	4	—	
1071		Nippon Steel Corporation/Blast Furnace Foundations in Japan	—	Japan	BF-47	47.2	87.8	1,827	-0.89	Impact drive	2	—	

1 inch = 25.4 mm; 1 ft = 0.305 m; 1 kip = 4,448.2216 N.

—No data.

Displ. = Displacement.

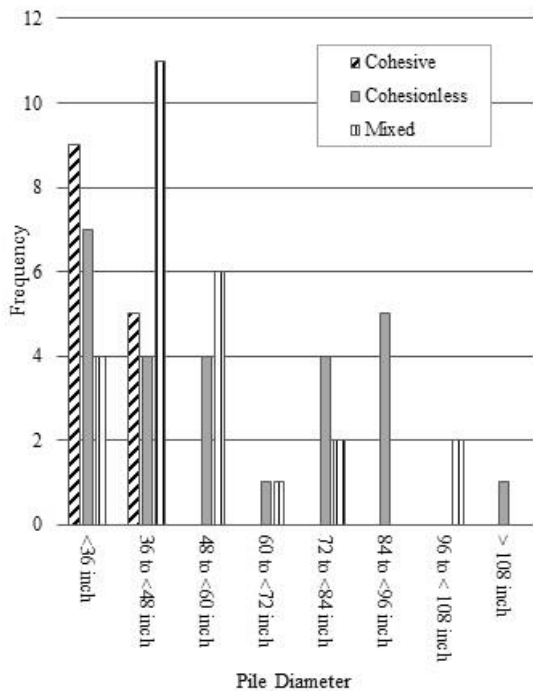
Note: Table formatted for 11x17 printing.

The resistance factor calibration was performed based on subsurface conditions at each load test site. The number of tests per each site condition are presented in table 2.

**Table 2. Number of test piles by site condition.**

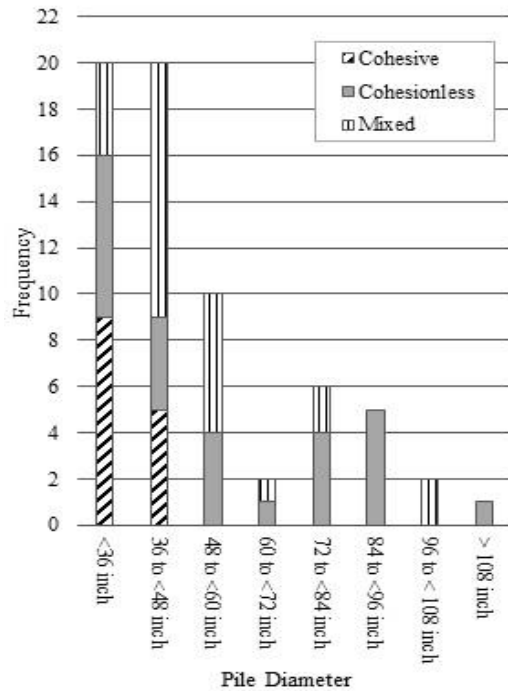
Site Condition	Number of Test Piles	Number of Projects
Cohesive	14	9
Cohesionless	26	18
Mixed	26	15

Figure 5-A and figure 5-B present histograms of pile diameters by site condition. Figure 6 shows the cumulative distribution function of pile diameters by site condition. Figure 7-A and figure 7-B show the range of pile diameters and maximum test loads of the data set piles.



Source: FHWA.  
1 inch = 25.4 mm.

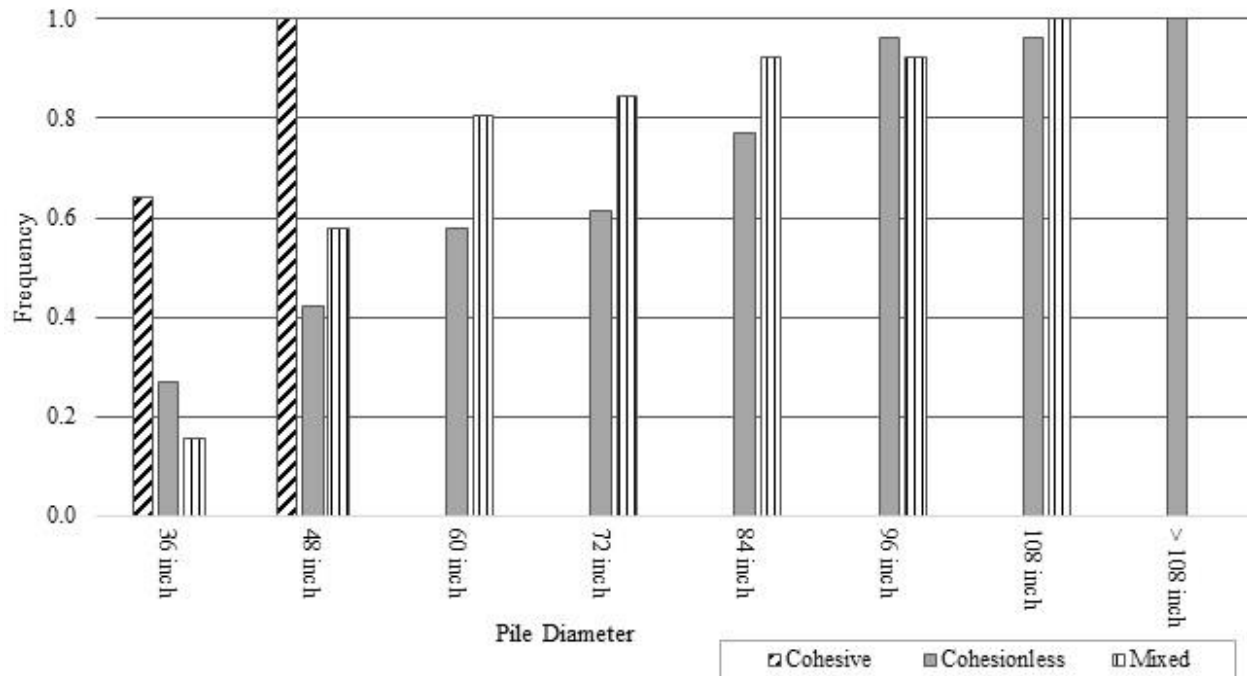
A. Frequency by soil type.



Source: FHWA.  
1 inch = 25.4 mm.

B. Cumulative frequency.

**Figure 5. Charts. Load test data set: histograms of pile diameter.**



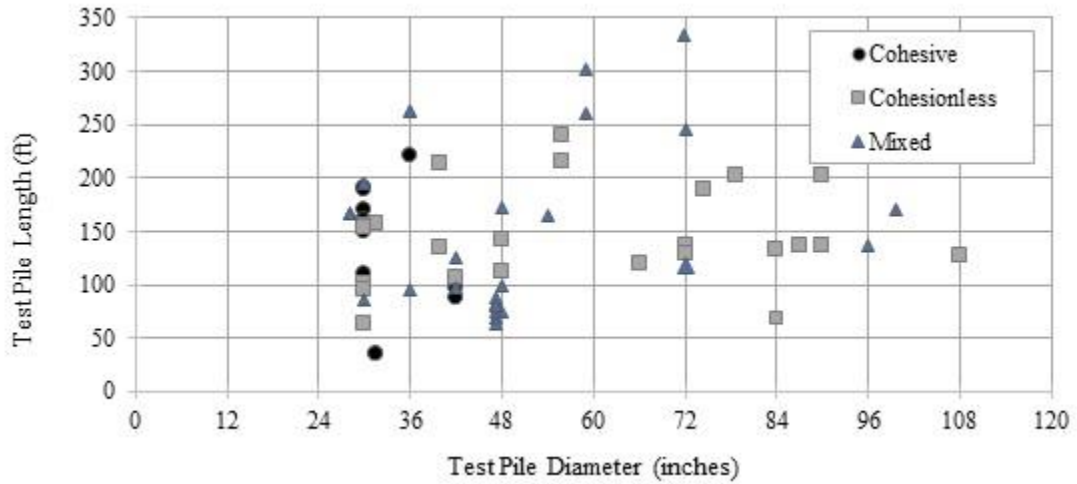
Source: FHWA.  
1 inch = 25.4 mm.

**Figure 6. Chart. Load test data set: cumulative distribution function of pile diameter by soil type.**

General comments on the resistance factor calibration load test data set include:

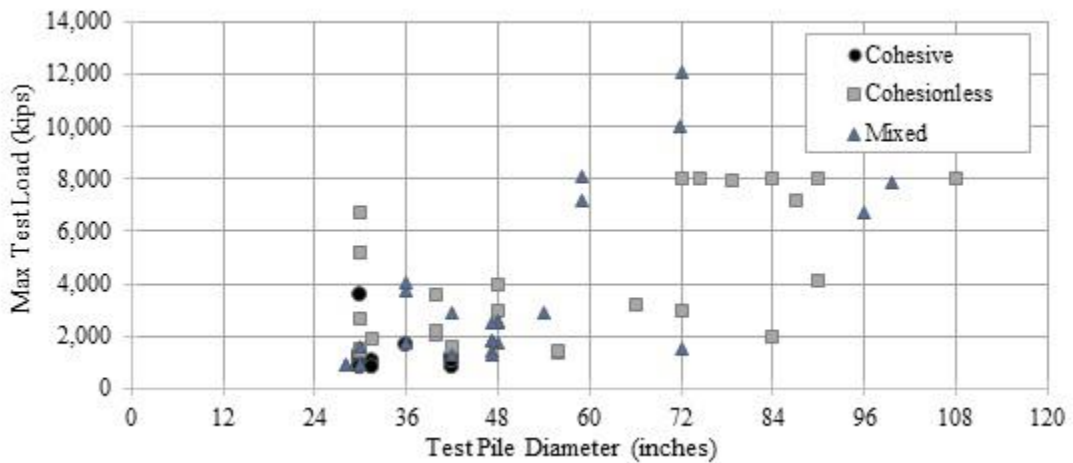
- The majority of the test piles, including all of the test piles at Cohesive sites, have diameters less than 48 inches. Therefore, the static design method analyses and resistance factor calibration for Cohesive sites may have uncertainty for larger diameters. The Cohesionless data set is relatively evenly distributed among diameters up to 96 inches and is considered to have greater applicability to a larger potential range of pile diameters.
- The number of load tests at Cohesive sites is lower than Cohesionless or Mixed sites. The lower number of tests may result in increased uncertainty of the resistance factor calibration.
- All site condition pile groups contain multiple test piles from the same project. In smaller data sets, this may reduce the applicability of the results due to potential overrepresentation of some test sites.

- The load test data set includes load tests conducted to varying ranges of displacement. Numerous tests were conducted to a plunging type failure with large displacements. Other load tests were conducted to lower Service Limit range displacements or were only loaded to required design loads that do not correspond to the true nominal resistance. The displacement magnitudes are discussed further in relation to the load test failure criteria.



Source: FHWA.  
 1 inch = 25.4 mm; 1 ft = 0.305 m.

A. Pile dimensions by soil type.



Source: FHWA.  
 1 inch = 25.4 mm; 1 kip = 4,448.2216 N.

B. Max test load by soil type.

**Figure 7. Graphs. Load test data set: plots of pile dimensions and maximum test loads.**

An alternative Variable Side data set was also included in the analysis. As noted above, the Cohesive site condition subset has only 14 load tests. Of the 66 load tests in the load test data set, an additional 9 piles have cohesive base conditions combined with cohesionless or mixed side conditions. To further evaluate cohesive base conditions, a separate data set was considered with cohesive base conditions and any potential side condition (cohesive, cohesionless, or mixed). The Variable Side condition was also considered with cohesionless-based conditions. The number of tests per each Variable Side condition is shown in table 3.

**Table 3. Number of test piles for alternate Variable Side site conditions.**

Site Condition	Number of Test Piles	Number of Projects
Variable Side + Cohesive Base	14 + 6 + 3 = 23	13
Variable Side + Cohesionless Base	26 + 5 + 12 = 43	30

### LOAD TEST FAILURE CRITERIA

Numerous failure criteria are available for evaluation of measured pile load test nominal resistance. This research performed a quantitative and qualitative assessment of the failure criteria based on their subjectivity and repeatability, required inputs, and mean statistics of the load test data set. Furthermore, the failure criteria were considered in relation to the load test data set displacements, accounting for the varying shapes and displacement magnitudes of the load displacement curves. As described in the preceding section, the load test data set includes load tests conducted to varying levels of displacement. In many cases, the shape of the load displacement curve and the magnitude of the load test displacement limit the applicability of some failure criteria. Load tests within the load test data set are excluded from the resistance factor calibration analysis when a failure criterion is not applicable, thereby reducing the size of the data set. In order to address data size considerations, multiple failure criteria were selected and utilized independently in the resistance factor calibration. The failure criteria were selected to balance consistent interpretations of the measured pile nominal resistance using a smaller data set along with more variable interpretations of measured pile nominal resistance with a larger data set.

The following three failure criteria were selected for use in the resistance factor calibration:

- Modified Davisson criterion. The Modified Davisson criterion is recommended for piles with diameters greater than 36 inches (914 mm) (AASHTO 2017). The nominal resistance is determined where the Modified Davisson offset line intersects the load test load displacement curve. The Modified Davisson line is computed as:

$$s_f = \frac{QL}{AE} + \frac{B}{30} \quad (1)$$

Where:

$s_f$  = pile top settlement (inch).  
 $Q$  = test load (kips).

$L$  = pile length (inch).  
 $A$  = pile cross-sectional area (inch<sup>2</sup>).  
 $E$  = pile modulus (ksi).  
 $B$  = pile diameter (inch).

- 5 Percent Diameter criterion. The nominal resistance is equal to the applied test load corresponding to a pile head displacement of 5 percent of the pile diameter.
- Max Load criterion. The Max Load criterion define the nominal resistance as the maximum load applied during the static load test. This criterion enable utilization of all tests in the load test data set.

Table 39 in appendix A presents the predicted nominal resistance loads and displacements using the three selected failure criteria for the Phase II data set. Table 4 below summarizes the number of load tests by site condition that are considered applicable to each of three failure criterion.

**Table 4. Number of test piles by site condition considered applicable to failure criteria.**

Site Condition	Test Pile Count by Failure Criterion		
	Modified Davisson	5 Percent Diameter	Max Load
Cohesive	11	10	14
Cohesionless	13	16	26
Mixed	12	15	26

## SOIL PROPERTY EVALUATION

Static axial resistance design methods require defined soil stratigraphy and engineering parameters for input into the design equations. Depending on the design method, required input parameters include unit weight, relative density, internal friction angle, undrained shear strength, and over-consolidation ratio (OCR). Each load test includes varying levels of detail pertaining to soil layer types, thicknesses, and engineering properties as provided in the available reports and references. In general, the resistance factor calibration analysis utilized reported soil layer properties when available. When information was not available, the approach considered the nearest boring and laboratory data as follows:

- Evaluation of soil layers. Soil layers were determined based on review of exploration logs for layers of similar soil type and density. In general, soil layer thicknesses were limited to a maximum thickness of 35 ft to provide discretization of engineering properties.
- Review of in-situ and laboratory data. Available in-situ data generally consisted of sample descriptions, standard penetration test (SPT) blow counts, and CPT data. Laboratory test data generally consisted of water content, unit weight, Atterberg limits, unconfined compression from a pocket penetrometer, unconfined compression, and triaxial strength test results. All sources of available data were reviewed and compared for evaluation of characteristic properties.

- Total unit weight is required by many cohesionless design methods to compute vertical effective stress. When available, total unit weight is calculated using the reported moisture content and an assumed specific gravity based on soil classification.
- Soil correlations were also considered to provide missing information. Correlations used for the project are provided in table 5.

The following hierarchy was employed in the selection of soil properties:

1. Average of reported lab data in layer (e.g., undrained strength, internal friction angle, unit weight).
2. Average or interpreted values provided in generalized borings and site data.
3. Correlated values based on SPT or CPT data. The closest boring was used in the case when multiple borings are available for a test pile. CPT results were considered in combination with SPT values, when available.

Table 5 includes four methods to correlate internal friction angle from SPT blow counts. In general, the Peck et al. (1974) correlation was considered to provide the most consistent, reasonable friction angle values. This correlation was also used to determine friction angles for NCHRP Report 507 (Paikowsky 2004). The Schmertmann (1975) correlation generally resulted in the highest values, followed by Hatanaka and Uchida (1996). The Naval Facilities Engineering Command (NAVFAC) approach generally resulted in the lowest friction angles in loose soil (NAVFAC 1992).

The OCR was computed in relation to undrained shear strength. For numerous projects, undrained shear strength was either reported or available from lab strength data. In some projects, undrained shear strength was determined from the CPT correlations. In these cases, the OCR was computed using Ladd and Foott (1974). Conversely, if OCR values were available or correlated using CPT results, undrained shear strength was computed using Ladd and Foott (1974). Undrained shear strength and OCR correlations with SPT N-values were used with caution.

The API method for cohesionless soil utilizes soil type and relative density condition (i.e., medium dense, dense) for selection of unit side resistance parameters. Relative density values were computed using multiple correlations in table 5. The API side resistance properties were selected in consideration of the computed relative density values and corresponding API relative density – soil type categories.

**Table 5. Soil property correlations.**

Soil Property	Correlation	Reference
Relative density (CPT)	$D_r = 100 \cdot 0.268 \cdot \ln \left( \frac{q_t/p_a}{\sigma_v/p_a} - 0.675 \right)^{0.5} \quad (2)$	Jamiolkowski et al. 2001
Relative density (SPT)	$D_r = \frac{N_{60}}{17 + 24 \left( \frac{\sigma_v}{p_a} \right)} \quad (3)$	Meyerhof 1957
Relative density (SPT)	<i>See tabulated values in Kulhawy and Mayne (1990).</i>	Kulhawy and Mayne 1990
Unit weight (CPT)	$\frac{\gamma}{\gamma_w} = \frac{0.27 \log R_f + 0.36 \log \frac{q_t}{p_a} + 1.236}{2.65} \cdot G_s \quad (4)$	Robertson and Cabal 2010
Unit weight (SPT)	<i>See tabulated values in Bowles (1996).</i>	Bowles 1996
Internal friction angle	$\phi' = 54 - 27.6034e^{-0.014N} \quad (5)$	Peck et al. 1974
Internal friction angle	$\phi' = 20 + \frac{15.4(N_{160})^{0.34}}{12.2 + 20.3 \frac{\sigma_v}{p_a}} \quad (6)$	Hatanaka and Uchida 1996
Internal friction angle	$\phi' = \tan^{-1} \frac{N_{60}}{12.2 + 20.3 \frac{\sigma_v}{p_a}} \quad (7)$	Schmertmann 1975
Internal friction angle	<i>See NAVFAC chapter 3, figure 7, Correlations of Strength Characteristics for Granular Soil (NAVFAC 1982).</i>	NAVFAC 1982
Undrained shear strength (CPT)	$S_u = \frac{q_t - \sigma_v}{N_k} \quad (8)$	Kulhawy and Mayne 1990
Undrained shear strength (SPT)	$S_u = 0.038 \cdot N \quad (9)$	Sowers 1979
Undrained shear strength (Correlated with OCR)	$\frac{S_u}{\sigma_v} = 0.23 \cdot OCR^{0.80} \quad (10)$	Ladd and Foott 1974
OCR (SPT)	$OCR = 0.193 \left( \frac{N_{60}}{\sigma_v} \right)^{0.689} \quad (11)$	Mayne and Kemper 1988
OCR (CPT)	$OCR = \frac{0.33(q_t - \sigma_v)}{\sigma_v} \quad (12)$	Kulhawy and Mayne 1990
OCR (Correlated with $S_u$ )	$\frac{S_u}{\sigma_v} = 0.23 \cdot OCR^{0.80} \quad (13)$	Ladd and Foott 1974

## ESTIMATED PILE NOMINAL RESISTANCE

### Static Axial Resistance Design Methods

Numerous static axial resistance design methods are available for calculation of predicted pile nominal resistance. These include well-known methods used for transportation infrastructure projects, such as those published in FHWA guidelines and provided in the AASHTO code (Hannigan et al. 2016 and AASHTO 2017). The API design guide describes other methods used for offshore foundations (API 2011). In recent years, new methods have been published specifically developed for steel and concrete open-end piles. In addition, several State departments of transportation (DOTs) have developed regional specific pile design methods.

A limited number of the static design methods were selected for LDOEP evaluation and resistance factor calibration as part of this study. The selected methods are listed in table 6.

**Table 6. Static design methods considered in LDOEP evaluation.**

Side Resistance		Base Resistance	
Cohesive Side	Cohesionless Side	Cohesive Base	Cohesionless Base
Tomlinson $\alpha$ -method	Nordlund method	Total stress approach (AASHTO/API)	Nordlund method
API $\alpha$ -method	API $\beta$ -method	Brown method	Bearing capacity API method
Saye method	Gudavalli method	—	Gudavalli method
Brown method	Brown method	—	Brown method

—No data.

The methods were selected considering multiple factors, including:

- Methods that are frequently used by State DOTs for design of LDOEPs as identified in the survey performed as part of NCHRP Synthesis 478 (Brown and Thompson 2015). Respondents indicated that the Tomlinson  $\alpha$ -method and Nordlund method are most commonly used for LDOEP design in cohesive and cohesionless soil, respectively.
- Methods that incorporated LDOEP load test data in their development. Many existing design methods are based on load tests on smaller diameter piles, resulting in uncertainty in their applicability to LDOEPs. Selected methods that included LDOEP data in their development include the API, Brown, and Gudavalli methods.
- Methods that directly account for potential pile plugging, such as the Gudavalli method.

- Availability of input parameters in collected load test data. The preference would be to include recent static design methods based on CPT results or those that directly incorporate laboratory data, such as plasticity index. However, the required design methods' input parameters were considered in terms of the available information in the collected load test data used for resistance factor calibration. Unfortunately, there is insufficient information in the calibration data to perform representative analyses of these design methods.
- Required input parameters for design methods. Input parameters for the selected methods generally include unit weight for the effective stress calculation, friction angle, undrained shear strength, OCR, relative density, and SPT blow count values. Other methods include properties that are difficult to determine, such as lateral stress index  $K_o$  and interface friction angle. Because these properties are difficult to determine and are not reported in the load test data, their usage in design methods is considered to introduce additional uncertainty into the analysis.

The majority of the selected methods are described in detail in the AASHTO *LRFD Bridge Design Specifications* and the FHWA *Design and Construction of Driven Pile Foundations* manual (AASHTO 2017 and Hannigan et al. 2016). The Saye (2013) and Gudavalli (2013) methods are described in their respective references. Table 3 and table 4 provide a summary of the side and base resistance methods, respectively.

It is noted that the Gudavalli method was developed for steel LDOEPs in dense sand, based on the load test data set used for the method development. However, the present analysis applies this method to all cohesionless layers, regardless of soil density. Therefore, the analysis checks the applicability of the method to an expanded set of cohesionless subsurface conditions for potential applicability to steel LDOEPs. For the Gudavalli side resistance method, the beta value was limited to a lower bound value of 0.1 based on data presented in the original reference. However, this lower bound is not specifically prescribed in the reference.

**Table 7. Selected side resistance design methods.**

Method	Design Equations	Equation Parameters
Tomlinson $\alpha$ (Tomlinson 1980)	$q_s = \alpha \cdot S_u$ (14) <i>[See reference for <math>\alpha</math> values (Hannigan et al. 2016 and AASHTO 2017).]</i>	$\alpha$ = adhesion factor $S_u$ = undrained shear strength
API $\alpha$ (API 2011)	$q_s = \alpha \cdot S_u$ (15) $\alpha$ is defined as: $\alpha = 0.5 \cdot \Psi^{-0.5}$ for $\Psi \leq 1.0$ (16) $\alpha = 0.5 \cdot \Psi^{-0.25}$ for $\Psi > 1.0$ (17) where $\Psi = S_u / (\sigma'_v)$ and $\alpha \leq 1.0$ (18)	$\alpha$ = adhesion factor $S_u$ = undrained shear strength $\sigma'_v$ = vertical effective stress
Saye (Saye et al. 2013)	$q_s / \sigma'_v = 0.19(\text{OCR})^{0.7}$ (19) $\text{OCR} = \frac{S_u / \sigma'_v}{0.32}^{1/0.8}$ (20)	$S_u$ = undrained shear strength $\sigma'_v$ = vertical effective stress OCR = over-consolidation ratio
Nordlund (Nordlund 1979)	$q_s = K_\delta \cdot C_F \cdot \sigma'_v \frac{\sin(\delta + \omega)}{\cos \omega}$ (21) <i>[See reference for input parameters <math>K_\delta</math> and <math>C_F</math> (Hannigan et al. 2016 and AASHTO 2017).]</i>	$K_\delta$ = coefficient of lateral earth pressure at mid-point of soil layer $C_F$ = Correction factor for $K_\delta$ $\sigma'_v$ = vertical effective stress $\delta$ = interface friction angle between pile and soil $\omega$ = angle of pile taper from vertical
API $\beta$ (API 2011)	$q_s = \beta \cdot \sigma'_v$ (22) <i>[See reference for <math>\beta</math> values (Hannigan et al. 2016).]</i>	$\beta$ = friction coefficient $\sigma'_v$ = vertical effective stress
Brown (Brown 2001)	$q_s$ (kPa) = $F_{vs}(A_b + B_b N_{60})$ (23) <i>[See reference for <math>A_b</math>, <math>B_b</math>, and <math>F_{vs}</math> values (Hannigan et al. 2016).]</i>	$N_{60}$ = SPT N-value corrected for 60 percent energy transfer $F_{vs}$ = reduction factor for vibratory installation
Gudavalli (Gudavalli et al. 2013)	For dense to very dense sand: $q_s = \beta \cdot \sigma'_v$ (24) $\beta = (3.5 - 3.2 \cdot \text{PLR})e^{-0.023 \cdot l}$ (25) $\text{PLR} = \frac{b_i}{1.4}^{0.19}$ (26)	$\beta$ = friction coefficient $\sigma'_v$ = vertical effective stress PLR = plug length ratio $l$ = pile penetration depth (m) $b_i$ = interior pile diameter (m)

**Table 8. Selected base resistance design methods.**

Method	Design Equations	Equation Parameters
Total stress approach (AASHTO 2017 and API 2011)	$q_p = N_c \cdot S_u$ (27) where $N_c = 9$	$S_u$ = undrained shear strength $N_c$ = bearing capacity factor
Bearing capacity approach (API 2011)	$q_p = N_q \cdot \sigma'_v$ (28) [See reference for $N_q$ parameters.]	$N_q$ = bearing capacity factor $\sigma'_v$ = vertical effective stress
Nordlund (Nordlund 1979)	$q_p = \alpha_t \cdot N_q \cdot \sigma'_v \leq q_L$ (29) [See reference for determination of input parameters $\alpha_t$ , $N_q$ , and $q_L$ . (Hannigan et al. 2016 and AASHTO 2017).]	$\alpha_t$ = dimensionless factor $N_q$ = bearing capacity factor $\sigma'_v$ = vertical effective stress at the pile base $\leq 3.2$ ksf $q_L$ = limiting unit base resistance (ksf)
Brown (Brown 2001)	For impact driven piles: $q_p$ (MPa) = $0.17 \cdot N_{60}$ (30) $q_p$ (ksf) = $3.55 \cdot N_{60}$ (31) For vibratory installation, multiply $q_p$ by 0.56. Total base resistance: $R_p = q_p (A_{tp} + A_t F_{plug})$ (32)	$N_{60}$ = SPT N-value corrected for 60 percent energy transfer (blows/0.3 m) $A_{tp}$ = annular area of pile base $A_t$ = plug area at pile base $F_{plug}$ = plug mobilization factor = 0.42 for open-end piles
Gudavalli (Gudavalli et al 2013)	For dense to very dense sand: $q_p = N_q \cdot \sigma'_v$ (33) $N_q = 12.3 \cdot \text{PLR}^{-8.4}$ (34) $\text{PLR} = \frac{b_i}{1.4}^{0.19}$ (35)	$N_q$ = bearing capacity factor $\sigma'_v$ = vertical effective stress PLR = plug length ratio $b_i$ = interior pile diameter (m)

### Static Axial Resistance Design Method Combinations

The resistance factor calibration was performed considering the load test data set by site condition: Cohesive, Cohesionless, Mixed, and Variable Side combinations. The majority of test sites, including uniform Cohesive and Cohesionless sites, have some combination of cohesive and cohesionless soil. Therefore, a combination of cohesive and cohesionless side resistance methods is required to estimate the pile nominal resistance. Some methods, such as API and Brown, include equations for both cohesive and cohesionless soil, and these combinations were used. However, other methods do not necessarily address all soil conditions. Therefore, the methods were combined, as shown in table 9.

**Table 9. Side resistance static design method combinations for cohesive and cohesionless sites.**

Cohesive Sites			Cohesionless Sites		
$\geq 70$ percent (primary) Cohesive side	+	$\leq 30$ percent Cohesionless side	$\geq 70$ percent (primary) Cohesionless side	+	$\leq 30$ percent Cohesive side
Tomlinson $\alpha$ -method	+	Nordlund method	Nordlund method	+	Tomlinson $\alpha$ -method
API $\alpha$ -method	+	API $\beta$ -method	API $\beta$ -method	+	API $\alpha$ -method
Saye method	+	Gudavalli method	Gudavalli method	+	Saye method
Brown method	+	Brown method	Brown method	+	Brown method

At uniform Cohesive and Cohesionless sites, the pile resistance is controlled by the primary soil type and the method combination is less significant. However, the side resistance method combination is significant for the Mixed and Variable Side cases. Therefore, the corresponding calculated resistance factor calibrations are specific to the side resistance method combinations.

### Side and Base Resistance Design Conditions

The development of pile plugging and its impact on base resistance is a source of uncertainty when evaluating LDOEP static resistance. If a pile plugs during driving, base resistance may act over the entire pile cross-sectional area. However, if a pile plug does not develop, base resistance may act only on the annular pile area. In this case, side resistance may develop on the internal pile surface area.

In order to evaluate potential pile plugging impacts on bearing resistance analysis, four alternate side and base resistance design conditions were considered. The combinations reflect common design practices and are intended to bracket the potential range of design values. The side and base resistance design conditions include:

- Plugged. Base resistance acts on the entire pile cross-sectional area. Side resistance develops on the pile exterior only.
- Unplugged with Interior Side Resistance. Base resistance acts on the annular pile end area only. Side resistance develops on the interior and exterior pile surfaces. Interior side resistance is assumed to be equal to the exterior pile side resistance.
- Unplugged Neglecting Interior Side Resistance. Base resistance acts on the annular pile end area only. Side resistance is assumed to act on the pile exterior only. Interior pile side resistance is neglected.
- Minimum of Plugged and Unplugged with Interior Side Resistance. Consistent with API guidelines and common engineering practice, total pile resistance is computed as the minimum of Plugged and Unplugged with Interior Side Resistance.

## Calculation Approach

The static axial pile resistance evaluation was performed considering the total pile resistance. All combinations of static side and base resistance design methods and design conditions were computed to estimate the predicted pile nominal resistance. The combined side and base resistance estimates were compared to the measured nominal resistance obtained from the load test failure criteria.

## RESISTANCE FACTOR CALIBRATION

Geotechnical resistance factors were developed based on reliability theory that evaluates the likelihood of failure where the applied loads are greater than the available resistance. The resistance factor calibration treats uncertainties in load and resistance separately to enable efficient design for a uniform level of acceptable risk (Studelein et al. 2012). The objective of calibration is to estimate the combination of load and resistance factors such that failure occurs for a prescribed probability of failure.

This analysis utilized three methods for resistance factor calibration: First Order Second Moment (FOSM), First Order Reliability Method (FORM), and the Monte Carlo method. Paikowsky (2004) recommended the target reliability in resistance factor calibration account for pile performance on the basis of redundancy. Resistance factors were developed for a target reliability index value  $\beta = 2.33$ , corresponding to a probability of failure  $p_f$  of 1 percent for redundant foundations. Resistance factors were also developed for a target reliability index of  $\beta = 3.0$ , corresponding to a probability of failure  $p_f$  of 0.1 percent for nonredundant foundations.

## Calibration Input

Resistance factor calibration requires statistical characterization of load and resistance. Load factors were based on AASHTO Strength Limit I with the assumed load statistics as follows:

- $\gamma_D$  = dead load factor = 1.25.
- $\gamma_L$  = live load factor = 1.75.
- $\lambda_D$  = mean dead load bias = 1.08.
- $\lambda_L$  = mean live load bias = 1.15.
- $COV_D$  = dead load coefficient of variation = 0.128.
- $COV_L$  = live load coefficient of variation = 0.18.

This analysis considered a dead load to live load ratio ( $Q_D/Q_L$ ) of 3.0, consistent with Allen (2005). The dead load to live load ratio is dependent on bridge span length. However, McVay et al. (2002) found that the calibrated resistance factor is generally insensitive to the dead load to live load ratio greater than 3.0.

Statistical characterization of the static design method mean resistance bias ( $\lambda_R$ ) and coefficient of variation ( $COV_R$ ) were based on the estimated pile nominal resistances predicted for each design method, side and base resistance combination, and failure criteria.

## FOSM

The FOSM method allows for direct computation of resistance factors based on the static design method mean resistance bias ( $\lambda_R$ ) and coefficient of variation ( $COV_R$ ) and the AASHTO load factors and statistics. The calculation is based on Paikowsky (2004) with Styler's (2006) correction for coefficient of variation of load as follows:

$$\phi = \frac{\lambda_R \left( \gamma_D \frac{Q_D}{Q_L} + \gamma_L \right) \sqrt{\left[ \frac{1 + COV_Q^2}{1 + COV_R^2} \right]}}{\left( \lambda_D \frac{Q_D}{Q_L} + \lambda_L \right) \exp \left\{ \beta \sqrt{\ln[(1 + COV_R^2)(1 + COV_Q^2)]} \right\}} \quad (36)$$

$$COV_Q^2 = \frac{\left( \frac{Q_D}{Q_L} \lambda_D COV_D \right)^2 (\lambda_L COV_L)^2}{\left( \frac{Q_D}{Q_L} \lambda_D COV_D \right)^2 + 2 \frac{Q_D}{Q_L} \lambda_D \lambda_L + \lambda_L^2} \quad (37)$$

## FORM

Resistance factor calibration using FORM, as developed by Hasofer and Lind (1974), is based on reliability theory where the limit state  $g(x)$  is defined as:

$$g = \phi R - \gamma_L Q_L - \gamma_D Q_D \quad (38)$$

In the process, loads  $Q_L$  and  $Q_D$  and resistance  $R$  are treated as random variables, and failure is defined when the limit state is less than zero.

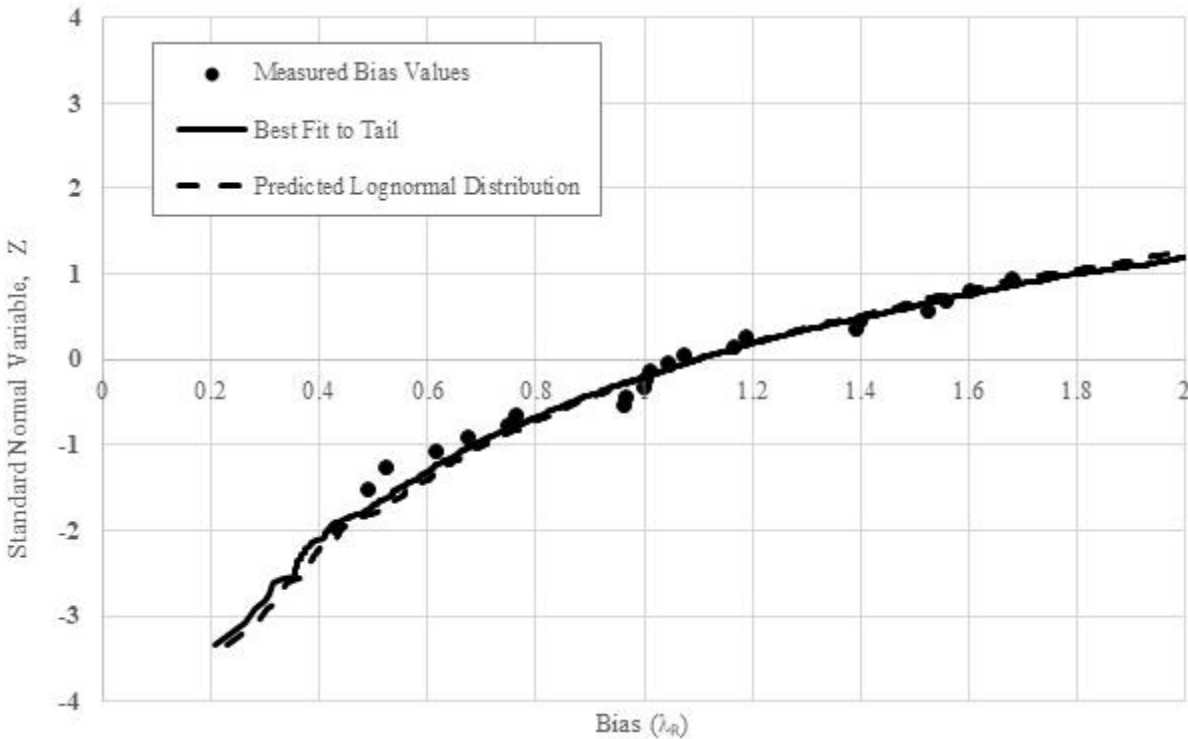
FORM uses an iterative calculation approach. The method determines a unique reliability index ( $\beta$ ) for a given resistance factor ( $\phi$ ) as the minimum distance between the origin and a point on a surface that represents the limit state. Iteratively, the limit state is evaluated at points  $R$ ,  $Q_L$ , and  $Q_D$  as functions of their standard normal variates until stable  $R$ ,  $Q_L$ , and  $Q_D$  points are achieved. The stable points correspond to the unique  $\beta$  for the given resistance factor  $\phi$ .

The FORM method assumes the load and resistance have lognormal distributions. Lognormal statistics are converted to equivalent normal statistics using the log of the resistance bias. The analysis considered a stability tolerance of  $10^{-7}$  with 9 significant figures.

## Monte Carlo

The Monte Carlo approach, as described by Allen et al. (2005), assesses random variables that contribute to the uncertainty in predicted loads and resistances in the limit state function expressed in equation 38. The method utilizes a random number generator to extrapolate the cumulative distribution function (CDF) values for each random variable. Extrapolation of the CDF enables calculation of the reliability index ( $\beta$ ), when there would otherwise be insufficient load and resistance data to reliably estimate  $\beta$ . The CDF of load is characterized by the mean, standard deviation, and an assumed lognormal distribution.

The CDF of the estimated pile nominal resistance bias was computed for combinations of failure criteria, static design method, and side and base condition with sufficiently sized data sets. A sample CDF is presented in figure 8 with the predicted lognormal distribution. As described by Allen et al. (2005), the left side of the resistance distribution, or the “tail,” controls the probability of failure. In this tail zone, where the bias is less than 1.0, the predicted resistance is less than the measured resistance, and potential failure may occur. Allen et al. (2005) recommend fitting the tail such that the curve is at or slightly to the left of the actual data for a more conservative resistance estimate. The “best fit to tail” line is shown in figure 8.



Source: FHWA.

**Figure 8. Graph. Cumulative distribution function of resistance bias values for sample results (Cohesionless site, Max Load failure criterion, Gudavalli side and base resistance, Plugged condition).**

Utilizing the CDFs of the load and resistance, the random number generator determines trial values of  $R$ ,  $Q_L$ , and  $Q_D$  for a selected resistance factor  $\phi$  and computes the limit state function  $g(x)$  in equation 38. Probability of failure is determined for the number of cases in which:

$$p_f = \frac{\text{count}(g \leq 0)}{N} \quad (39)$$

where  $N$  is equal to 50,000 trials for this analysis. Using the inverse of the standard normal cumulative distribution function  $\Phi$ , the reliability index of the selected resistance factor is computed as:

$$\beta = \Phi^{-1}(p_f) \quad (40)$$

The process is repeated for multiple resistance factors  $\phi$  to achieve the target reliability index  $\beta$ .

As noted above, the CDF of the estimated pile nominal resistance bias was computed only for sufficiently sized data sets to allow for reasonable characterization of the data. For this effort, the minimum data set size was set to 20. Based on this minimum requirement, the CDF was computed and subsequent Monte Carlo resistance factor calibrations were performed for the Max Load failure criterion with the Cohesionless and Mixed data sets. There was insufficient data with the Cohesive data set and other failure criteria for the calibration.

### **Data Filtering**

The resistance factor calibration performed in NCHRP Report 507 used a filtered data set that excluded data that were more than two standard deviations from the mean to assess the resistance bias statistical parameters (Paikowsky 2004). Allen et al. (2005) discuss that the removal of outliers may be justified so the statistical parameters are not skewed by a few data points that do not appear to be a part of the data set. Typical reasons to remove outliers include:

- Different failure criterion.
- Different measurement techniques.
- Data that are affected by regional factors.
- Data from a source that may be suspect.

Allen et al. (2005) further discuss that the removal of outliers is subjective and must be performed cautiously. The authors do not recommend the removal of outliers not meeting the above criteria for the cumulative distribution function fitting in the Monte Carlo calibration. The removal of data in the tails simply to obtain a better fit may lead to significant errors in the resistance factor calibration.

For this analysis, the Monte Carlo cumulative distribution function fitting process included all data points. In general, the outlier criteria by Allen et al. (2005) were considered not applicable to the selected load test data set or were already applied in the data set evaluation. The FORM and FOSM resistance factor calibration was performed using both the unfiltered data set and a filtered data with removal of outliers exceeding  $\pm$  two standard deviations from the mean.

## CHAPTER 4. LDOEP RESISTANCE FACTOR CALIBRATION RESULTS

### NOMINAL PILE RESISTANCE

LDOEP nominal pile resistance was computed for the load test data set using the design methods and side and base resistance combinations described in chapter 3. The predicted nominal pile resistance was then compared to the measured load test nominal resistance to evaluate the accuracy of the prediction for the unfiltered and filtered data sets, as described in this chapter. Additional information can be found in appendix B.

### RESISTANCE FACTOR COMBINATIONS

Results of the nominal pile resistance predictions and measured values determined from the load test failure criteria are used to compute LDOEP-specific resistance factors for the load test data set. The resistance factor calibration encompasses the numerous combinations of data groups, failure criteria, design methods, side and base combinations, and target reliability described herein to result in over 6,000 different resistance factor values. Table 10 provides a listing of the multiple analysis components and combinations considered in the resistance factor calibration.

The following sections summarize and discuss the results of the resistance factor calibration. Due to the volume of resistance factors computed in the analysis, only select values are included in this report.

### FOSM AND FORM RESISTANCE FACTORS

Table 11 through table 25 present FORM resistance factors for all data groups, failure criteria, design methods, and side and base resistance combinations for filtered data with a target reliability index  $\beta = 2.33$ , corresponding to redundant foundations. The tables include the summary statistics of the mean resistance bias, along with the individual resistance factors ( $\phi$ ) and efficiency ( $\phi/\lambda$ ) values for FORM methods.

**Table 10. Summary of analysis components considered in resistance factor calibration.**

<b>Analysis Component</b>	<b>Analysis Subcomponents</b>
Five data groups	Cohesive
	Cohesionless
	Mixed
	Variable Side + Cohesive Base
	Variable Side + Cohesionless Base
Three failure criteria	Modified Davisson
	5 Percent Diameter
	Max Load
Four side resistance methods	Tomlinson $\alpha$ -method + Nordlund
	API
	Saye + Gudavalli
	Brown
Five base resistance methods	Total Stress Approach (AASHTO/API) ( <i>Cohesive base only</i> )
	Bearing Capacity Approach (API) ( <i>Cohesionless base only</i> )
	Nordlund ( <i>Cohesionless base only</i> )
	Gudavalli ( <i>Cohesionless base only</i> )
	Brown
Four side and base combinations	Plugged
	Unplugged with Interior Side Resistance
	Unplugged Neglecting Interior Side Resistance
	Minimum of Plugged, Unplugged with Interior Side Resistance
Two target reliability indices	$\beta = 2.33$ for redundant foundations
	$\beta = 3.0$ for nonredundant foundations
Three resistance factor methods	FOSM
	FORM
	Monte Carlo ( <i>only Cohesionless and Mixed data sets with Max Load failure criteria</i> )
Two data versions	Unfiltered data
	Filtered data

Table 11. FORM resistance factors for Cohesive sites—Modified Davisson failure criterion with Filtered data and target reliability  $\beta = 2.33$ .

Cohesive Failure Criterion: Modified Davisson Filtered Data Beta = 2.33		Side Method: Tomlinson $\alpha$ + Nordlund				Side Method: API				Side Method: Saye + Gudavalli				Side Method: Brown			
		Base Method				Base Method				Base Method				Base Method			
		AASHTO/API	Nordlund	Gudavalli	Brown	AASHTO/API	Nordlund	Gudavalli	Brown	AASHTO/API	Nordlund	Gudavalli	Brown	AASHTO/API	Nordlund	Gudavalli	Brown
Plugged	Mean	0.86	—	—	0.66	0.79	—	—	0.62	0.84	—	—	0.67	0.82	—	—	0.67
	COV	0.19	—	—	0.30	0.24	—	—	0.32	0.24	—	—	0.37	0.24	—	—	0.41
	Count	10	—	—	11	10	—	—	11	10	—	—	11	10	—	—	11
	<b>FORM Resistance Factor, <math>\phi</math></b>	<b>0.64</b>	—	—	<b>0.38</b>	<b>0.53</b>	—	—	<b>0.34</b>	<b>0.56</b>	—	—	<b>0.32</b>	<b>0.55</b>	—	—	<b>0.30</b>
	FORM Efficiency, $\phi/\lambda$	0.75	—	—	0.58	0.67	—	—	0.55	0.67	—	—	0.49	0.68	—	—	0.45
Unplugged with Interior Side Resistance	Mean	0.51	—	—	0.50	0.47	—	—	0.46	0.48	—	—	0.47	0.47	—	—	0.46
	COV	0.28	—	—	0.26	0.34	—	—	0.31	0.24	—	—	0.24	0.27	—	—	0.26
	Count	10	—	—	10	10	—	—	10	10	—	—	10	10	—	—	10
	<b>FORM Resistance Factor, <math>\phi</math></b>	<b>0.31</b>	—	—	<b>0.32</b>	<b>0.25</b>	—	—	<b>0.26</b>	<b>0.32</b>	—	—	<b>0.31</b>	<b>0.29</b>	—	—	<b>0.29</b>
	FORM Efficiency, $\phi/\lambda$	0.60	—	—	0.64	0.53	—	—	0.57	0.67	—	—	0.67	0.62	—	—	0.64
Unplugged Neglecting Interior Side Resistance	Mean	0.99	—	—	0.95	0.91	—	—	0.87	0.93	—	—	0.91	0.92	—	—	0.88
	COV	0.27	—	—	0.23	0.33	—	—	0.28	0.24	—	—	0.25	0.27	—	—	0.25
	Count	10	—	—	10	10	—	—	10	10	—	—	10	10	—	—	10
	<b>FORM Resistance Factor, <math>\phi</math></b>	<b>0.62</b>	—	—	<b>0.66</b>	<b>0.49</b>	—	—	<b>0.53</b>	<b>0.63</b>	—	—	<b>0.60</b>	<b>0.58</b>	—	—	<b>0.57</b>
	FORM Efficiency, $\phi/\lambda$	0.62	—	—	0.69	0.54	—	—	0.61	0.67	—	—	0.66	0.62	—	—	0.65
Minimum of Plugged and Unplugged with Interior Side Resistance	Mean	0.86	—	—	0.73	0.79	—	—	0.68	0.84	—	—	0.75	0.82	—	—	0.71
	COV	0.19	—	—	0.20	0.24	—	—	0.25	0.24	—	—	0.32	0.24	—	—	0.32
	Count	10	—	—	10	10	—	—	10	10	—	—	11	10	—	—	11
	<b>FORM Resistance Factor, <math>\phi</math></b>	<b>0.64</b>	—	—	<b>0.53</b>	<b>0.53</b>	—	—	<b>0.45</b>	<b>0.56</b>	—	—	<b>0.41</b>	<b>0.55</b>	—	—	<b>0.39</b>
	FORM Efficiency, $\phi/\lambda$	0.75	—	—	0.73	0.67	—	—	0.66	0.67	—	—	0.55	0.68	—	—	0.55

—No data.

Note: Table formatted for 11x17 printing.

Table 12. FORM resistance factors for Cohesive sites—5 Percent Diameter failure criterion with Filtered data and target reliability  $\beta = 2.33$ .

Cohesive Failure Criterion: 5 Percent Diameter Filtered Data Beta = 2.33		Side Method: Tomlinson $\alpha$ + Nordlund				Side Method: API				Side Method: Saye + Gudavalli				Side Method: Brown			
		Base Method				Base Method				Base Method				Base Method			
		AASHTO/API	Nordlund	Gudavalli	Brown	AASHTO/API	Nordlund	Gudavalli	Brown	AASHTO/API	Nordlund	Gudavalli	Brown	AASHTO/API	Nordlund	Gudavalli	Brown
Plugged	Mean	0.83	—	—	0.70	0.80	—	—	0.65	0.80	—	—	0.70	0.81	—	—	0.72
	COV	0.14	—	—	0.26	0.23	—	—	0.29	0.19	—	—	0.33	0.24	—	—	0.36
	Count	9	—	—	10	10	—	—	10	9	—	—	10	9	—	—	10
	<b>FORM Resistance Factor, <math>\phi</math></b>	<b>0.69</b>	—	—	<b>0.45</b>	<b>0.54</b>	—	—	<b>0.39</b>	<b>0.60</b>	—	—	<b>0.38</b>	<b>0.54</b>	—	—	<b>0.36</b>
	FORM Efficiency, $\phi/\lambda$	0.84	—	—	0.64	0.68	—	—	0.60	0.75	—	—	0.54	0.67	—	—	0.50
Unplugged with Interior Side Resistance	Mean	0.48	—	—	0.51	0.44	—	—	0.46	0.46	—	—	0.45	0.47	—	—	0.46
	COV	0.23	—	—	0.25	0.27	—	—	0.30	0.18	—	—	0.18	0.28	—	—	0.27
	Count	9	—	—	10	9	—	—	10	9	—	—	9	9	—	—	9
	<b>FORM Resistance Factor, <math>\phi</math></b>	<b>0.33</b>	—	—	<b>0.33</b>	<b>0.27</b>	—	—	<b>0.27</b>	<b>0.35</b>	—	—	<b>0.35</b>	<b>0.29</b>	—	—	<b>0.29</b>
	FORM Efficiency, $\phi/\lambda$	0.69	—	—	0.65	0.63	—	—	0.58	0.77	—	—	0.77	0.61	—	—	0.62
Unplugged Neglecting Interior Side Resistance	Mean	0.94	—	—	0.96	0.85	—	—	0.88	0.89	—	—	0.86	0.92	—	—	0.89
	COV	0.22	—	—	0.22	0.26	—	—	0.27	0.18	—	—	0.18	0.28	—	—	0.26
	Count	9	—	—	10	9	—	—	10	9	—	—	9	9	—	—	9
	<b>FORM Resistance Factor, <math>\phi</math></b>	<b>0.67</b>	—	—	<b>0.67</b>	<b>0.55</b>	—	—	<b>0.54</b>	<b>0.69</b>	—	—	<b>0.66</b>	<b>0.56</b>	—	—	<b>0.57</b>
	FORM Efficiency, $\phi/\lambda$	0.71	—	—	0.70	0.65	—	—	0.62	0.77	—	—	0.76	0.61	—	—	0.64
Minimum of Plugged and Unplugged with Interior Side Resistance	Mean	0.83	—	—	0.74	0.80	—	—	0.68	0.80	—	—	0.72	0.81	—	—	0.74
	COV	0.14	—	—	0.20	0.23	—	—	0.24	0.19	—	—	0.30	0.24	—	—	0.31
	Count	9	—	—	10	10	—	—	10	9	—	—	10	9	—	—	10
	<b>FORM Resistance Factor, <math>\phi</math></b>	<b>0.69</b>	—	—	<b>0.54</b>	<b>0.54</b>	—	—	<b>0.46</b>	<b>0.60</b>	—	—	<b>0.42</b>	<b>0.54</b>	—	—	<b>0.42</b>
	FORM Efficiency, $\phi/\lambda$	0.84	—	—	0.73	0.68	—	—	0.67	0.75	—	—	0.58	0.67	—	—	0.56

—No data.

Note: Table formatted for 11x17 printing.

Table 13. FORM resistance factors for Cohesive sites—Max Load failure criterion with Filtered data and target reliability  $\beta = 2.33$

Cohesive Failure Criterion: Max Load Filtered Data Beta = 2.33		Side Method: Tomlinson $\alpha$ + Nordlund				Side Method: API				Side Method: Saye + Gudavalli				Side Method: Brown			
		Base Method				Base Method				Base Method				Base Method			
		AASHTO/API	Nordlund	Gudavalli	Brown	AASHTO/API	Nordlund	Gudavalli	Brown	AASHTO/API	Nordlund	Gudavalli	Brown	AASHTO/API	Nordlund	Gudavalli	Brown
Plugged	Mean	0.91	—	—	0.64	0.84	—	—	0.60	0.89	—	—	0.61	0.80	—	—	0.63
	COV	0.18	—	—	0.31	0.21	—	—	0.32	0.20	—	—	0.33	0.21	—	—	0.43
	Count	13	—	—	14	13	—	—	14	13	—	—	13	13	—	—	14
	FORM Resistance Factor, $\phi$	<b>0.69</b>	—	—	<b>0.36</b>	<b>0.60</b>	—	—	<b>0.33</b>	<b>0.65</b>	—	—	<b>0.33</b>	<b>0.58</b>	—	—	<b>0.27</b>
	FORM Efficiency, $\phi/\lambda$	0.76	—	—	0.56	0.71	—	—	0.56	0.73	—	—	0.54	0.72	—	—	0.42
Unplugged with Interior Side Resistance	Mean	0.55	—	—	0.53	0.50	—	—	0.49	0.52	—	—	0.51	0.47	—	—	0.45
	COV	0.26	—	—	0.24	0.30	—	—	0.28	0.21	—	—	0.21	0.25	—	—	0.23
	Count	13	—	—	13	13	—	—	13	13	—	—	13	13	—	—	13
	FORM Resistance Factor, $\phi$	<b>0.35</b>	—	—	<b>0.35</b>	<b>0.29</b>	—	—	<b>0.30</b>	<b>0.37</b>	—	—	<b>0.36</b>	<b>0.31</b>	—	—	<b>0.31</b>
	FORM Efficiency, $\phi/\lambda$	0.64	—	—	0.67	0.58	—	—	0.61	0.71	—	—	0.71	0.66	—	—	0.68
Unplugged Neglecting Interior Side Resistance	Mean	1.06	—	—	1.01	0.98	—	—	0.93	1.01	—	—	0.97	0.91	—	—	0.87
	COV	0.25	—	—	0.22	0.29	—	—	0.25	0.21	—	—	0.21	0.24	—	—	0.23
	Count	13	—	—	13	13	—	—	13	13	—	—	13	13	—	—	13
	FORM Resistance Factor, $\phi$	<b>0.69</b>	—	—	<b>0.71</b>	<b>0.58</b>	—	—	<b>0.60</b>	<b>0.72</b>	—	—	<b>0.69</b>	<b>0.61</b>	—	—	<b>0.60</b>
	FORM Efficiency, $\phi/\lambda$	0.65	—	—	0.71	0.59	—	—	0.65	0.71	—	—	0.72	0.67	—	—	0.69
Minimum of Plugged and Unplugged with Interior Side Resistance	Mean	0.91	—	—	0.71	0.84	—	—	0.67	0.89	—	—	0.73	0.80	—	—	0.63
	COV	0.18	—	—	0.21	0.21	—	—	0.23	0.20	—	—	0.30	0.21	—	—	0.33
	Count	13	—	—	13	13	—	—	13	13	—	—	14	13	—	—	13
	FORM Resistance Factor, $\phi$	<b>0.69</b>	—	—	<b>0.51</b>	<b>0.60</b>	—	—	<b>0.45</b>	<b>0.65</b>	—	—	<b>0.43</b>	<b>0.58</b>	—	—	<b>0.35</b>
	FORM Efficiency, $\phi/\lambda$	0.76	—	—	0.71	0.71	—	—	0.68	0.73	—	—	0.59	0.72	—	—	0.55

—No data.

Note: Table formatted for 11x17 printing.

Table 14. FORM resistance factors for Cohesionless sites—Modified Davison failure criterion with Filtered data and target reliability  $\beta = 2.33$ .

Cohesionless Failure Criterion: Modified Davison Filtered Data Beta = 2.33		Side Method: Tomlinson $\alpha$ + Nordlund				Side Method: API				Side Method: Saye + Gudavalli				Side Method: Brown			
		Base Method				Base Method				Base Method				Base Method			
		AASHTO/API	Nordlund	Gudavalli	Brown	AASHTO/API	Nordlund	Gudavalli	Brown	AASHTO/API	Nordlund	Gudavalli	Brown	AASHTO/API	Nordlund	Gudavalli	Brown
Plugged	Mean	0.51	0.48	0.55	0.41	0.68	0.70	0.86	0.53	0.72	0.86	1.04	0.62	0.62	0.63	0.82	0.54
	COV	0.51	0.49	0.40	0.48	0.50	0.64	0.46	0.52	0.44	0.66	0.45	0.52	0.45	0.59	0.43	0.51
	Count	15	14	14	14	15	14	15	14	14	14	14	14	15	14	15	15
	<b>FORM Resistance Factor, <math>\phi</math></b>	<b>0.18</b>	<b>0.18</b>	<b>0.25</b>	<b>0.16</b>	<b>0.24</b>	<b>0.19</b>	<b>0.35</b>	<b>0.19</b>	<b>0.31</b>	<b>0.22</b>	<b>0.42</b>	<b>0.21</b>	<b>0.25</b>	<b>0.19</b>	<b>0.35</b>	<b>0.20</b>
	FORM Efficiency, $\phi/\lambda$	0.36	0.37	0.46	0.39	0.36	0.27	0.40	0.35	0.42	0.26	0.41	0.34	0.41	0.30	0.42	0.36
Unplugged with Interior Side Resistance	Mean	0.43	0.42	0.43	0.42	0.75	0.70	0.72	0.68	1.13	1.12	1.11	1.08	0.71	0.70	0.69	0.69
	COV	0.50	0.48	0.48	0.48	0.45	0.42	0.42	0.41	0.37	0.37	0.35	0.38	0.33	0.33	0.41	0.32
	Count	14	14	14	14	15	14	14	14	15	15	14	15	14	14	15	14
	<b>FORM Resistance Factor, <math>\phi</math></b>	<b>0.16</b>	<b>0.16</b>	<b>0.16</b>	<b>0.16</b>	<b>0.31</b>	<b>0.30</b>	<b>0.31</b>	<b>0.30</b>	<b>0.56</b>	<b>0.55</b>	<b>0.57</b>	<b>0.52</b>	<b>0.39</b>	<b>0.38</b>	<b>0.31</b>	<b>0.39</b>
	FORM Efficiency, $\phi/\lambda$	0.37	0.38	0.38	0.38	0.41	0.43	0.44	0.44	0.50	0.49	0.51	0.48	0.55	0.55	0.45	0.56
Unplugged Neglecting Interior Side Resistance	Mean	0.80	0.79	0.81	0.76	1.29	1.28	1.33	1.21	2.00	2.02	2.04	1.78	1.31	1.22	1.30	1.24
	COV	0.49	0.47	0.47	0.47	0.41	0.42	0.41	0.41	0.36	0.39	0.37	0.36	0.32	0.40	0.41	0.31
	Count	14	14	14	14	14	14	14	14	15	15	14	14	14	15	15	14
	<b>FORM Resistance Factor, <math>\phi</math></b>	<b>0.30</b>	<b>0.31</b>	<b>0.31</b>	<b>0.30</b>	<b>0.58</b>	<b>0.55</b>	<b>0.60</b>	<b>0.55</b>	<b>1.02</b>	<b>0.96</b>	<b>1.02</b>	<b>0.90</b>	<b>0.74</b>	<b>0.56</b>	<b>0.58</b>	<b>0.71</b>
	FORM Efficiency, $\phi/\lambda$	0.37	0.39	0.39	0.39	0.45	0.43	0.45	0.45	0.51	0.47	0.50	0.50	0.56	0.45	0.45	0.57
Minimum of Plugged and Unplugged with Interior Side Resistance	Mean	0.52	0.52	0.56	0.46	0.79	0.80	0.89	0.69	1.15	1.16	1.21	1.09	0.73	0.73	0.82	0.69
	COV	0.49	0.46	0.40	0.47	0.47	0.52	0.45	0.41	0.36	0.45	0.41	0.37	0.41	0.46	0.43	0.40
	Count	15	14	14	14	15	14	15	14	15	14	15	15	15	14	15	15
	<b>FORM Resistance Factor, <math>\phi</math></b>	<b>0.19</b>	<b>0.21</b>	<b>0.26</b>	<b>0.18</b>	<b>0.31</b>	<b>0.28</b>	<b>0.37</b>	<b>0.31</b>	<b>0.57</b>	<b>0.47</b>	<b>0.54</b>	<b>0.54</b>	<b>0.33</b>	<b>0.29</b>	<b>0.35</b>	<b>0.32</b>
	FORM Efficiency, $\phi/\lambda$	0.37	0.40	0.46	0.40	0.39	0.35	0.41	0.44	0.50	0.40	0.45	0.49	0.45	0.40	0.43	0.46

Note: Table formatted for 11x17 printing.

Table 15. FORM resistance factors for Cohesionless sites—5 Percent Diameter failure criterion with Filtered data and target reliability  $\beta = 2.33$

Cohesionless Failure Criterion: 5 Percent Diameter Filtered Data Beta = 2.33		Side Method: Tomlinson $\alpha$ + Nordlund				Side Method: API				Side Method: Saye + Gudavalli				Side Method: Brown			
		Base Method				Base Method				Base Method				Base Method			
		AASHTO/API	Nordlund	Gudavalli	Brown	AASHTO/API	Nordlund	Gudavalli	Brown	AASHTO/API	Nordlund	Gudavalli	Brown	AASHTO/API	Nordlund	Gudavalli	Brown
Plugged	Mean	0.52	0.50	0.57	0.45	0.64	0.66	0.76	0.63	0.74	0.81	0.88	0.72	0.58	0.65	0.76	0.53
	COV	0.47	0.51	0.41	0.47	0.47	0.56	0.43	0.54	0.43	0.54	0.36	0.52	0.42	0.55	0.44	0.45
	Count	16	15	16	15	15	15	15	16	15	15	14	16	15	16	16	15
	<b>FORM Resistance Factor, <math>\phi</math></b>	<b>0.20</b>	<b>0.18</b>	<b>0.26</b>	<b>0.18</b>	<b>0.25</b>	<b>0.21</b>	<b>0.32</b>	<b>0.21</b>	<b>0.32</b>	<b>0.27</b>	<b>0.45</b>	<b>0.25</b>	<b>0.26</b>	<b>0.21</b>	<b>0.32</b>	<b>0.22</b>
	FORM Efficiency, $\phi/\lambda$	0.39	0.36	0.45	0.40	0.39	0.32	0.43	0.34	0.43	0.33	0.51	0.34	0.44	0.32	0.42	0.41
Unplugged with Interior Side Resistance	Mean	0.46	0.43	0.46	0.42	0.72	0.72	0.73	0.71	1.02	1.07	1.04	1.05	0.63	0.65	0.64	0.62
	COV	0.47	0.44	0.47	0.44	0.45	0.46	0.44	0.45	0.36	0.38	0.36	0.39	0.41	0.33	0.42	0.40
	Count	16	15	16	15	16	16	16	16	15	16	15	16	16	15	16	16
	<b>FORM Resistance Factor, <math>\phi</math></b>	<b>0.18</b>	<b>0.18</b>	<b>0.18</b>	<b>0.18</b>	<b>0.30</b>	<b>0.29</b>	<b>0.30</b>	<b>0.29</b>	<b>0.52</b>	<b>0.51</b>	<b>0.52</b>	<b>0.49</b>	<b>0.29</b>	<b>0.36</b>	<b>0.28</b>	<b>0.28</b>
	FORM Efficiency, $\phi/\lambda$	0.39	0.42	0.39	0.42	0.41	0.40	0.41	0.41	0.51	0.48	0.50	0.47	0.45	0.54	0.44	0.46
Unplugged Neglecting Interior Side Resistance	Mean	0.86	0.80	0.81	0.78	1.33	1.23	1.35	1.20	1.92	1.81	1.91	1.74	1.17	1.19	1.20	1.13
	COV	0.47	0.43	0.43	0.43	0.44	0.43	0.44	0.42	0.37	0.36	0.38	0.36	0.39	0.32	0.42	0.39
	Count	16	15	15	15	16	15	16	15	16	15	15	15	16	15	16	16
	<b>FORM Resistance Factor, <math>\phi</math></b>	<b>0.34</b>	<b>0.34</b>	<b>0.35</b>	<b>0.33</b>	<b>0.56</b>	<b>0.53</b>	<b>0.57</b>	<b>0.53</b>	<b>0.94</b>	<b>0.92</b>	<b>0.93</b>	<b>0.87</b>	<b>0.54</b>	<b>0.66</b>	<b>0.53</b>	<b>0.53</b>
	FORM Efficiency, $\phi/\lambda$	0.39	0.42	0.43	0.43	0.42	0.43	0.42	0.44	0.49	0.51	0.49	0.50	0.46	0.56	0.44	0.47
Minimum of Plugged and Unplugged with Interior Side Resistance	Mean	0.53	0.53	0.58	0.49	0.77	0.75	0.83	0.73	1.11	1.09	0.99	1.06	0.70	0.73	0.76	0.67
	COV	0.45	0.47	0.41	0.45	0.47	0.45	0.45	0.44	0.39	0.39	0.32	0.38	0.43	0.44	0.43	0.41
	Count	16	15	16	15	16	15	16	16	16	15	14	16	16	16	16	16
	<b>FORM Resistance Factor, <math>\phi</math></b>	<b>0.21</b>	<b>0.21</b>	<b>0.26</b>	<b>0.20</b>	<b>0.30</b>	<b>0.31</b>	<b>0.34</b>	<b>0.30</b>	<b>0.52</b>	<b>0.51</b>	<b>0.55</b>	<b>0.51</b>	<b>0.30</b>	<b>0.31</b>	<b>0.32</b>	<b>0.30</b>
	FORM Efficiency, $\phi/\lambda$	0.41	0.39	0.45	0.41	0.39	0.41	0.41	0.42	0.47	0.46	0.56	0.48	0.43	0.42	0.42	0.45

Note: Table formatted for 11x17 printing.

Table 16. FORM resistance factors for Cohesionless sites—Max Load failure criterion with Filtered data and target reliability  $\beta = 2.33$

Cohesionless Failure Criterion: Max Load Filtered Data Beta = 2.33		Side Method: Tomlinson $\alpha$ + Nordlund				Side Method: API				Side Method: Saye + Gudavalli				Side Method: Brown			
		Base Method				Base Method				Base Method				Base Method			
		AASHTO/API	Nordlund	Gudavalli	Brown	AASHTO/API	Nordlund	Gudavalli	Brown	AASHTO/API	Nordlund	Gudavalli	Brown	AASHTO/API	Nordlund	Gudavalli	Brown
Plugged	Mean	0.54	0.52	0.61	0.50	0.67	0.71	0.89	0.64	0.81	0.88	1.18	0.75	0.63	0.64	0.87	0.56
	COV	0.57	0.58	0.49	0.61	0.49	0.64	0.43	0.54	0.46	0.64	0.44	0.53	0.44	0.59	0.42	0.45
	Count	25	24	25	25	24	24	25	25	24	24	25	25	24	24	26	24
	<b>FORM Resistance Factor, <math>\phi</math></b>	<b>0.17</b>	<b>0.16</b>	<b>0.23</b>	<b>0.14</b>	<b>0.25</b>	<b>0.19</b>	<b>0.38</b>	<b>0.21</b>	<b>0.32</b>	<b>0.23</b>	<b>0.49</b>	<b>0.25</b>	<b>0.26</b>	<b>0.19</b>	<b>0.38</b>	<b>0.23</b>
	FORM Efficiency, $\phi/\lambda$	0.31	0.31	0.37	0.28	0.37	0.27	0.43	0.33	0.40	0.27	0.42	0.34	0.42	0.29	0.43	0.41
Unplugged with Interior Side Resistance	Mean	0.47	0.47	0.47	0.46	0.77	0.76	0.79	0.75	1.23	1.20	1.27	1.23	0.69	0.68	0.70	0.67
	COV	0.60	0.59	0.59	0.59	0.47	0.47	0.46	0.46	0.39	0.37	0.39	0.39	0.41	0.41	0.42	0.40
	Count	25	25	25	25	25	25	25	25	25	25	25	26	25	25	25	25
	<b>FORM Resistance Factor, <math>\phi</math></b>	<b>0.14</b>	<b>0.14</b>	<b>0.14</b>	<b>0.14</b>	<b>0.30</b>	<b>0.30</b>	<b>0.31</b>	<b>0.30</b>	<b>0.58</b>	<b>0.60</b>	<b>0.59</b>	<b>0.57</b>	<b>0.31</b>	<b>0.31</b>	<b>0.31</b>	<b>0.31</b>
	FORM Efficiency, $\phi/\lambda$	0.29	0.30	0.30	0.30	0.39	0.39	0.40	0.40	0.47	0.50	0.47	0.46	0.45	0.45	0.44	0.46
Unplugged Neglecting Interior Side Resistance	Mean	0.89	0.96	0.99	0.86	1.43	1.34	1.47	1.31	2.28	2.13	2.34	2.08	1.28	1.24	1.37	1.22
	COV	0.58	0.67	0.72	0.57	0.45	0.43	0.44	0.41	0.38	0.36	0.38	0.36	0.39	0.40	0.42	0.37
	Count	25	26	26	25	25	24	25	24	26	25	25	25	25	25	26	25
	<b>FORM Resistance Factor, <math>\phi</math></b>	<b>0.27</b>	<b>0.24</b>	<b>0.22</b>	<b>0.27</b>	<b>0.58</b>	<b>0.57</b>	<b>0.61</b>	<b>0.58</b>	<b>1.10</b>	<b>1.09</b>	<b>1.13</b>	<b>1.05</b>	<b>0.60</b>	<b>0.58</b>	<b>0.60</b>	<b>0.60</b>
	FORM Efficiency, $\phi/\lambda$	0.30	0.25	0.23	0.31	0.40	0.42	0.42	0.45	0.48	0.51	0.48	0.51	0.47	0.46	0.44	0.49
Minimum of Plugged and Unplugged with Interior Side Resistance	Mean	0.56	0.59	0.61	0.54	0.82	0.84	0.95	0.79	1.27	1.28	1.30	1.21	0.76	0.76	0.87	0.72
	COV	0.60	0.60	0.49	0.59	0.49	0.49	0.44	0.44	0.39	0.38	0.40	0.36	0.43	0.44	0.42	0.39
	Count	25	24	25	25	25	24	26	25	25	24	25	25	25	24	26	25
	<b>FORM Resistance Factor, <math>\phi</math></b>	<b>0.16</b>	<b>0.17</b>	<b>0.23</b>	<b>0.16</b>	<b>0.31</b>	<b>0.31</b>	<b>0.39</b>	<b>0.33</b>	<b>0.60</b>	<b>0.61</b>	<b>0.59</b>	<b>0.61</b>	<b>0.33</b>	<b>0.32</b>	<b>0.38</b>	<b>0.34</b>
	FORM Efficiency, $\phi/\lambda$	0.29	0.29	0.37	0.29	0.37	0.37	0.41	0.42	0.47	0.48	0.46	0.50	0.43	0.42	0.44	0.47

Note: Table formatted for 11x17 printing.

Table 17. FORM resistance factors for Mixed sites—Modified Davisson failure criterion with Filtered data and target reliability  $\beta = 2.33$ .

Mixed Failure Criterion: Modified Davisson Filtered Data Beta = 2.33		Side Method: Tomlinson $\alpha$ + Nordlund				Side Method: API				Side Method: Saye + Gudavalli				Side Method: Brown			
		Base Method				Base Method				Base Method				Base Method			
		AASHTO/API	Nordlund	Gudavalli	Brown	AASHTO/API	Nordlund	Gudavalli	Brown	AASHTO/API	Nordlund	Gudavalli	Brown	AASHTO/API	Nordlund	Gudavalli	Brown
Plugged	Mean	0.44	0.35	0.53	0.46	0.58	0.50	0.70	0.60	0.66	0.56	0.88	0.65	0.57	0.49	0.67	0.58
	COV	0.33	0.21	0.38	0.37	0.19	0.36	0.34	0.17	0.36	0.55	0.30	0.42	0.19	0.34	0.37	0.15
	Count	12	10	11	13	13	10	11	12	13	10	10	13	13	10	11	12
	<b>FORM Resistance Factor, <math>\phi</math></b>	<b>0.24</b>	<b>0.25</b>	<b>0.26</b>	<b>0.23</b>	<b>0.44</b>	<b>0.25</b>	<b>0.37</b>	<b>0.47</b>	<b>0.33</b>	<b>0.18</b>	<b>0.51</b>	<b>0.29</b>	<b>0.43</b>	<b>0.26</b>	<b>0.33</b>	<b>0.47</b>
	FORM Efficiency, $\phi/\lambda$	0.55	0.72	0.49	0.49	0.75	0.50	0.53	0.79	0.51	0.33	0.58	0.44	0.75	0.53	0.49	0.81
Unplugged with Interior Side Resistance	Mean	0.40	0.38	0.39	0.40	0.58	0.60	0.61	0.58	0.74	0.84	0.87	0.73	0.55	0.57	0.55	0.55
	COV	0.50	0.42	0.44	0.50	0.26	0.22	0.24	0.26	0.43	0.30	0.29	0.42	0.25	0.24	0.22	0.25
	Count	12	10	10	12	13	11	11	13	13	10	10	13	13	11	10	13
	<b>FORM Resistance Factor, <math>\phi</math></b>	<b>0.15</b>	<b>0.17</b>	<b>0.17</b>	<b>0.15</b>	<b>0.37</b>	<b>0.41</b>	<b>0.41</b>	<b>0.37</b>	<b>0.32</b>	<b>0.50</b>	<b>0.52</b>	<b>0.32</b>	<b>0.36</b>	<b>0.38</b>	<b>0.38</b>	<b>0.36</b>
	FORM Efficiency, $\phi/\lambda$	0.37	0.44	0.42	0.37	0.65	0.69	0.66	0.64	0.43	0.59	0.59	0.43	0.65	0.66	0.69	0.65
Unplugged Neglecting Interior Side Resistance	Mean	0.77	0.71	0.76	0.77	1.09	1.11	1.17	1.09	1.37	1.56	1.65	1.37	1.04	1.06	1.04	1.04
	COV	0.49	0.40	0.44	0.49	0.24	0.22	0.25	0.25	0.41	0.30	0.29	0.41	0.24	0.24	0.23	0.24
	Count	12	10	10	12	13	11	11	13	13	10	10	13	13	11	10	13
	<b>FORM Resistance Factor, <math>\phi</math></b>	<b>0.29</b>	<b>0.33</b>	<b>0.32</b>	<b>0.28</b>	<b>0.73</b>	<b>0.79</b>	<b>0.76</b>	<b>0.72</b>	<b>0.61</b>	<b>0.90</b>	<b>0.98</b>	<b>0.61</b>	<b>0.70</b>	<b>0.72</b>	<b>0.72</b>	<b>0.70</b>
	FORM Efficiency, $\phi/\lambda$	0.37	0.46	0.42	0.37	0.67	0.71	0.65	0.66	0.44	0.58	0.60	0.45	0.68	0.68	0.69	0.67
Minimum of Plugged and Unplugged with Interior Side Resistance	Mean	0.47	0.44	0.56	0.47	0.66	0.69	0.72	0.67	0.84	0.77	0.94	0.79	0.62	0.61	0.65	0.62
	COV	0.34	0.27	0.41	0.34	0.12	0.23	0.29	0.14	0.28	0.39	0.28	0.39	0.18	0.21	0.26	0.18
	Count	12	10	11	12	12	11	11	12	12	10	10	13	13	10	10	13
	<b>FORM Resistance Factor, <math>\phi</math></b>	<b>0.25</b>	<b>0.28</b>	<b>0.25</b>	<b>0.25</b>	<b>0.57</b>	<b>0.47</b>	<b>0.43</b>	<b>0.56</b>	<b>0.51</b>	<b>0.36</b>	<b>0.58</b>	<b>0.37</b>	<b>0.48</b>	<b>0.44</b>	<b>0.42</b>	<b>0.47</b>
	FORM Efficiency, $\phi/\lambda$	0.53	0.63	0.45	0.53	0.86	0.69	0.59	0.84	0.60	0.47	0.62	0.47	0.77	0.71	0.64	0.76

Note: Table formatted for 11x17 printing.

Table 18. FORM resistance factors for Mixed sites—5 Percent Diameter failure criterion with Filtered data and target reliability  $\beta = 2.33$

Mixed Failure Criterion: 5 Percent Diameter Filtered Data Beta = 2.33		Side Method: Tomlinson $\alpha$ + Nordlund				Side Method: API				Side Method: Saye + Gudavalli				Side Method: Brown			
		Base Method				Base Method				Base Method				Base Method			
		AASHTO/API	Nordlund	Gudavalli	Brown	AASHTO/API	Nordlund	Gudavalli	Brown	AASHTO/API	Nordlund	Gudavalli	Brown	AASHTO/API	Nordlund	Gudavalli	Brown
Plugged	Mean	0.45	0.32	0.50	0.41	0.56	0.45	0.64	0.54	0.65	0.49	0.75	0.57	0.54	0.44	0.56	0.53
	COV	0.39	0.19	0.43	0.32	0.21	0.30	0.39	0.15	0.22	0.46	0.42	0.33	0.18	0.30	0.34	0.15
	Count	14	10	11	14	14	10	11	14	14	10	11	15	14	10	10	14
	<b>FORM Resistance Factor, <math>\phi</math></b>	<b>0.22</b>	<b>0.24</b>	<b>0.21</b>	<b>0.22</b>	<b>0.40</b>	<b>0.26</b>	<b>0.31</b>	<b>0.44</b>	<b>0.46</b>	<b>0.20</b>	<b>0.32</b>	<b>0.31</b>	<b>0.41</b>	<b>0.26</b>	<b>0.30</b>	<b>0.43</b>
	FORM Efficiency, $\phi/\lambda$	0.48	0.75	0.43	0.55	0.71	0.58	0.47	0.82	0.70	0.40	0.43	0.54	0.76	0.58	0.53	0.82
Unplugged with Interior Side Resistance	Mean	0.44	0.36	0.42	0.44	0.55	0.55	0.57	0.54	0.69	0.76	0.78	0.68	0.51	0.49	0.50	0.51
	COV	0.53	0.49	0.53	0.52	0.27	0.27	0.29	0.27	0.31	0.26	0.27	0.31	0.26	0.22	0.23	0.27
	Count	15	10	11	15	15	11	11	15	14	10	10	14	14	10	10	14
	<b>FORM Resistance Factor, <math>\phi</math></b>	<b>0.15</b>	<b>0.14</b>	<b>0.14</b>	<b>0.15</b>	<b>0.34</b>	<b>0.35</b>	<b>0.33</b>	<b>0.34</b>	<b>0.39</b>	<b>0.48</b>	<b>0.49</b>	<b>0.39</b>	<b>0.32</b>	<b>0.35</b>	<b>0.34</b>	<b>0.32</b>
	FORM Efficiency, $\phi/\lambda$	0.34	0.37	0.34	0.35	0.63	0.63	0.59	0.62	0.57	0.64	0.62	0.57	0.64	0.70	0.69	0.63
Unplugged Neglecting Interior Side Resistance	Mean	0.84	0.67	0.79	0.82	1.04	1.02	1.08	1.02	1.29	1.39	1.49	1.27	0.96	0.92	0.95	0.96
	COV	0.52	0.47	0.52	0.52	0.26	0.25	0.30	0.26	0.29	0.26	0.27	0.29	0.24	0.22	0.23	0.25
	Count	15	10	11	15	15	11	11	15	14	10	10	14	14	10	10	14
	<b>FORM Resistance Factor, <math>\phi</math></b>	<b>0.29</b>	<b>0.26</b>	<b>0.27</b>	<b>0.29</b>	<b>0.67</b>	<b>0.67</b>	<b>0.63</b>	<b>0.65</b>	<b>0.77</b>	<b>0.89</b>	<b>0.92</b>	<b>0.75</b>	<b>0.64</b>	<b>0.65</b>	<b>0.65</b>	<b>0.63</b>
	FORM Efficiency, $\phi/\lambda$	0.35	0.39	0.34	0.35	0.65	0.66	0.58	0.64	0.60	0.64	0.62	0.59	0.67	0.71	0.69	0.65
Minimum of Plugged and Unplugged with Interior Side Resistance	Mean	0.49	0.41	0.52	0.48	0.63	0.63	0.67	0.59	0.77	0.69	0.85	0.72	0.58	0.56	0.59	0.54
	COV	0.40	0.33	0.44	0.39	0.21	0.22	0.34	0.18	0.22	0.35	0.28	0.28	0.19	0.22	0.27	0.14
	Count	14	10	11	15	15	11	11	15	14	10	10	14	14	10	10	13
	<b>FORM Resistance Factor, <math>\phi</math></b>	<b>0.23</b>	<b>0.23</b>	<b>0.22</b>	<b>0.23</b>	<b>0.45</b>	<b>0.44</b>	<b>0.35</b>	<b>0.46</b>	<b>0.53</b>	<b>0.36</b>	<b>0.51</b>	<b>0.44</b>	<b>0.44</b>	<b>0.40</b>	<b>0.37</b>	<b>0.45</b>
	FORM Efficiency, $\phi/\lambda$	0.46	0.55	0.41	0.47	0.71	0.70	0.53	0.77	0.70	0.52	0.60	0.61	0.76	0.70	0.63	0.83

Note: Table formatted for 11x17 printing.

Table 19. FORM resistance factors for Mixed sites—Max Load failure criterion with Filtered data and target reliability  $\beta = 2.33$

Mixed Failure Criterion: Max Load Filtered Data Beta = 2.33		Side Method: Tomlinson $\alpha$ + Nordlund				Side Method: API				Side Method: Saye + Gudavalli				Side Method: Brown			
		Base Method				Base Method				Base Method				Base Method			
		AASHTO/API	Nordlund	Gudavalli	Brown	AASHTO/API	Nordlund	Gudavalli	Brown	AASHTO/API	Nordlund	Gudavalli	Brown	AASHTO/API	Nordlund	Gudavalli	Brown
Plugged	Mean	0.62	0.41	0.54	0.59	0.67	0.50	0.67	0.63	0.71	0.54	0.72	0.67	0.62	0.45	0.62	0.58
	COV	0.51	0.35	0.33	0.50	0.40	0.39	0.36	0.36	0.44	0.52	0.41	0.41	0.39	0.42	0.45	0.35
	Count	24	16	16	25	24	16	17	25	24	16	16	25	24	16	17	25
	<b>FORM Resistance Factor, <math>\phi</math></b>	<b>0.22</b>	<b>0.21</b>	<b>0.29</b>	<b>0.21</b>	<b>0.31</b>	<b>0.24</b>	<b>0.34</b>	<b>0.32</b>	<b>0.29</b>	<b>0.19</b>	<b>0.33</b>	<b>0.30</b>	<b>0.29</b>	<b>0.20</b>	<b>0.26</b>	<b>0.30</b>
	FORM Efficiency, $\phi/\lambda$	0.35	0.52	0.54	0.36	0.46	0.47	0.51	0.50	0.41	0.35	0.45	0.44	0.47	0.44	0.41	0.52
Unplugged with Interior Side Resistance	Mean	0.58	0.42	0.46	0.57	0.62	0.60	0.59	0.62	0.74	0.72	0.69	0.74	0.57	0.52	0.53	0.57
	COV	0.55	0.37	0.44	0.55	0.31	0.23	0.28	0.31	0.45	0.45	0.41	0.44	0.39	0.40	0.41	0.39
	Count	24	15	16	24	24	16	17	24	25	17	16	25	25	17	17	25
	<b>FORM Resistance Factor, <math>\phi</math></b>	<b>0.19</b>	<b>0.21</b>	<b>0.19</b>	<b>0.19</b>	<b>0.35</b>	<b>0.41</b>	<b>0.36</b>	<b>0.35</b>	<b>0.31</b>	<b>0.29</b>	<b>0.31</b>	<b>0.31</b>	<b>0.27</b>	<b>0.24</b>	<b>0.24</b>	<b>0.27</b>
	FORM Efficiency, $\phi/\lambda$	0.32	0.49	0.42	0.32	0.57	0.68	0.61	0.57	0.41	0.41	0.45	0.42	0.47	0.46	0.45	0.48
Unplugged Neglecting Interior Side Resistance	Mean	1.11	0.78	0.88	1.09	1.19	1.12	1.13	1.17	1.41	1.33	1.32	1.38	1.10	0.98	1.01	1.08
	COV	0.56	0.36	0.43	0.56	0.31	0.22	0.29	0.31	0.44	0.44	0.40	0.43	0.39	0.39	0.41	0.38
	Count	24	15	16	24	24	16	17	24	25	17	16	25	25	17	17	25
	<b>FORM Resistance Factor, <math>\phi</math></b>	<b>0.35</b>	<b>0.40</b>	<b>0.38</b>	<b>0.35</b>	<b>0.67</b>	<b>0.78</b>	<b>0.68</b>	<b>0.67</b>	<b>0.58</b>	<b>0.55</b>	<b>0.60</b>	<b>0.59</b>	<b>0.52</b>	<b>0.45</b>	<b>0.45</b>	<b>0.52</b>
	FORM Efficiency, $\phi/\lambda$	0.32	0.50	0.43	0.32	0.57	0.70	0.60	0.57	0.42	0.41	0.45	0.43	0.47	0.46	0.44	0.48
Minimum of Plugged and Unplugged with Interior Side Resistance	Mean	0.67	0.51	0.59	0.62	0.73	0.66	0.69	0.67	0.81	0.72	0.80	0.79	0.66	0.56	0.61	0.63
	COV	0.48	0.35	0.38	0.46	0.33	0.20	0.32	0.26	0.40	0.40	0.43	0.40	0.35	0.36	0.39	0.34
	Count	24	16	17	24	24	15	17	24	24	16	17	25	24	16	16	25
	<b>FORM Resistance Factor, <math>\phi</math></b>	<b>0.25</b>	<b>0.27</b>	<b>0.28</b>	<b>0.25</b>	<b>0.39</b>	<b>0.48</b>	<b>0.38</b>	<b>0.43</b>	<b>0.37</b>	<b>0.33</b>	<b>0.35</b>	<b>0.36</b>	<b>0.34</b>	<b>0.29</b>	<b>0.29</b>	<b>0.34</b>
	FORM Efficiency, $\phi/\lambda$	0.38	0.52	0.49	0.40	0.54	0.73	0.55	0.64	0.46	0.46	0.43	0.45	0.51	0.51	0.47	0.53

Note: Table formatted for 11x17 printing.

Table 20. FORM resistance factors for Variable Side with Cohesive Base sites—Modified Davison failure criterion with Filtered data and target reliability  $\beta = 2.33$ .

Variable Side + Cohesive Base Failure Criterion: Modified Davison Filtered Data Beta = 2.33		Side Method: Tomlinson $\alpha$ + Nordlund				Side Method: API				Side Method: Saye + Gudavalli				Side Method: Brown			
		Base Method				Base Method				Base Method				Base Method			
		AASHTO/API	Nordlund	Gudavalli	Brown	AASHTO/API	Nordlund	Gudavalli	Brown	AASHTO/API	Nordlund	Gudavalli	Brown	AASHTO/API	Nordlund	Gudavalli	Brown
Plugged	Mean	0.82	—	—	0.64	0.76	—	—	0.60	0.81	—	—	0.65	0.78	—	—	0.65
	COV	0.26	—	—	0.33	0.25	—	—	0.31	0.24	—	—	0.36	0.24	—	—	0.39
	Count	12	—	—	13	12	—	—	13	12	—	—	13	12	—	—	13
	<b>FORM Resistance Factor, <math>\phi</math></b>	<b>0.52</b>	—	—	<b>0.35</b>	<b>0.50</b>	—	—	<b>0.34</b>	<b>0.54</b>	—	—	<b>0.33</b>	<b>0.52</b>	—	—	<b>0.30</b>
	FORM Efficiency, $\phi/\lambda$	0.64	—	—	0.54	0.66	—	—	0.57	0.66	—	—	0.51	0.67	—	—	0.47
Unplugged with Interior Side Resistance	Mean	0.51	—	—	0.50	0.47	—	—	0.46	0.47	—	—	0.47	0.47	—	—	0.46
	COV	0.36	—	—	0.34	0.34	—	—	0.31	0.22	—	—	0.22	0.27	—	—	0.25
	Count	12	—	—	12	12	—	—	12	12	—	—	12	12	—	—	12
	<b>FORM Resistance Factor, <math>\phi</math></b>	<b>0.26</b>	—	—	<b>0.26</b>	<b>0.25</b>	—	—	<b>0.26</b>	<b>0.33</b>	—	—	<b>0.32</b>	<b>0.29</b>	—	—	<b>0.30</b>
	FORM Efficiency, $\phi/\lambda$	0.51	—	—	0.53	0.53	—	—	0.56	0.70	—	—	0.69	0.63	—	—	0.65
Unplugged Neglecting Interior Side Resistance	Mean	0.99	—	—	0.95	0.90	—	—	0.87	0.92	—	—	0.90	0.91	—	—	0.87
	COV	0.35	—	—	0.33	0.33	—	—	0.29	0.22	—	—	0.23	0.26	—	—	0.25
	Count	12	—	—	12	12	—	—	12	12	—	—	12	12	—	—	12
	<b>FORM Resistance Factor, <math>\phi</math></b>	<b>0.51</b>	—	—	<b>0.52</b>	<b>0.49</b>	—	—	<b>0.52</b>	<b>0.64</b>	—	—	<b>0.62</b>	<b>0.58</b>	—	—	<b>0.58</b>
	FORM Efficiency, $\phi/\lambda$	0.51	—	—	0.54	0.54	—	—	0.59	0.70	—	—	0.69	0.64	—	—	0.66
Minimum of Plugged and Unplugged with Interior Side Resistance	Mean	0.82	—	—	0.70	0.76	—	—	0.66	0.81	—	—	0.72	0.78	—	—	0.69
	COV	0.26	—	—	0.26	0.25	—	—	0.25	0.24	—	—	0.32	0.24	—	—	0.32
	Count	12	—	—	12	12	—	—	12	12	—	—	13	12	—	—	13
	<b>FORM Resistance Factor, <math>\phi</math></b>	<b>0.52</b>	—	—	<b>0.44</b>	<b>0.50</b>	—	—	<b>0.43</b>	<b>0.54</b>	—	—	<b>0.40</b>	<b>0.52</b>	—	—	<b>0.38</b>
	FORM Efficiency, $\phi/\lambda$	0.64	—	—	0.64	0.66	—	—	0.65	0.66	—	—	0.55	0.67	—	—	0.55

—No data.

Note: Table formatted for 11x17 printing.

Table 21. FORM resistance factors for Variable Side with Cohesive Base sites—5 Percent Diameter failure criterion with Filtered data and target reliability  $\beta = 2.33$ .

Variable Side + Cohesive Base Failure Criterion: 5 Percent Diameter Filtered Data Beta = 2.33		Side Method: Tomlinson $\alpha$ + Nordlund				Side Method: API				Side Method: Saye + Gudavalli				Side Method: Brown			
		Base Method				Base Method				Base Method				Base Method			
		AASHTO/API	Nordlund	Gudavalli	Brown	AASHTO/API	Nordlund	Gudavalli	Brown	AASHTO/API	Nordlund	Gudavalli	Brown	AASHTO/API	Nordlund	Gudavalli	Brown
Plugged	Mean	0.83	—	—	0.64	0.78	—	—	0.61	0.78	—	—	0.62	0.80	—	—	0.66
	COV	0.15	—	—	0.32	0.23	—	—	0.29	0.18	—	—	0.30	0.25	—	—	0.36
	Count	12	—	—	14	14	—	—	14	13	—	—	13	13	—	—	14
	<b>FORM Resistance Factor, <math>\phi</math></b>	<b>0.68</b>	—	—	<b>0.36</b>	<b>0.54</b>	—	—	<b>0.36</b>	<b>0.59</b>	—	—	<b>0.36</b>	<b>0.52</b>	—	—	<b>0.33</b>
	FORM Efficiency, $\phi/\lambda$	0.82	—	—	0.56	0.69	—	—	0.59	0.76	—	—	0.58	0.65	—	—	0.50
Unplugged with Interior Side Resistance	Mean	0.52	—	—	0.51	0.46	—	—	0.47	0.46	—	—	0.46	0.49	—	—	0.48
	COV	0.35	—	—	0.33	0.27	—	—	0.29	0.17	—	—	0.17	0.32	—	—	0.31
	Count	14	—	—	14	13	—	—	14	13	—	—	13	13	—	—	13
	<b>FORM Resistance Factor, <math>\phi</math></b>	<b>0.27</b>	—	—	<b>0.27</b>	<b>0.29</b>	—	—	<b>0.28</b>	<b>0.36</b>	—	—	<b>0.36</b>	<b>0.27</b>	—	—	<b>0.27</b>
	FORM Efficiency, $\phi/\lambda$	0.52	—	—	0.54	0.62	—	—	0.60	0.78	—	—	0.78	0.55	—	—	0.56
Unplugged Neglecting Interior Side Resistance	Mean	1.01	—	—	1.01	0.89	—	—	0.90	0.91	—	—	0.88	0.96	—	—	0.93
	COV	0.34	—	—	0.26	0.27	—	—	0.27	0.17	—	—	0.18	0.32	—	—	0.30
	Count	14	—	—	13	13	—	—	14	13	—	—	13	13	—	—	13
	<b>FORM Resistance Factor, <math>\phi</math></b>	<b>0.53</b>	—	—	<b>0.65</b>	<b>0.56</b>	—	—	<b>0.56</b>	<b>0.71</b>	—	—	<b>0.68</b>	<b>0.53</b>	—	—	<b>0.54</b>
	FORM Efficiency, $\phi/\lambda$	0.53	—	—	0.65	0.63	—	—	0.62	0.78	—	—	0.77	0.55	—	—	0.58
Minimum of Plugged and Unplugged with Interior Side Resistance	Mean	0.83	—	—	0.71	0.78	—	—	0.65	0.78	—	—	0.63	0.80	—	—	0.70
	COV	0.15	—	—	0.21	0.23	—	—	0.24	0.18	—	—	0.26	0.25	—	—	0.32
	Count	12	—	—	13	14	—	—	14	13	—	—	13	13	—	—	14
	<b>FORM Resistance Factor, <math>\phi</math></b>	<b>0.68</b>	—	—	<b>0.50</b>	<b>0.54</b>	—	—	<b>0.43</b>	<b>0.59</b>	—	—	<b>0.40</b>	<b>0.52</b>	—	—	<b>0.39</b>
	FORM Efficiency, $\phi/\lambda$	0.82	—	—	0.71	0.69	—	—	0.66	0.76	—	—	0.63	0.65	—	—	0.55

—No data.

Note: Table formatted for 11x17 printing.

Table 22. FORM resistance factors for Variable Side with Cohesive Base sites—Max Load failure criterion with Filtered data and target reliability  $\beta = 2.33$ .

Variable Side + Cohesive Base Failure Criterion: Max Load Filtered Data Beta = 2.33		Side Method: Tomlinson $\alpha$ + Nordlund				Side Method: API				Side Method: Saye + Gudavalli				Side Method: Brown			
		Base Method				Base Method				Base Method				Base Method			
		AASHTO/API	Nordlund	Gudavalli	Brown	AASHTO/API	Nordlund	Gudavalli	Brown	AASHTO/API	Nordlund	Gudavalli	Brown	AASHTO/API	Nordlund	Gudavalli	Brown
Plugged	Mean	0.99	—	—	0.70	0.97	—	—	0.67	0.99	—	—	0.68	0.85	—	—	0.66
	COV	0.33	—	—	0.41	0.35	—	—	0.36	0.33	—	—	0.35	0.24	—	—	0.38
	Count	21	—	—	22	22	—	—	22	22	—	—	22	21	—	—	22
	<b>FORM Resistance Factor, <math>\phi</math></b>	<b>0.54</b>	—	—	<b>0.32</b>	<b>0.50</b>	—	—	<b>0.33</b>	<b>0.54</b>	—	—	<b>0.35</b>	<b>0.58</b>	—	—	<b>0.32</b>
	FORM Efficiency, $\phi/\lambda$	0.54	—	—	0.45	0.52	—	—	0.50	0.55	—	—	0.52	0.68	—	—	0.49
Unplugged with Interior Side Resistance	Mean	0.68	—	—	0.65	0.63	—	—	0.61	0.58	—	—	0.59	0.57	—	—	0.55
	COV	0.52	—	—	0.47	0.50	—	—	0.45	0.33	—	—	0.36	0.36	—	—	0.36
	Count	21	—	—	21	21	—	—	21	20	—	—	21	22	—	—	22
	<b>FORM Resistance Factor, <math>\phi</math></b>	<b>0.24</b>	—	—	<b>0.25</b>	<b>0.23</b>	—	—	<b>0.25</b>	<b>0.31</b>	—	—	<b>0.30</b>	<b>0.29</b>	—	—	<b>0.28</b>
	FORM Efficiency, $\phi/\lambda$	0.35	—	—	0.39	0.36	—	—	0.40	0.54	—	—	0.51	0.51	—	—	0.51
Unplugged Neglecting Interior Side Resistance	Mean	1.33	—	—	1.22	1.23	—	—	1.13	1.20	—	—	1.11	1.10	—	—	1.06
	COV	0.51	—	—	0.45	0.50	—	—	0.40	0.42	—	—	0.32	0.36	—	—	0.36
	Count	21	—	—	21	21	—	—	21	21	—	—	21	22	—	—	22
	<b>FORM Resistance Factor, <math>\phi</math></b>	<b>0.47</b>	—	—	<b>0.49</b>	<b>0.44</b>	—	—	<b>0.52</b>	<b>0.53</b>	—	—	<b>0.62</b>	<b>0.56</b>	—	—	<b>0.54</b>
	FORM Efficiency, $\phi/\lambda$	0.35	—	—	0.40	0.36	—	—	0.46	0.44	—	—	0.56	0.51	—	—	0.51
Minimum of Plugged and Unplugged with Interior Side Resistance	Mean	1.00	—	—	0.77	0.93	—	—	0.73	0.99	—	—	0.73	0.85	—	—	0.69
	COV	0.37	—	—	0.34	0.30	—	—	0.33	0.33	—	—	0.29	0.24	—	—	0.33
	Count	21	—	—	21	21	—	—	21	22	—	—	21	21	—	—	22
	<b>FORM Resistance Factor, <math>\phi</math></b>	<b>0.49</b>	—	—	<b>0.41</b>	<b>0.54</b>	—	—	<b>0.40</b>	<b>0.54</b>	—	—	<b>0.44</b>	<b>0.58</b>	—	—	<b>0.38</b>
	FORM Efficiency, $\phi/\lambda$	0.49	—	—	0.53	0.58	—	—	0.55	0.55	—	—	0.60	0.68	—	—	0.54

—No data.

Note: Table formatted for 11x17 printing.

Table 23. FORM resistance factors for Variable Side with Cohesionless Base sites—Modified Davisson failure criterion with Filtered data and target reliability  $\beta = 2.33$ .

Variable Side + Cohesionless Base Failure Criterion: Modified Davisson Filtered Data Beta = 2.33		Side Method: Tomlinson $\alpha$ + Nordlund				Side Method: API				Side Method: Saye + Gudavalli				Side Method: Brown			
		Base Method				Base Method				Base Method				Base Method			
		AASHTO/API	Nordlund	Gudavalli	Brown	AASHTO/API	Nordlund	Gudavalli	Brown	AASHTO/API	Nordlund	Gudavalli	Brown	AASHTO/API	Nordlund	Gudavalli	Brown
Plugged	Mean	0.46	0.45	0.54	0.43	0.55	0.58	0.76	0.55	0.66	0.70	0.89	0.64	0.55	0.59	0.75	0.51
	COV	0.43	0.51	0.39	0.42	0.31	0.51	0.41	0.41	0.39	0.58	0.40	0.49	0.32	0.54	0.43	0.35
	Count	25	25	25	25	23	24	25	25	24	24	24	25	24	25	26	24
	<b>FORM Resistance Factor, <math>\phi</math></b>	<b>0.20</b>	<b>0.16</b>	<b>0.26</b>	<b>0.19</b>	<b>0.32</b>	<b>0.21</b>	<b>0.34</b>	<b>0.25</b>	<b>0.31</b>	<b>0.21</b>	<b>0.41</b>	<b>0.24</b>	<b>0.31</b>	<b>0.19</b>	<b>0.32</b>	<b>0.26</b>
	FORM Efficiency, $\phi/\lambda$	0.43	0.36	0.47	0.44	0.57	0.36	0.45	0.45	0.47	0.30	0.46	0.38	0.56	0.33	0.43	0.51
Unplugged with Interior Side Resistance	Mean	0.41	0.40	0.41	0.40	0.66	0.65	0.67	0.64	0.98	0.98	0.97	0.92	0.67	0.66	0.68	0.66
	COV	0.48	0.46	0.47	0.46	0.37	0.37	0.37	0.36	0.35	0.36	0.40	0.32	0.28	0.28	0.30	0.26
	Count	24	24	24	24	25	25	25	25	24	24	25	23	24	24	24	24
	<b>FORM Resistance Factor, <math>\phi</math></b>	<b>0.16</b>	<b>0.16</b>	<b>0.16</b>	<b>0.16</b>	<b>0.32</b>	<b>0.32</b>	<b>0.33</b>	<b>0.33</b>	<b>0.51</b>	<b>0.49</b>	<b>0.44</b>	<b>0.51</b>	<b>0.41</b>	<b>0.41</b>	<b>0.40</b>	<b>0.42</b>
	FORM Efficiency, $\phi/\lambda$	0.39	0.40	0.39	0.40	0.49	0.49	0.49	0.51	0.52	0.50	0.45	0.56	0.62	0.61	0.59	0.64
Unplugged Neglecting Interior Side Resistance	Mean	0.77	0.75	0.79	0.75	1.22	1.20	1.26	1.18	1.78	1.71	1.73	1.70	1.25	1.19	1.22	1.20
	COV	0.46	0.45	0.46	0.45	0.35	0.37	0.37	0.34	0.34	0.41	0.38	0.34	0.26	0.25	0.32	0.24
	Count	24	24	24	24	25	25	25	25	24	25	24	24	24	23	24	24
	<b>FORM Resistance Factor, <math>\phi</math></b>	<b>0.30</b>	<b>0.31</b>	<b>0.31</b>	<b>0.31</b>	<b>0.62</b>	<b>0.60</b>	<b>0.63</b>	<b>0.62</b>	<b>0.95</b>	<b>0.76</b>	<b>0.84</b>	<b>0.90</b>	<b>0.80</b>	<b>0.78</b>	<b>0.67</b>	<b>0.80</b>
	FORM Efficiency, $\phi/\lambda$	0.39	0.41	0.40	0.41	0.51	0.50	0.50	0.52	0.53	0.45	0.49	0.53	0.64	0.65	0.55	0.67
Minimum of Plugged and Unplugged with Interior Side Resistance	Mean	0.49	0.51	0.56	0.48	0.70	0.71	0.78	0.68	0.97	0.97	0.97	0.91	0.72	0.70	0.77	0.70
	COV	0.43	0.44	0.40	0.43	0.38	0.37	0.39	0.33	0.38	0.43	0.37	0.35	0.28	0.41	0.40	0.25
	Count	25	25	25	25	25	24	25	25	25	24	24	24	24	25	26	24
	<b>FORM Resistance Factor, <math>\phi</math></b>	<b>0.21</b>	<b>0.21</b>	<b>0.25</b>	<b>0.20</b>	<b>0.34</b>	<b>0.35</b>	<b>0.37</b>	<b>0.37</b>	<b>0.46</b>	<b>0.41</b>	<b>0.48</b>	<b>0.47</b>	<b>0.44</b>	<b>0.32</b>	<b>0.35</b>	<b>0.46</b>
	FORM Efficiency, $\phi/\lambda$	0.43	0.41	0.46	0.43	0.48	0.50	0.47	0.54	0.48	0.43	0.50	0.52	0.61	0.45	0.45	0.66

Note: Table formatted for 11x17 printing.

Table 24. FORM resistance factors for Variable Side with Cohesionless Base sites—5 Percent Diameter failure criterion with Filtered data and target reliability  $\beta = 2.33$ .

Variable Side + Cohesionless Base Failure Criterion: 5 Percent Diameter Filtered Data Beta = 2.33		Side Method: Tomlinson $\alpha$ + Nordlund				Side Method: API				Side Method: Saye + Gudavalli				Side Method: Brown			
		Base Method				Base Method				Base Method				Base Method			
		AASHTO/API	Nordlund	Gudavalli	Brown	AASHTO/API	Nordlund	Gudavalli	Brown	AASHTO/API	Nordlund	Gudavalli	Brown	AASHTO/API	Nordlund	Gudavalli	Brown
Plugged	Mean	0.46	0.44	0.52	0.43	0.59	0.55	0.71	0.53	0.67	0.67	0.82	0.61	0.55	0.52	0.70	0.52
	COV	0.43	0.52	0.41	0.43	0.41	0.47	0.43	0.37	0.41	0.54	0.39	0.43	0.36	0.46	0.44	0.37
	Count	26	26	26	26	26	25	26	25	26	25	25	25	26	25	27	26
	<b>FORM Resistance Factor, <math>\phi</math></b>	<b>0.20</b>	<b>0.16</b>	<b>0.24</b>	<b>0.19</b>	<b>0.27</b>	<b>0.21</b>	<b>0.31</b>	<b>0.26</b>	<b>0.30</b>	<b>0.22</b>	<b>0.38</b>	<b>0.26</b>	<b>0.28</b>	<b>0.21</b>	<b>0.29</b>	<b>0.26</b>
	FORM Efficiency, $\phi/\lambda$	0.43	0.35	0.45	0.43	0.45	0.39	0.43	0.49	0.45	0.33	0.47	0.43	0.51	0.40	0.42	0.49
Unplugged with Interior Side Resistance	Mean	0.44	0.42	0.44	0.42	0.63	0.62	0.64	0.62	0.89	0.85	0.87	0.84	0.59	0.62	0.58	0.60
	COV	0.50	0.48	0.50	0.48	0.40	0.40	0.40	0.39	0.40	0.39	0.38	0.38	0.33	0.29	0.37	0.34
	Count	27	26	27	26	26	26	26	26	26	25	25	25	25	25	26	26
	<b>FORM Resistance Factor, <math>\phi</math></b>	<b>0.16</b>	<b>0.16</b>	<b>0.16</b>	<b>0.16</b>	<b>0.29</b>	<b>0.29</b>	<b>0.29</b>	<b>0.29</b>	<b>0.40</b>	<b>0.40</b>	<b>0.42</b>	<b>0.41</b>	<b>0.32</b>	<b>0.36</b>	<b>0.28</b>	<b>0.32</b>
	FORM Efficiency, $\phi/\lambda$	0.37	0.38	0.37	0.38	0.46	0.46	0.46	0.47	0.45	0.48	0.48	0.49	0.54	0.59	0.49	0.54
Unplugged Neglecting Interior Side Resistance	Mean	0.79	0.78	0.80	0.78	1.17	1.14	1.20	1.14	1.61	1.59	1.60	1.61	1.16	1.13	1.09	1.14
	COV	0.48	0.47	0.47	0.47	0.38	0.39	0.39	0.38	0.32	0.40	0.37	0.35	0.29	0.28	0.37	0.28
	Count	26	26	26	26	26	26	26	26	24	26	25	25	25	25	26	25
	<b>FORM Resistance Factor, <math>\phi</math></b>	<b>0.30</b>	<b>0.30</b>	<b>0.31</b>	<b>0.30</b>	<b>0.56</b>	<b>0.54</b>	<b>0.56</b>	<b>0.55</b>	<b>0.89</b>	<b>0.73</b>	<b>0.79</b>	<b>0.84</b>	<b>0.70</b>	<b>0.69</b>	<b>0.54</b>	<b>0.70</b>
	FORM Efficiency, $\phi/\lambda$	0.38	0.39	0.39	0.39	0.48	0.47	0.47	0.49	0.56	0.46	0.49	0.52	0.60	0.61	0.50	0.61
Minimum of Plugged and Unplugged with Interior Side Resistance	Mean	0.50	0.50	0.54	0.47	0.67	0.67	0.73	0.63	0.92	0.95	0.90	0.86	0.62	0.63	0.71	0.65
	COV	0.44	0.46	0.41	0.43	0.41	0.35	0.41	0.34	0.40	0.44	0.36	0.35	0.36	0.35	0.42	0.26
	Count	27	26	26	26	26	25	26	25	26	26	25	25	26	25	27	24
	<b>FORM Resistance Factor, <math>\phi</math></b>	<b>0.21</b>	<b>0.20</b>	<b>0.24</b>	<b>0.20</b>	<b>0.30</b>	<b>0.34</b>	<b>0.33</b>	<b>0.34</b>	<b>0.42</b>	<b>0.40</b>	<b>0.45</b>	<b>0.45</b>	<b>0.31</b>	<b>0.32</b>	<b>0.31</b>	<b>0.42</b>
	FORM Efficiency, $\phi/\lambda$	0.42	0.40	0.45	0.43	0.45	0.51	0.45	0.53	0.45	0.42	0.50	0.52	0.50	0.52	0.44	0.64

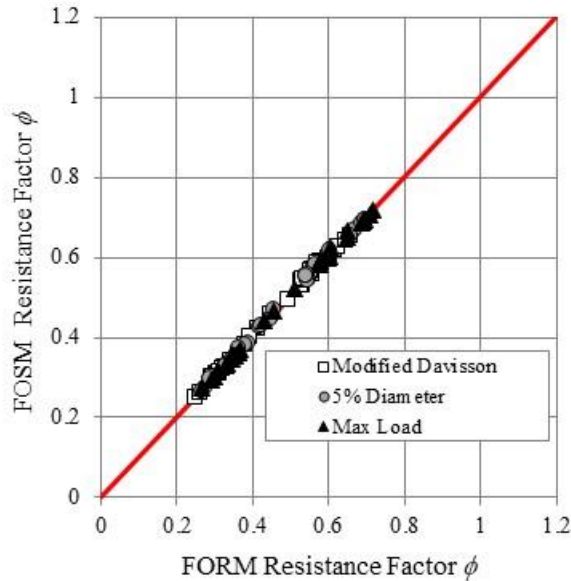
Note: Table formatted for 11x17 printing.

Table 25. FORM resistance factors for Variable Side with Cohesionless Base sites—Max Load failure criterion with Filtered data and target reliability  $\beta = 2.33$ .

Variable Side + Cohesionless Base Failure Criterion: Max Load Filtered Data Beta = 2.33		Side Method: Tomlinson $\alpha$ + Nordlund				Side Method: API				Side Method: Saye + Gudavalli				Side Method: Brown			
		Base Method				Base Method				Base Method				Base Method			
		AASHTO/API	Nordlund	Gudavalli	Brown	AASHTO/API	Nordlund	Gudavalli	Brown	AASHTO/API	Nordlund	Gudavalli	Brown	AASHTO/API	Nordlund	Gudavalli	Brown
Plugged	Mean	0.49	0.49	0.57	0.46	0.59	0.58	0.76	0.57	0.70	0.73	0.95	0.68	0.56	0.56	0.75	0.54
	COV	0.48	0.54	0.43	0.47	0.38	0.50	0.39	0.40	0.43	0.62	0.43	0.49	0.37	0.55	0.45	0.42
	Count	41	41	41	40	40	39	40	40	40	40	40	41	40	40	42	41
	<b>FORM Resistance Factor, <math>\phi</math></b>	<b>0.19</b>	<b>0.16</b>	<b>0.24</b>	<b>0.18</b>	<b>0.28</b>	<b>0.21</b>	<b>0.35</b>	<b>0.26</b>	<b>0.30</b>	<b>0.20</b>	<b>0.40</b>	<b>0.25</b>	<b>0.27</b>	<b>0.18</b>	<b>0.31</b>	<b>0.24</b>
	FORM Efficiency, $\phi/\lambda$	0.38	0.33	0.43	0.39	0.48	0.36	0.47	0.46	0.43	0.28	0.42	0.37	0.49	0.33	0.41	0.44
Unplugged with Interior Side Resistance	Mean	0.48	0.47	0.48	0.47	0.64	0.67	0.67	0.66	0.97	1.00	1.02	0.97	0.62	0.61	0.62	0.61
	COV	0.55	0.55	0.55	0.54	0.38	0.42	0.41	0.41	0.44	0.46	0.46	0.45	0.43	0.43	0.43	0.42
	Count	42	42	42	42	39	41	40	41	40	42	41	41	42	42	41	42
	<b>FORM Resistance Factor, <math>\phi</math></b>	<b>0.16</b>	<b>0.16</b>	<b>0.16</b>	<b>0.16</b>	<b>0.31</b>	<b>0.29</b>	<b>0.30</b>	<b>0.30</b>	<b>0.40</b>	<b>0.40</b>	<b>0.41</b>	<b>0.40</b>	<b>0.26</b>	<b>0.26</b>	<b>0.27</b>	<b>0.27</b>
	FORM Efficiency, $\phi/\lambda$	0.33	0.33	0.33	0.33	0.48	0.43	0.45	0.45	0.42	0.40	0.40	0.41	0.42	0.43	0.43	0.44
Unplugged Neglecting Interior Side Resistance	Mean	0.90	0.89	0.91	0.88	1.23	1.23	1.30	1.22	1.82	1.76	1.90	1.74	1.16	1.14	1.17	1.13
	COV	0.54	0.53	0.53	0.53	0.39	0.40	0.40	0.38	0.44	0.43	0.44	0.42	0.41	0.42	0.42	0.39
	Count	42	42	42	42	40	41	41	41	41	41	41	41	42	42	41	42
	<b>FORM Resistance Factor, <math>\phi</math></b>	<b>0.30</b>	<b>0.30</b>	<b>0.31</b>	<b>0.30</b>	<b>0.58</b>	<b>0.56</b>	<b>0.59</b>	<b>0.59</b>	<b>0.76</b>	<b>0.75</b>	<b>0.79</b>	<b>0.76</b>	<b>0.51</b>	<b>0.50</b>	<b>0.52</b>	<b>0.53</b>
	FORM Efficiency, $\phi/\lambda$	0.33	0.34	0.34	0.34	0.47	0.46	0.45	0.48	0.42	0.43	0.41	0.44	0.44	0.44	0.44	0.47
Minimum of Plugged and Unplugged with Interior Side Resistance	Mean	0.53	0.55	0.60	0.54	0.69	0.74	0.80	0.69	1.03	1.04	1.03	1.01	0.64	0.69	0.76	0.65
	COV	0.49	0.50	0.45	0.52	0.39	0.42	0.41	0.36	0.45	0.45	0.43	0.42	0.37	0.45	0.43	0.37
	Count	41	40	42	42	40	40	41	40	41	40	40	41	40	41	42	41
	<b>FORM Resistance Factor, <math>\phi</math></b>	<b>0.20</b>	<b>0.20</b>	<b>0.24</b>	<b>0.19</b>	<b>0.33</b>	<b>0.33</b>	<b>0.36</b>	<b>0.35</b>	<b>0.42</b>	<b>0.42</b>	<b>0.44</b>	<b>0.44</b>	<b>0.32</b>	<b>0.28</b>	<b>0.32</b>	<b>0.32</b>
	FORM Efficiency, $\phi/\lambda$	0.37	0.36	0.41	0.35	0.47	0.44	0.44	0.51	0.41	0.41	0.43	0.44	0.49	0.41	0.42	0.49

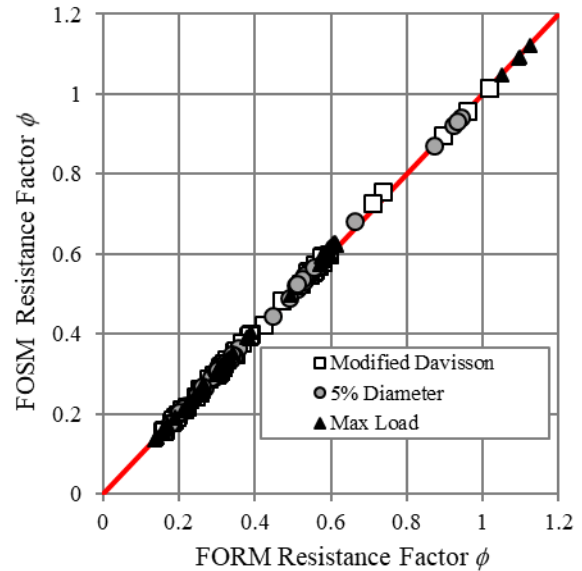
Note: Table formatted for 11x17 printing.

In general, resistance factors computed using the FOSM method were similar to those computed using the FORM method. Figure 9-A and figure 9-B compare resistance factors computed using the FOSM and FORM methods for Cohesive and Cohesionless sites. The trends are similar for other site conditions analyzed. As reflected in the figures, the difference in the FOSM and FORM resistance factors is generally less than 3 percent. Paikowsky (2004) indicated that FORM provides resistance factors approximately 10 percent higher than those obtained from FOSM. The improved agreement between the FOSM and FORM values in this study is attributed to Styler's (2006) correction for coefficient of variation of load.



Source: FHWA.

A. Cohesive sites.

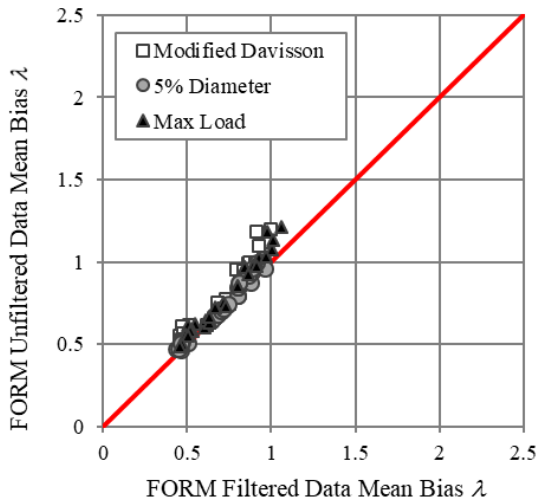


Source: FHWA.

B. Cohesionless sites.

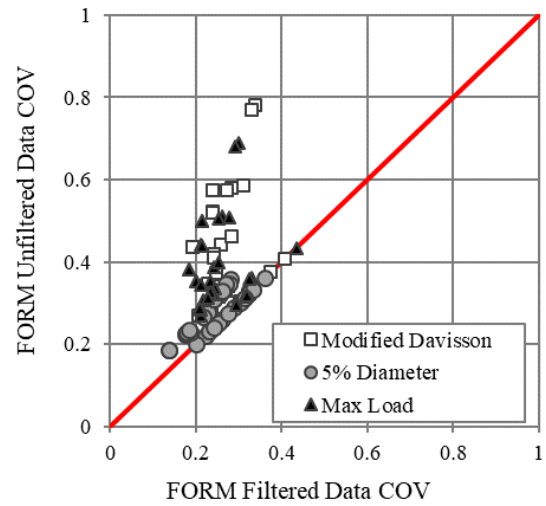
**Figure 9. Graphs. Comparison of FORM and FOSM resistance factors for filtered data with target reliability  $\beta = 2.33$ .**

Figure 10-A through figure 10-C and figure 11-A through figure 11-C compare mean resistance bias, coefficient of variation (COV), and resistance factors for filtered and unfiltered data sets with the FORM method for Cohesive and Cohesionless sites, respectively. As shown in the figures, the mean bias values are similar between the filtered and unfiltered data sets. However, as anticipated, the COV is greater for the unfiltered data set (especially Cohesive sites with a smaller data population) resulting in lower resistance factors. The trends are similar for other site conditions analyzed.



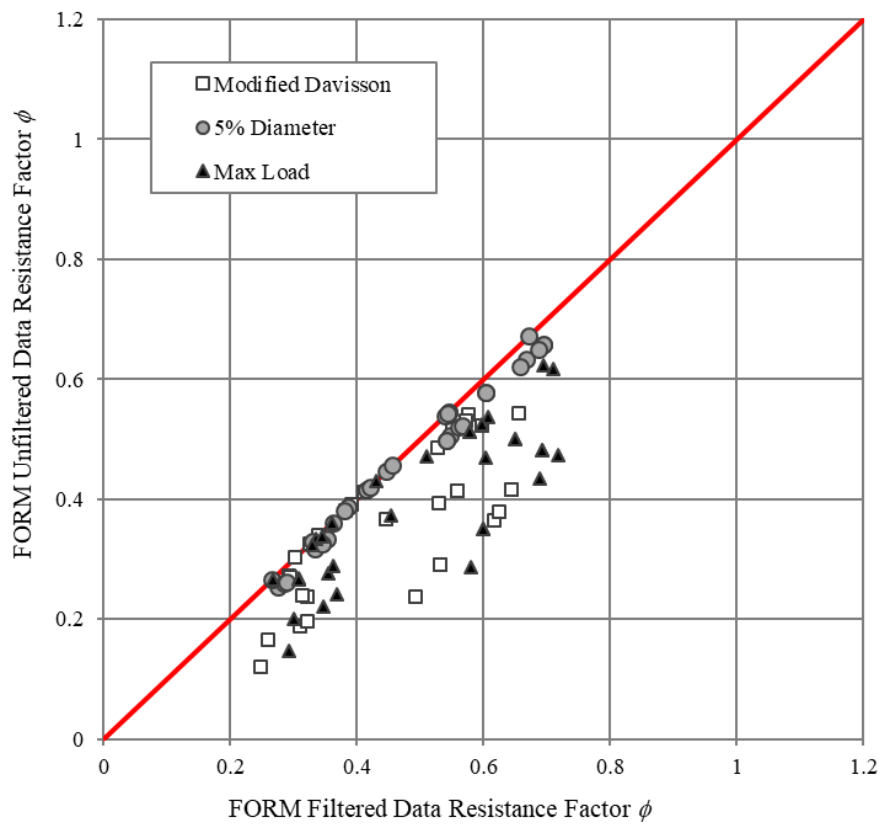
Source: FHWA.

A. Mean bias comparison.



Source: FHWA.

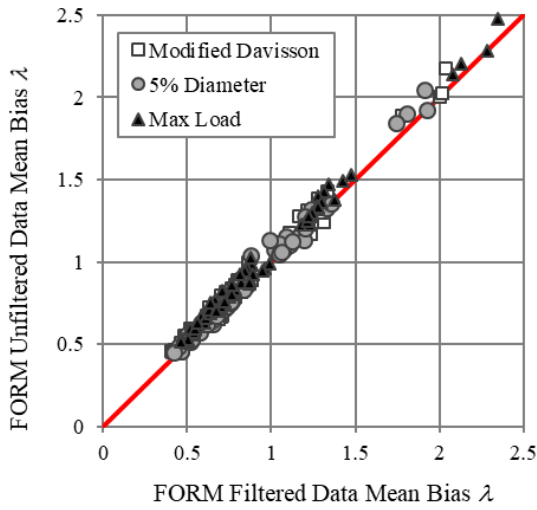
B. COV comparison.



Source: FHWA.

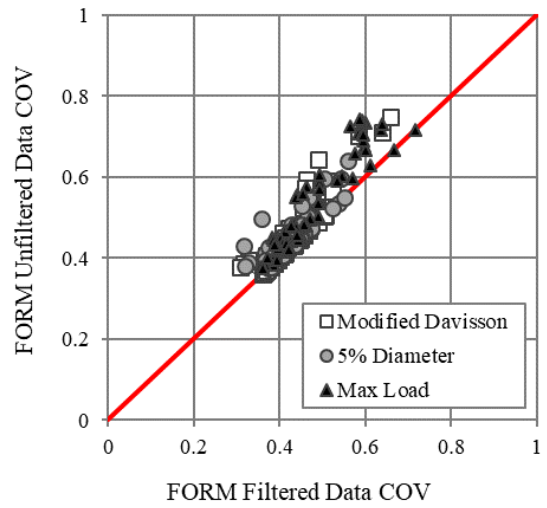
C. Resistance factor comparison.

**Figure 10. Graphs. Comparison of FORM mean bias, COV, and resistance factors for Cohesive sites, filtered and unfiltered data sets with target reliability  $\beta = 2.33$ .**



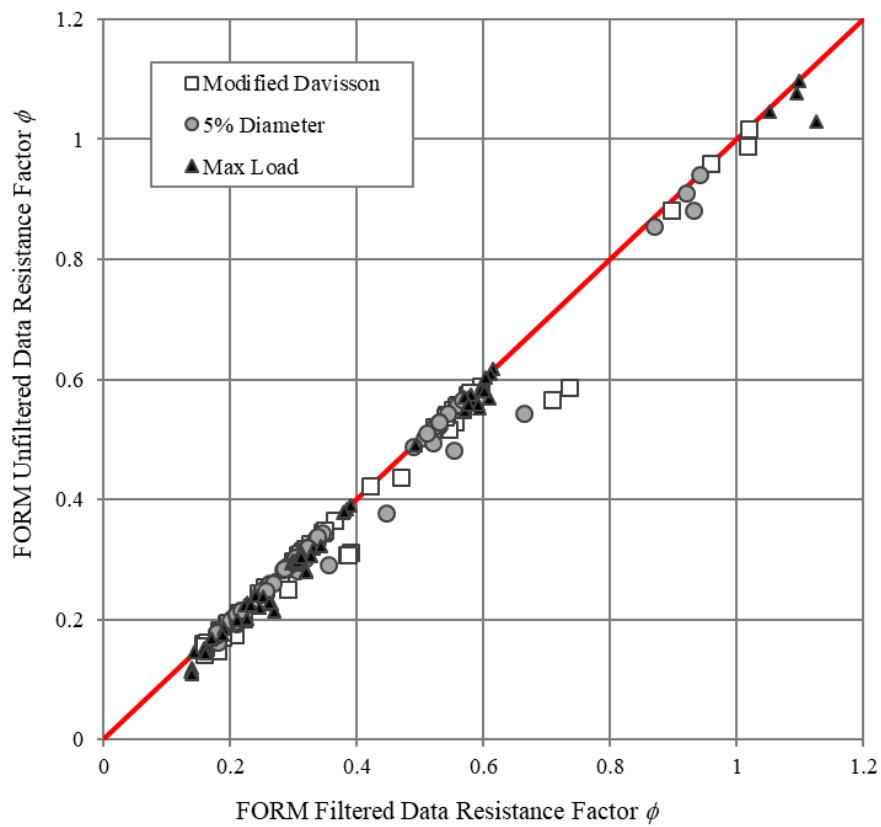
Source: FHWA.

A. Mean bias comparison.



Source: FHWA.

B. COV comparison.

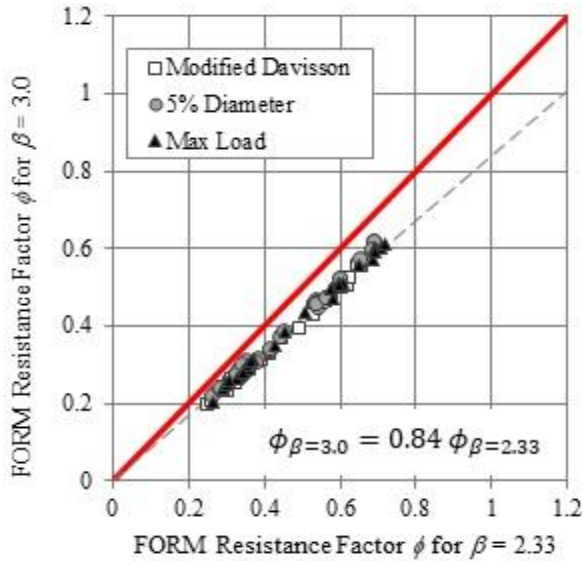


Source: FHWA.

C. Resistance factor comparison.

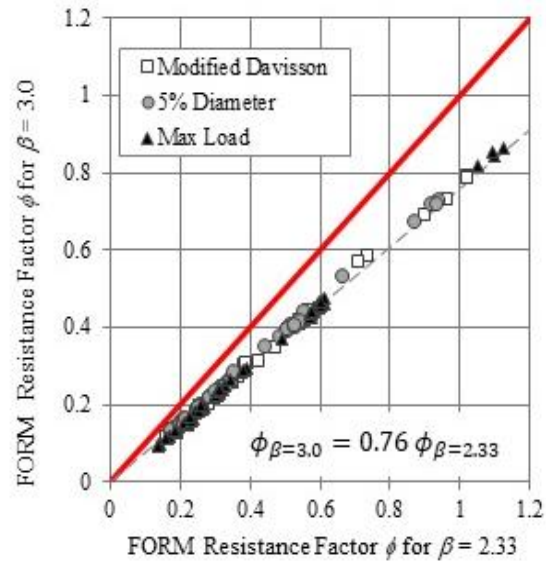
**Figure 11. Graphs. Comparison of FORM mean bias, COV, and resistance factors for Cohesionless sites, filtered and unfiltered data sets with target reliability  $\beta = 2.33$ .**

Figure 12-A and figure 12-B compare FORM resistance factors for target reliabilities of  $\beta = 2.33$  for redundant foundations and  $\beta = 3.0$  for nonredundant foundations at Cohesive and Cohesionless sites. Accounting for values computed for all site conditions, the resistance factors based on  $\beta = 3.0$  for nonredundant foundations range are approximately 80 percent of those for redundant foundations. The reduction for nonredundant LDOEPs computed in this analysis is consistent with the AASHTO *LRFD Bridge Design Specifications* recommendation for drilled shaft nonredundant foundations (AASHTO 2017).



Source: FHWA.

A. Cohesive sites.



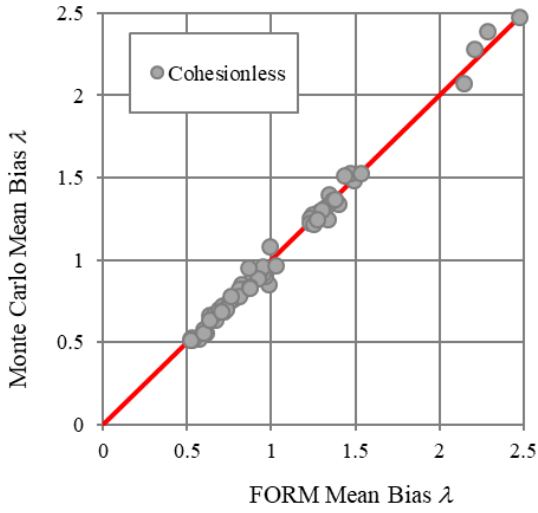
Source: FHWA.

B. Cohesionless sites.

**Figure 12. Graphs. Comparison of FORM resistance factors for target reliabilities of  $\beta = 2.33$  and  $\beta = 3.0$ .**

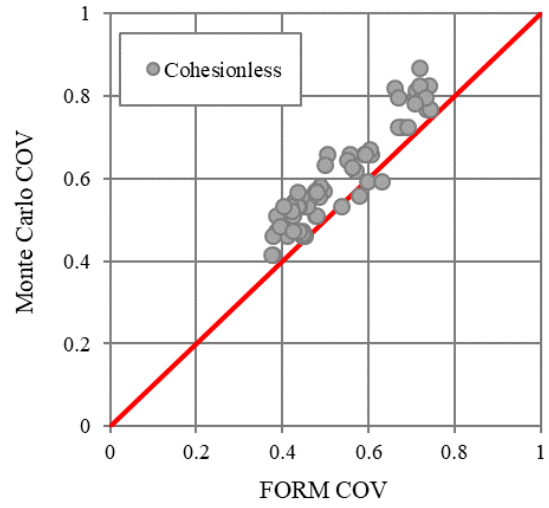
## MONTE CARLO RESISTANCE FACTORS

This analysis computed resistance factors using the Monte Carlo method for Cohesionless and Mixed unfiltered data sets with the Max Load failure criterion and target reliabilities of  $\beta = 2.33$  and  $\beta = 3.0$ . As previously discussed, the Monte Carlo resistance factor calibration was limited to these conditions to enable a sufficiently sized data set for evaluation of the resistance bias CDF. Figure 13-A through figure 13-C and figure 14-A through figure 14-C compare the mean resistance bias, COV, and resistance factors computed using the FORM and Monte Carlo methods for the Cohesionless and Mixed sites, respectively. As shown in figure 13-A through figure 13-C and figure 14-A through figure 14-C, the Monte Carlo results typically show higher variability and lower resistance factors compared to the FORM results. This effect is attributed in part to the CDF evaluation process. As discussed above, the CDF evaluation targets the tails of the data, focusing on resistance bias  $\lambda$  values less than 1.0. However, outliers with mean  $\lambda \leq 1.0$  remain in the data group and impact the fit to the tails. Therefore, increased variability may be anticipated for many of the methods.



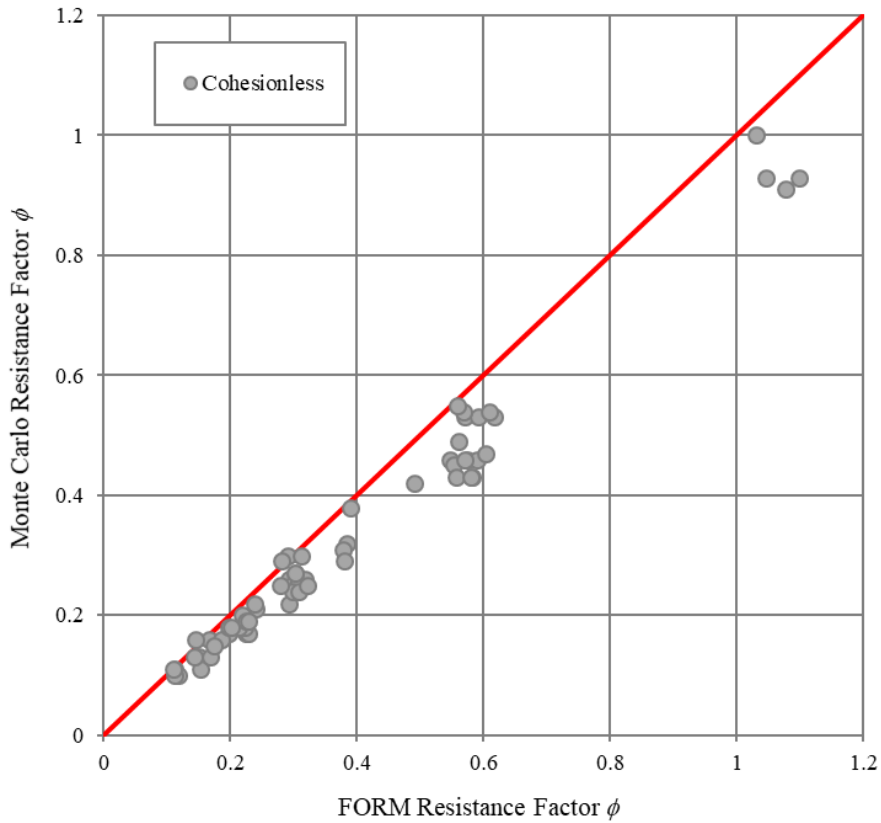
Source: FHWA.

A. Mean bias comparison.



Source: FHWA.

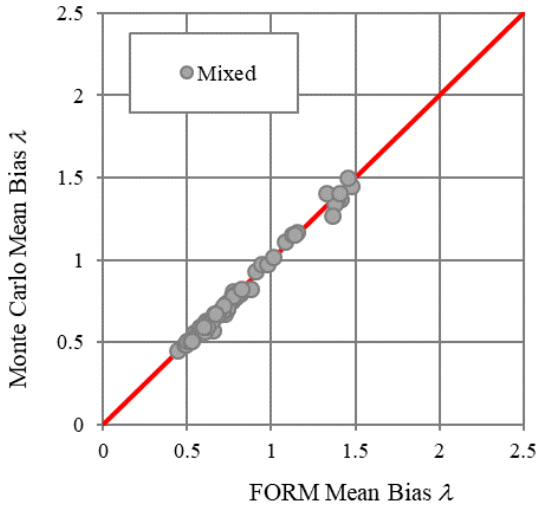
B. COV comparison.



Source: FHWA.

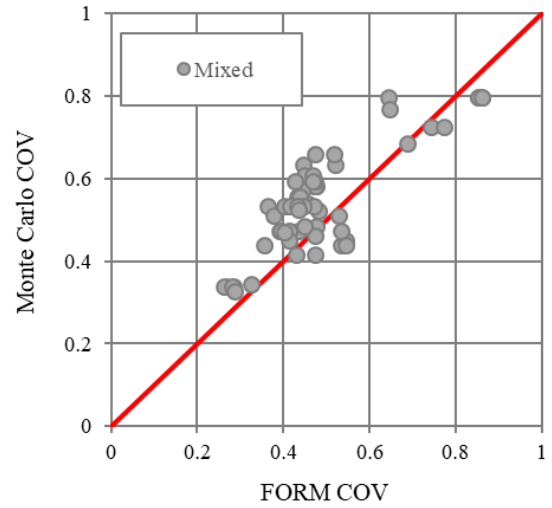
C. Resistance factor comparison.

**Figure 13. Graphs. Comparison of FORM and Monte Carlo mean bias, COV, and resistance factors for Cohesionless sites, unfiltered data set, and target reliability  $\beta = 2.33$ .**



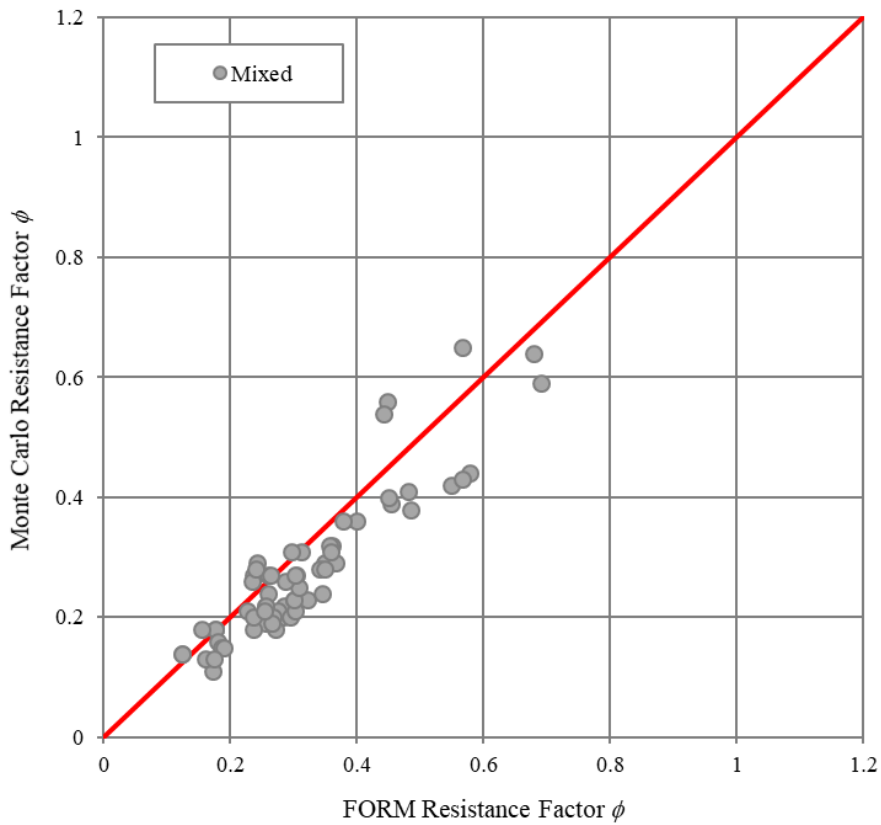
Source: FHWA.

A. Mean bias comparison.



Source: FHWA.

B. COV comparison.



Source: FHWA.

C. Resistance factor comparison.

**Figure 14. Graphs. Comparison of FORM and Monte Carlo mean bias, COV, and resistance factors for Mixed sites, unfiltered data set, and target reliability  $\beta = 2.33$ .**

Additionally, the Monte Carlo analysis utilizes the Max Load failure criterion to enable a sufficiently sized data set for estimating the resistance bias CDF. The Max Load failure criterion may introduce additional uncertainty into the analysis due to the inconsistent resistance mobilization and displacement of the data set test piles.

## **DISCUSSION**

The numerous combinations of data groups, failure criteria, design methods, side and base combinations, target reliability, and calibration methods complicate the selection of preferred resistance factors for potential application to LDOEP design. The following includes general trends observed in the resistance factor results for consideration. In general, favorable methods are considered to be good predictors of pile nominal resistance with a bias ( $\lambda$ ) close to 1.0 and low variability, as reflected in the COV value. In addition, favorable methods have a high efficiency ( $\phi/\lambda$ ). The efficiency term identifies the percentage of measured resistance available for design and reflects the relative economic value of the method. A method with a higher efficiency will result in a higher factored load, and thereby either shorter pile lengths or a fewer number of piles. The more precise (lower COV) a design method is in predicting resistances, the higher its efficiency and the more economical the method (Abu-Helje et al. 2011).

### **Resistance Factor Calibration Method**

Based on the tabulated resistance factor results and the comparisons presented in figure 9 through figure 14, the FORM method using the filtered results is most suitable for the resistance factor calibration. The filtered data are considered to reflect more representative predictions and exclude outliers that skew the summary statistics and reduce the estimated resistance factors.

The Monte Carlo resistance factors are considered to have limited applicability due to the data limitations. The Monte Carlo process requires a sufficiently sized data set that was only available for Cohesionless and Mixed sites with the Max Load failure criterion. The Max Load failure criterion reflects inconsistent resistance mobilization in the data set that potentially increases the variability. The CDF tail fitting process is also based on the unfiltered data set, including all data points. Inclusion of the outliers may affect the quality of the results; however, outliers were included consistent with Allen et al. (2005). Individual review of data outliers may be warranted for future individual Monte Carlo evaluation; however, individual data point review was not feasible in the current effort due to the quantity of calibrations performed.

### **Failure Criterion Method**

Three failure criteria were considered in the resistance factor calibration to address the variability in the shape of the load test data load displacement curves and the varying magnitudes of the load test displacements. The use of the Modified Davisson and the 5 Percent Diameter criteria enabled evaluation of the load tests using a consistent approach. Given limitations in the data, the use of these failure criteria resulted in smaller data sets, as indicated in the counts shown in table 4 and table 9 through table 19. The Max Load criterion enables consideration of all load test data in the resistance factor calibration. However, this failure criterion results in inconsistent interpretations of pile nominal resistance that are dependent on the magnitude of displacement.

Results presented in table 11 through table 25. do not show clear trends in the resistance factor calibration considering the three failure criteria. The failure criterion resulting in highest and lowest resistance factors and efficiencies varies by design method, side and base resistance combination, and site condition. A single preferred failure criterion is not identified in the analysis.

## **Trends by Site Condition**

### ***Cohesive Sites***

General resistance factor trends for Cohesive sites include:

- Resistance factors developed for the Cohesive soil sites should be considered with caution due to the small data group. In addition, the low COV values may be misleading. Instead of relating to the accuracy of the predictions, the low COV may reflect the limited variability of the data group. As discussed in the description of the load test data set, the 14 Cohesive site test piles were performed for 9 individual projects, indicating multiple projects are attributed to a single project or site. In addition, the range of pile diameters for the Cohesive sites is all less than or equal to 48 inches, which is at the low end of the range of LDOEP diameters. The limitations of the Cohesive data group should be considered for application of the resistance factor results.
- Side resistance methods are considered in combinations for this analysis (i.e., Tomlinson  $\alpha$ -method + Nordlund and Saye + Gudavalli). For uniform Cohesive sites, side resistance method combinations results are considered to primarily reflect the cohesive soil contribution, as piles in the data group have 70 percent or greater cohesive soil. Therefore, results for the Cohesive sites are considered to be applicable to the Tomlinson  $\alpha$ -method, API cohesive, Saye, and Brown cohesive methods individually instead of combined with the cohesionless methods.
- Resistance factors computed for the Tomlinson  $\alpha$ -method are greater than the currently recommended AASHTO resistance factor of 0.35.
- The mean resistance bias values are less than 1.0 for nearly all design methods, side and base resistance combinations, and failure criteria. In general, the Unplugged with Interior Side Resistance condition has the lowest mean bias values, indicating the greatest overprediction. The Unplugged Neglecting Interior Side Resistance condition typically exhibited mean bias values closest to 1.0. These results imply that inclusion of interior side resistance overestimates nominal pile resistance. The effect could be attributed to potential disturbance of the soil on the pile interior during pile driving or potential lack of setup prior to static load testing.
- The Plugged condition shows that the mean bias and efficiency values for all side resistance methods combined with the Brown base resistance method are lower than the side resistance methods combined with the AASHTO/API base resistance method. Furthermore, the COV values are greater for the Brown method. These results suggest

that the AASHTO/API method may be a better predictor of base resistance compared to the Brown method.

- In general, the highest efficiency values are observed for the Minimum of Plugged and Unplugged with Interior Side Resistance side and base resistance combination. The high efficiency values suggest this is a favorable design approach for piles in Cohesive sites.

### *Cohesionless Sites*

General resistance factor trends for Cohesionless sites include:

- Side resistance methods are considered in combinations for this analysis (i.e., Tomlinson  $\alpha$ -method + Nordlund and Saye + Gudavalli). For uniform Cohesionless sites, side resistance method combinations results are considered to primarily reflect the cohesionless soil contribution as piles in the data group have 70 percent or greater cohesionless soil. Therefore, results for the Cohesionless sites are considered to be applicable to the Nordlund, API cohesionless, Gudavalli, and Brown cohesionless methods individually instead of combined with the cohesive methods.
- Computed resistance factors for the Nordlund side resistance method are less than the currently recommended AASHTO resistance factor of 0.45.
- The Nordlund side resistance method generally showed resistance bias values in the range of about 0.5 to 0.8, indicating potentially significant overprediction. These results are consistent with commentary in Hannigan et al. (2016) that the Nordlund method tends to overpredict nominal resistance for pile diameters greater than 24 inches. The resistance bias values for the Nordlund method were generally the lowest of the cohesionless side resistance methods. Based on its poor prediction ability, the Nordlund side resistance method is considered unfavorable for LDOEP design.
- The API and Brown side resistance method results generally show resistance bias values in the range of 0.7 to 0.8 for Unplugged with Interior Side Resistance and around 1.3 for Unplugged Neglecting Interior Side Resistance. The average of these two side and base resistance design conditions would be close to 1.0. The results suggest that inclusion of reduced interior side resistance may provide a better prediction of nominal pile resistance.
- The Gudavalli side resistance method shows favorable results for all base resistance methods considering the Unplugged with Interior Side Resistance condition.
- The Gudavalli side resistance method shows significant underprediction for the Unplugged Neglecting Interior Side Resistance condition. This combination is not recommended for LDOEP design.
- The Plugged condition reflects the highest overprediction and generally lowest resistance factors and efficiency values for the Cohesionless data group. The overprediction was typically greatest for the Brown method.

- In general, the highest efficiency values are observed for the Unplugged with Interior Side Resistance and the Minimum of Plugged and Unplugged with Interior Side Resistance side and base resistance combination. The high efficiency values suggest these are favorable design approaches for piles in Cohesionless sites.

### ***Mixed and Variable Side Sites***

General resistance factor trends for Mixed and Variable Side sites include:

- Side resistance methods are considered in combinations for this analysis (i.e., Tomlinson  $\alpha$ -method + Nordlund and Saye + Gudavalli). Resistance factors developed for Mixed and Variable Side sites are specific to the side resistance method combinations.
- Similar trends in the resistance factor results are generally observed for the Variable Side + Cohesive Base and Cohesive sites along with the Variable Side + Cohesionless Base and Cohesionless sites.
- The API and Brown side resistance methods with the Unplugged Neglecting Interior Side Resistance and Minimum of Plugged and Unplugged conditions consistently resulted in favorable predictions, resistance factors, and efficiency values for the Mixed and Variable Side sites.
- The Saye + Gudavalli side resistance method with the Minimum of Plugged and Unplugged conditions consistently resulted in favorable predictions, resistance factors, and efficiency values for the Mixed and Variable Side sites.

### **Consideration of Minimum of Plugged and Unplugged with Interior Side Resistance**

The preceding discussion identifies resistance factor trends per site condition considering the various side and base resistance combinations considered in the analysis. In general, the favorable combination of side and base resistance varies within soil types, by design method, and by failure criterion. In order to develop a consistent calculation approach for all conditions, resistance factors based on the Minimum of Plugged and Unplugged with Interior Side Resistance are given additional consideration. This calculation approach, as recommended by Paikowsky and Whitman (1990), is commonly used in LDOEP design and is incorporated in API guidance (API 2011). Reviewing the results presented in table 11 through table 25, the efficiencies of the Minimum of Plugged and Unplugged with Interior Side Resistance combination are generally at the upper bound of the side and base resistance combinations, indicating the economic value of the approach.

The resistance factors and efficiency values for the Minimum of Plugged and Unplugged with Interior Side Resistance combination are presented by design method in table 26 through table 33. The tables enable a review of the range of values computed for the three failure criteria to identify trends in the resistance factors for the development of recommended values.

## Cohesive Sites

Table 26 and table 27 present resistance factors and efficiency values by side resistance methods for piles in Cohesive site conditions using the AASHTO/API and Brown base resistance methods, respectively. Due to the limited data available for Cohesive sites, the results are reviewed in conjunction with table 28 and table 29, which present the same results for Variable Side with Cohesive Base conditions. Chapter 3 and the preceding section discuss the use of this site condition to provide a larger data set that can be applied to Cohesive site conditions. In general, the resistance factors and efficiency values are lower for the Variable Side with Cohesive Base conditions compared to the Cohesive site conditions. The lower values are more reasonable and reflect a larger and more representative data set. Other observed trends and comments include:

- Similar ranges of resistance factors are observed between all side resistance methods for given base resistance methods.
- The resistance factors and efficiency factors show limited variation with failure criterion.
- Similar ranges of efficiencies are observed across the methods, implying similar economy in design regardless of the resistance factor. The Tomlinson  $\alpha$ -method generally has the highest efficiencies, and the Brown side resistance method generally has the lowest.
- Resistance factors and efficiencies are higher for all side resistance methods in conjunction with the AASHTO/API base resistance method compared to the Brown base resistance method.

**Table 26. Resistance factors and efficiency values for Cohesive sites with the Minimum of Plugged and Unplugged with Interior Side Resistance calculation approach and the AASHTO/API base resistance method.**

Term	Failure Criterion	Side Resistance Method			
		Tomlinson $\alpha$	API	Saye	Brown
Resistance factors	Modified Davisson	0.64	0.53	0.56	0.55
	5 Percent Diameter	0.69	0.54	0.60	0.54
	Max Load	0.69	0.60	0.65	0.58
Efficiency values	Modified Davisson	0.75	0.67	0.67	0.68
	5 Percent Diameter	0.84	0.68	0.75	0.67
	Max Load	0.76	0.71	0.73	0.72

**Table 27. Resistance factors and efficiency values for Cohesive sites with the Minimum of Plugged and Unplugged with Interior Side Resistance calculation approach and the Brown base resistance method.**

Term	Failure Criterion	Side Resistance Method			
		Tomlinson $\alpha$	API	Saye	Brown
Resistance factors	Modified Davisson	0.53	0.45	0.41	0.39
	5 Percent Diameter	0.54	0.46	0.42	0.42
	Max Load	0.51	0.45	0.43	0.35
Efficiency values	Modified Davisson	0.73	0.66	0.55	0.55
	5 Percent Diameter	0.73	0.67	0.58	0.56
	Max Load	0.71	0.68	0.59	0.55

**Table 28. Resistance factors and efficiency values for Variable Side with Cohesive Base sites with the Minimum of Plugged and Unplugged with Interior Side Resistance calculation approach and the Total Stress AASHTO/API base resistance method.**

Term	Failure Criterion	Side Resistance Method			
		Tomlinson $\alpha$	API	Saye	Brown
Resistance factors	Modified Davisson	0.52	0.50	0.54	0.52
	5 Percent Diameter	0.68	0.54	0.59	0.52
	Max Load	0.49	0.54	0.54	0.58
Efficiency values	Modified Davisson	0.64	0.66	0.66	0.67
	5 Percent Diameter	0.82	0.69	0.76	0.65
	Max Load	0.49	0.58	0.55	0.66

**Table 29. Resistance factors and efficiency values for Variable Side with Cohesive Base sites with the Minimum of Plugged and Unplugged with Interior Side Resistance calculation approach and the Total Stress Brown base resistance method.**

Term	Failure Criterion	Side Resistance Method			
		Tomlinson $\alpha$	API	Saye	Brown
Resistance factors	Modified Davisson	0.44	0.43	0.40	0.38
	5 Percent Diameter	0.50	0.43	0.40	0.39
	Max Load	0.41	0.40	0.44	0.38
Efficiency values	Modified Davisson	0.64	0.65	0.55	0.55
	5 Percent Diameter	0.71	0.66	0.63	0.55
	Max Load	0.53	0.55	0.60	0.54

### *Cohesionless Sites*

Table 30 through table 33 present resistance factors and efficiency values by side resistance method for piles in Cohesionless site conditions using the API, Nordlund, Gudavalli, and Brown base resistance methods, respectively. The Nordlund side resistance method is not considered further due to its poor prediction ability, as discussed in the preceding section. However, the Nordlund base resistance method is included in the tables. Observed trends and comments include:

- The design method efficiencies are lower for the Cohesionless sites design methods compared to those for Cohesive sites.
- The resistance factors and efficiency factors show limited variation with failure criteria.
- The API and Brown side resistance methods generally reflect lower resistance factors and efficiency values compared to the Gudavalli side resistance method.
- The Gudavalli method results are considered cautiously as a new, relatively untested method that is applied beyond its intended soil conditions. As described in chapter 3, the Gudavalli method was in dense sand. However, it is applied in this analysis to all cohesionless deposits.

**Table 30. Resistance factors and efficiency values for Cohesionless sites with the Minimum of Plugged and Unplugged with Interior Side Resistance calculation approach and the bearing capacity API base resistance method.**

Term	Failure Criterion	Side Resistance Method			
		Nordlund	API	Gudavalli	Brown
Resistance factors	Modified Davisson	0.31	0.57	0.33	0.31
	5 Percent Diameter	0.30	0.52	0.30	0.30
	Max Load	0.31	0.60	0.33	0.31
Efficiency values	Modified Davisson	0.39	0.50	0.45	0.39
	5 Percent Diameter	0.39	0.47	0.43	0.39
	Max Load	0.37	0.47	0.43	0.37

**Table 31. Resistance factors and efficiency values for Cohesionless sites with the Minimum of Plugged and Unplugged with Interior Side Resistance calculation approach and the Nordlund base resistance method.**

Term	Failure Criterion	Side Resistance Method			
		Nordlund	API	Gudavalli	Brown
Resistance factors	Modified Davisson	0.28	0.47	0.29	0.28
	5 Percent Diameter	0.31	0.51	0.31	0.31
	Max Load	0.31	0.61	0.32	0.31
Efficiency values	Modified Davisson	0.35	0.40	0.40	0.35
	5 Percent Diameter	0.41	0.46	0.42	0.41
	Max Load	0.37	0.48	0.42	0.37

**Table 32. Resistance factors and efficiency values for Cohesionless sites with the Minimum of Plugged and Unplugged with Interior Side Resistance calculation approach and the Gudavalli base resistance method.**

Term	Failure Criterion	Side Resistance Method			
		Nordlund	API	Gudavalli	Brown
Resistance factors	Modified Davisson	0.37	0.54	0.35	0.37
	5 Percent Diameter	0.34	0.55	0.32	0.34
	Max Load	0.39	0.59	0.38	0.39
Efficiency values	Modified Davisson	0.41	0.45	0.43	0.41
	5 Percent Diameter	0.41	0.56	0.42	0.41
	Max Load	0.41	0.46	0.44	0.41

**Table 33. Resistance factors and efficiency values for Cohesionless sites with the Minimum of Plugged and Unplugged with Interior Side Resistance calculation approach and the Brown base resistance method.**

Term	Failure Criterion	Side Resistance Method			
		Nordlund	API	Gudavalli	Brown
Resistance factors	Modified Davisson	0.31	0.54	0.32	0.31
	5 Percent Diameter	0.30	0.51	0.30	0.30
	Max Load	0.33	0.61	0.34	0.33
Efficiency values	Modified Davisson	0.44	0.49	0.46	0.44
	5 Percent Diameter	0.42	0.48	0.45	0.42
	Max Load	0.42	0.50	0.47	0.42



## CHAPTER 5. LDOEP DESIGN RECOMMENDATIONS

The development of LDOEP bearing resistance design recommendations requires consideration of the combinations of design methods and side and base resistance combinations presented herein, along with the applied failure criteria and resulting summary statistics (bias,  $\lambda$ , and COV values) and efficiency ( $\phi/\lambda$ ) values. In addition, the design recommendations are intended to enable a rational, consistent calculation approach that can be applied for all recommended methods and resistance factors. Based on the analysis, results, and discussion provided in chapter 4, the following sections summarize recommendations for the design of steel LDOEPs.

### RECOMMENDED STATIC DESIGN METHODS

Table 34 presents recommended side and base resistance static design methods for the design of steel LDOEPs. These methods were included in the resistance factor calibration and demonstrated reasonable ranges of summary statistics, resistance factors, and efficiency values in the calibration effort. The Nordlund side resistance method is not recommended for steel LDOEP evaluation due to its significant overprediction of pile resistance.

**Table 34. Recommended static design methods for the design of steel LDOEPs.**

Side Resistance		Base Resistance	
Cohesive Side	Cohesionless Side	Cohesive Base	Cohesionless Base
Tomlinson $\alpha$ -method	API $\beta$ -method	Total stress approach (AASHTO/API)	Nordlund method
API $\alpha$ -method	Gudavalli method	Brown method	Bearing capacity API method
Saye method	Brown method	—	Gudavalli method
Brown method	—	—	Brown method

—No data.

### RECOMMENDED CALCULATION APPROACH

The Minimum of Plugged and Unplugged with Interior Side Resistance combination is recommended to provide a consistent design approach suitable for all soil types and design methods. Using selected static design method(s), steel LDOEP resistance is calculated as follows:

1. Compute pile resistance assuming a Plugged pile condition. Calculate side resistance acting on the pile exterior. Calculate base resistance acting on the entire pile cross-sectional area.
2. Compute pile resistance assuming an Unplugged with Interior Side Resistance condition. Calculate side resistance acting on the pile interior and exterior. Interior side unit side resistance is equal to that acting on the pile exterior. Calculate base resistance acting on the annular pile end area only.

3. Consider nominal pile resistance equal to the minimum of (1) and (2).
4. Apply appropriate resistance factors.

### RECOMMENDED RESISTANCE FACTORS

Based on the discussion provided in chapter 4, table 35 and table 36 present recommended resistance factors for LDOEP design in Cohesive and Cohesionless site conditions. The resistance factors are for impact driven piles or piles installed with a combination of vibratory and impact driving methods. The resistance factors are specific to the combination of side and base resistance design methods, as provided in the tables, and generally reflect the lower bound values of combinations presented in table 26 through table 33. The recommended resistance factors are based on the FORM method using the filtered data.

**Table 35. Recommended resistance factors for piles in Cohesive sites using Minimum of Plugged and Unplugged with Interior Side Resistance calculation approach.**

Side Resistance Method	Base Resistance Method	Recommended Resistance Factor
Tomlinson $\alpha$	AASHTO/API	0.50
	Brown	0.40
API	AASHTO/API	0.50
	Brown	0.40
Saye	AASHTO/API	0.50
	Brown	0.40
Brown	AASHTO/API	0.50
	Brown	0.35

**Table 36. Recommended resistance factors for piles in Cohesionless sites using Minimum of Plugged and Unplugged with Interior Side Resistance calculation approach.**

Side Resistance Method	Base Resistance Method	Recommended Resistance Factor
API	API	0.30
	Nordlund	0.28
	Gudavalli	0.35
	Brown	0.30
Gudavalli	API	0.50
	Nordlund	0.45
	Gudavalli	0.50
	Brown	0.50
Brown	API	0.30
	Nordlund	0.30
	Gudavalli	0.30
	Brown	0.30

The resistance factors presented in table 35 and table 36 correspond to a target reliability  $\beta$  equal to 2.33 for redundant foundations. For nonredundant foundations, these resistance factors should be multiplied by a reduction factor of 0.8.

Resistance factors in table 35 and table 36 assume uniform Cohesive or Cohesionless site conditions. The resistance factors are differentiated for Mixed soil conditions, where the pile side and tip are in different soil types. Table 37 and table 38 present resistance factor values for independent consideration of the design methods in Mixed site conditions. The values are not calibrated, but reflect lower bound resistance factors of the combinations considered in table 35 and table 36.

Resistance factors presented in table 35 through table 37 reflect conditions of the load test data set described in chapter 3. Other considerations, such as the duration of pile setup and the influence of partial vibratory installation, may affect the measured nominal pile resistance. Unfortunately, limitations in load test details and the number of available load tests prevent the consideration of such influences on pile resistance. The analysis and resistance factors presented herein reflect the best effort LDOEP resistance factor calibration, accounting for known limitations in the load test data set.

**Table 37. Recommended resistance factors for side resistance of piles in Mixed sites using Minimum of Plugged and Unplugged with Interior Side Resistance calculation approach.**

Soil Type	Side Resistance Methods	Recommended Resistance Factor
Cohesive	Tomlinson $\alpha$	0.40
	API	0.40
	Saye	0.40
	Brown	0.35
Cohesionless	API	0.30
	Gudavalli	0.45
	Brown	0.30

**Table 38. Recommended resistance factors for base resistance of piles in Mixed sites using Minimum of Plugged and Unplugged with Interior Side Resistance calculation approach.**

Soil Type	Base Resistance Methods	Recommended Resistance Factor
Cohesive	AASHTO/API	0.50
	Brown	0.35
Cohesionless	API	0.30
	Nordlund	0.30
	Gudavalli	0.30
	Brown	0.30

## RECOMMENDED FAILURE CRITERIA

The resistance factor calibration considered the Modified Davisson, 5 Percent Diameter, and Max Load failure criteria. Evaluation of the load test data considered in this analysis and the resistance factor calibration results yielded no singular most favorable failure criterion for the evaluation of pile nominal resistance. Due to their nonsubjective nature, ease of use, and applicability to large diameter piles, the Modified Davisson and 5 Percent Diameter failure criteria are recommended for the evaluation of LDOEP nominal resistance. The nominal resistances determined from the two methods should be compared and considered in relation to the associated top of pile displacement. The final recommended value should be selected in conjunction with project owners and design team members.

The Max Load criterion was considered in this analysis due to the varying levels of displacement in the load test data set that limited the applicability of the other failure criteria. As described in chapter 3, use of the Max Load criterion enabled the consideration of the full load test data set in the resistance factor calibration. However, the Max Load failure criterion is generally not

recommended for the evaluation of LDOEP nominal resistance. The criterion is dependent on the magnitude of the load test displacement and does not provide a consistent approach to determine the pile nominal resistance.

## **FUTURE RESEARCH**

This study performed a comprehensive resistance factor calibration of select static design methods for steel LDOEPs. However, in many instances, the research was constrained by limitations in the available load test data set. Additionally, the research focused on predictive methods for bearing resistance, but was unable to evaluate actual LDOEP behavior. There are numerous future research needs related to LDOEPs, with many identified in NCHRP Synthesis 478 (Brown and Thompson 2015). The following presents a list of research needs directly related to the work presented herein:

- The current study excluded concrete cylinder LDOPs from the resistance factor calibration due to the limited available concrete LDOEP static load test data. A greater volume of static load tests is needed for concrete LDOEPs to enable similar resistance factor calibration, as performed in this study.
- The available static load test data limited the ability to develop resistance factors using the Monte Carlo method for all site conditions. Additionally, the available static load test data limited the effectiveness of the resistance factor calibrations for steel LDOEPs at cohesive sites. Additional load tests are needed for steel LDOEPs in both cohesive and cohesionless site conditions.
- The current research did not identify a single, appropriate failure criterion for steel LDOEPs due to variable, and at times limited, displacement mobilization of the static load test data set. Additional load tests are needed that are conducted to large pile displacements.
- Preliminary analysis performed as part of the project compared nominal resistance determined from dynamic testing with signal matching to static load test results. As described in chapter 1, the preliminary analysis was limited by insufficient available dynamic load test data, and resistance factor calibration was not performed. Additional dynamic testing should be performed in conjunction with static load testing to enable future dynamic testing resistance factor calibration. Dynamic testing with signal matching of LDOEPs should consider appropriately sized pile driving hammers to mobilize the full nominal pile resistance. Additionally, the setup time for dynamic pile testing with signal matching should be similar to that of a static load test to enable a comparison of the static and dynamic load tests.
- Instrumented static load test data are needed to evaluate LDOEP behavior and pile plugging mechanisms. As noted above, this research focused on predictive static design methods. Additional instrumented, full-scale static load test data is needed to enable the differentiation of pile side and base resistance and pile plugging mechanisms.



## **APPENDIX A. RESISTANCE FACTOR CALIBRATION LOAD TEST DATA SET**

Appendix A provides an overview of the load test data set used in the resistance factor calibration. Table 39 summarizes the load tests, including details of the test location, site conditions, pile dimensions, test loads and displacements, and nominal resistances determined by the failure criteria. Figure 15 through figure 80 present the corresponding force displacement curves for each load test. The nominal resistances are indicated in the plots for applicable failure criteria.

**Table 39. Resistance factor calibration load test data set: load test nominal resistance.**

Subsurface Conditions	Project	Project Name	Pile Designation	Diameter (inch)	Length (ft)	Max Force (kips)	Max Displ. (inch)	Modified Davisson		5 Percent Diameter		Max Load	
								Nominal Resist. (kips)	Displ. (inch)	Nominal Resist. (kips)	Displ. (inch)	Nominal Resist. (kips)	Displ. (inch)
Cohesive	1006	I-880 Port of Oakland Connector Viaduct (Caltrans Bridge No. 33-0612E)	TP-9	42.0	88.3	1,245	-1.38	—	—	—	—	1,245	-0.7
	1007	I-880 Oakland Bridge Replacement	Pile3-H	42.0	105.5	1,209	-1.24	—	—	—	—	1,209	-0.5
	1009	Noto Peninsula New Highway Route Bridges (Japan)	TP-1	31.5	36.1	1,057	-7.79	1,051	-1.4	1,048	-1.6	1,057	-1.5
	1009	Noto Peninsula New Highway Route Bridges (Japan)	TP-2	31.5	36.1	832	-1.30	832	-1.3	—	—	832	-1.3
	1010	Pentre Site	TP-NC	30.0	191.9	1,349	-4.22	1,227	-2.8	1,330	-1.5	1,349	-1.4
	1021	Annacis Throughway Bridge Project – Highway 91	TP-D67m	36.0	220.8	1,693	-3.72	1,569	-2.8	1,655	-1.8	1,693	-2.0
	1031	Gulf Intracoastal Waterway West Closure Complex Test Site 1	TP-3	30.0	160.5	830	-4.50	830	-2.0	830	-1.5	830	-0.8
	1031	Gulf Intracoastal Waterway West Closure Complex Test Site 1	TP-4	30.0	170.3	1,060	-4.50	1,060	-2.3	1,060	-1.5	1,060	-1.2
	1031	Gulf Intracoastal Waterway West Closure Complex Test Site 1	TP-5	30.0	161.0	900	-4.59	900	-2.1	900	-1.5	900	-0.9
	1031	Gulf Intracoastal Waterway West Closure Complex Test Site 1	TP-6	30.0	150.0	830	-4.48	830	-1.9	830	-1.5	830	-0.9
	1024	Gulf Intracoastal Waterway West Closure Complex Test Site 3	TP-11	30.0	190.0	1,215	-4.60	1,188	-2.7	1,172	-1.5	1,215	-4.6
	1063	Port of Oakland Connector Viaduct Maritime On/Off-Ramps (Caltrans Bridge No. 33-612E)	TP3-10NCI	42.0	98.0	845	-3.50	832	-1.7	825	-2.1	845	-0.7
	1063	Port of Oakland Connector Viaduct Maritime On/Off-Ramps (Caltrans Bridge No. 33-612E)	TP6-17NCI	42.0	103.0	1,037	-0.83	—	—	—	—	1,037	-0.6
1072	Tilbrook Grange Site	TP-OC	30.0	109.9	3,619	-4.02	3,400	-2.4	3,486	-1.5	3,619	-1.1	
Cohesionless	1002	Red Sea Coast, Saudi Arabia	TP-A1	56.0	216.5	1,397	-3.94	1,341	-2.8	1,340	-2.8	1,397	-3.9
	1002	Red Sea Coast, Saudi Arabia	TP-A2	56.0	239.5	1,454	-3.94	1,403	-2.9	1,397	-2.8	1,454	-3.9
	1008	Santa Clara River Bridge (Caltrans Bridge No. 52-0449)	Test-1	84.0	68.7	1,995	-8.10	1,959	-3.0	1,930	-4.2	1,995	-1.0
	1008	Santa Clara River Bridge (Caltrans Bridge No. 52-0449)	Test-2	84.0	134.0	8,000	-4.10	7,702	-3.8	—	—	8,000	-4.1
	1013	Hokkaido, Japan	TP-1	40.0	134.5	3,552	-3.84	3,531	-3.2	3,187	-2.0	3,552	-2.3
	1014	Chiba, Japan	TP-2	31.5	157.5	1,888	-2.78	—	—	1,655	-1.6	1,888	-2.4
	1019	EURIPIDES Joint Industry Project – offshore test piles	TP-1.1	29.9	100.9	2,653	-10.27	1,690	-1.5	1,692	-1.5	2,653	-10.3
	1019	EURIPIDES Joint Industry Project – offshore test piles	TP-1.3	29.9	155.0	5,202	-15.33	3,883	-2.8	3,429	-1.5	5,202	-10.3
	1019	EURIPIDES Joint Industry Project – offshore test piles	TP-2	29.9	154.0	5,195	-13.57	3,929	-2.8	3,589	-1.5	5,195	-13.6
	1019	EURIPIDES Joint Industry Project – offshore test piles	TP-2	29.9	154.0	6,708	-2.59	—	—	4,553	-1.5	6,708	-2.6
	1020	Sakonnet River Bridge (Route 138)	TestPile	72.0	136.2	2,990	-2.85	—	—	—	—	2,990	-2.9
	1023	Berenda Slough Bridge (Caltrans Bridge No. 41-0009R)	TestPile	42.0	106.0	1,618	-1.85	—	—	—	—	1,618	-1.9
	1027	Seal Beach Blvd OC (Caltrans Bridge No. 55-1099)	TP-2A2	48.0	112.5	3,003	-0.88	—	—	—	—	3,003	-0.9
	1056	Mad River Bridge (Caltrans Bridge No. 04-0025L)	TestPile	87.0	136.4	7,191	-11.02	6,405	-3.8	6,494	-4.4	7,191	-8.7
	1057	Russian River Bridge (Caltrans Bridge No. 10-0301)	TestPile	66.0	120.7	3,200	-1.30	—	—	—	—	3,200	-1.3
	1058	San Joaquin River Bridge (Caltrans Bridge No. 41-90)	TestPile	74.5	188.5	8,012	-2.15	—	—	—	—	8,012	-2.2
	1059	Colorado River Bridge (Caltrans Bridge No. 54-1272)	TestPile	108.0	127.0	8,000	-0.97	—	—	—	—	8,000	-1.0
	1060	Russian River Bridge (Caltrans Bridge No. 20-38)	TestPile	48.0	143.3	3,975	-5.20	3,600	-3.1	3,445	-2.4	3,975	-5.2
	1061	Feather River Bridge (Caltrans Bridge No. 18-0026R)	TP-1	90.0	136.0	4,090	-8.00	3,721	-3.5	3,805	-4.5	4,090	-8.0
	1061	Feather River Bridge (Caltrans Bridge No. 18-0026R)	TP-2	90.0	202.0	8,000	-3.00	—	—	—	—	8,000	-3.0
1062	Santa Clara River Bridge (Caltrans Bridge No. 53-2925)	TestPile	72.0	128.7	8,045	-6.17	7,175	-3.5	7,211	-3.6	8,045	-6.2	
1068	Port of Toamasina Offshore Jetty	12A	40.0	213.3	2,029	-2.60	—	—	2,002	-2.0	2,029	-2.6	
1068	Port of Toamasina Offshore Jetty	4B	40.0	213.3	2,205	-1.38	—	—	—	—	2,205	-1.4	
1069	Trans-Tokyo Bay Highway	TP-1	78.7	203.4	7,945	-8.20	—	—	2,002	-2.0	7,945	-8.2	
1070	Legislative Route 795 section B-6 Philadelphia, PA	TP-C	30.0	64.2	1,499	-1.31	—	—	—	—	1,499	-1.3	
1070	Legislative Route 795 section B-6 Philadelphia, PA	TP-E	30.0	96.0	1,436	-4.15	882	-1.7	879	-1.5	1,436	-4.2	

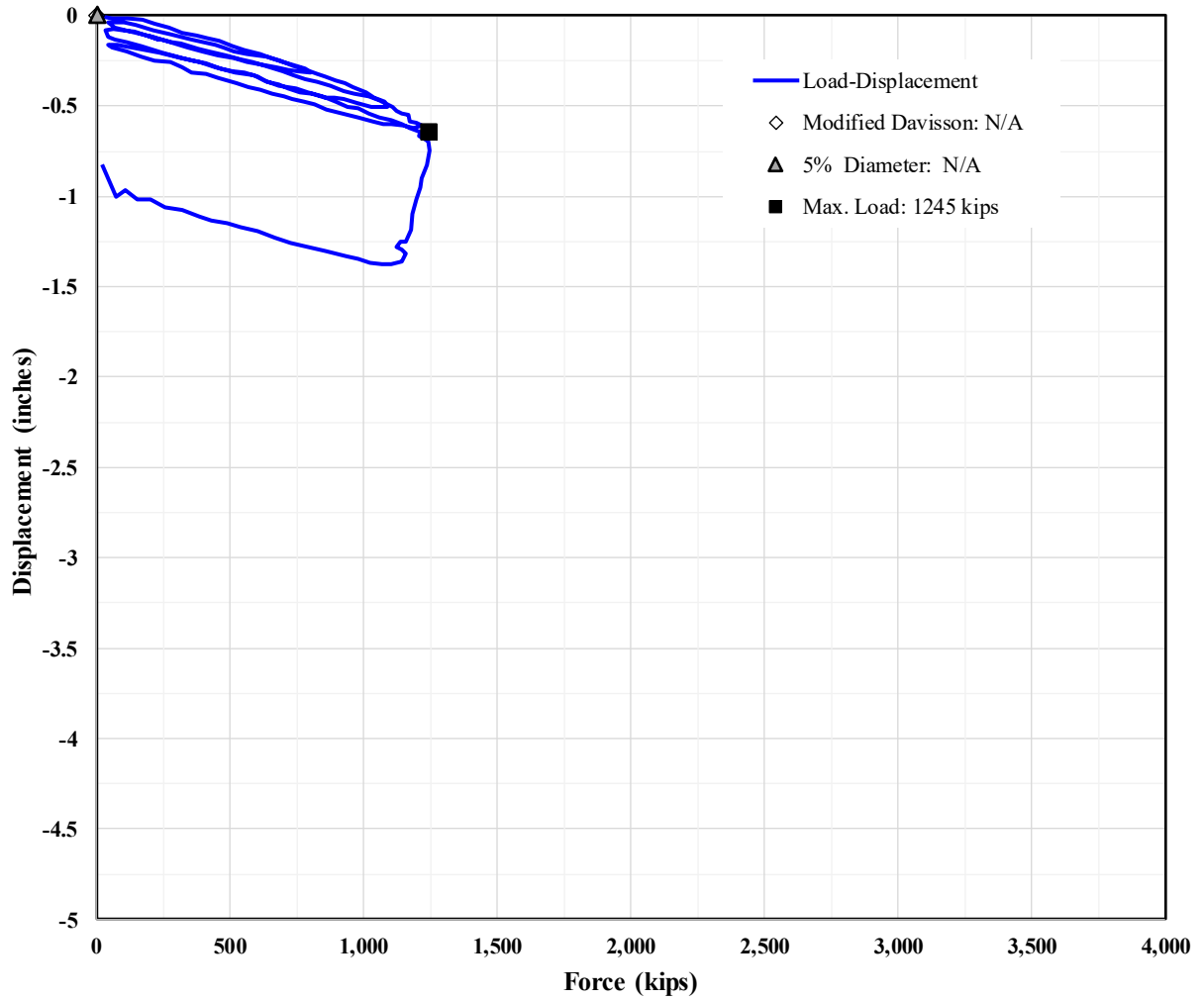
Subsurface Conditions	Project	Project Name	Pile Designation	Diameter (inch)	Length (ft)	Max Force (kips)	Max Displ. (inch)	Modified Davisson		5 Percent Diameter		Max Load		
								Nominal Resist. (kips)	Displ. (inch)	Nominal Resist. (kips)	Displ. (inch)	Nominal Resist. (kips)	Displ. (inch)	
Mixed	Side: Cohesive Base: Cohesionless	1003	Louisiana Highway 1 Improvements Load Test Data Phase 1B	T-3-1	30.0	1,597	-3.23	1,597	-3.2	1,365	-1.5	1,597	-3.2	
		1025	I-880 5th Street Overhead Bridge (Caltrans Bridge No. 33-27)	TestPile	96.0	136.6	6,742	-8.86	6,625	-4.0	6,679	-4.8	6,742	-8.9
		1063	Port of Oakland Connector Viaduct Maritime On/Off-Ramps (Caltrans Bridge No. 33-612E)	TP9-27NCI	42.0	97.0	1,288	-1.21	—	—	—	—	1,288	-0.7
		1067	Port Said	TP-22	28.0	167.3	899	-1.25	—	—	—	—	899	-1.3
		1067	Port Said	TP-136	28.0	167.3	899	-1.19	—	—	—	—	899	-1.2
	Side: Cohesionless Base: Cohesive	1011	Woodrow Wilson Bridge over Potomac River, VA and MD, USA	PL-3	36.0	96.3	1,764	-0.75	—	—	—	—	1,764	-0.5
		1055	Feather River Bridge (Caltrans Bridge No. 18-0009)	Pile-3	48.0	173.1	2,500	-3.60	2,430	-2.8	2,363	-2.4	2,500	-3.6
		1071	Nippon Steel Corporation/Blast Furnace Foundations in Japan	BF-61	47.2	75.6	1,834	-0.78	—	—	—	—	1,834	-0.8
		1071	Nippon Steel Corporation/Blast Furnace Foundations in Japan	H-27	47.2	69.7	2,518	-0.92	—	—	—	—	2,518	-0.9
		1071	Nippon Steel Corporation/Blast Furnace Foundations in Japan	HS-40	47.2	63.2	1,469	-1.68	—	—	—	—	1,469	-1.7
	Side: Mixed Base: Cohesive	1001	Port Mann Bridge	TestPile	72.0	245.7	12,061	-6.59	—	—	10,071	-3.6	12,061	-6.6
		1011	Woodrow Wilson Bridge over Potomac River, VA and MD, USA	PL-1	54.0	165.2	2,925	-2.68	—	—	2,783	-2.7	2,925	-2.3
		1071	Nippon Steel Corporation/Blast Furnace Foundations in Japan	HS-97	47.2	82.0	1,822	-0.94	—	—	—	—	1,822	-0.9
	Side: Mixed Base: Cohesionless	1004	Tokyo Port Bay Bridge	TP-4	59.1	260.8	7,194	-10.08	6,070	-5.2	5,100	-3.0	7,194	-10.1
		1004	Tokyo Port Bay Bridge	TP-5	59.1	301.8	8,093	-9.24	7,474	-6.6	6,422	-3.0	8,093	-9.2
		1005	Salinas River Bridge (Caltrans Bridge No. 44-216R/L)	TestPile	72.0	118.0	1,513	-0.96	—	—	—	—	1,513	-1.0
		1011	Woodrow Wilson Bridge over Potomac River, VA and MD, USA	PL-2	42.0	125.5	2,920	-2.68	—	—	2,783	-2.7	2,920	-1.7
		1012	Jin Mao Building	ST-1	36.0	262.5	3,698	-9.98	3,398	-5.4	2,679	-1.8	3,698	-9.5
		1012	Jin Mao Building	ST-2	36.0	262.5	4,073	-7.63	3,892	-6.0	3,007	-1.8	4,073	-7.3
		1022	Pitt River Bridge	Pile-P5	71.8	333.0	10,029	-3.26	—	—	—	—	10,029	-3.3
1026		I-405 and SR-22 HOV Connector Separation Bridge (Caltrans Bridge No. 55-1103E)	TP-9	48.0	75.0	1,772	-4.08	1,706	-2.1	1,724	-2.4	1,772	-3.8	
1026		I-405 and SR-22 HOV Connector Separation Bridge (Caltrans Bridge No. 55-1103E)	TP-10	48.0	100.0	2,600	-5.31	2,470	-2.5	2,480	-2.4	2,600	-1.0	
1035		Highway 32 Stony Creek Bridge (Caltrans Bridge No. 11-0029)	TP-6	99.6	169.9	7,859	-10.51	6,637	-4.1	6,381	-4.8	7,859	-1.7	
1070	Legislative Route 795 section B-6 Philadelphia, PA	TP-D	30.0	86.2	896	-2.74	882	-1.7	879	-1.5	896	-2.7		
1071	Nippon Steel Corporation/Blast Furnace Foundations in Japan	BF-47	47.2	87.8	1,827	-0.89	—	—	—	—	1,827	-0.9		

1 inch = 25.4 mm; 1 ft = 0.305 m; 1 kip = 4,448.2216 N.

—No data.

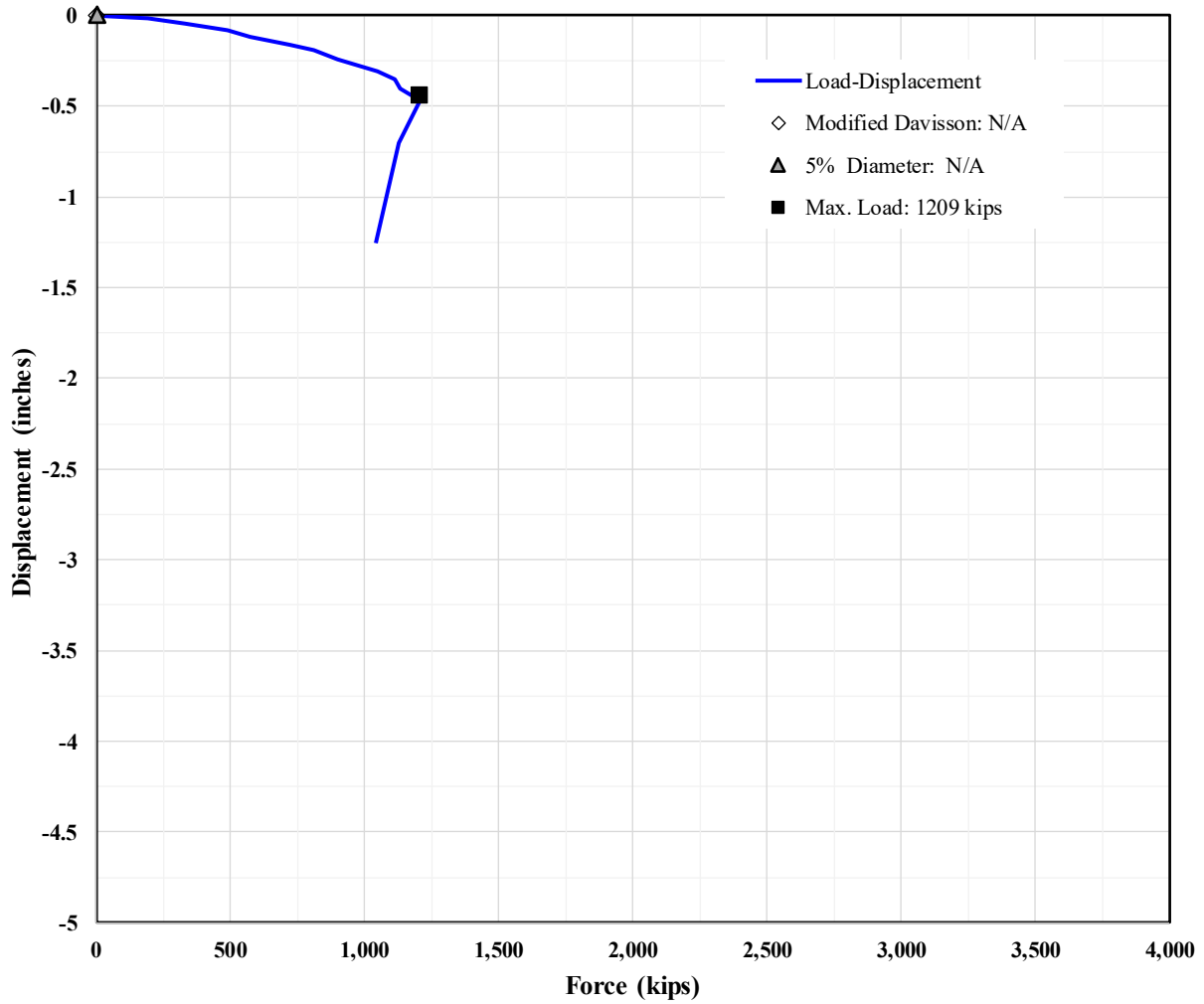
Displ. = Displacement; Resist. = Resistance.

Note: Table formatted for 11x17 printing.



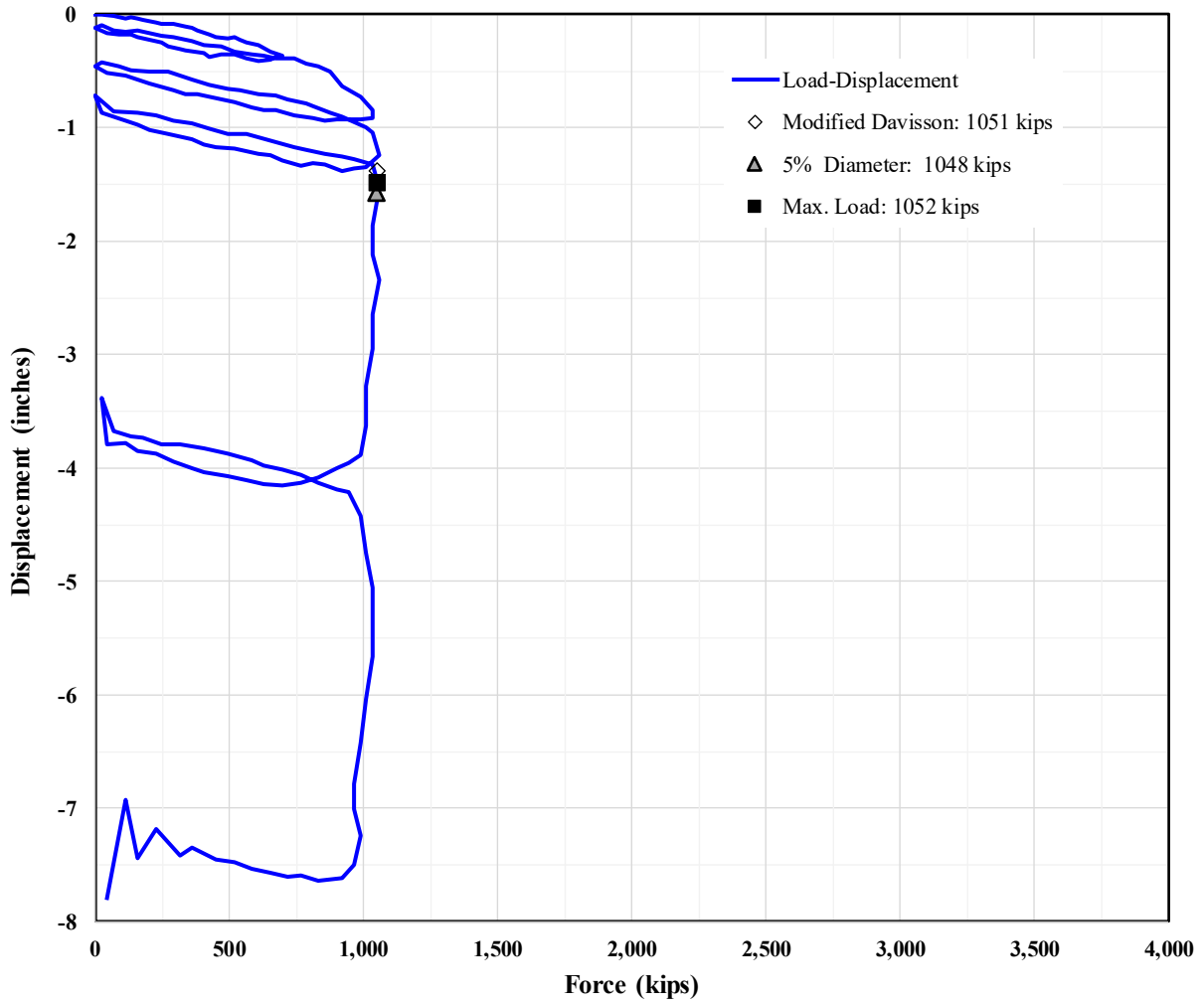
Source: FHWA.  
 1 inch = 25.4 mm; 1 kip = 4,448.2216 N.

**Figure 15. Graph. Force displacement curve. Project: I-880 Port of Oakland Connector Viaduct (Caltrans Bridge No. 33-0612E). Pile designation: TP-9.**



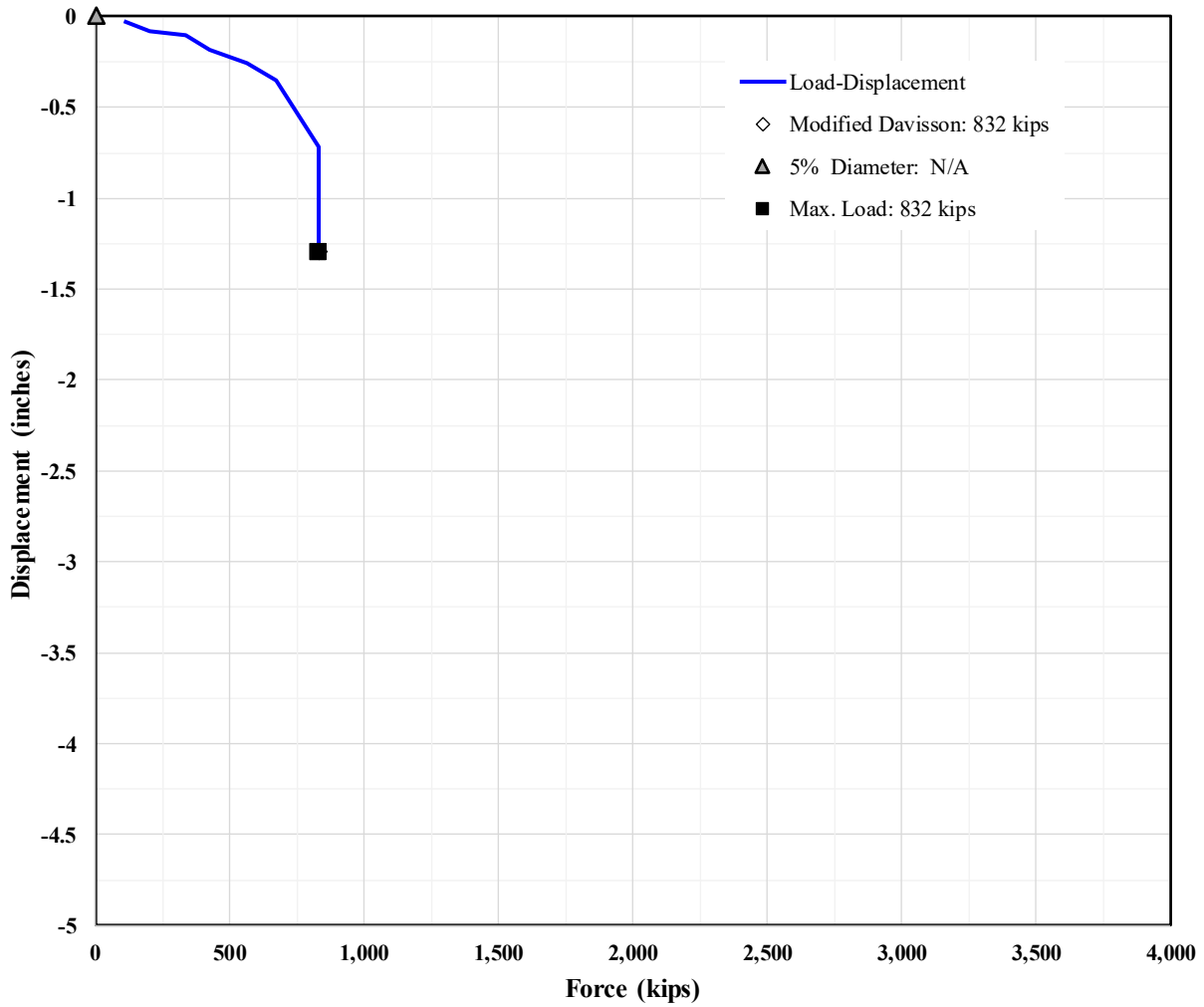
Source: FHWA.  
 1 inch = 25.4 mm; 1 kip = 4,448.2216 N.

**Figure 16. Graph. Force displacement curve. Project: I-880 Oakland Bridge Replacement.  
 Pile designation: Pile 3-H.**



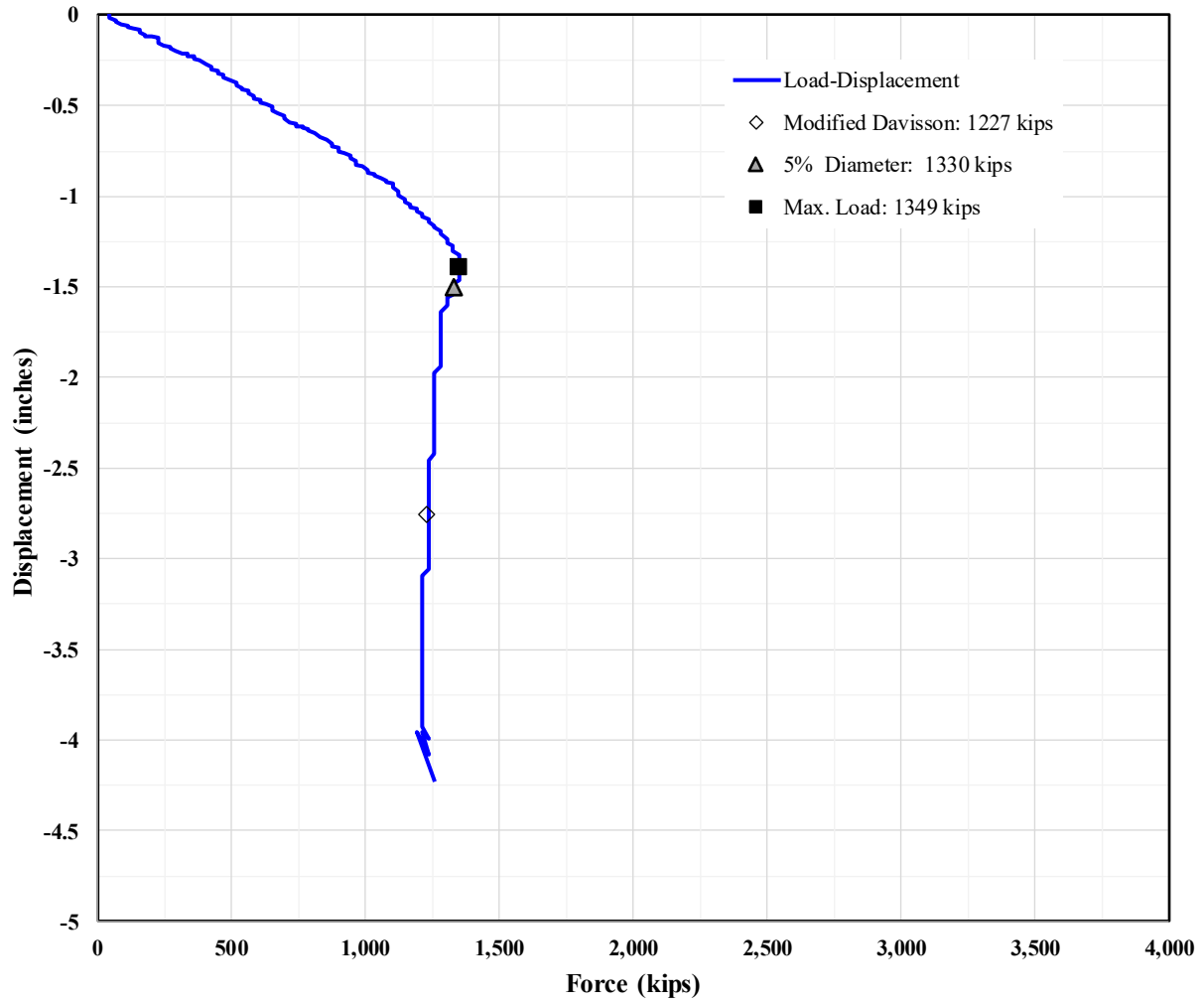
Source: FHWA.  
 1 inch = 25.4 mm; 1 kip = 4,448.2216 N.

**Figure 17. Graph. Force displacement curve. Project: Noto Peninsula New Highway Route Bridges (Japan). Pile designation: TP-1.**



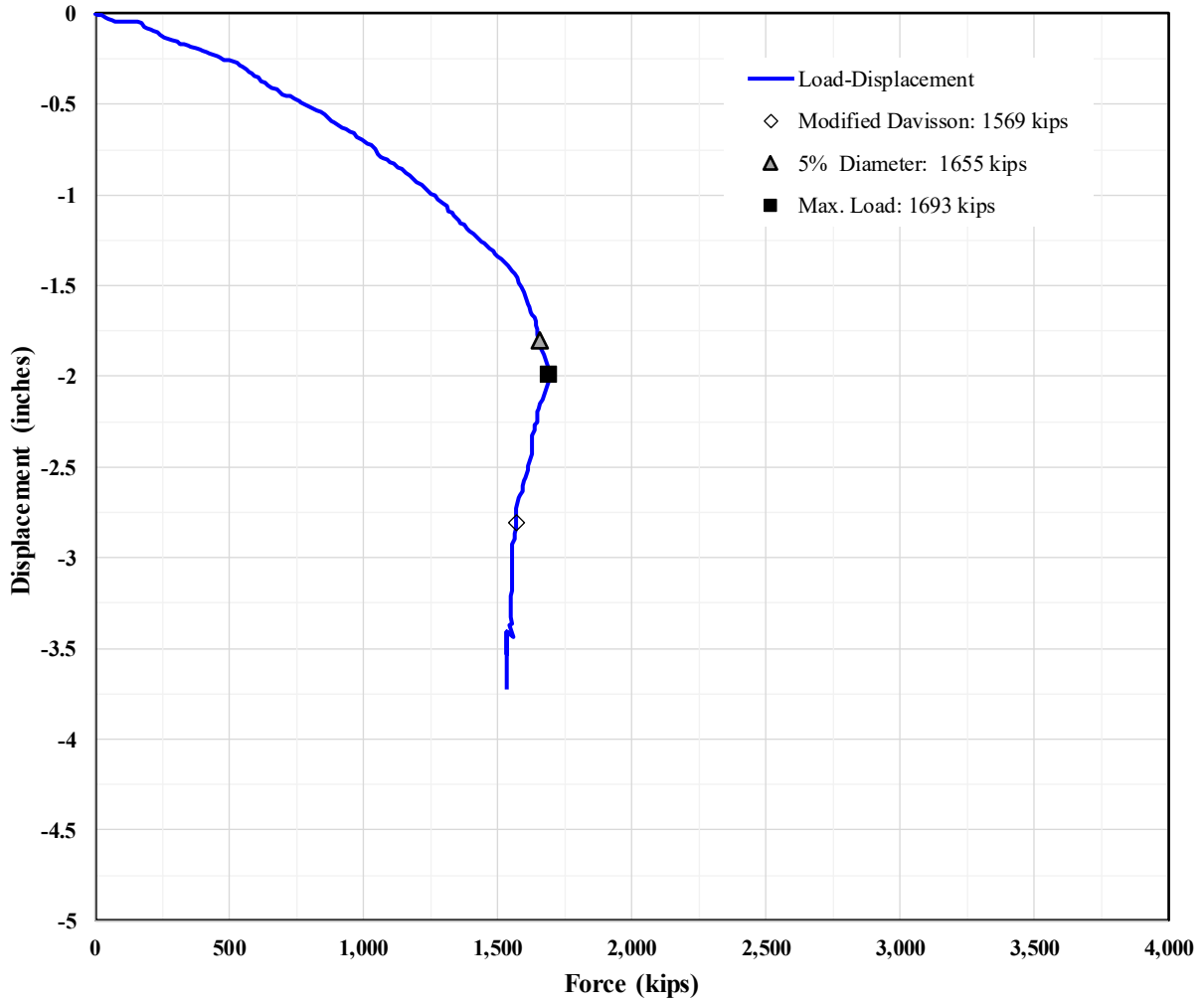
Source: FHWA.  
 1 inch = 25.4 mm; 1 kip = 4,448.2216 N.

**Figure 18. Graph. Force displacement curve. Project: Noto Peninsula New Highway Route Bridges (Japan). Pile designation: TP-2.**



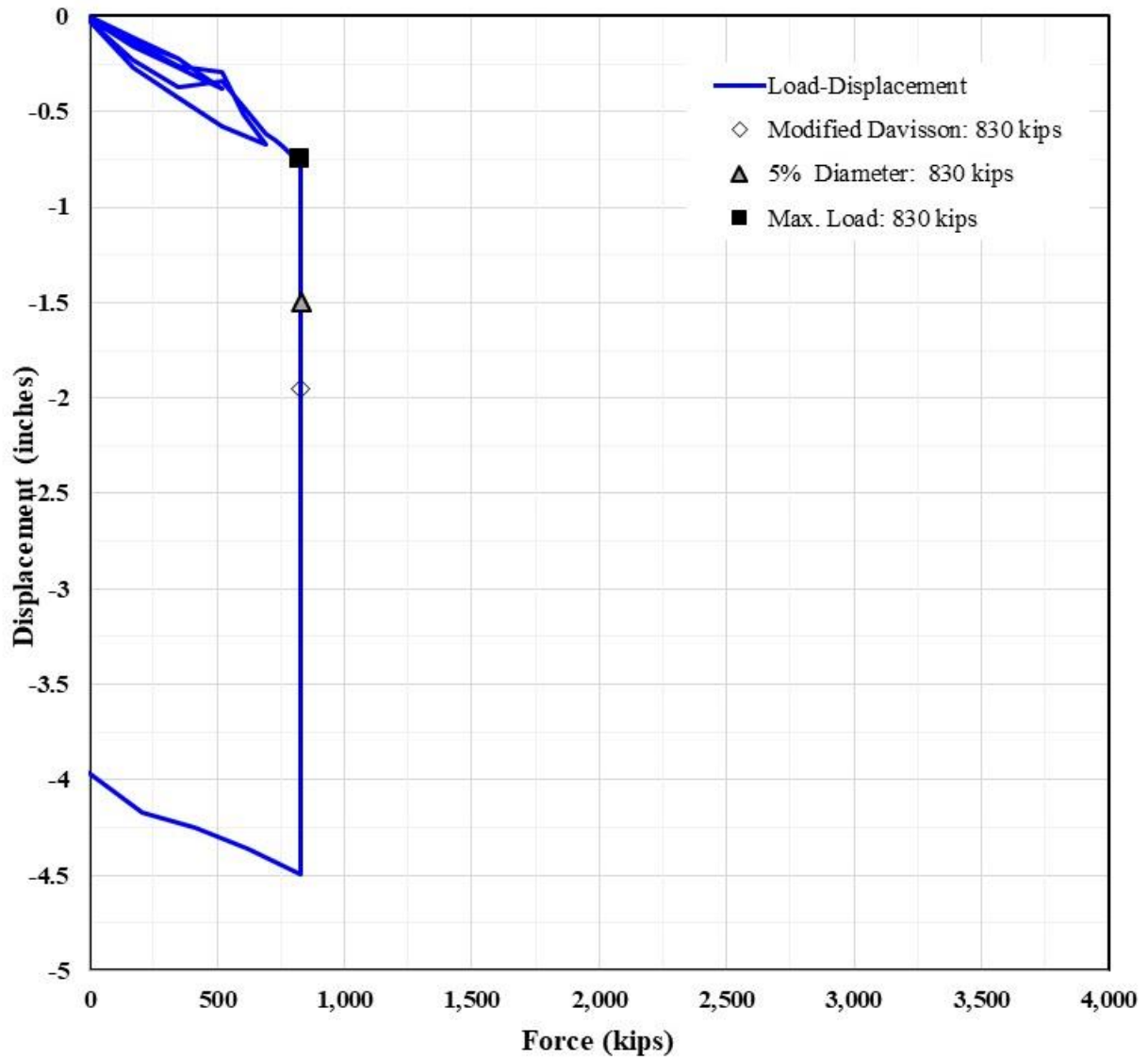
Source: FHWA.  
 1 inch = 25.4 mm; 1 kip = 4,448.2216 N.

**Figure 19. Graph. Force displacement curve. Project: Pentre Site. Pile designation: TP-NC.**



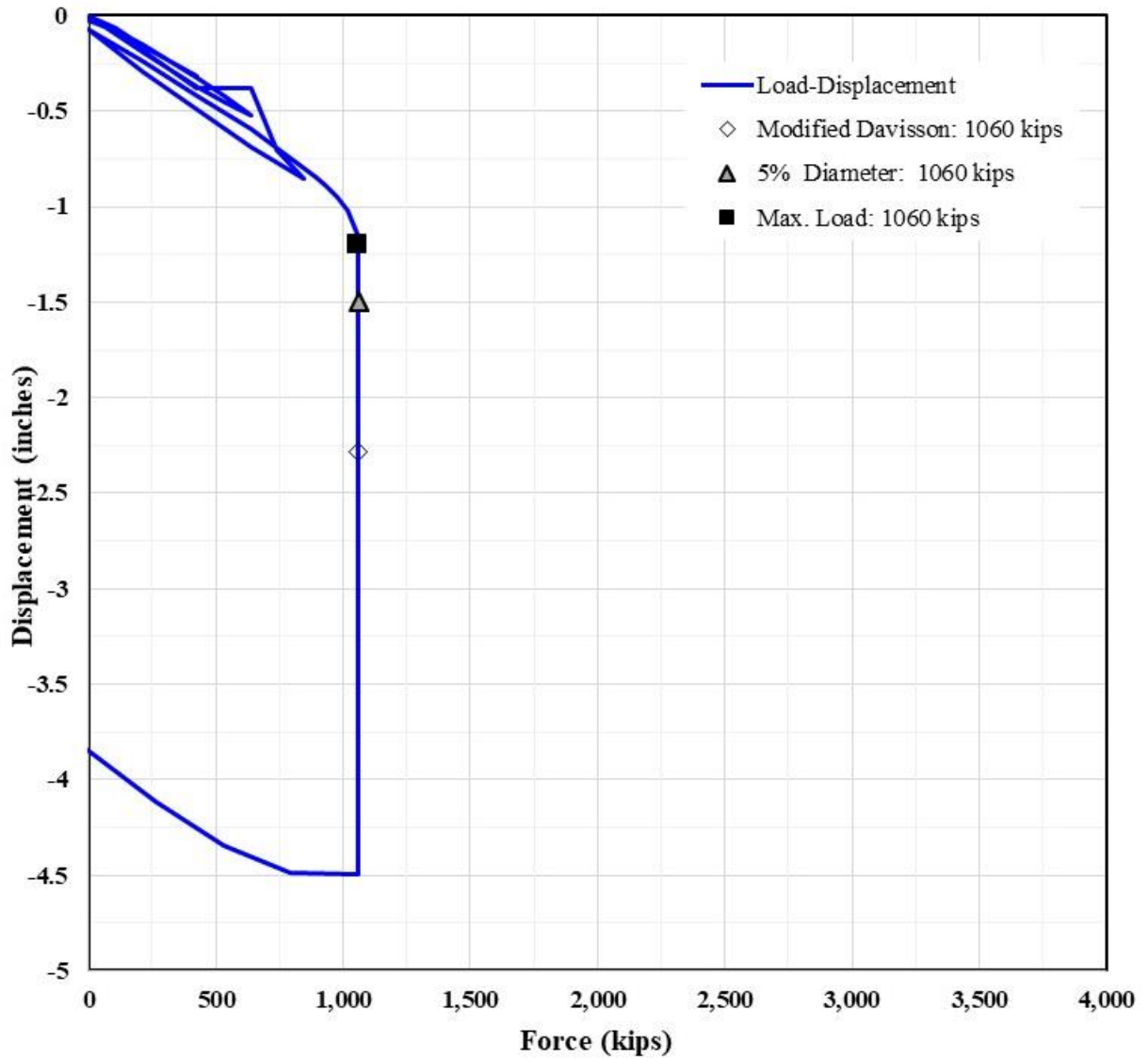
Source: FHWA.  
 1 inch = 25.4 mm; 1 kip = 4,448.2216 N.

**Figure 20. Graph. Force displacement curve. Project: Annacis Throughway Bridge Project – Highway 91. Pile designation: TP-D67m.**



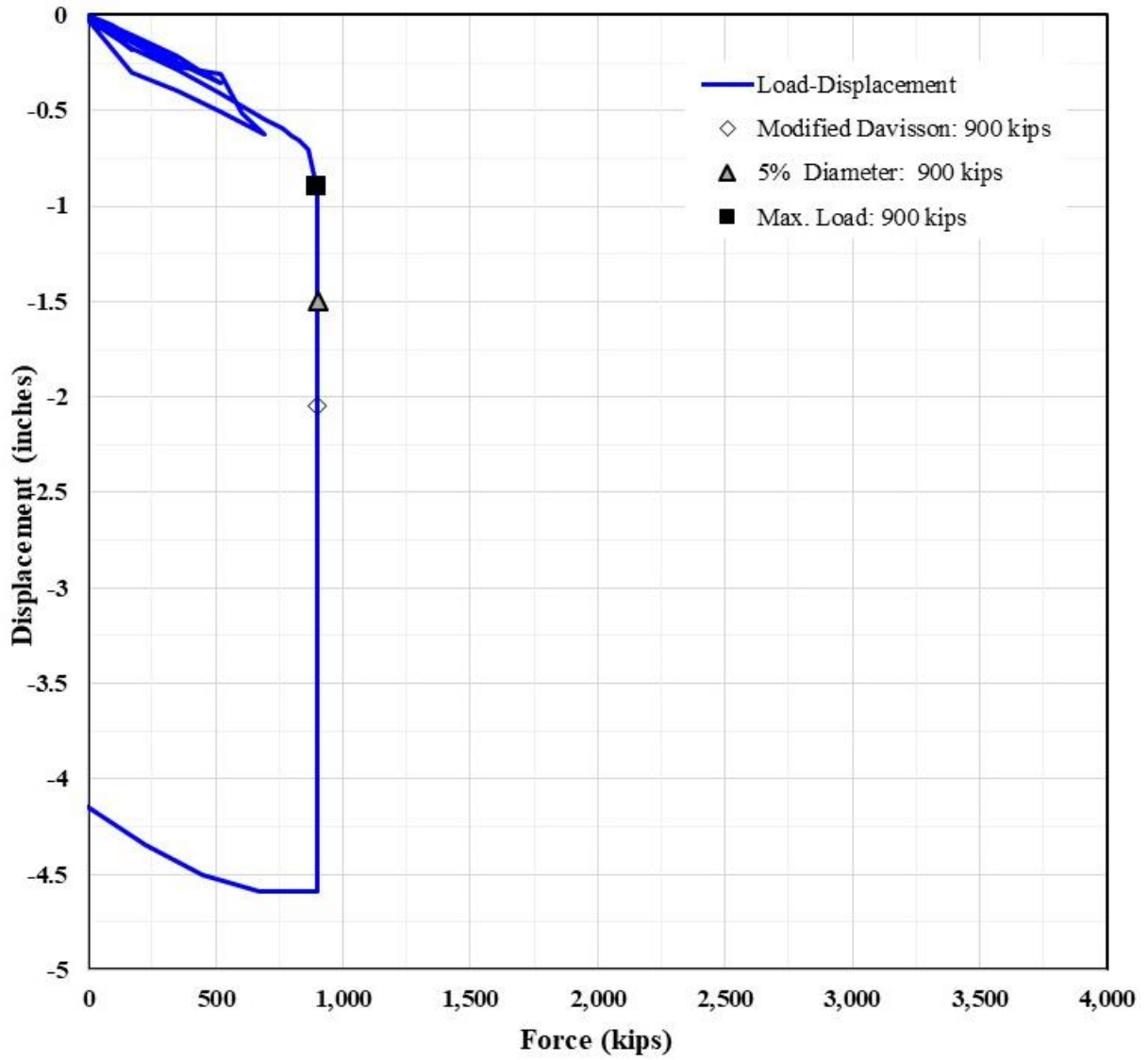
Source: FHWA.  
 1 inch = 25.4 mm; 1 kip = 4,448.2216 N.

**Figure 21. Graph. Force displacement curve. Project: Gulf Intracoastal Waterway West Closure Complex Test Site 1. Pile designation: TP-3.**



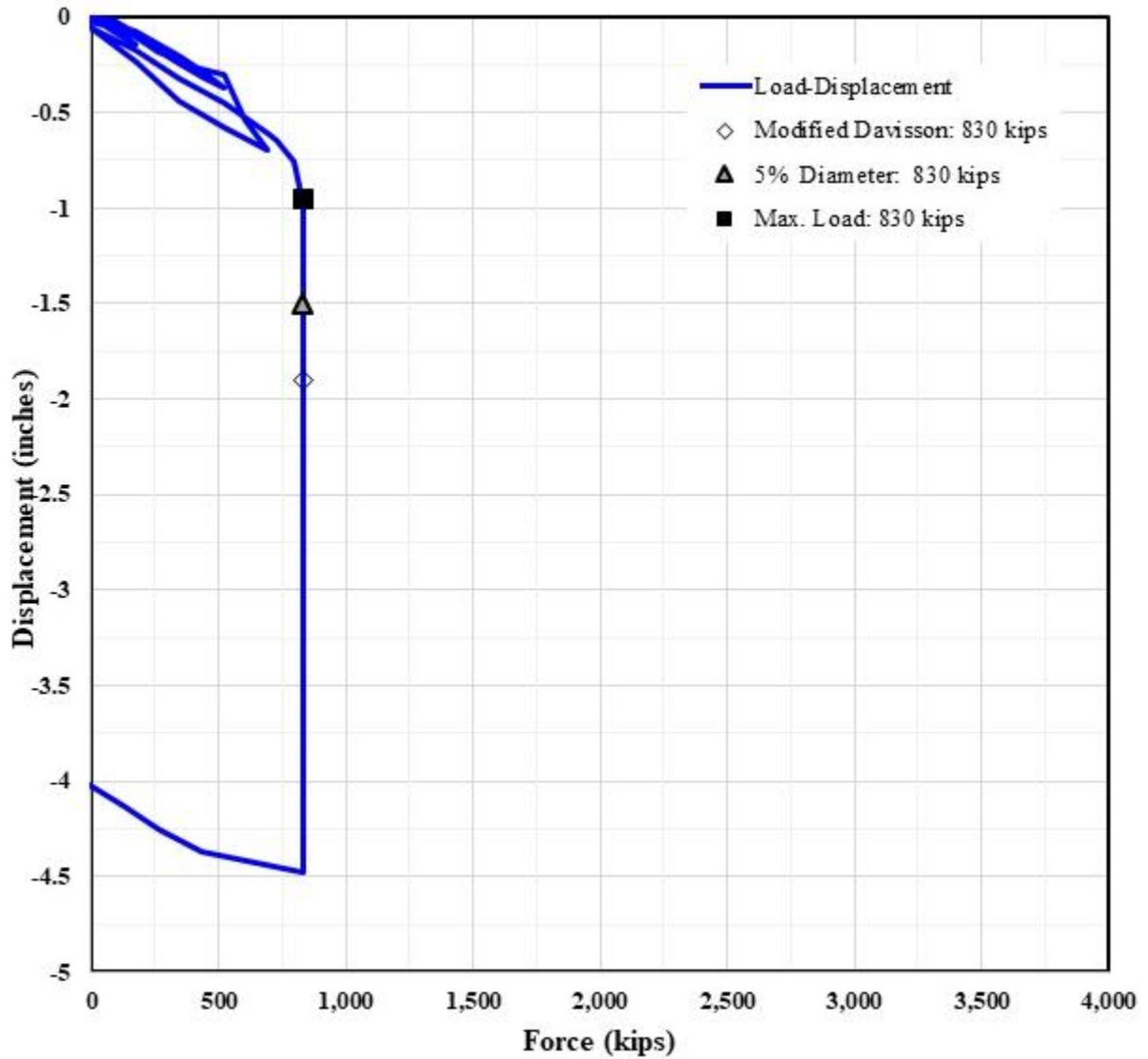
Source: FHWA.  
 1 inch = 25.4 mm; 1 kip = 4,448.2216 N.

**Figure 22. Graph. Force displacement curve. Project: Gulf Intracoastal Waterway West Closure Complex Test Site 1. Pile designation: TP-4.**



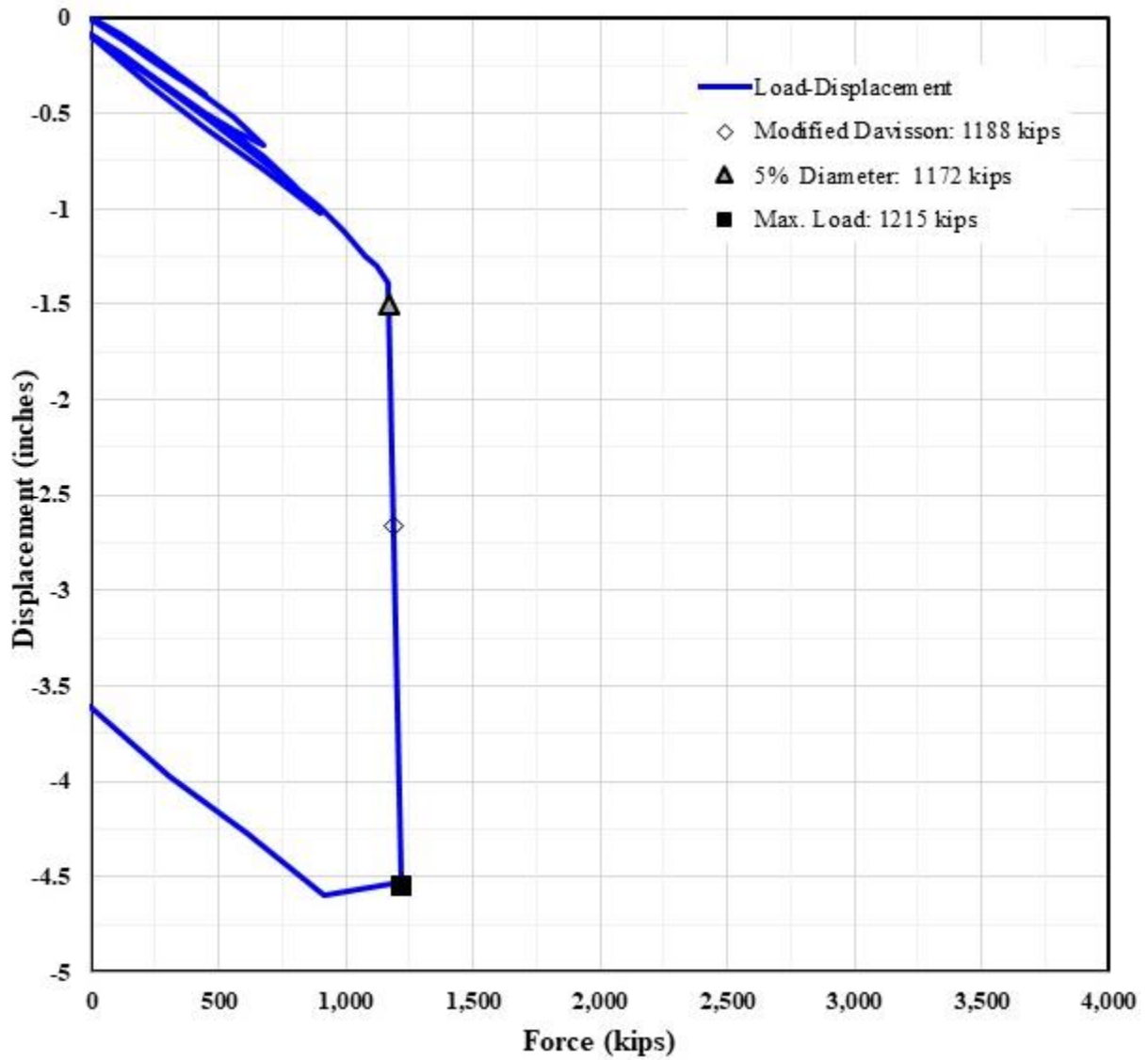
Source: FHWA.  
 1 inch = 25.4 mm; 1 kip = 4,448.2216 N.

**Figure 23. Graph. Force displacement curve. Project: Gulf Intracoastal Waterway West Closure Complex Test Site 1. Pile designation: TP-5.**



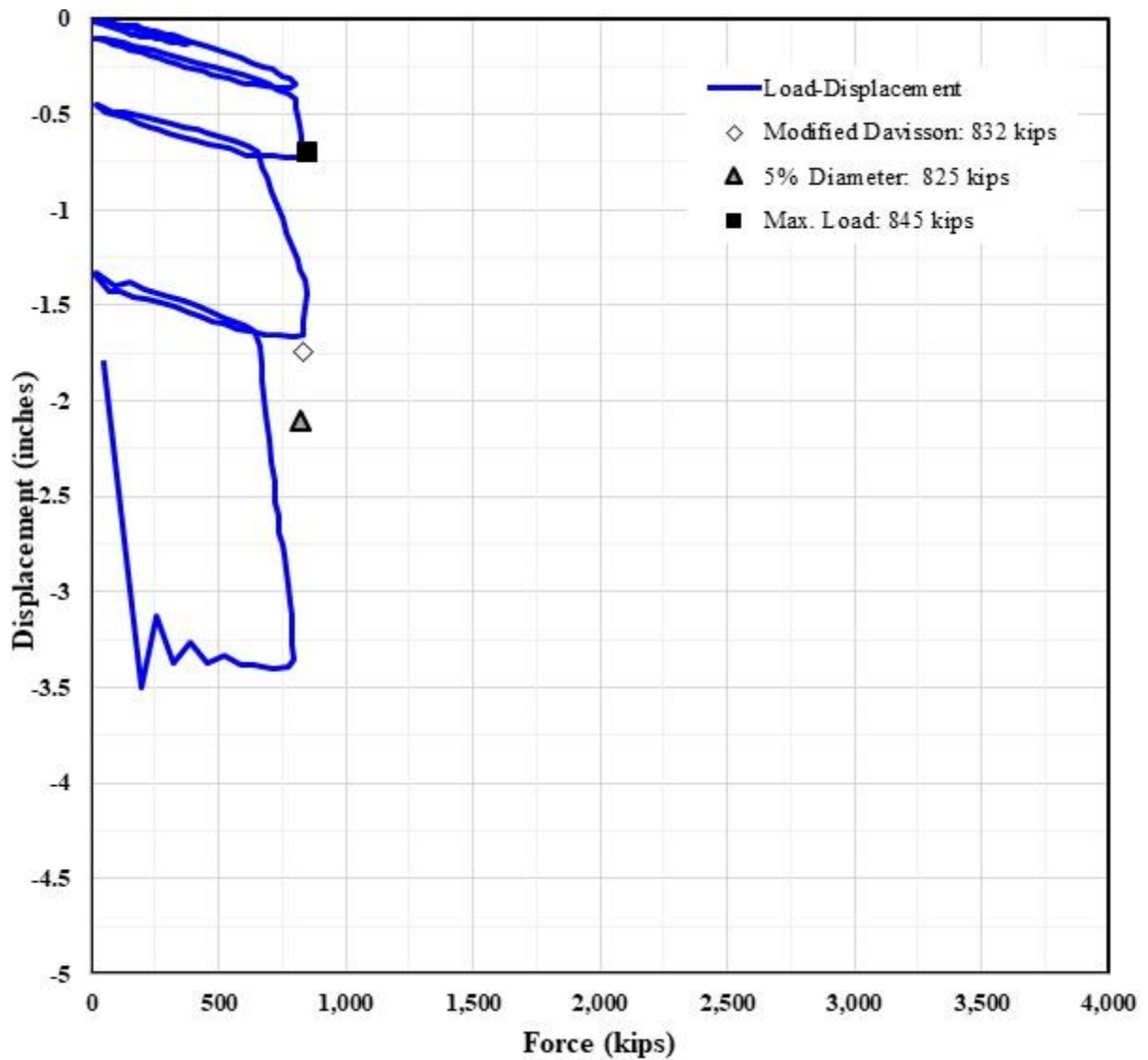
Source: FHWA.  
 1 inch = 25.4 mm; 1 kip = 4,448.2216 N.

**Figure 24. Graph. Force displacement curve. Project: Gulf Intracoastal Waterway West Closure Complex Test Site 1. Pile designation: TP-6.**



Source: FHWA.  
 1 inch = 25.4 mm; 1 kip = 4,448.2216 N.

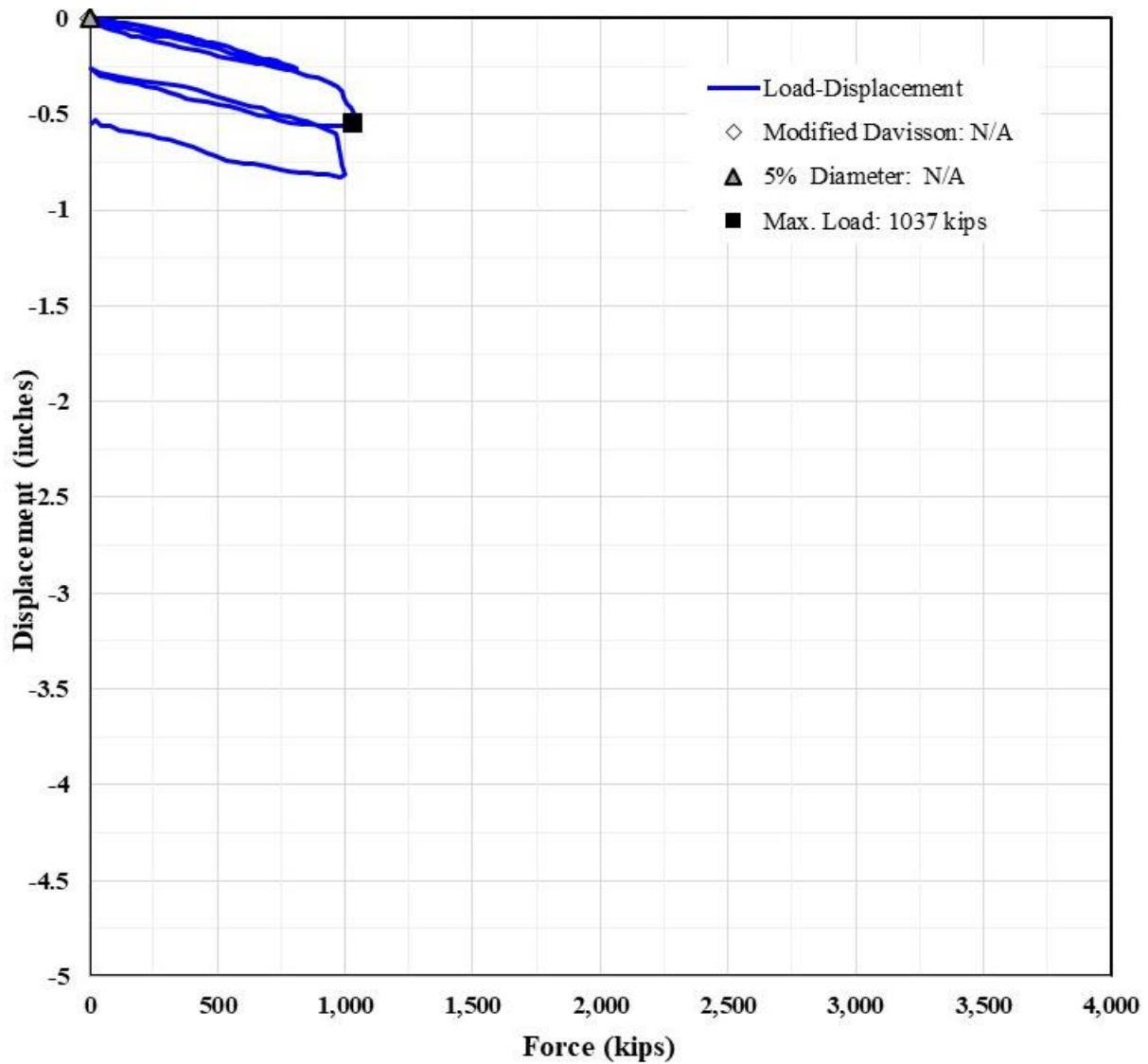
**Figure 25. Graph. Force displacement curve. Project: Gulf Intracoastal Waterway West Closure Complex Test Site 3. Pile designation: TP-11.**



Source: FHWA.

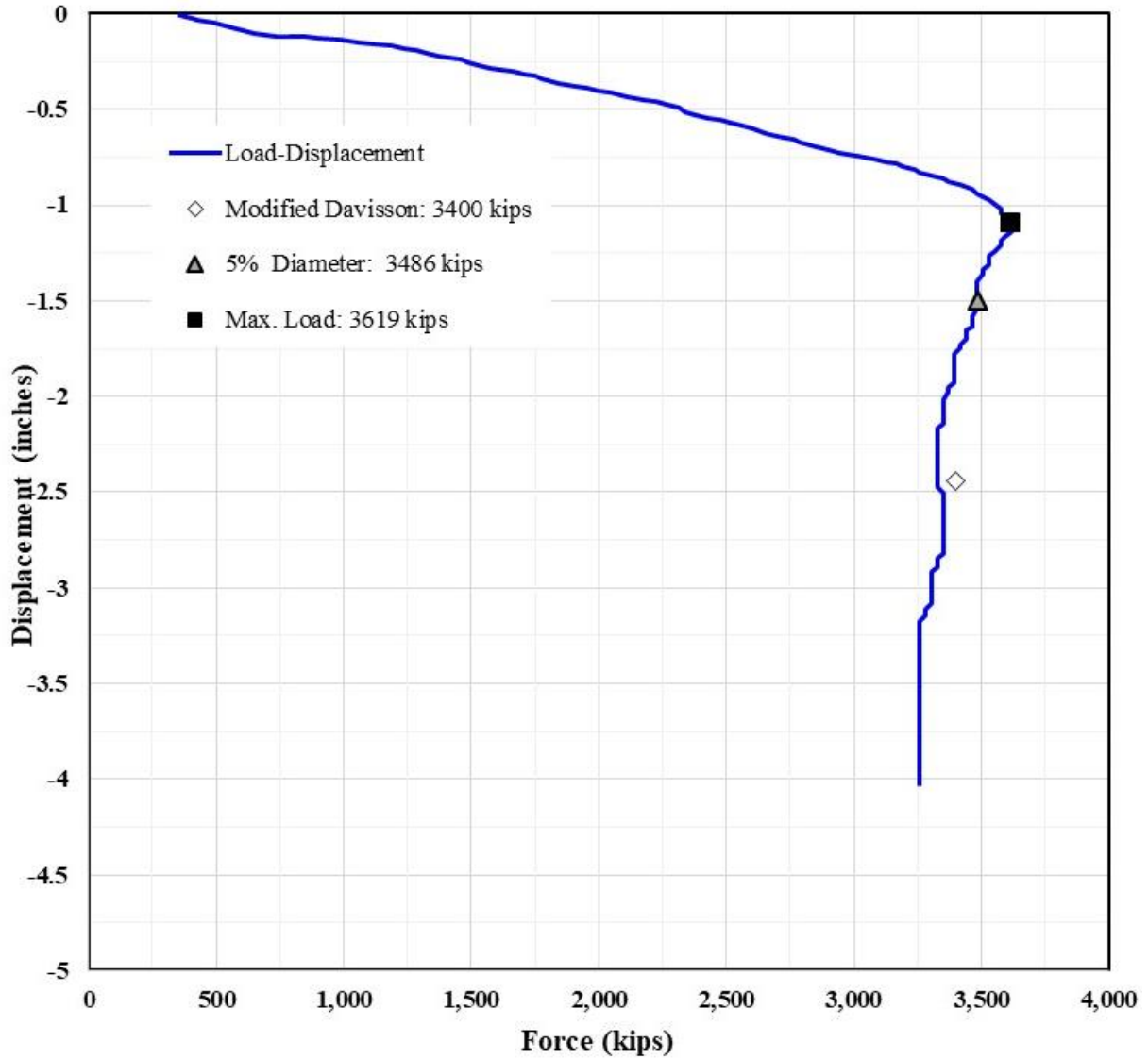
1 inch = 25.4 mm; 1 kip = 4,448.2216 N.

**Figure 26. Graph. Force displacement curve. Project: Port of Oakland Connector Viaduct Maritime On/Off-Ramps (Caltrans Bridge No. 33-612E). Pile designation: TP3-10NCI.**



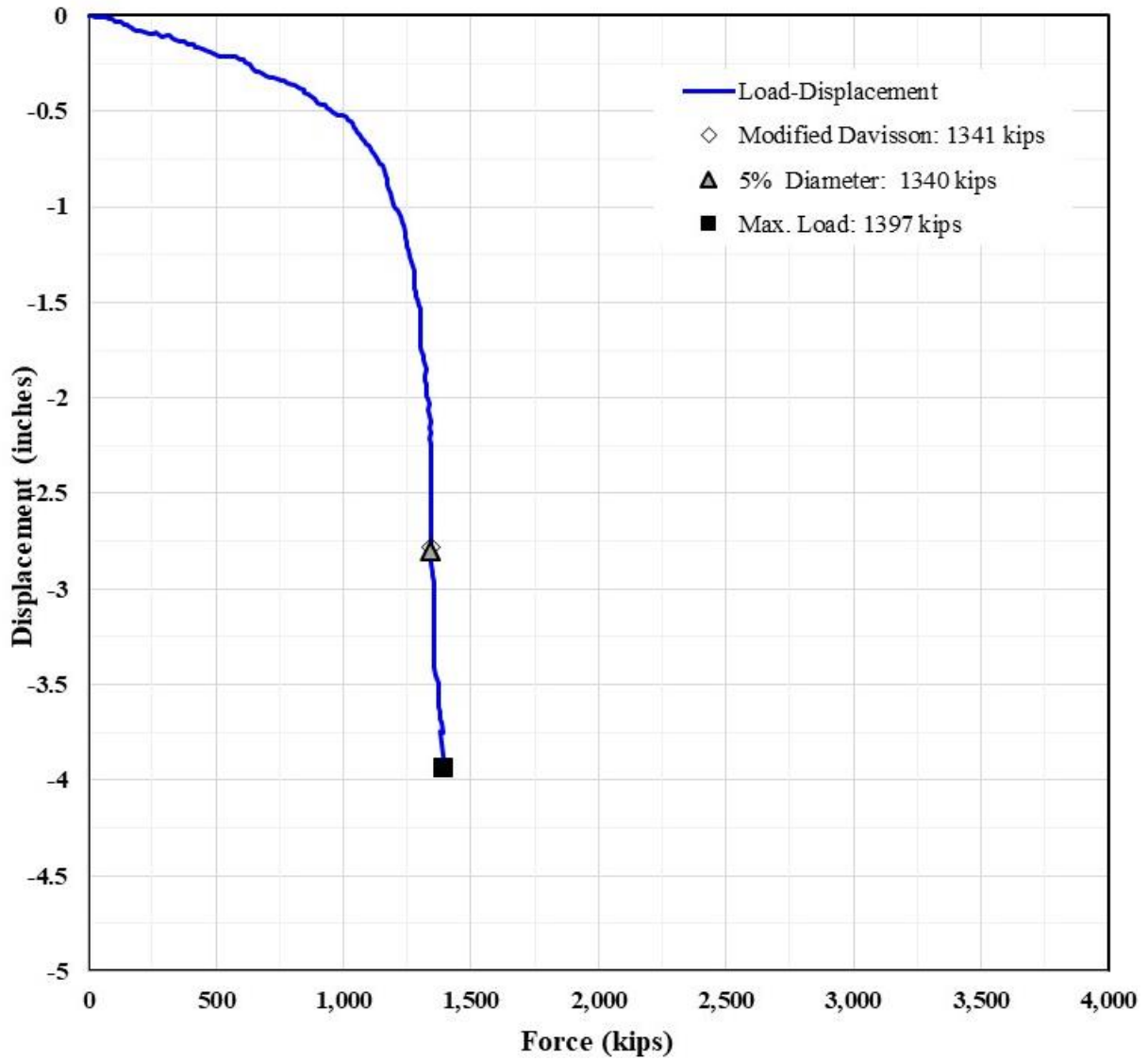
Source: FHWA.  
 1 inch = 25.4 mm; 1 kip = 4,448.2216 N.

**Figure 27. Graph. Force displacement curve. Project: Port of Oakland Connector Viaduct Maritime On/Off-Ramps (Caltrans Bridge No. 33-612E). Pile designation: TP6-17NCL.**



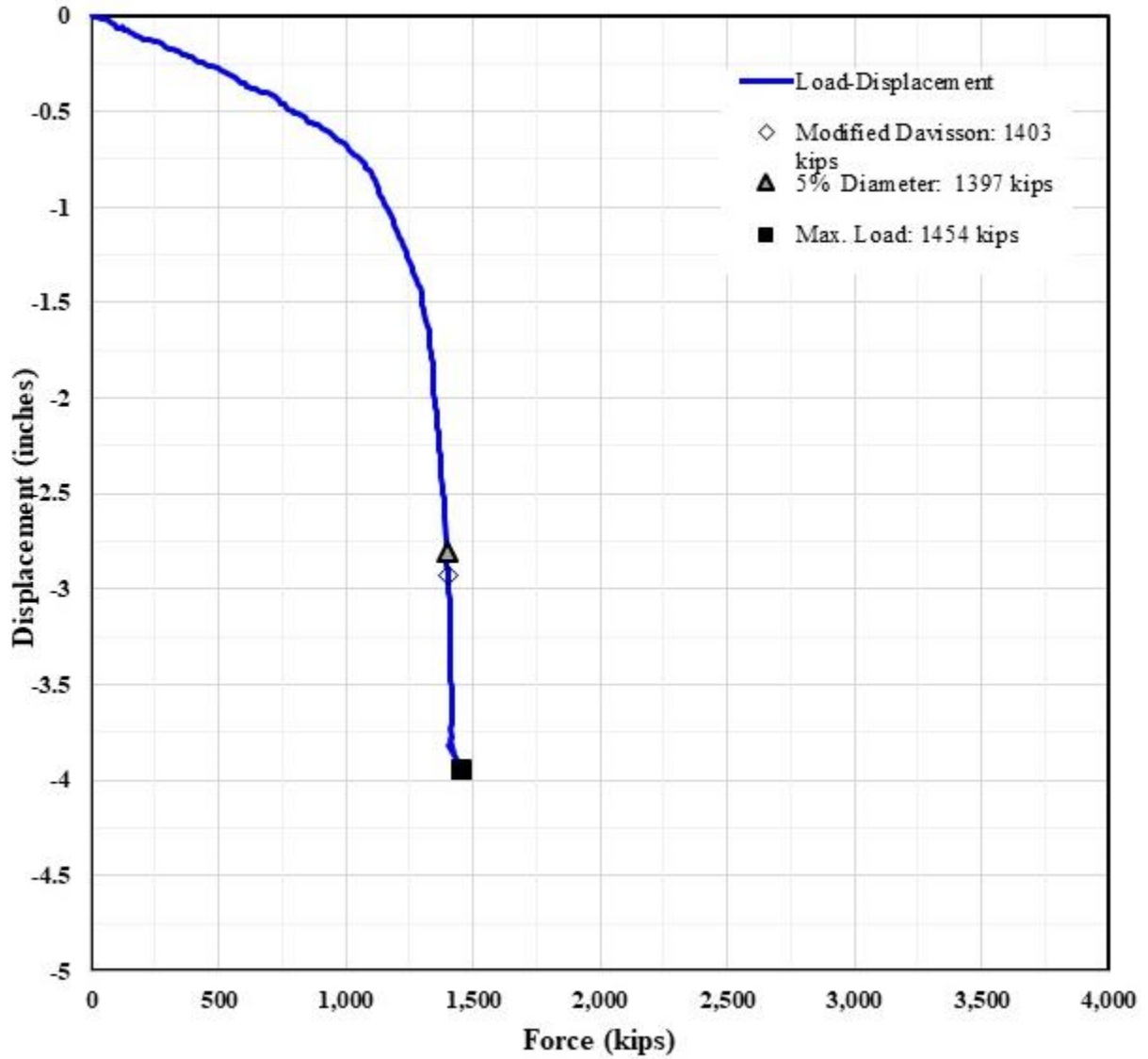
Source: FHWA.  
 1 inch = 25.4 mm; 1 kip = 4,448.2216 N.

**Figure 28. Graph. Force displacement curve. Project: Tilbrook Grange Site.  
 Pile designation: TP-OC.**



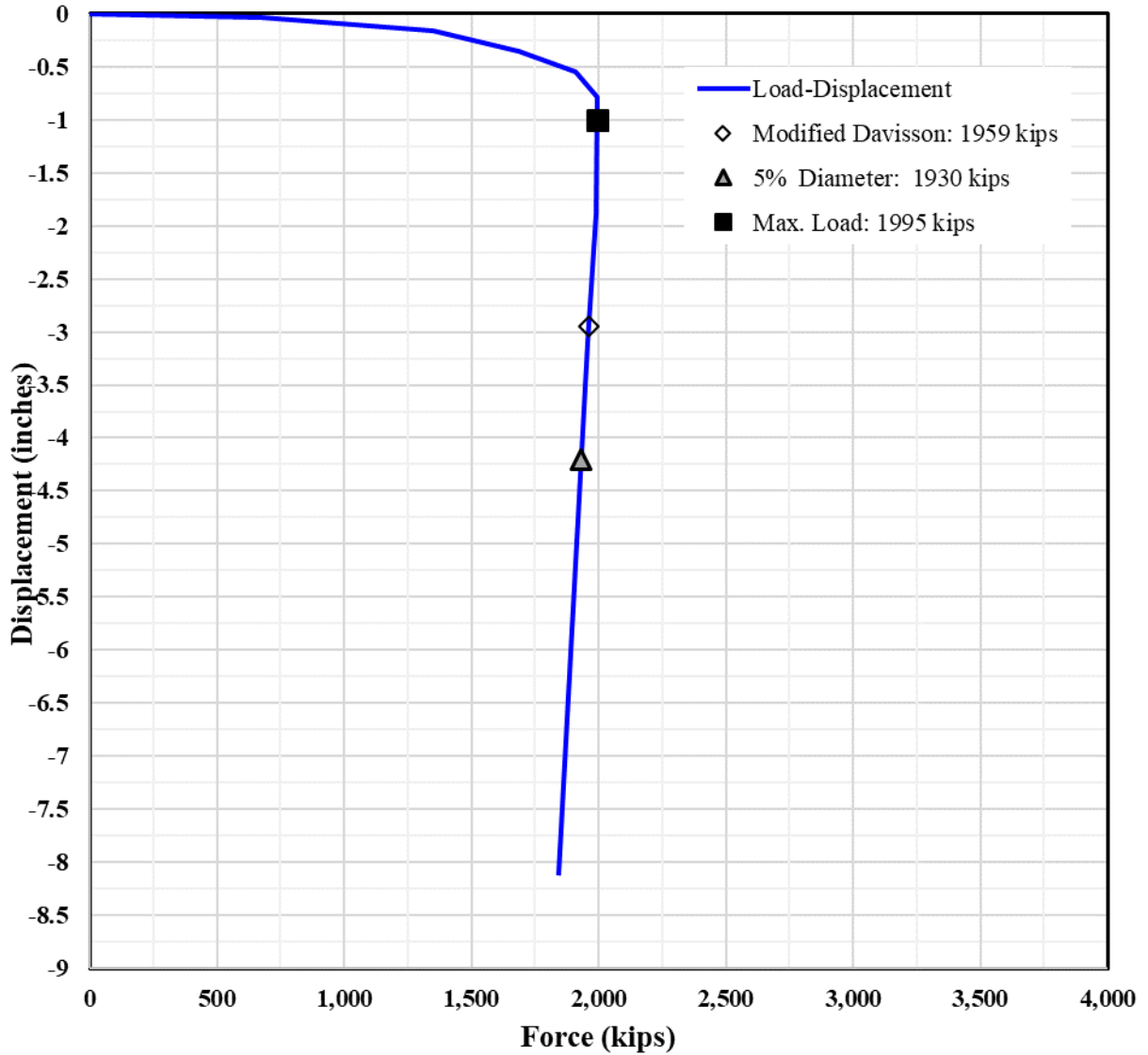
Source: FHWA.  
 1 inch = 25.4 mm; 1 kip = 4,448.2216 N.

**Figure 29. Graph. Force displacement curve. Project: Red Sea Coast, Saudi Arabia. Pile designation: TP-A1.**



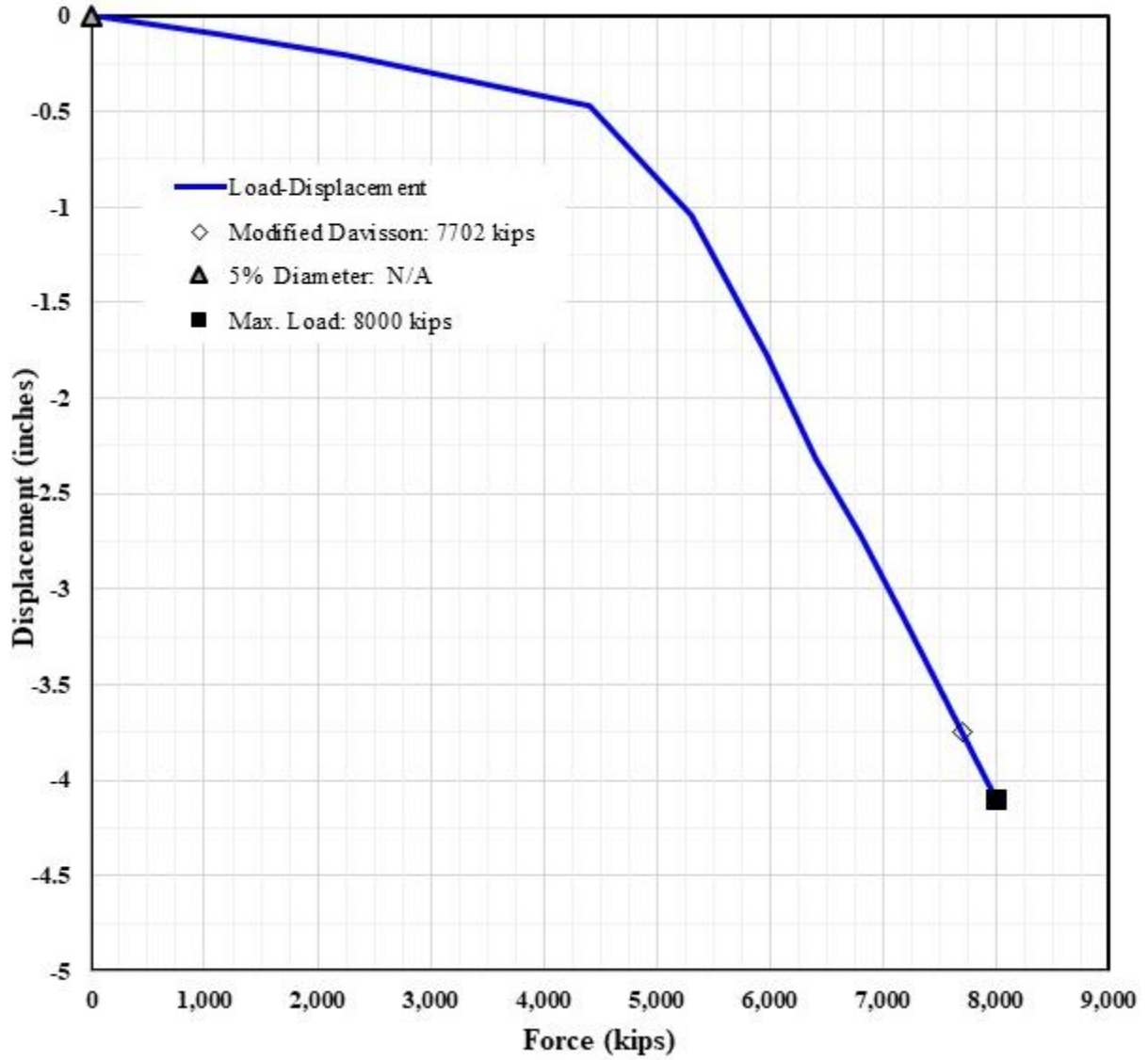
Source: FHWA.  
 1 inch = 25.4 mm; 1 kip = 4,448.2216 N.

**Figure 30. Graph. Force displacement curve. Project: Red Sea Coast, Saudi Arabia. Pile designation: TP-A2.**



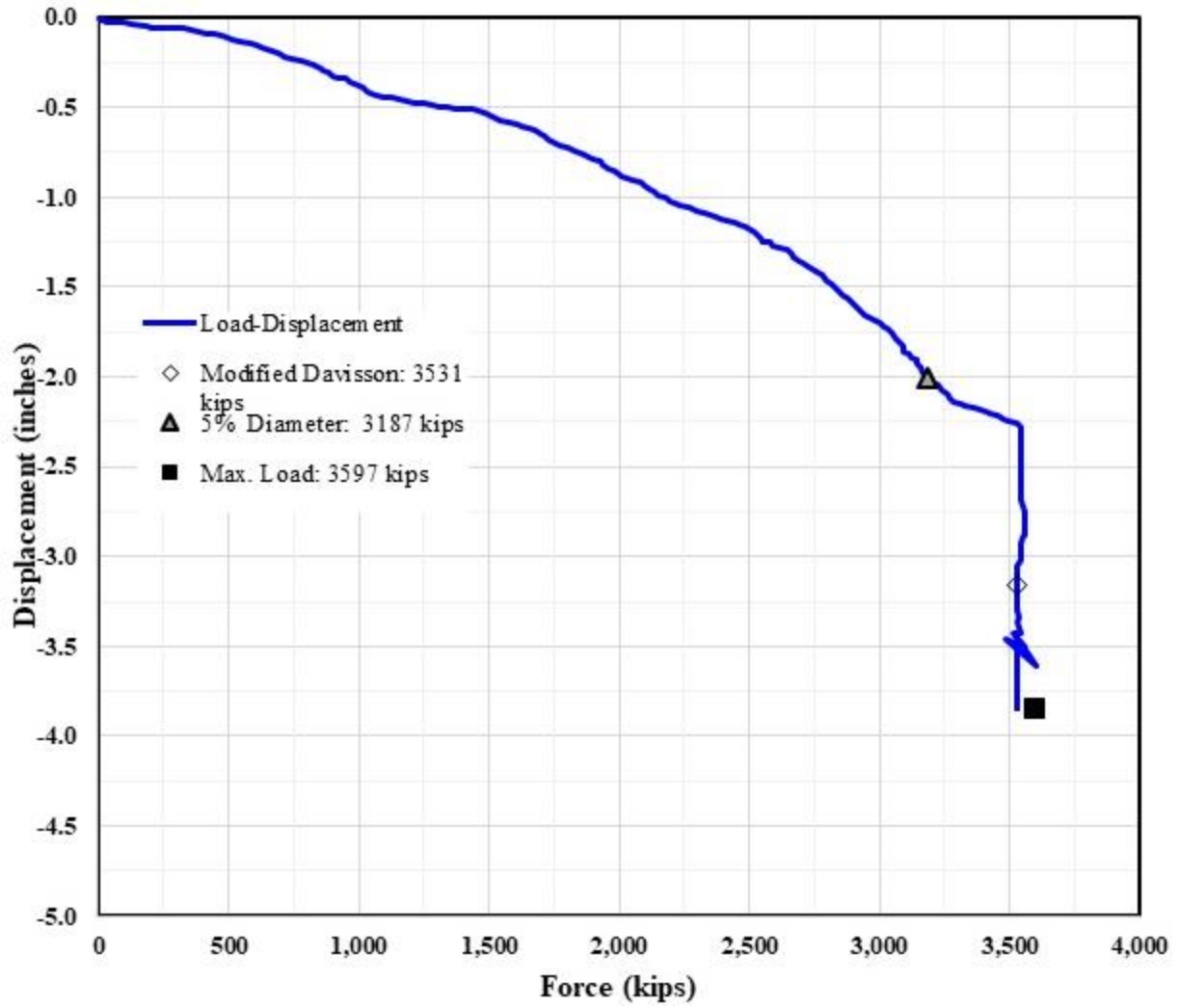
Source: FHWA.  
 1 inch = 25.4 mm; 1 kip = 4,448.2216 N.

**Figure 31. Graph. Force displacement curve. Project: Santa Clara River Bridge (Caltrans Bridge No. 52-0449). Pile designation: Test-1.**



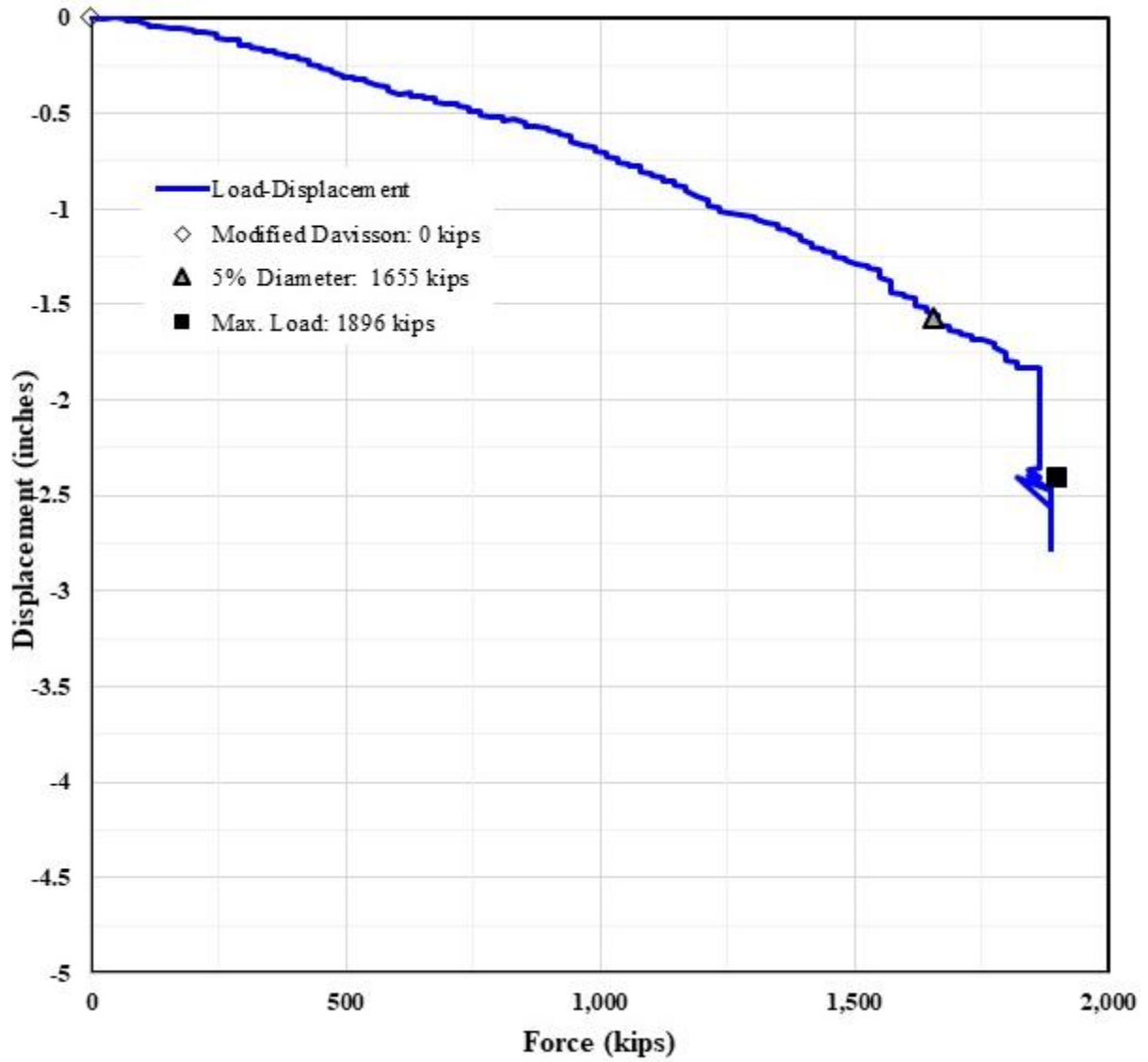
Source: FHWA.  
 1 inch = 25.4 mm; 1 kip = 4,448.2216 N.

**Figure 32. Graph. Force displacement curve. Project: Santa Clara River Bridge (Caltrans Bridge No. 52-0449). Pile designation: Test-2.**



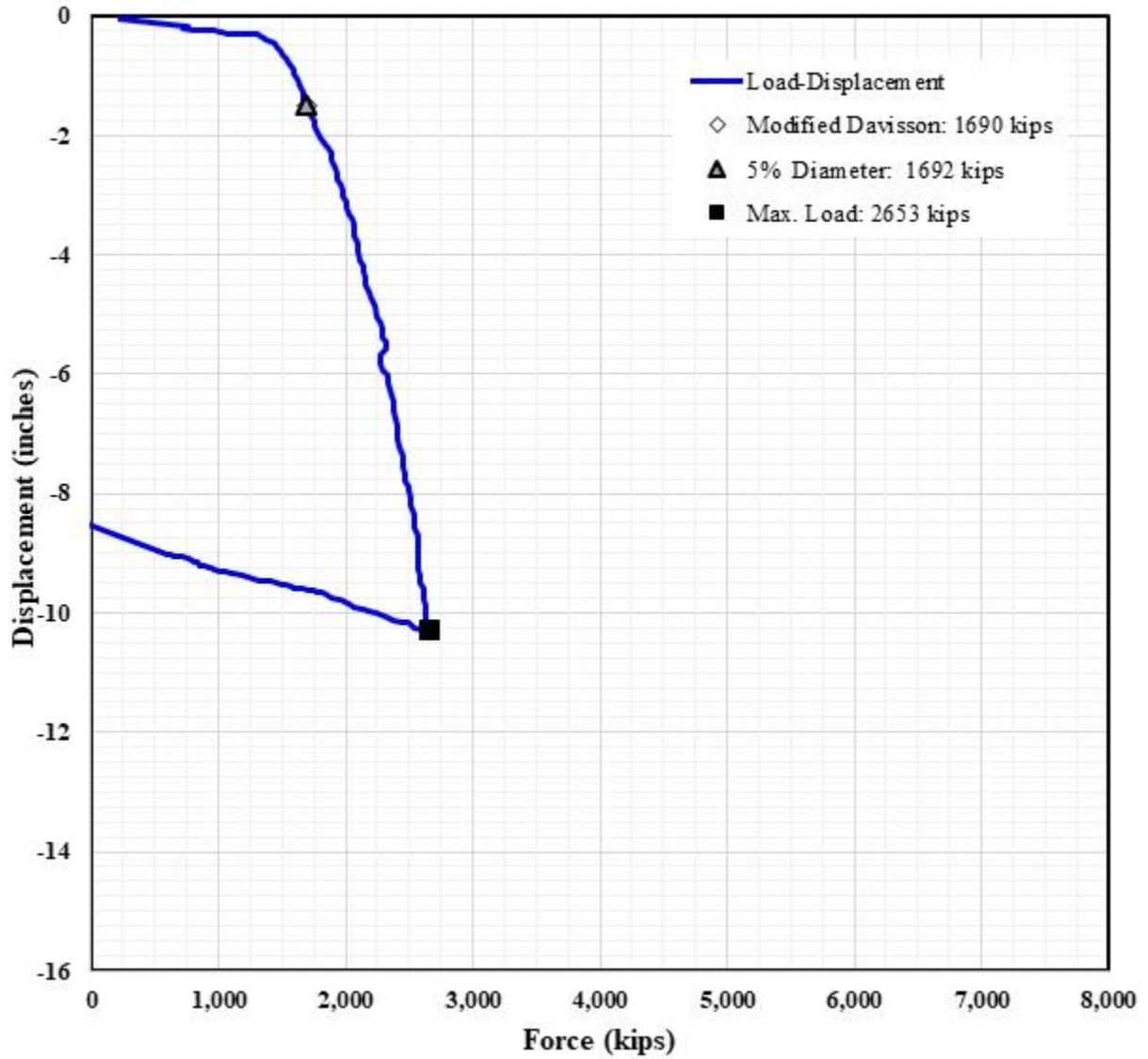
Source: FHWA.  
 1 inch = 25.4 mm; 1 kip = 4,448.2216 N.

**Figure 33. Graph. Force displacement curve. Project: Hokkaido, Japan.  
 Pile designation: TP-1.**



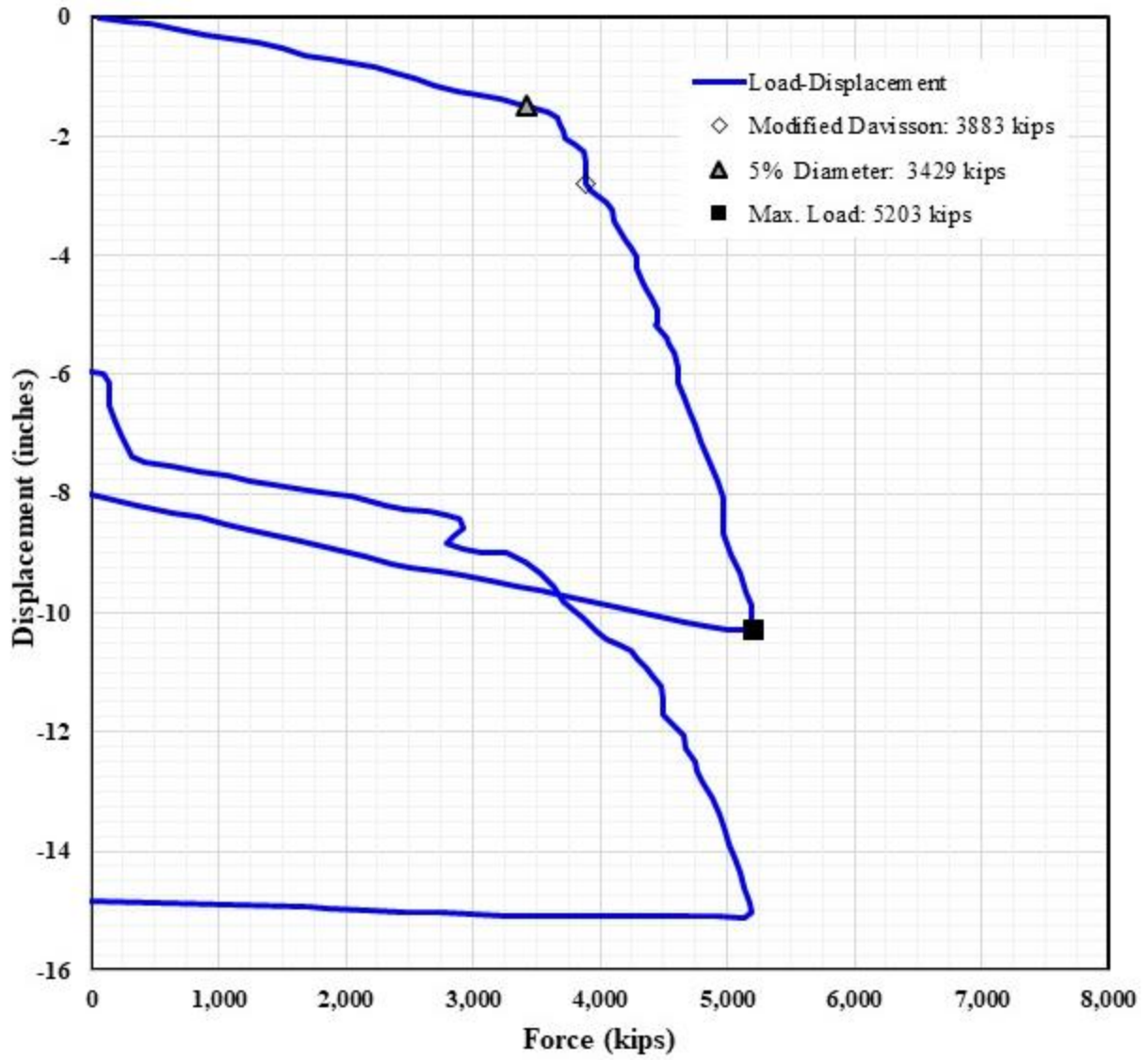
Source: FHWA.  
 1 inch = 25.4 mm; 1 kip = 4,448.2216 N.

**Figure 34. Graph. Force displacement curve. Project: Chiba, Japan. Pile designation: TP-2.**



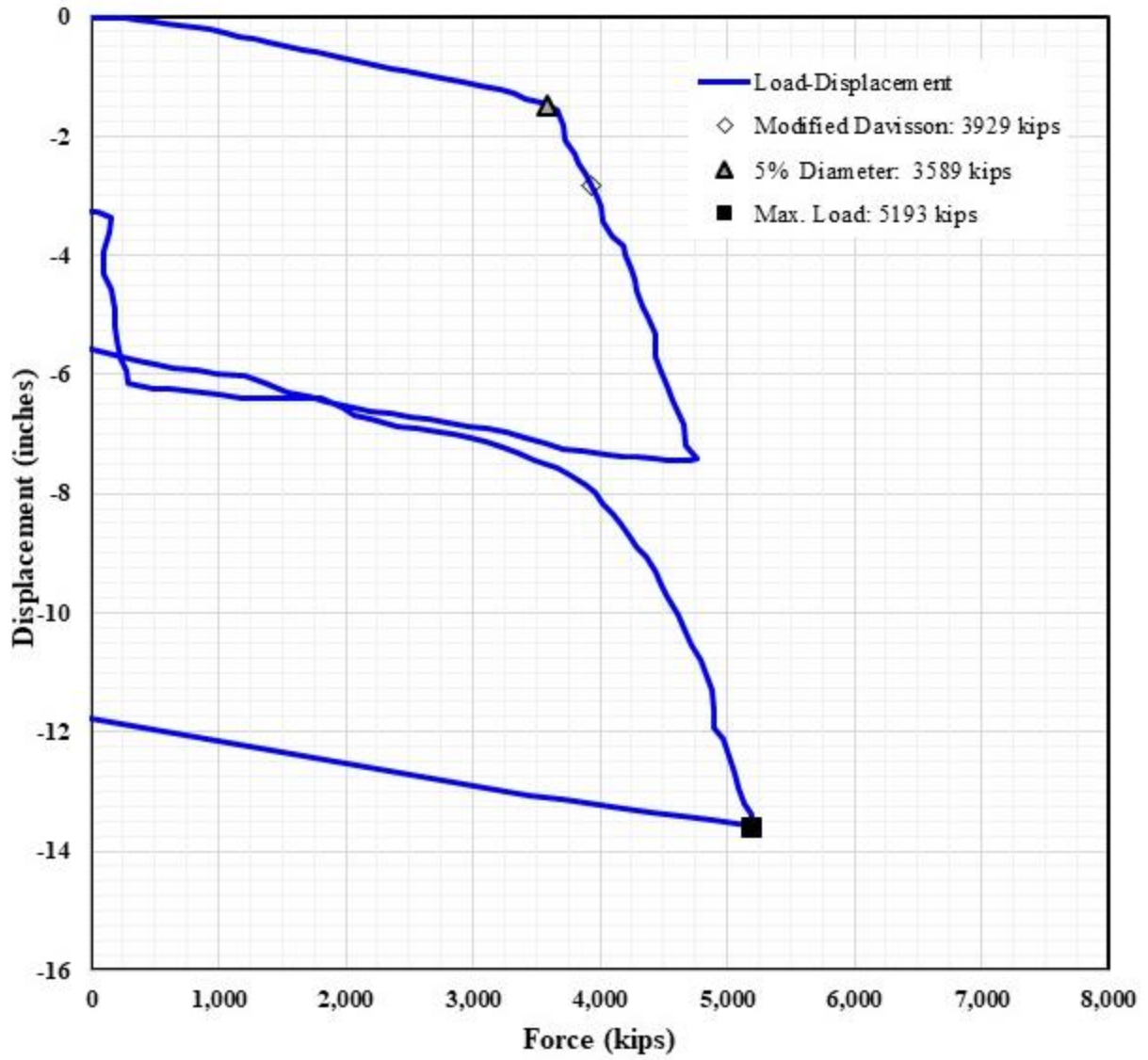
Source: FHWA.  
 1 inch = 25.4 mm; 1 kip = 4,448.2216 N.

**Figure 35. Graph. Force displacement curve. Project: EURIPIDES Joint Industry Project – offshore test piles. Pile designation: TP-1.1.**



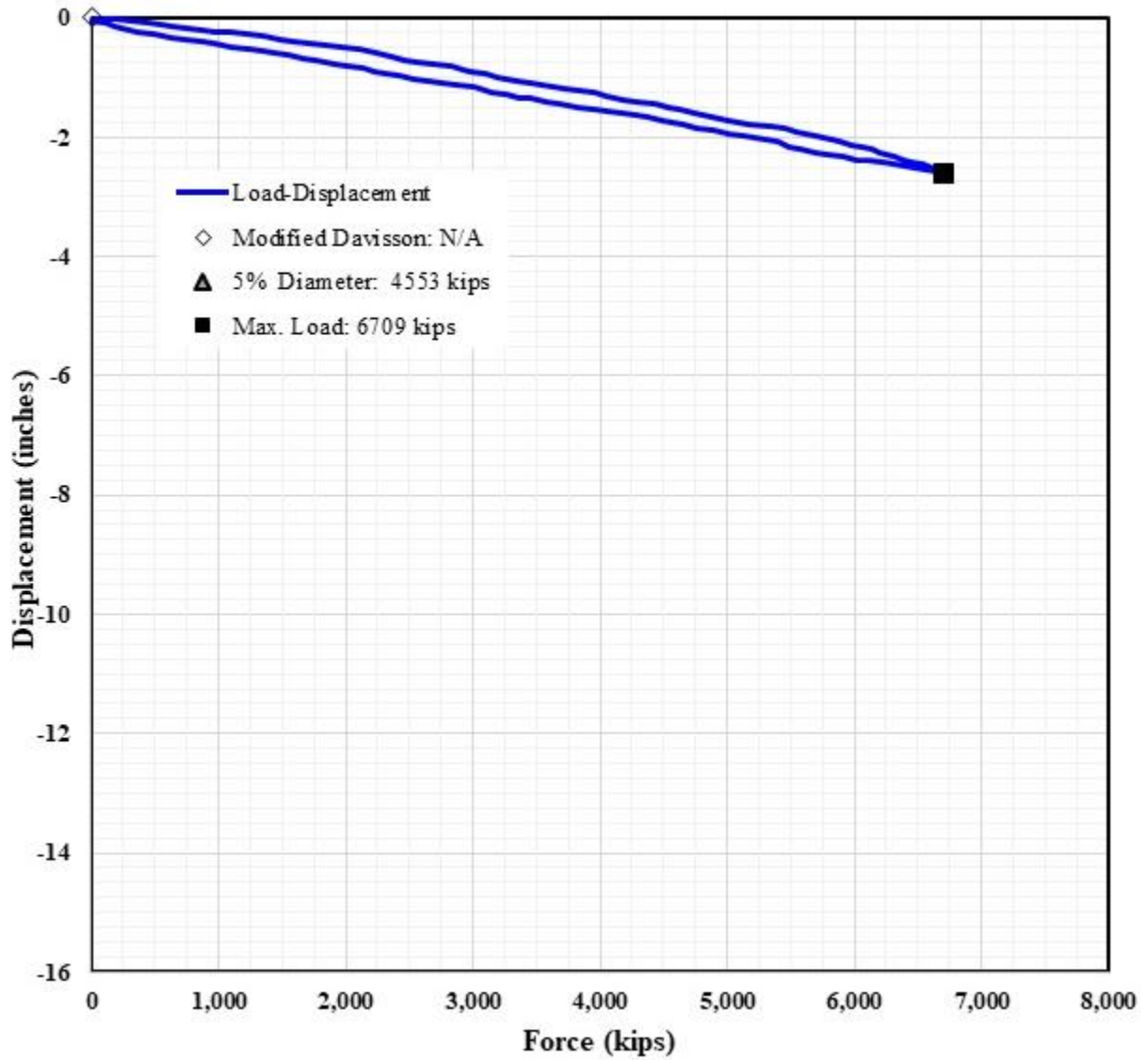
Source: FHWA.  
 1 inch = 25.4 mm; 1 kip = 4,448.2216 N.

**Figure 36. Graph. Force displacement curve. Project: EURIPIDES Joint Industry Project – offshore test piles. Pile designation: TP-1.3.**



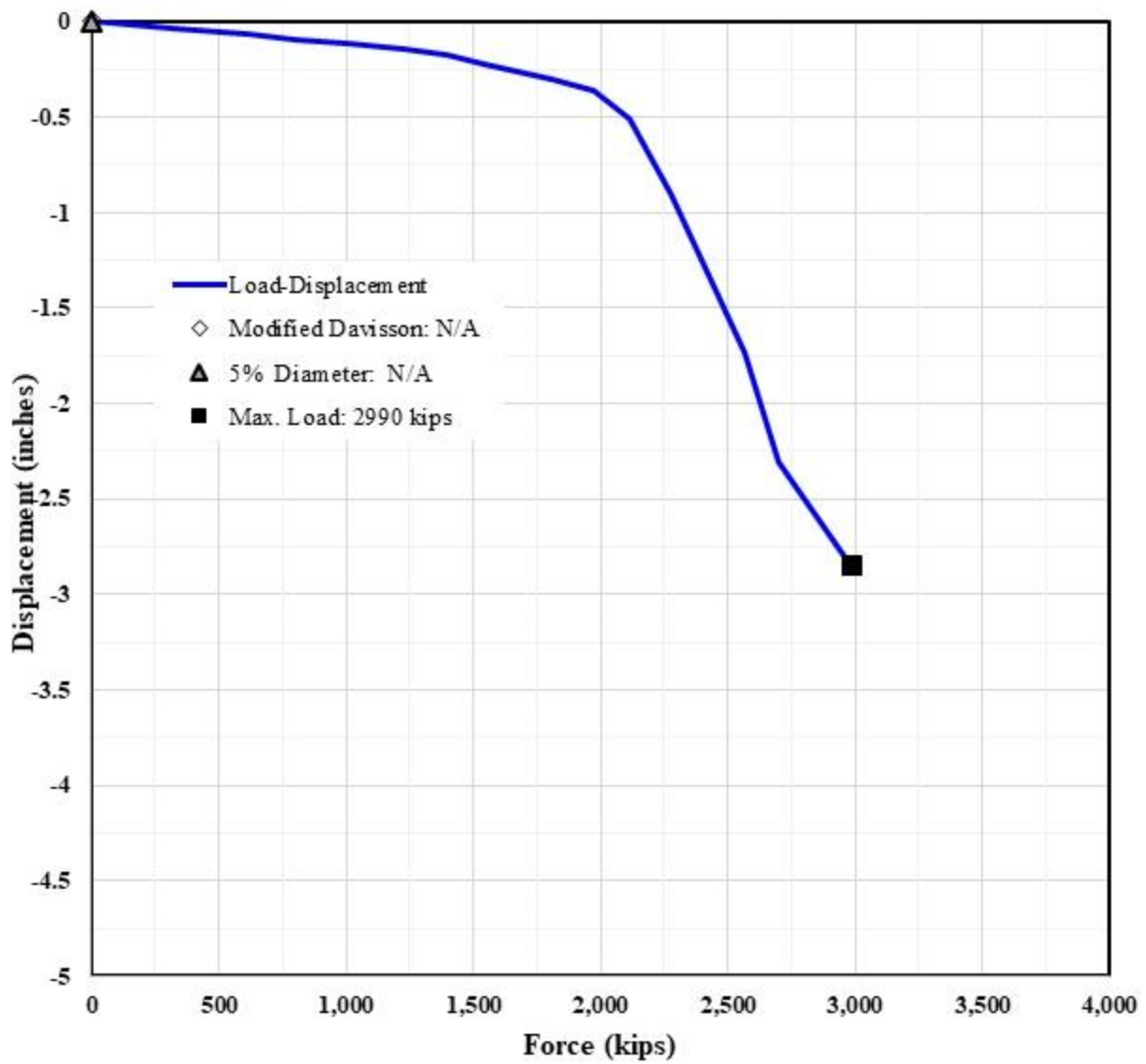
Source: FHWA.  
 1 inch = 25.4 mm; 1 kip = 4,448.2216 N.

**Figure 37. Graph. Force displacement curve. Project: EURIPIDES Joint Industry Project – offshore test piles. Pile designation: TP-2.**



Source: FHWA.  
 1 inch = 25.4 mm; 1 kip = 4,448.2216 N.

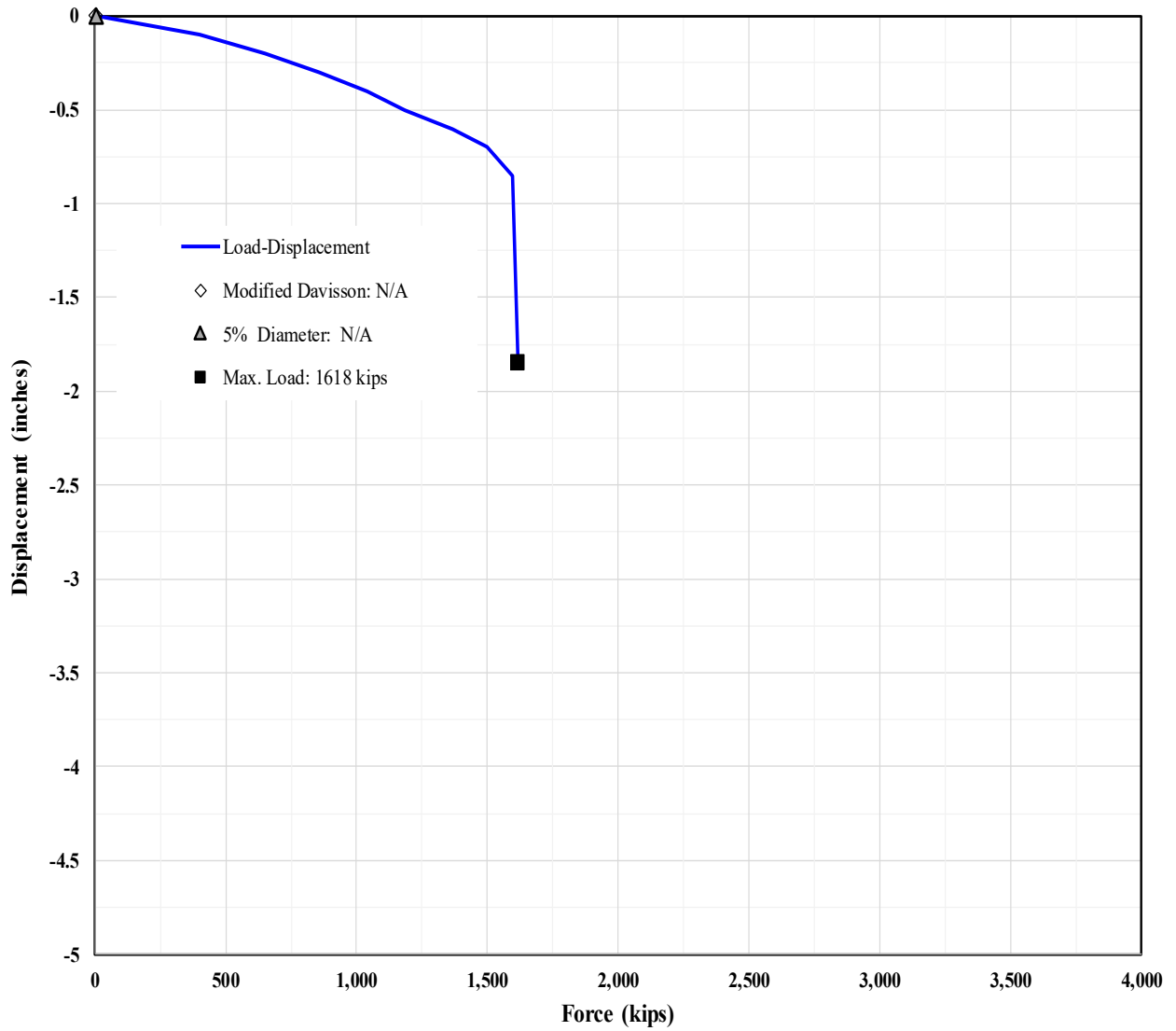
**Figure 38. Graph. Force displacement curve. Project: EURIPIDES Joint Industry Project – offshore test piles. Pile designation: TP-2.**



Source: FHWA.

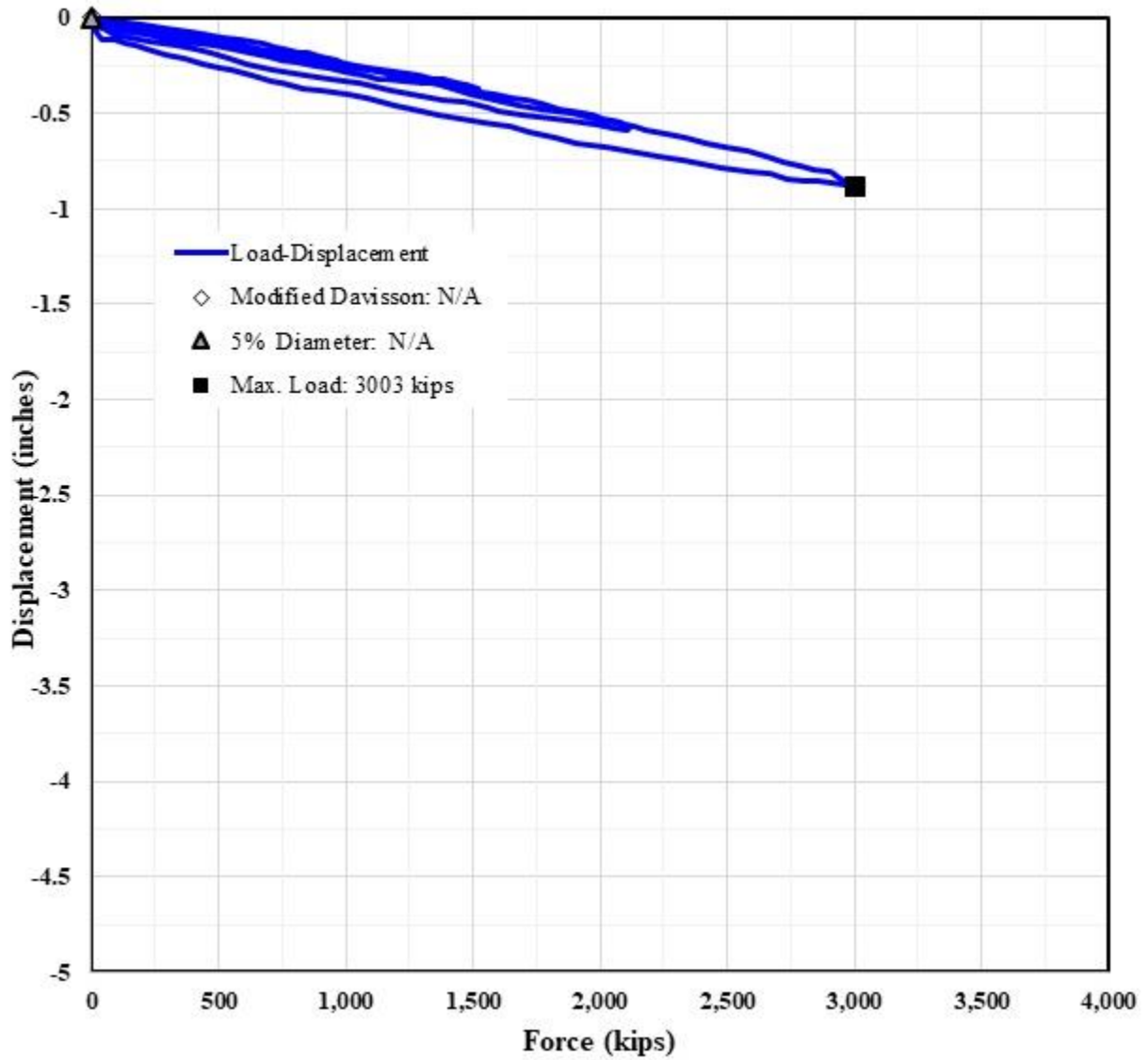
1 inch = 25.4 mm; 1 kip = 4,448.2216 N.

**Figure 39. Graph. Force displacement curve. Project: Sakonnet River Bridge (Route 138). Pile designation: TestPile.**



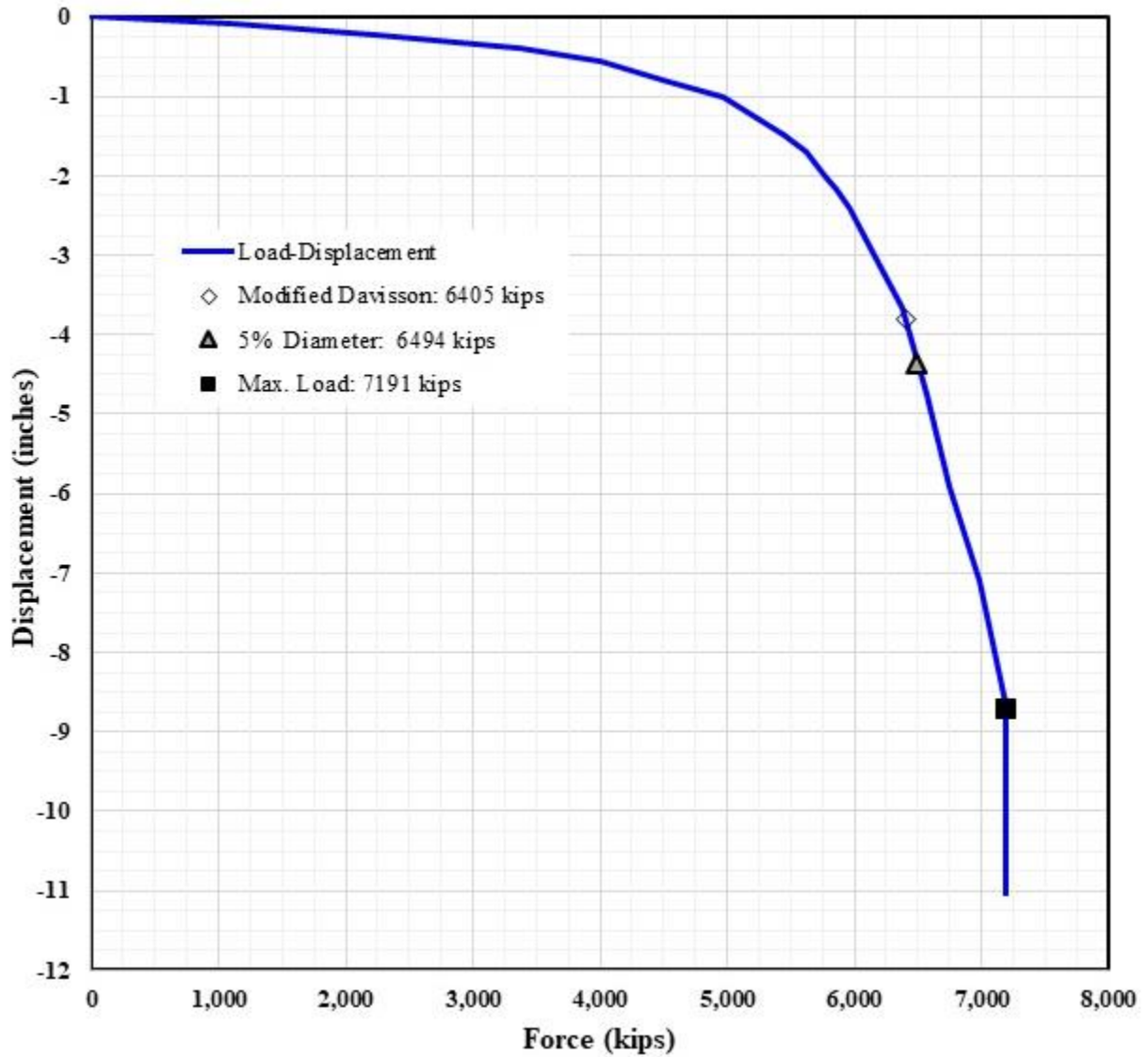
Source: FHWA.  
 1 inch = 25.4 mm; 1 kip = 4,448.2216 N.

**Figure 40. Graph. Force displacement curve. Project: Berenda Slough Bridge (Caltrans Bridge No. 41-0009R). Pile designation: TestPile.**



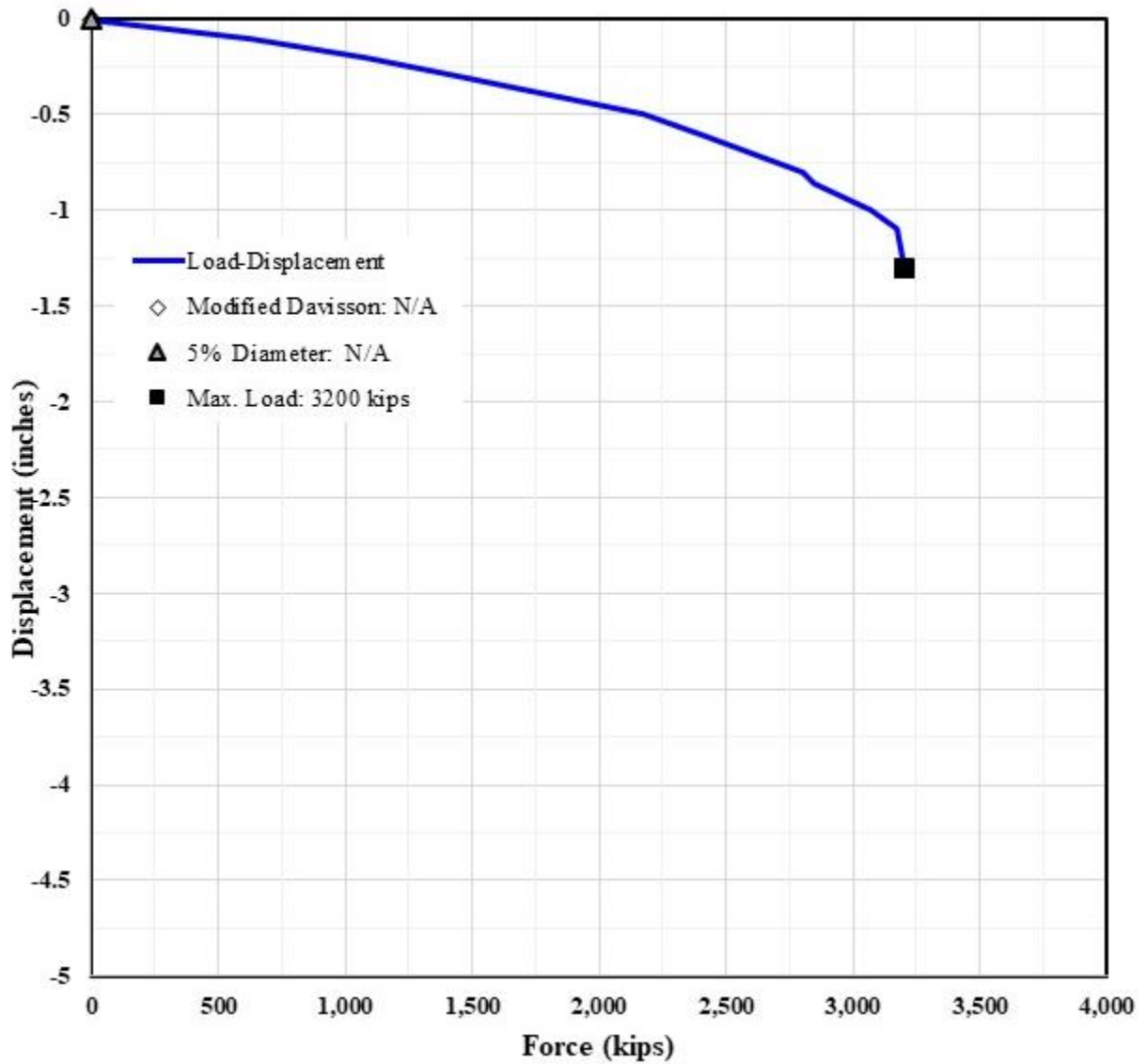
Source: FHWA.  
 1 inch = 25.4 mm; 1 kip = 4,448.2216 N.

**Figure 41. Graph. Force displacement curve. Project: Seal Beach Blvd OC (Caltrans Bridge No. 55-1099). Pile designation: TP-2A2.**



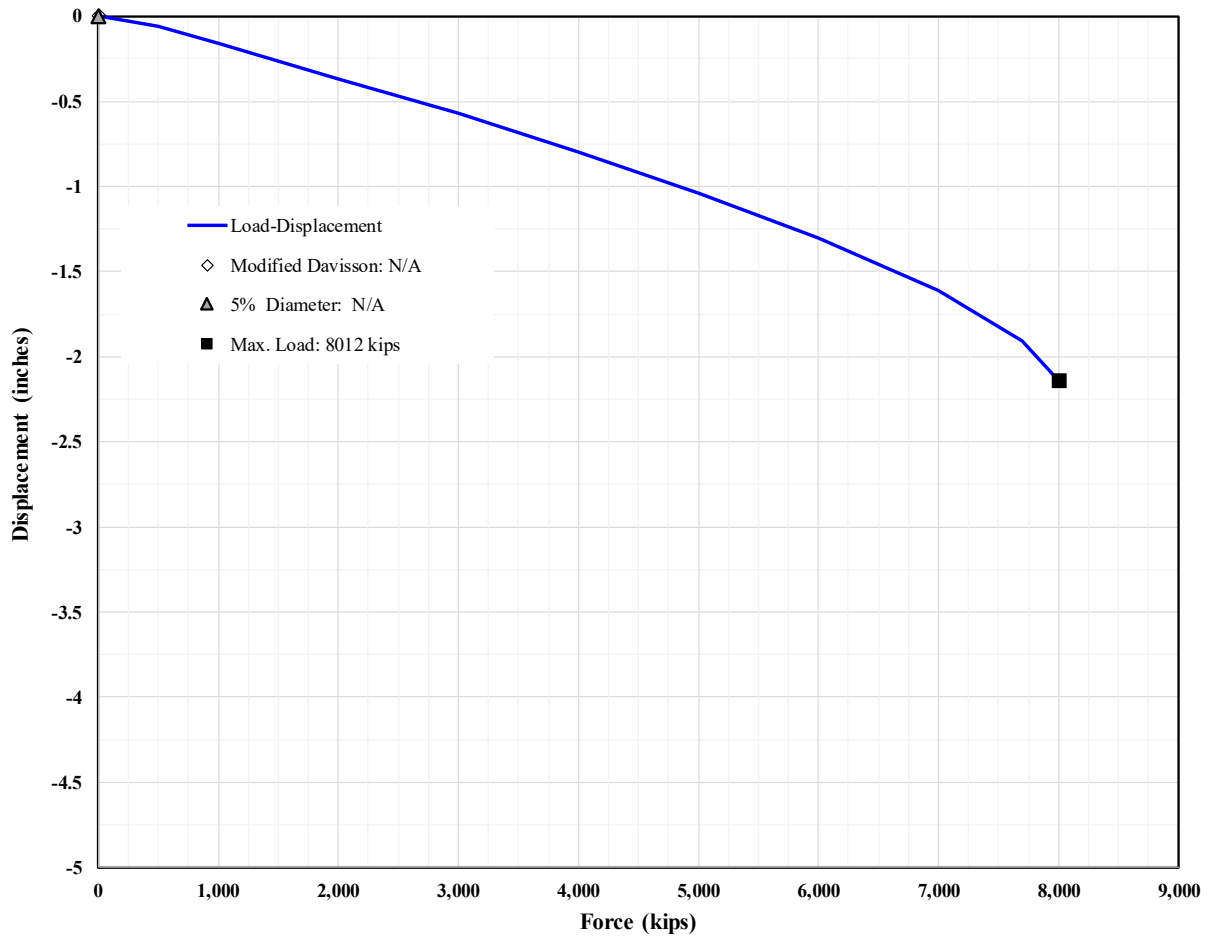
Source: FHWA.  
 1 inch = 25.4 mm; 1 kip = 4,448.2216 N.

**Figure 42. Graph. Force displacement curve. Project: Mad River Bridge (Caltrans Bridge No. 04-0025L). Pile designation: TestPile.**



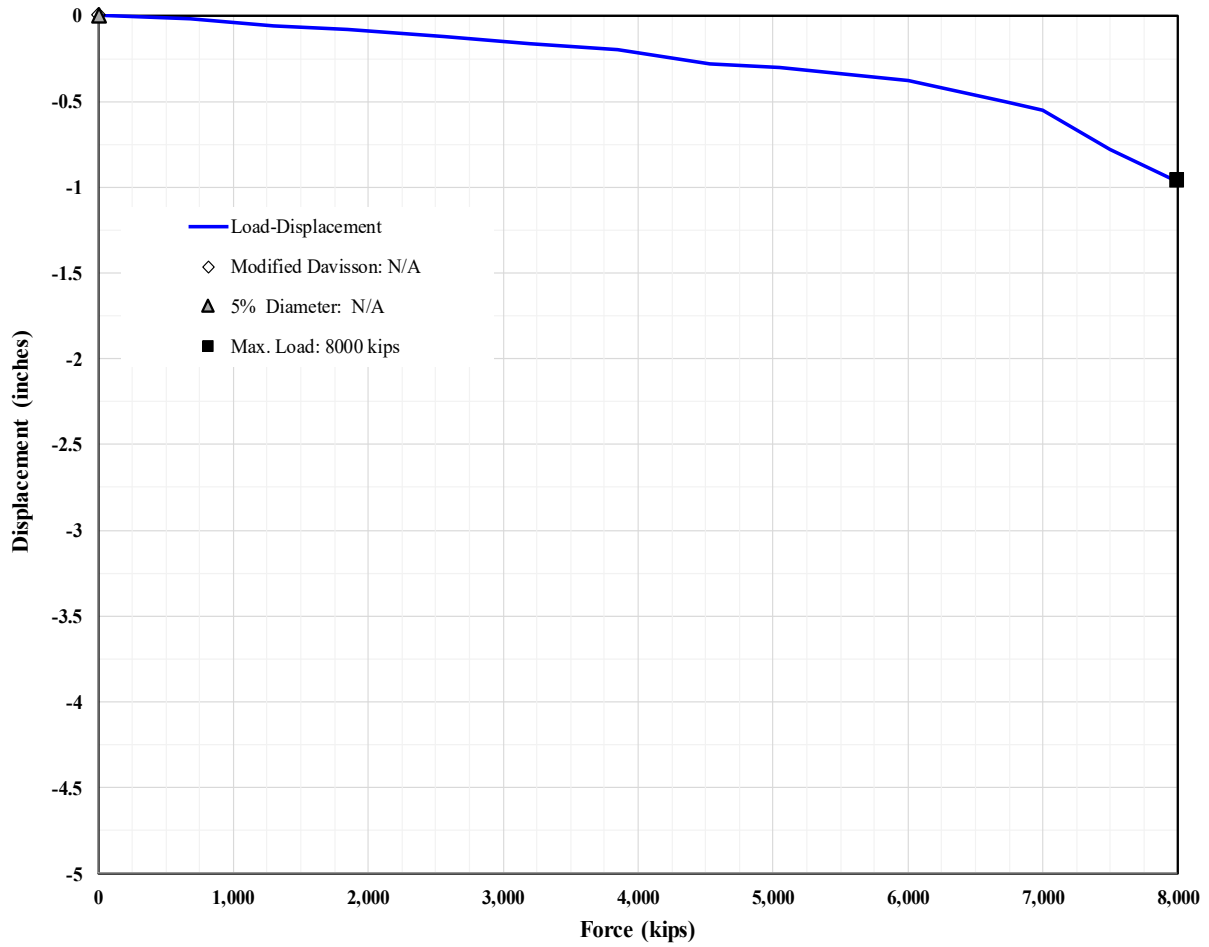
Source: FHWA.  
 1 inch = 25.4 mm; 1 kip = 4,448.2216 N.

**Figure 43. Graph. Force displacement curve. Project: Russian River Bridge (Caltrans Bridge No. 10-0301). Pile designation: TestPile.**



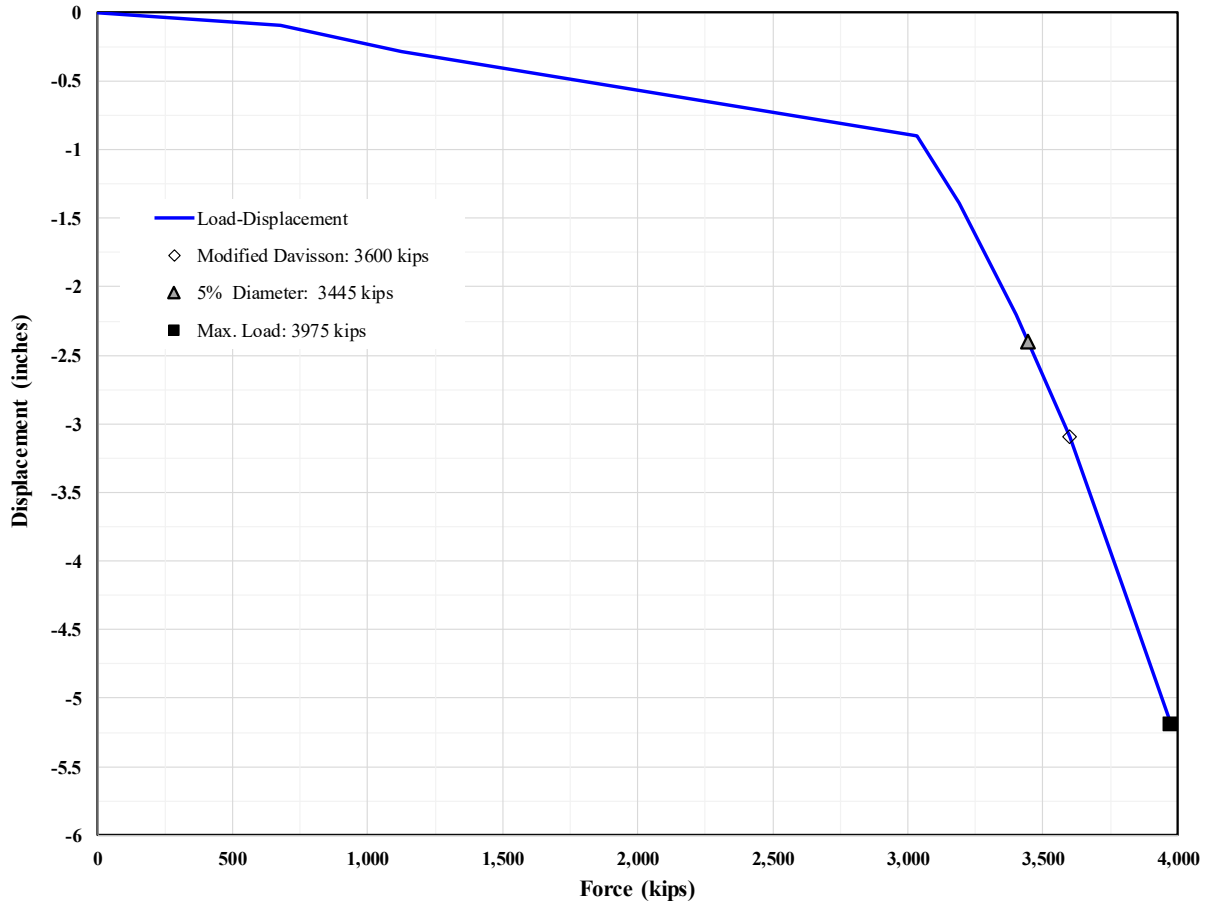
Source: FHWA.  
 1 inch = 25.4 mm; 1 kip = 4,448.2216 N.

**Figure 44. Graph. Force displacement curve. Project: San Joaquin River Bridge (Caltrans Bridge No. 41-90). Pile designation: TestPile.**



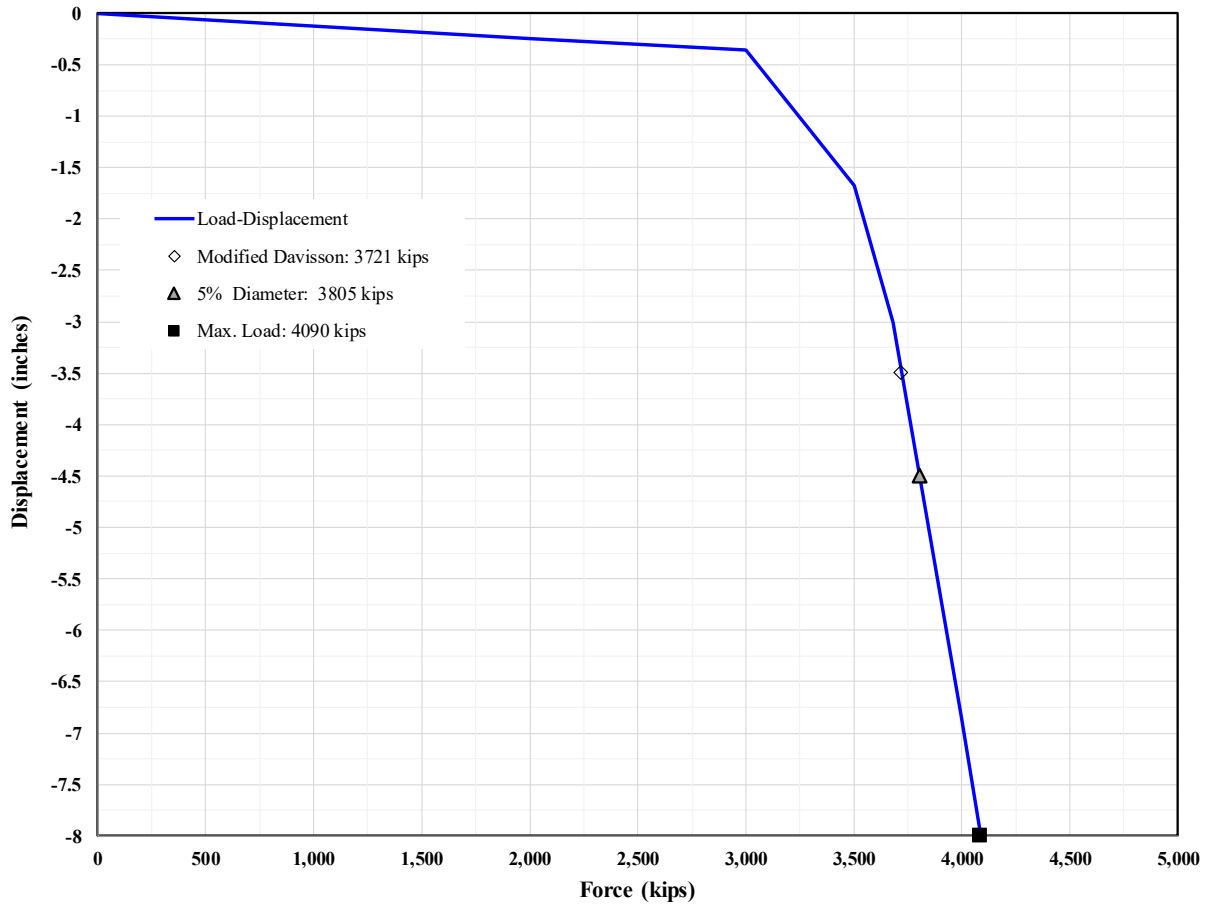
Source: FHWA.  
 1 inch = 25.4 mm; 1 kip = 4,448.2216 N.

**Figure 45. Graph. Force displacement curve. Project: Colorado River Bridge (Caltrans Bridge No. 54-1272). Pile designation: TestPile.**



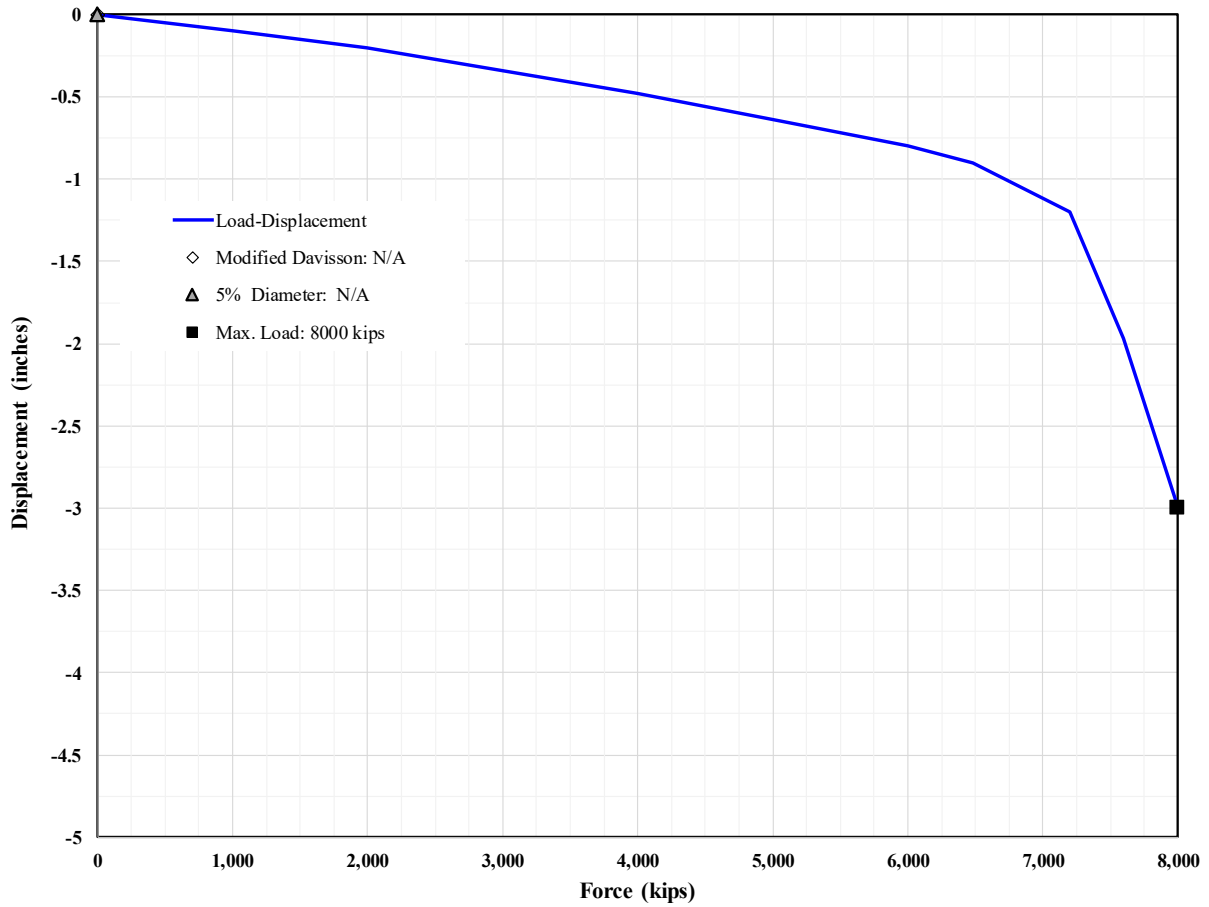
Source: FHWA.  
 1 inch = 25.4 mm; 1 kip = 4,448.2216 N.

**Figure 46. Graph. Force displacement curve. Project: Russian River Bridge (Caltrans Bridge No. 20-38). Pile designation: TestPile.**



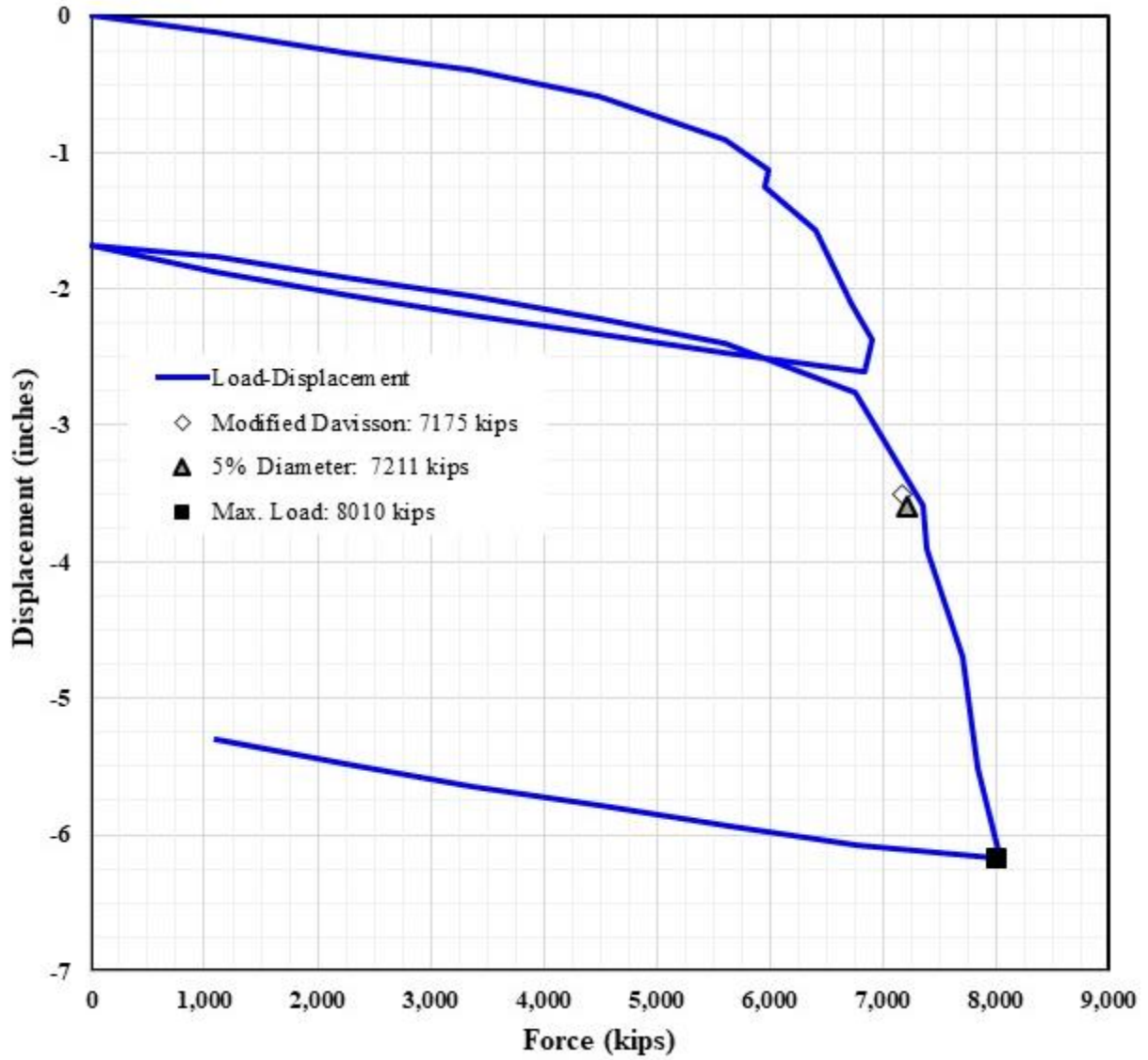
Source: FHWA.  
 1 inch = 25.4 mm; 1 kip = 4,448.2216 N.

**Figure 47. Graph. Force displacement curve. Project: Feather River Bridge (Caltrans Bridge No. 18-0026R). Pile designation: TP-1.**



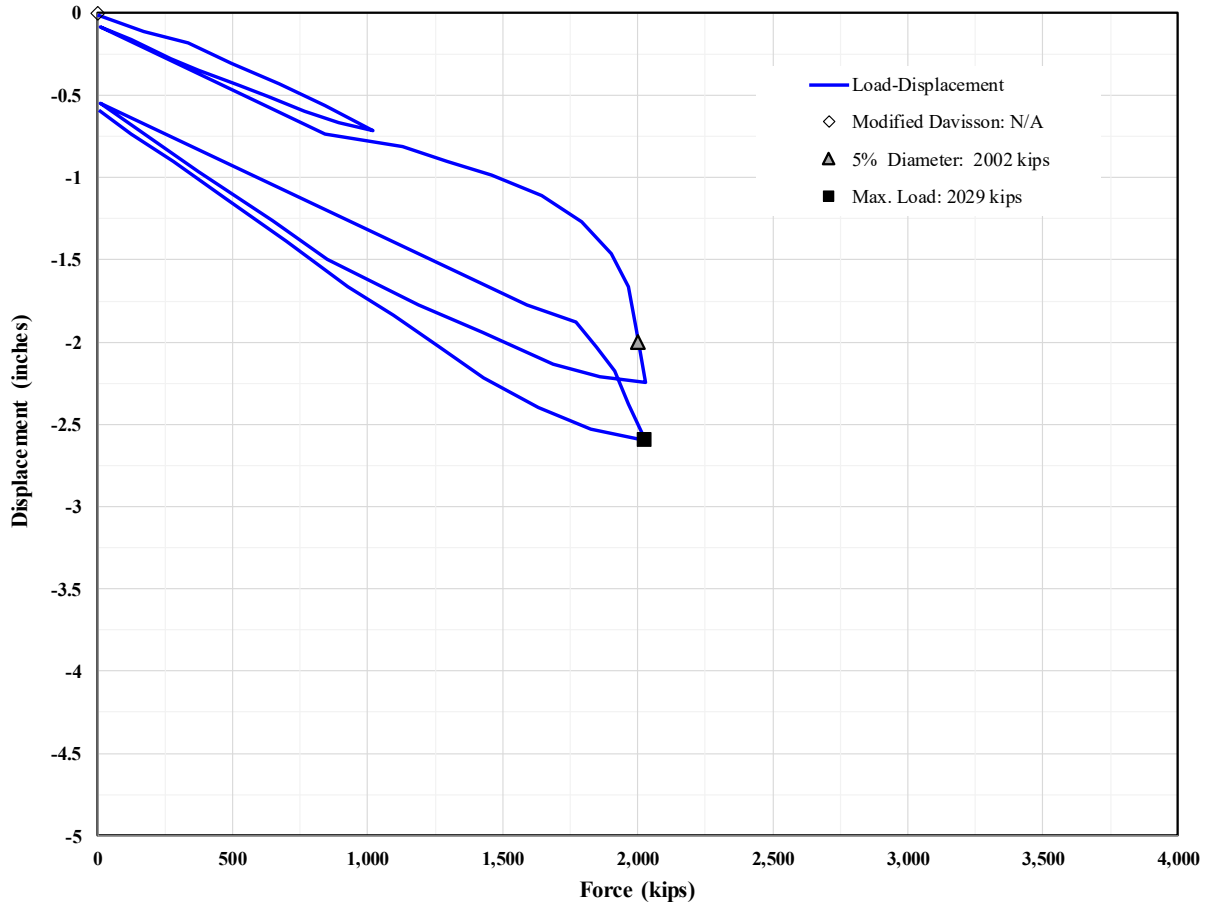
Source: FHWA.  
 1 inch = 25.4 mm; 1 kip = 4,448.2216 N.

**Figure 48. Graph. Force displacement curve. Project: Feather River Bridge (Caltrans Bridge No. 18-0026R). Pile designation: TP-2.**



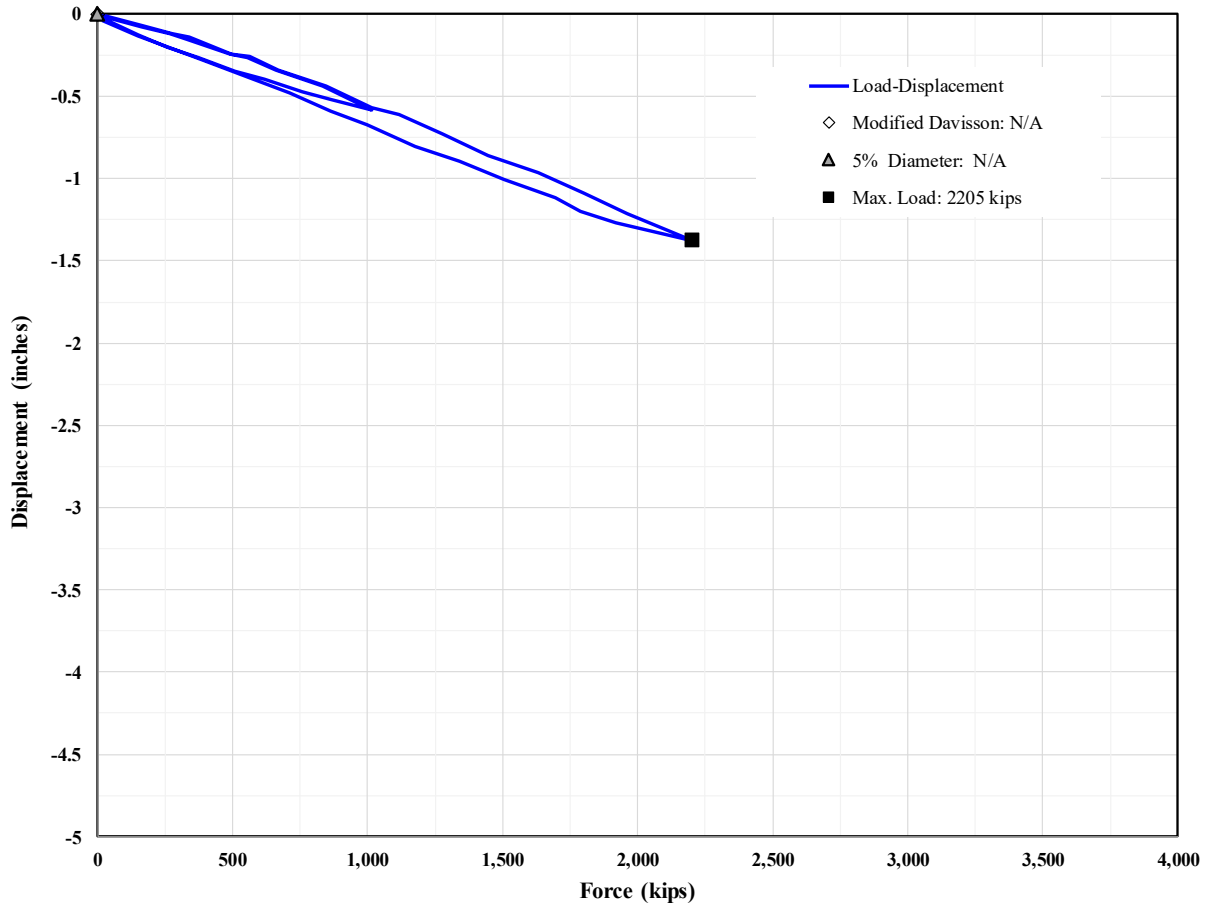
Source: FHWA.  
 1 inch = 25.4 mm; 1 kip = 4,448.2216 N.

**Figure 49. Graph. Force displacement curve. Project: Santa Clara River Bridge (Caltrans Bridge No. 53-2925). Pile designation: TestPile.**



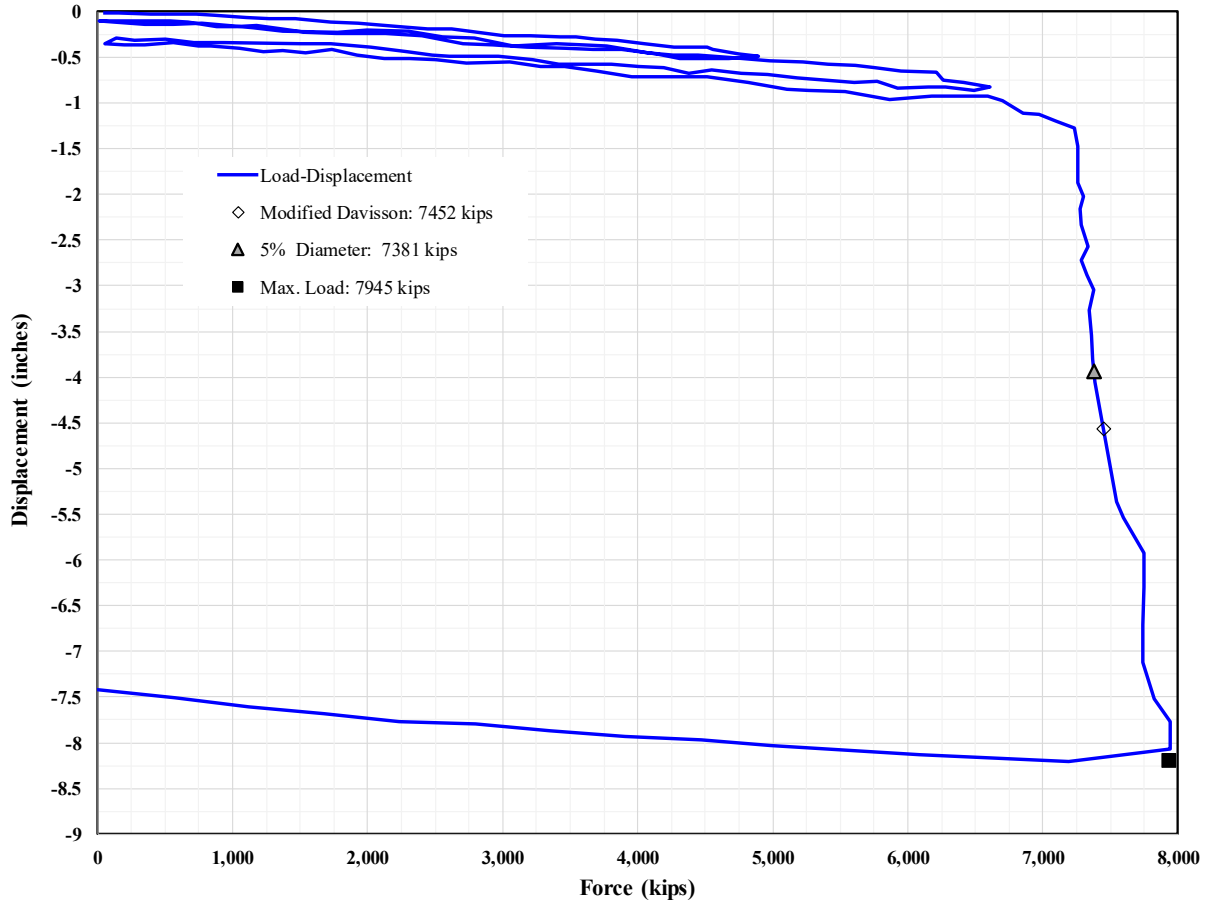
Source: FHWA.  
 1 inch = 25.4 mm; 1 kip = 4,448.2216 N.

**Figure 50. Graph. Force displacement curve. Project: Port of Toamasina Offshore Jetty. Pile designation: 12A.**



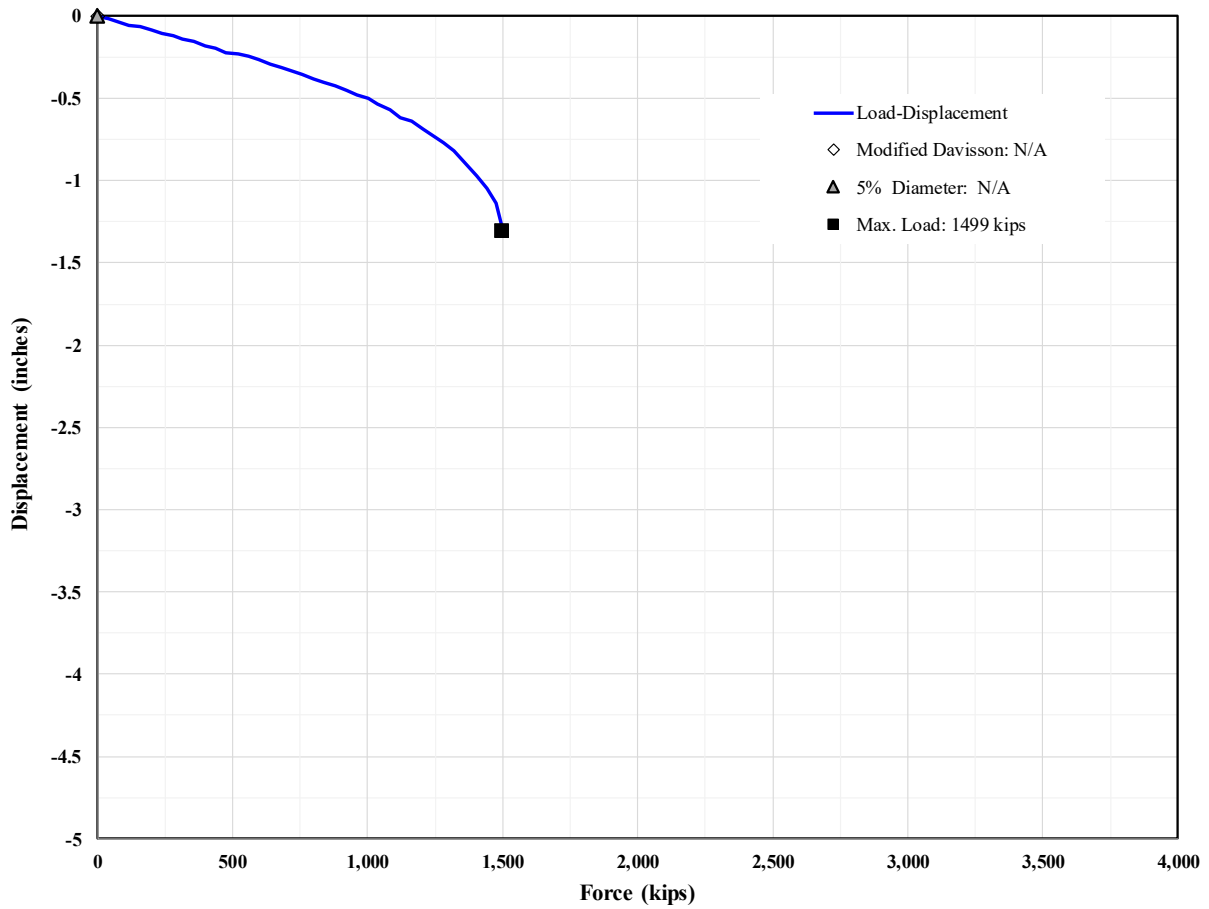
Source: FHWA.  
 1 inch = 25.4 mm; 1 kip = 4,448.2216 N.

**Figure 51. Graph. Force displacement curve. Project: Port of Toamasina Offshore Jetty. Pile designation: 4B.**



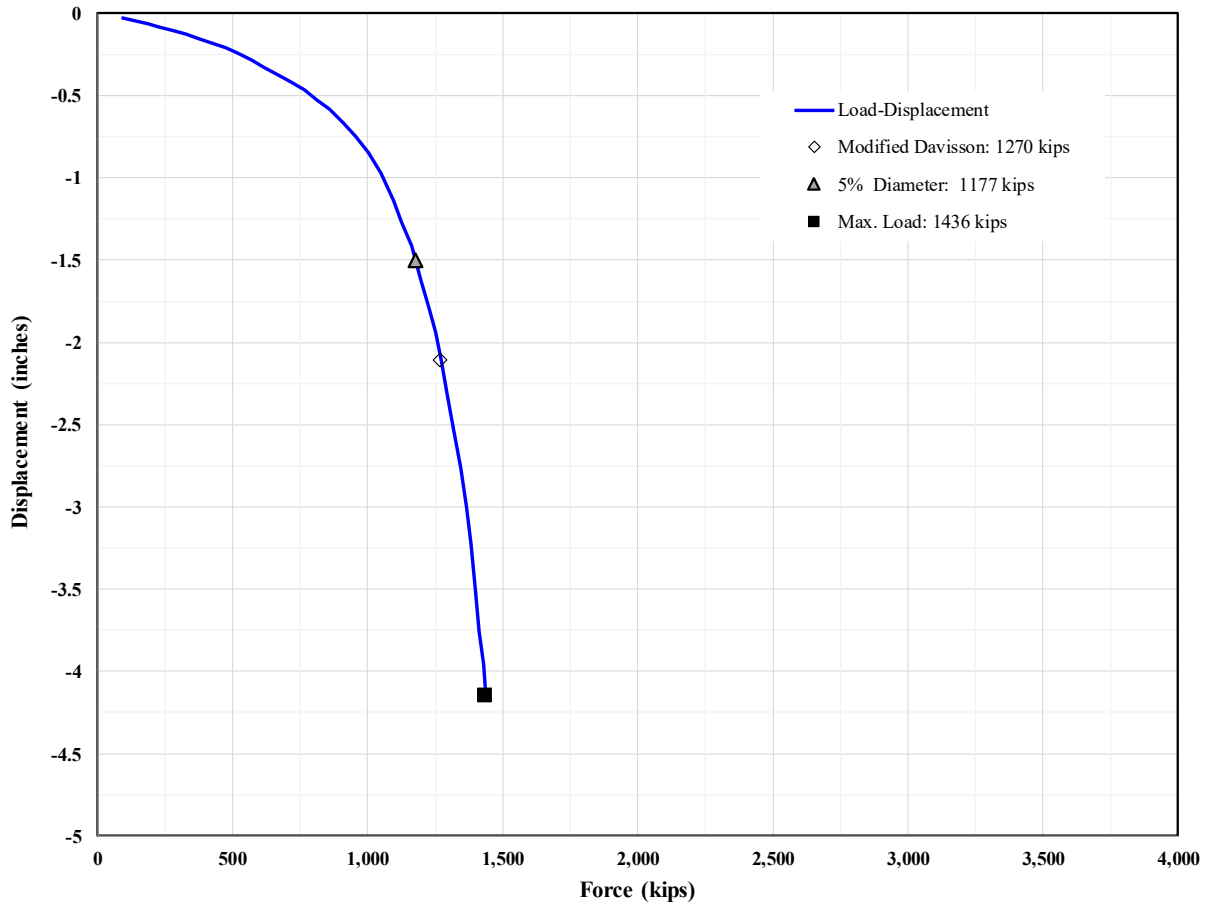
Source: FHWA.  
 1 inch = 25.4 mm; 1 kip = 4,448.2216 N.

**Figure 52. Graph. Force displacement curve. Project: Trans-Tokyo Bay Highway. Pile designation: TP-1.**



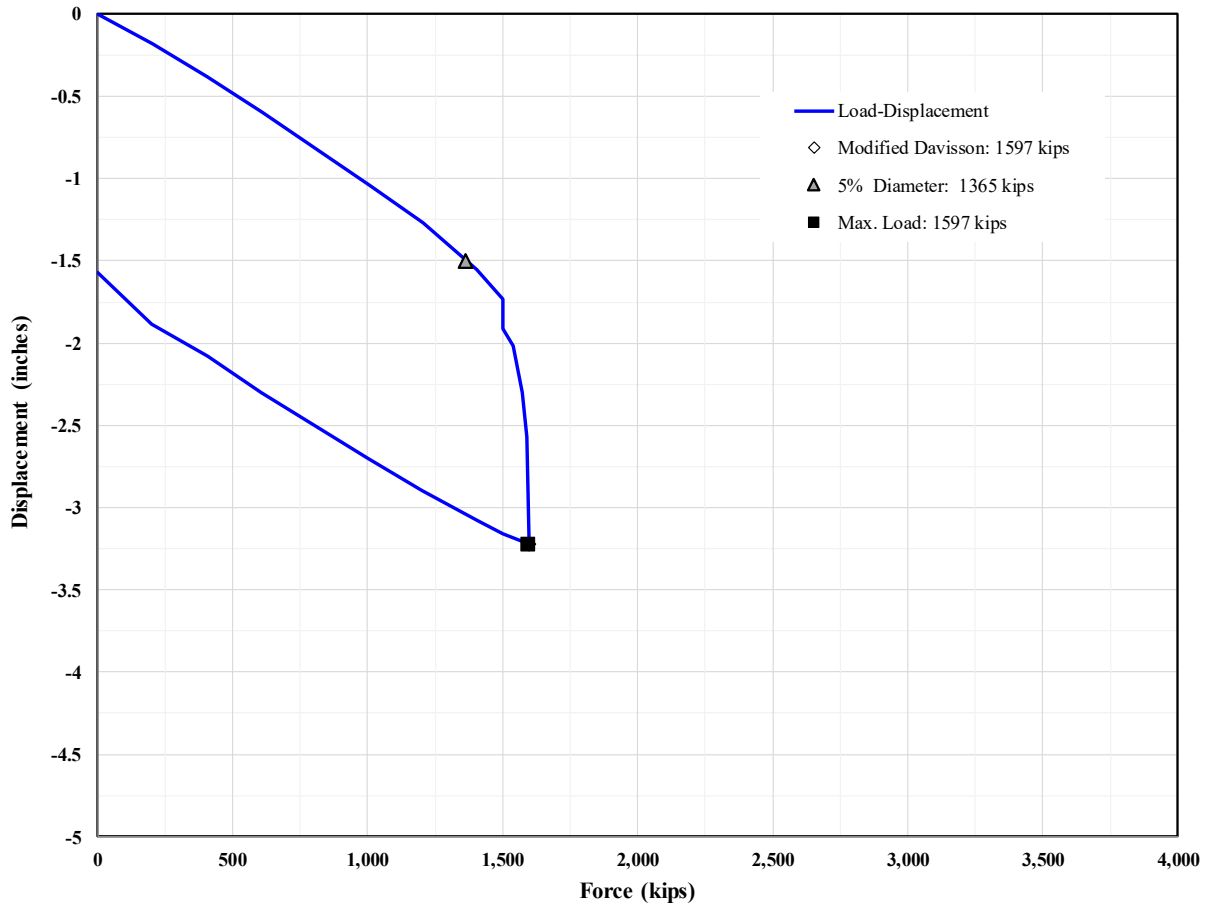
Source: FHWA.  
 1 inch = 25.4 mm; 1 kip = 4,448.2216 N.

**Figure 53. Graph. Force displacement curve. Project: Legislative Route 795 Section B-6 Philadelphia, PA. Pile designation: TP-C.**



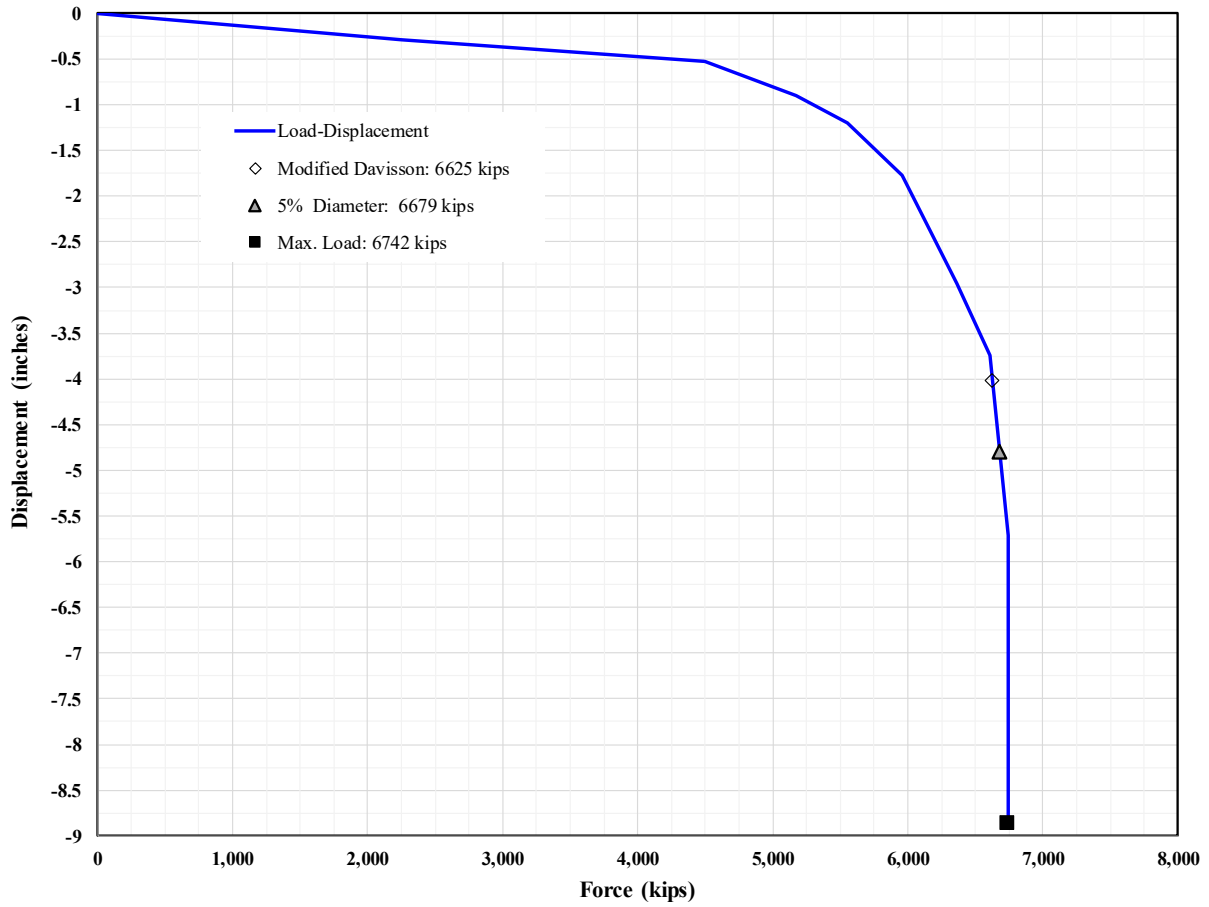
Source: FHWA.  
 1 inch = 25.4 mm; 1 kip = 4,448.2216 N.

**Figure 54. Graph. Force displacement curve. Project: Legislative Route 795 Section B-6 Philadelphia, PA. Pile designation: TP-E.**



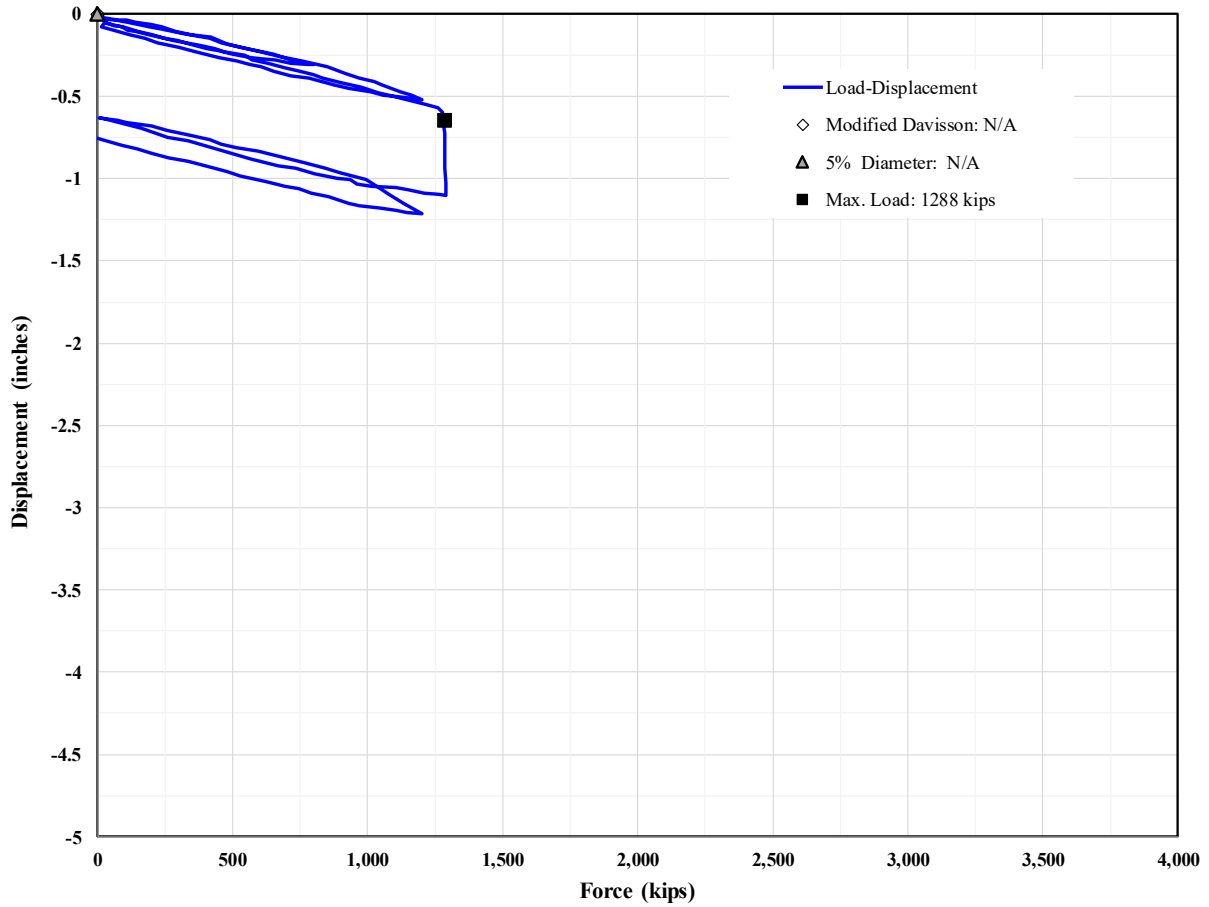
Source: FHWA.  
 1 inch = 25.4 mm; 1 kip = 4,448.2216 N.

**Figure 55. Graph. Force displacement curve. Project: Louisiana Highway 1 Improvements Load Test Data Phase 1B. Pile designation: T-3-1.**



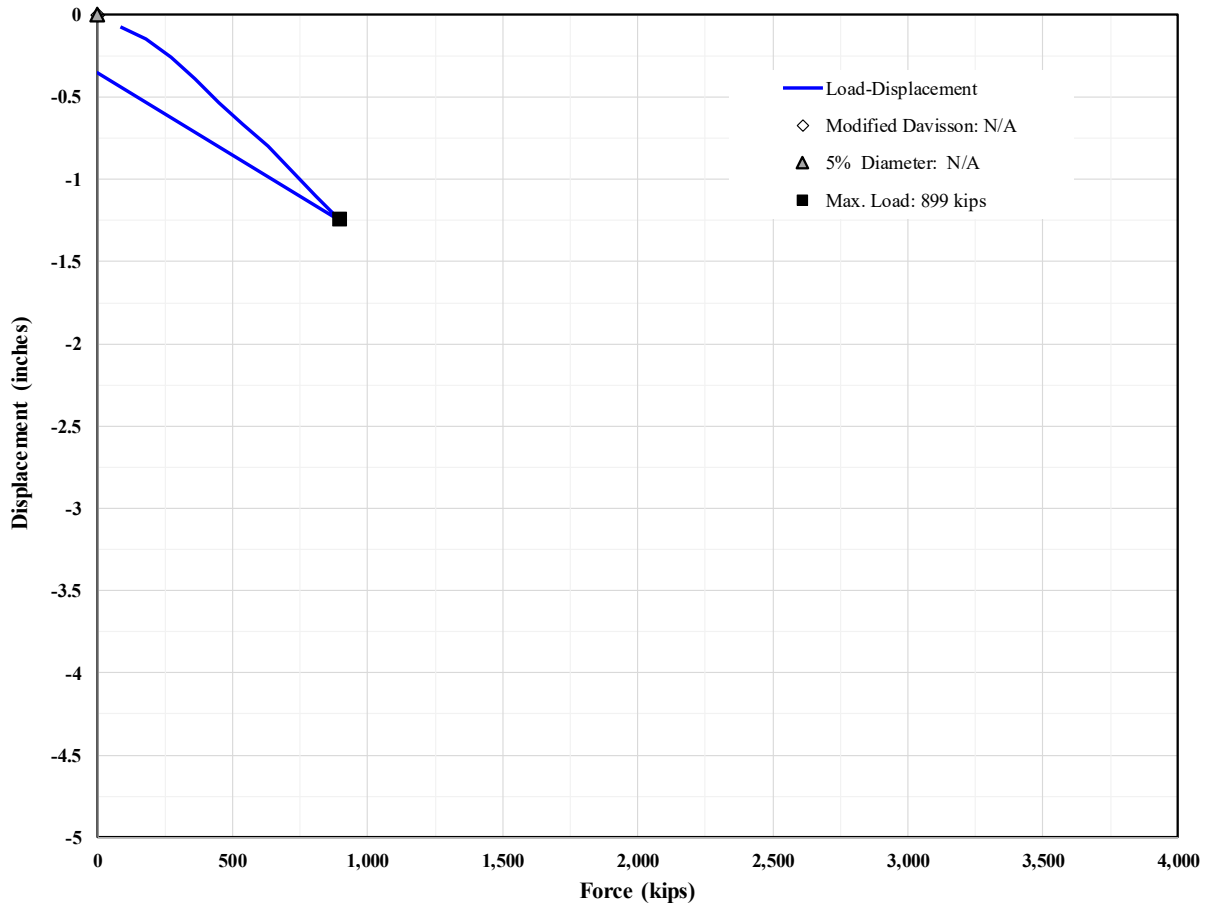
Source: FHWA.  
 1 inch = 25.4 mm; 1 kip = 4,448.2216 N.

**Figure 56. Graph. Force displacement curve. Project: I-880 5th Street Overhead Bridge (Caltrans Bridge No. 33-27). Pile designation: TestPile.**



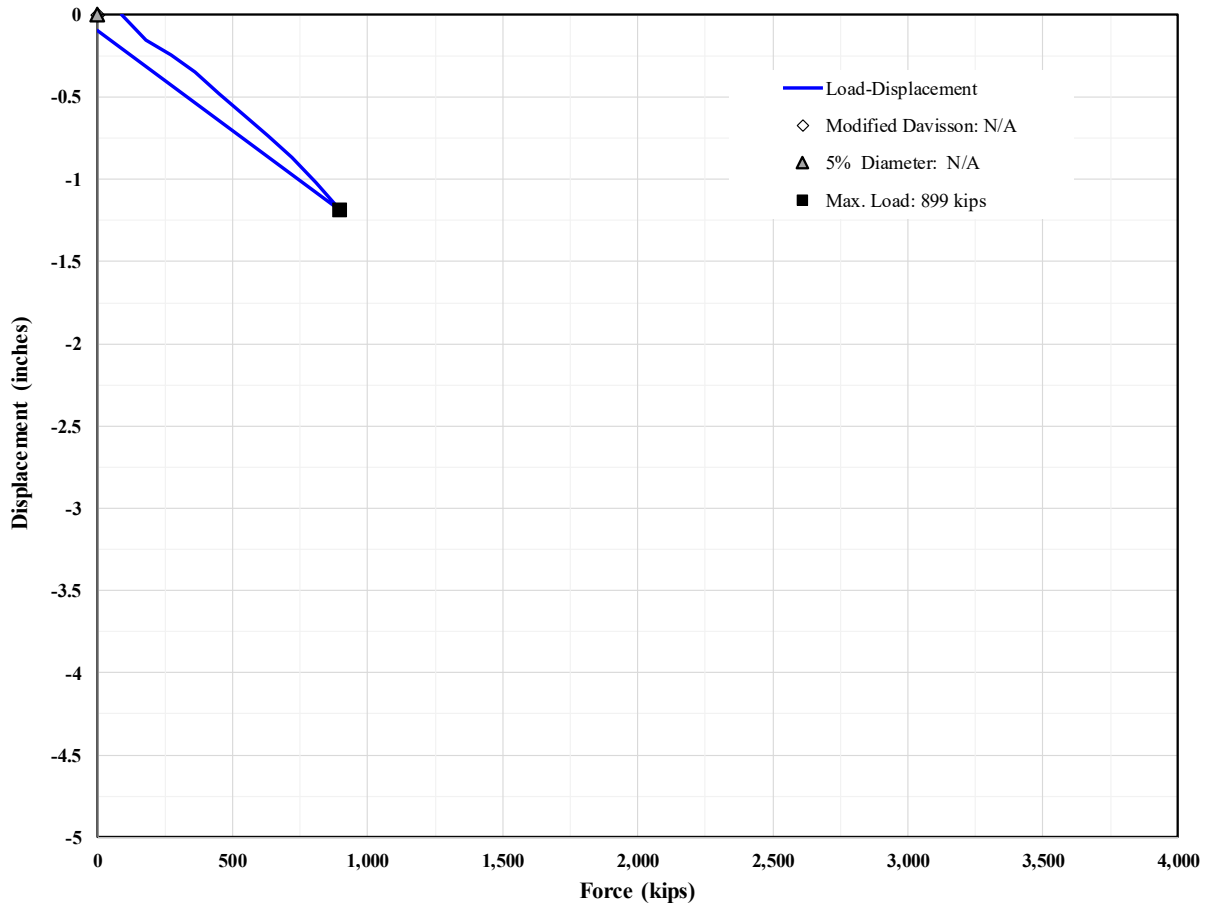
Source: FHWA.  
 1 inch = 25.4 mm; 1 kip = 4,448.2216 N.

**Figure 57. Graph. Force displacement curve. Project: Port of Oakland Connector Viaduct Maritime On/Off-Ramps (Caltrans Bridge No. 33-612E). Pile designation: TP9-27NCL.**



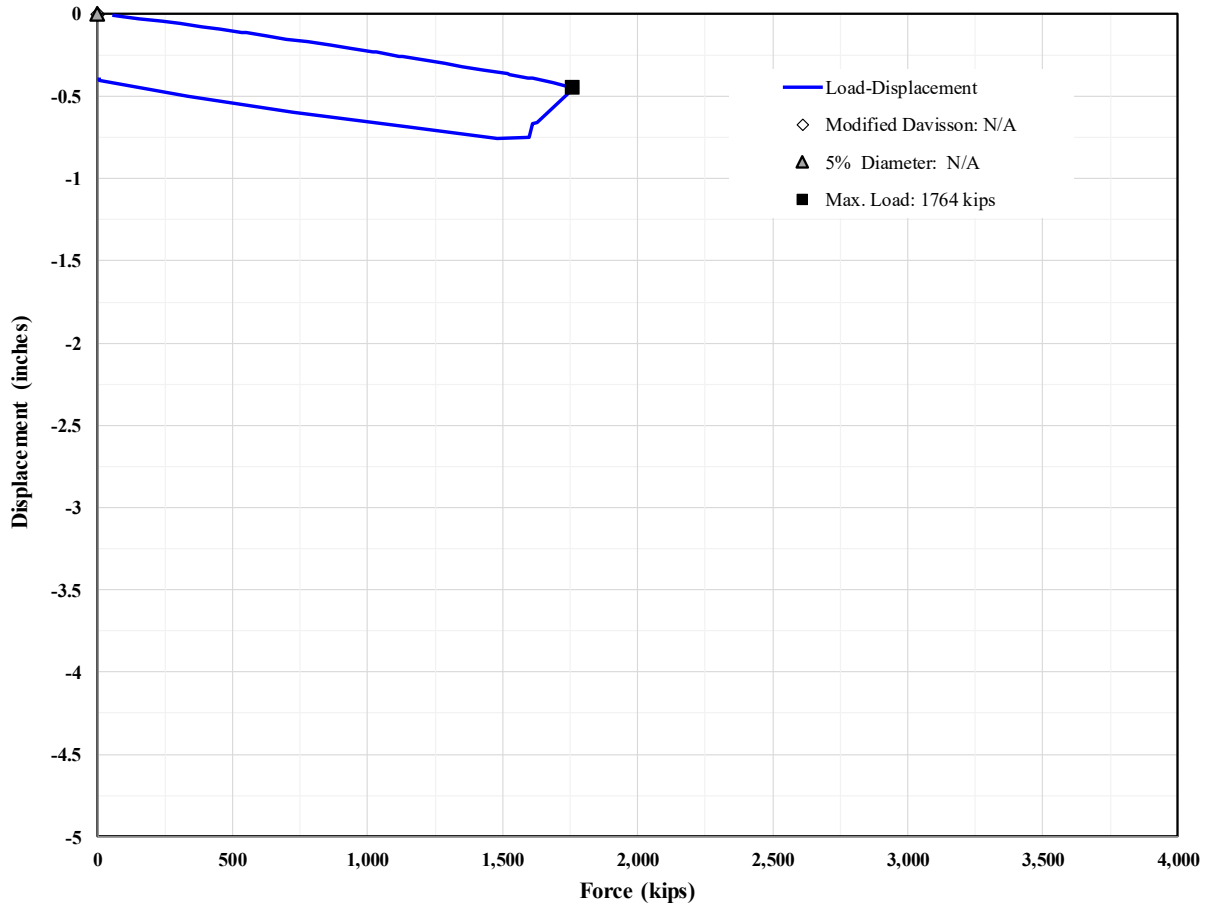
Source: FHWA.  
 1 inch = 25.4 mm; 1 kip = 4,448.2216 N.

**Figure 58. Graph. Force displacement curve. Project: Port Said. Pile designation: TP-22.**



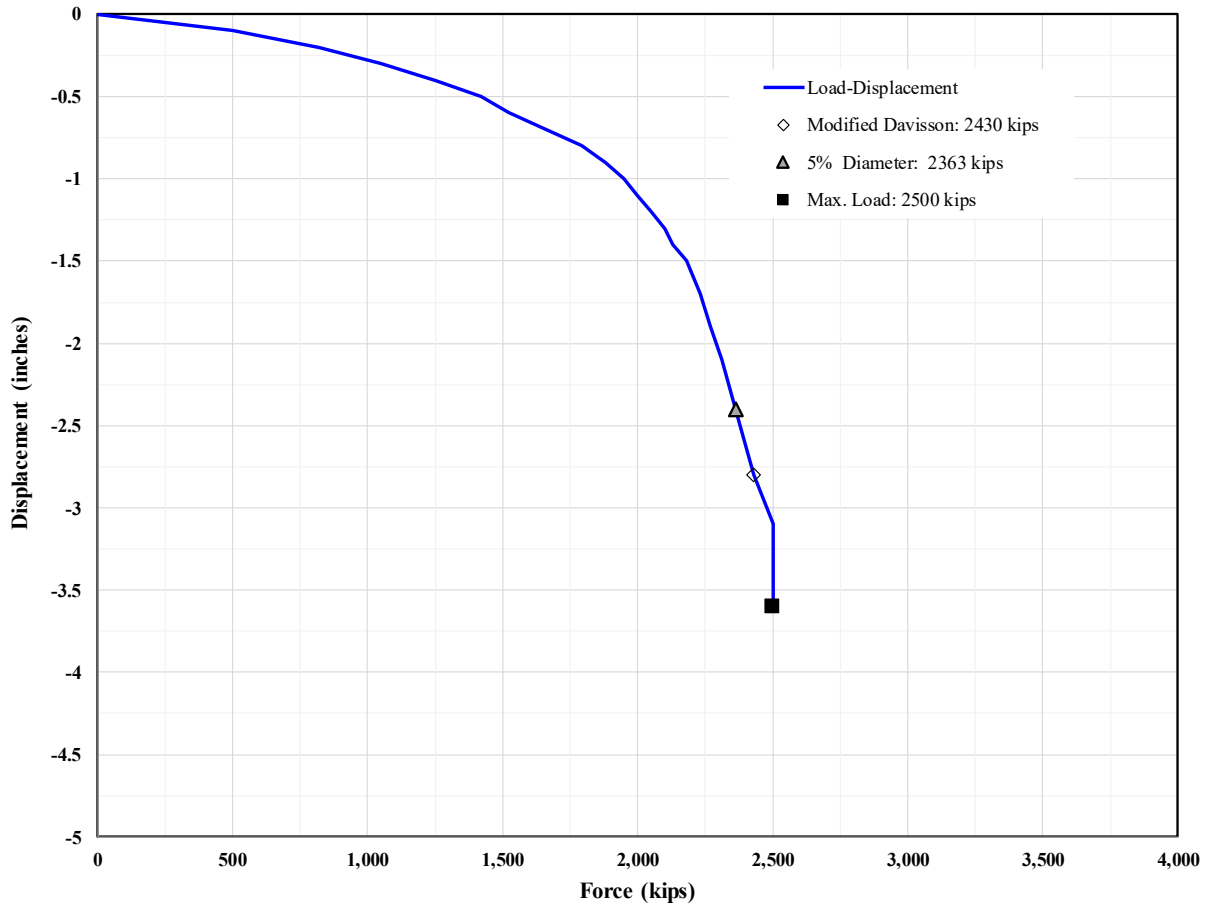
Source: FHWA.  
 1 inch = 25.4 mm; 1 kip = 4,448.2216 N.

**Figure 59. Graph. Force displacement curve. Project: Port Said. Pile designation: TP-136.**



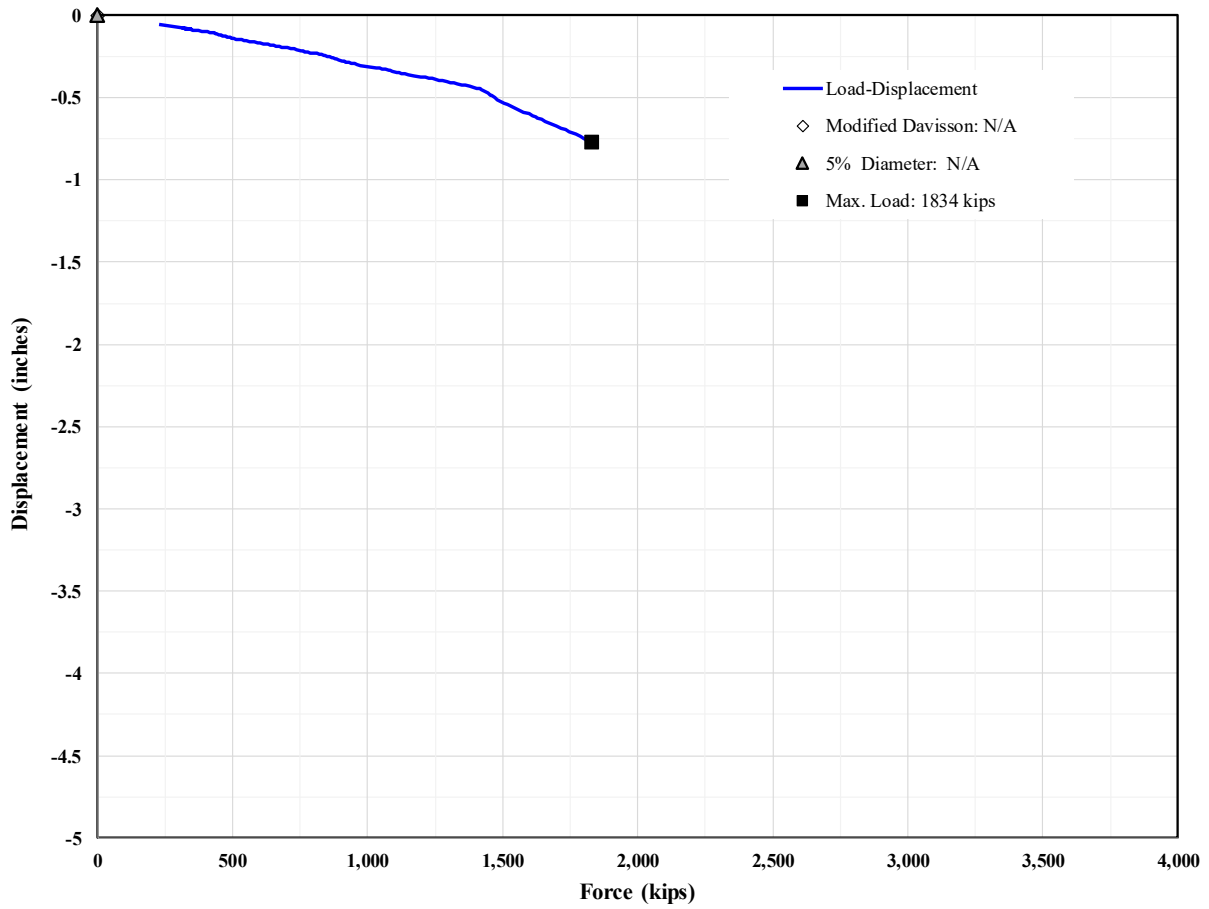
Source: FHWA.  
 1 inch = 25.4 mm; 1 kip = 4,448.2216 N.

**Figure 60. Graph. Force displacement curve. Project: Woodrow Wilson Bridge over Potomac River, VA and MD, USA. Pile designation: PL-3.**



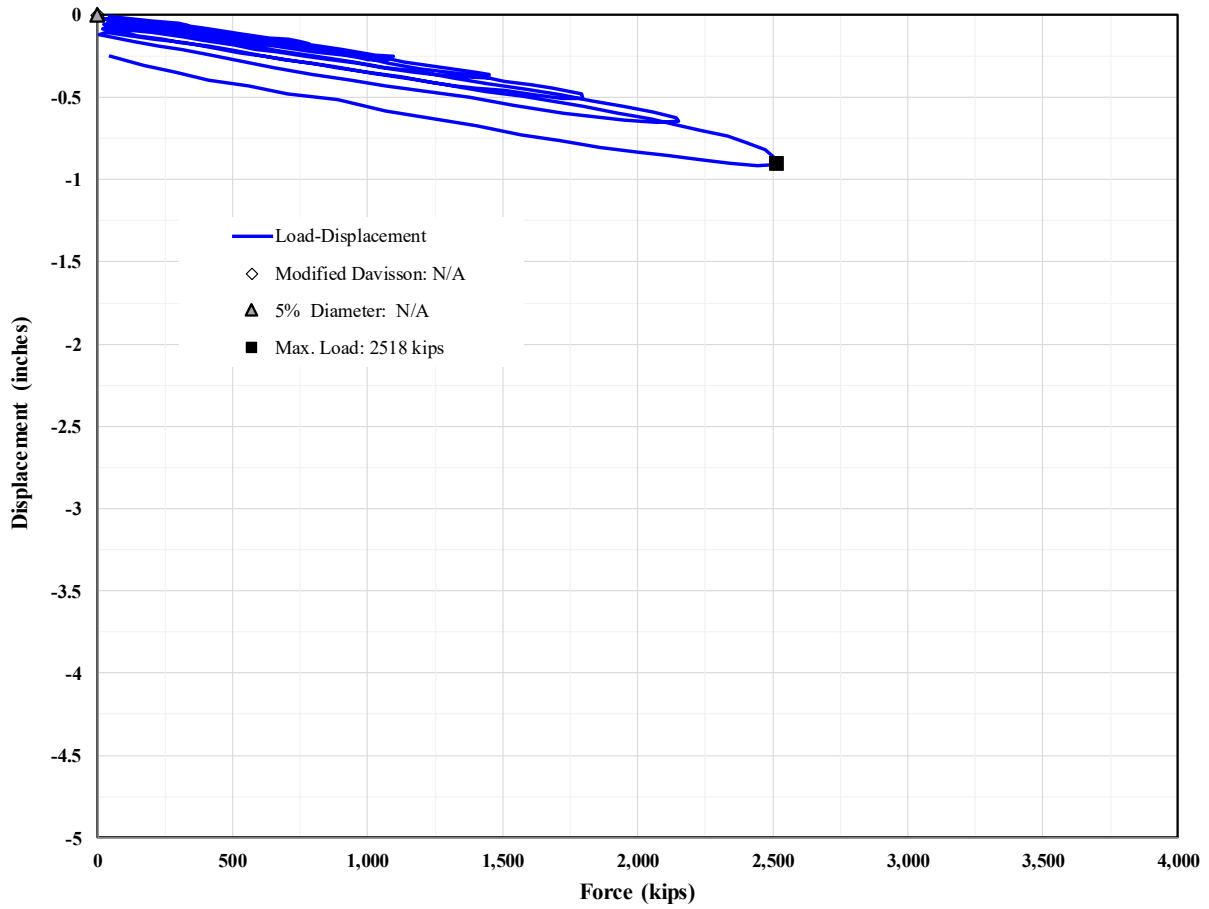
Source: FHWA.  
 1 inch = 25.4 mm; 1 kip = 4,448.2216 N.

**Figure 61. Graph. Force displacement curve. Project: Feather River Bridge (Caltrans Bridge No. 18-0009). Pile designation: Pile-3.**



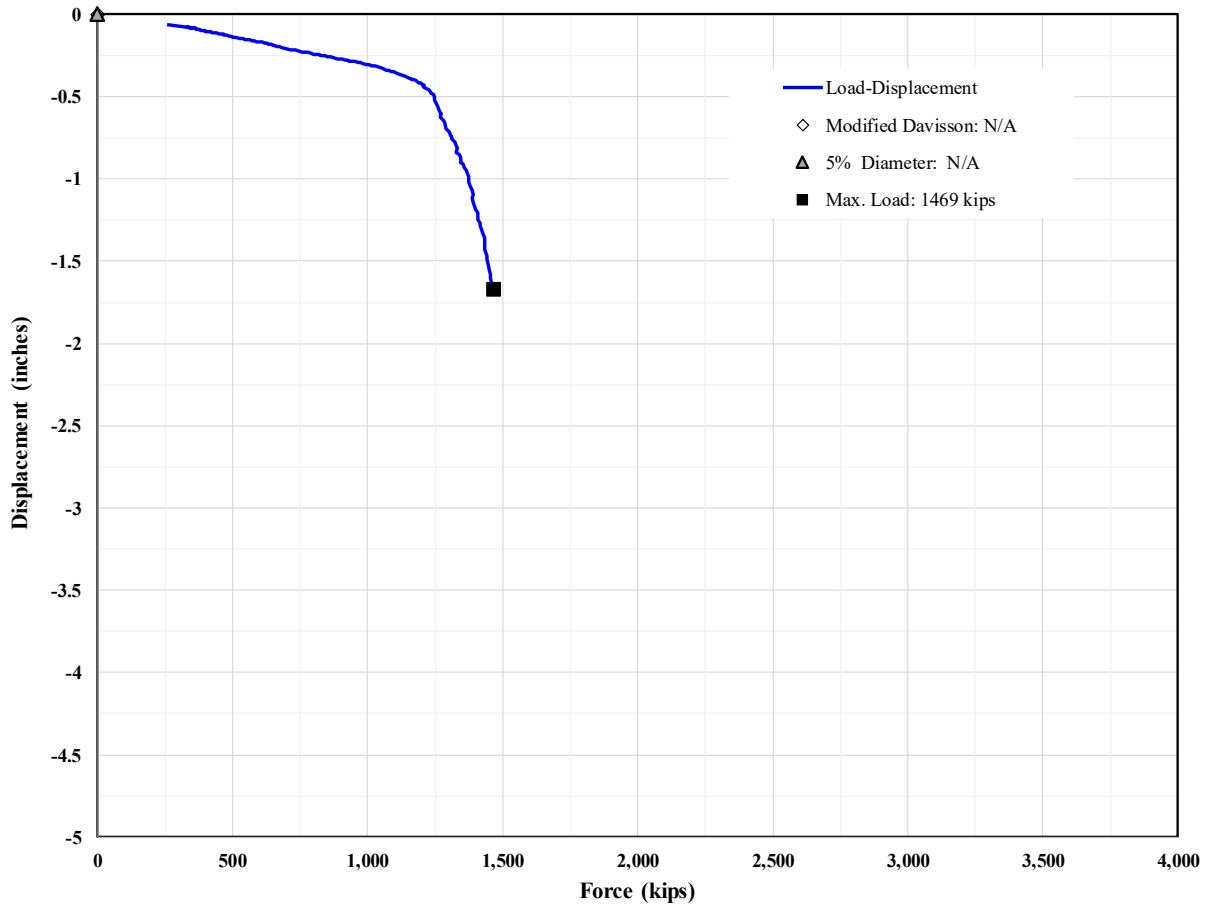
Source: FHWA.  
 1 inch = 25.4 mm; 1 kip = 4,448.2216 N.

**Figure 62. Graph. Force displacement curve. Project: Nippon Steel Corporation/Blast Furnace Foundations in Japan. Pile designation: BF-61.**



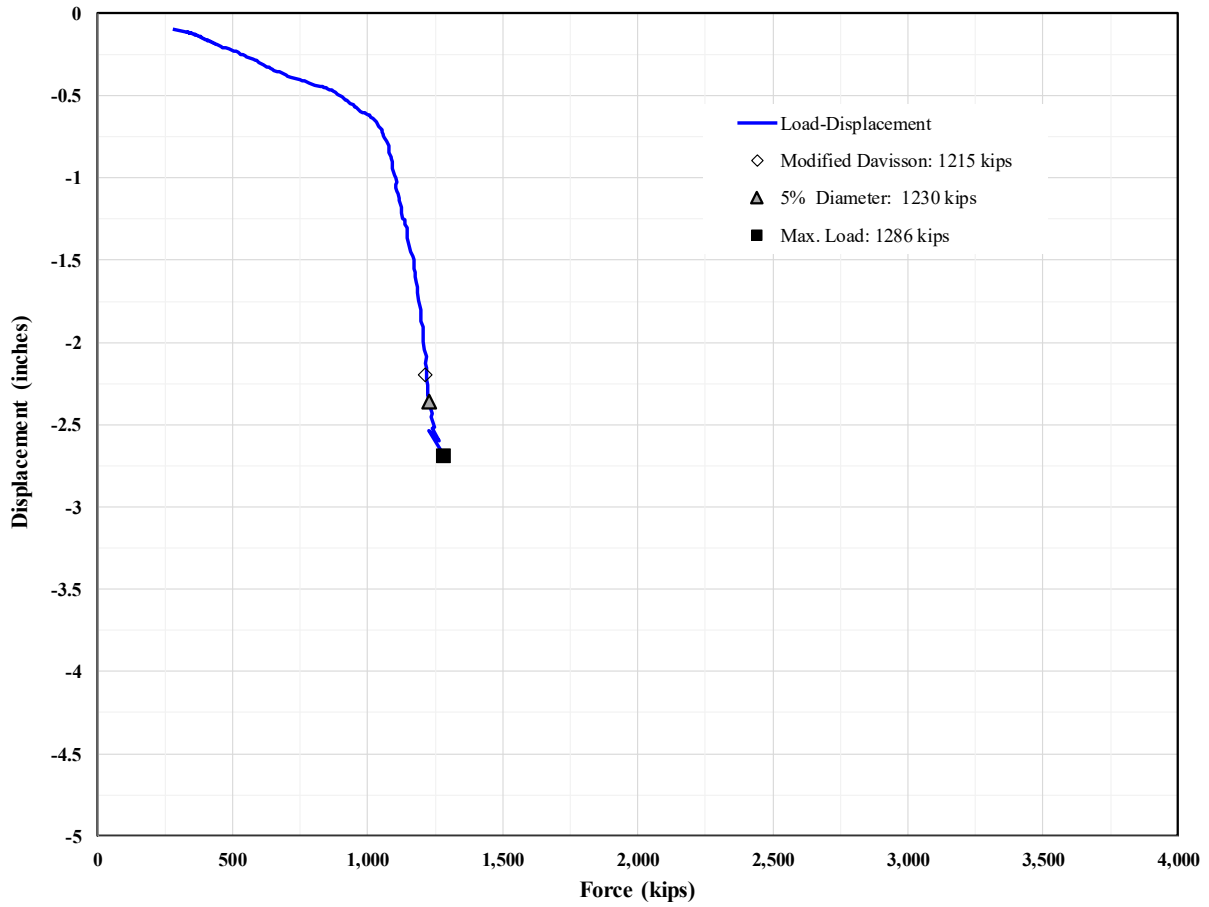
Source: FHWA.  
 1 inch = 25.4 mm; 1 kip = 4,448.2216 N.

**Figure 63. Graph. Force displacement curve. Project: Nippon Steel Corporation/Blast Furnace Foundations in Japan. Pile designation: H-27.**



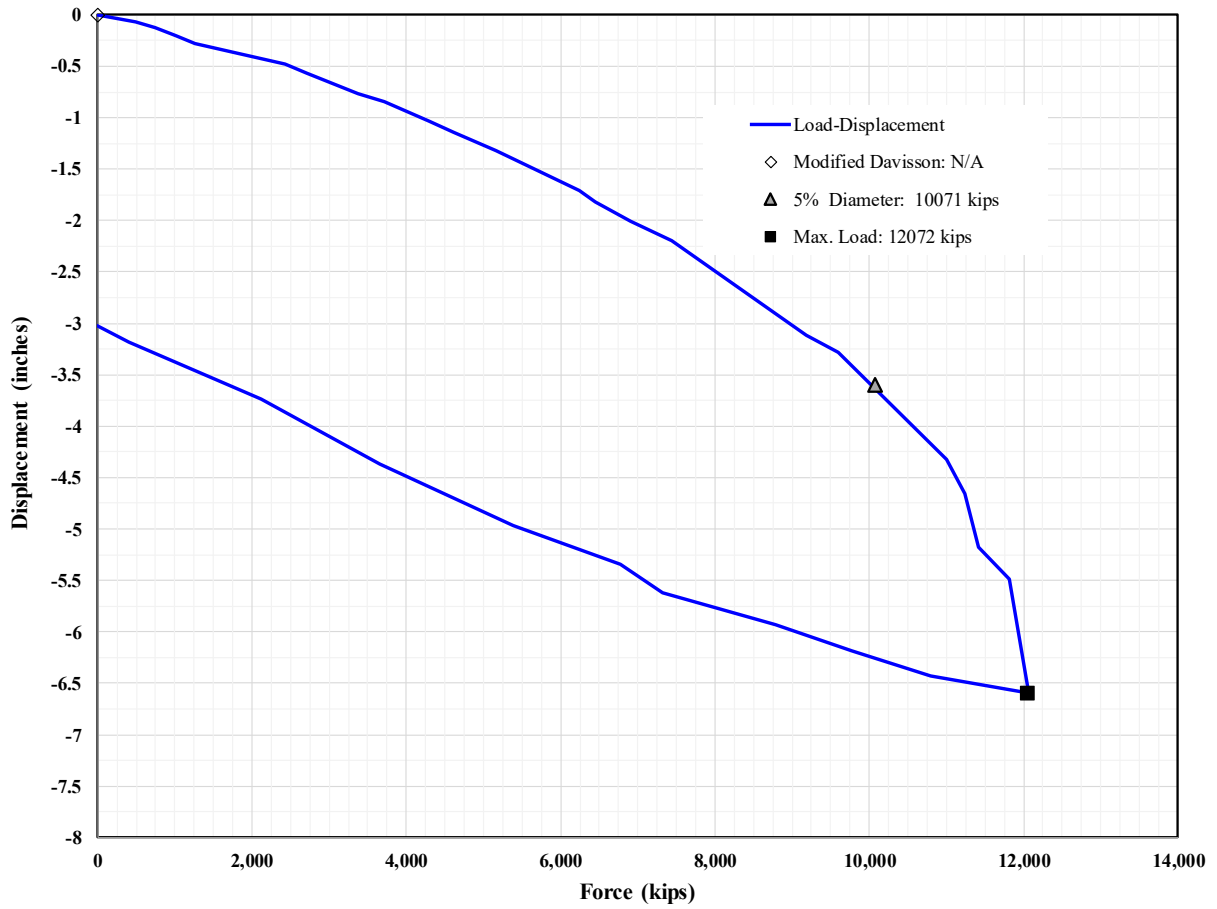
Source: FHWA.  
 1 inch = 25.4 mm; 1 kip = 4,448.2216 N.

**Figure 64. Graph. Force displacement curve. Project: Nippon Steel Corporation/Blast Furnace Foundations in Japan. Pile designation: HS-40.**



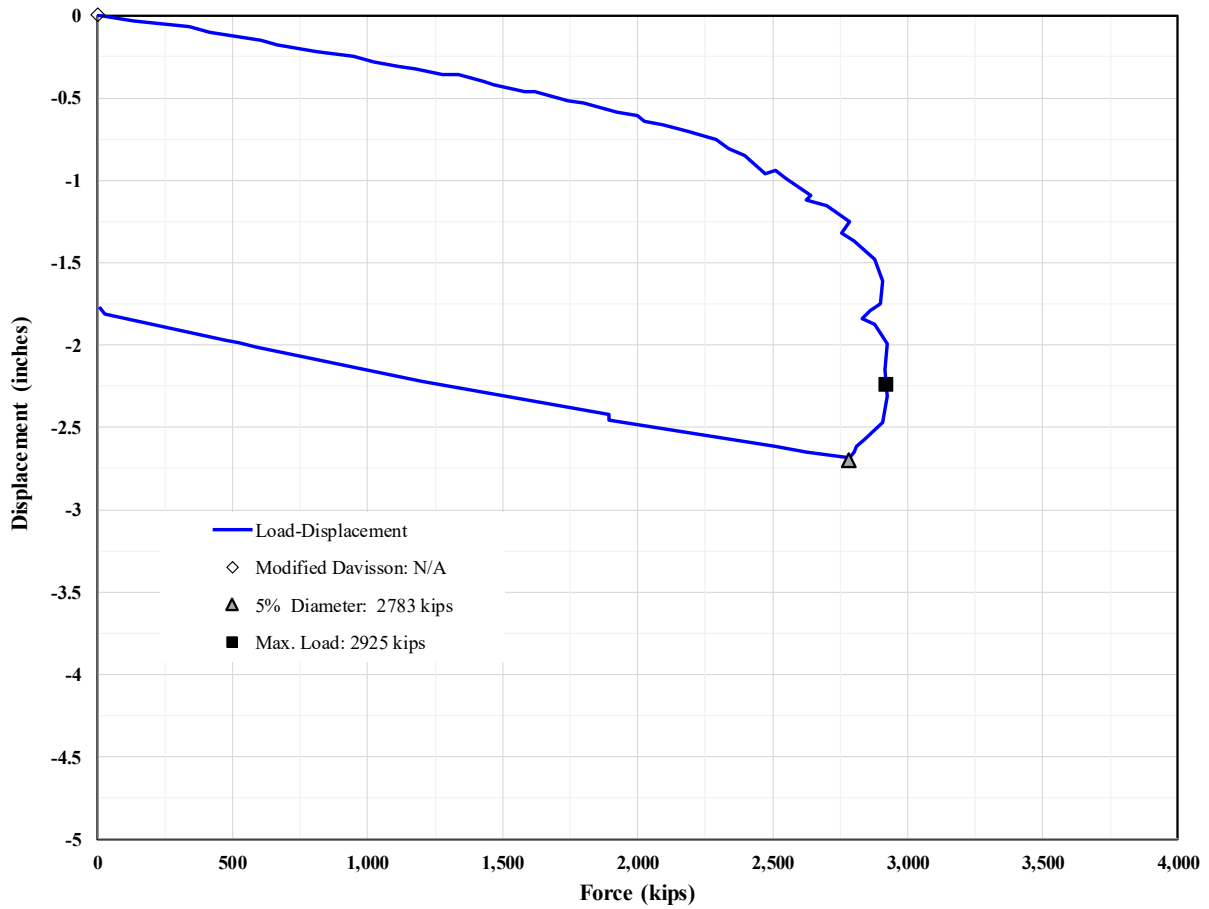
Source: FHWA.  
 1 inch = 25.4 mm; 1 kip = 4,448.2216 N.

**Figure 65. Graph. Force displacement curve. Project: Nippon Steel Corporation/Blast Furnace Foundations in Japan. Pile designation: HS-41.**



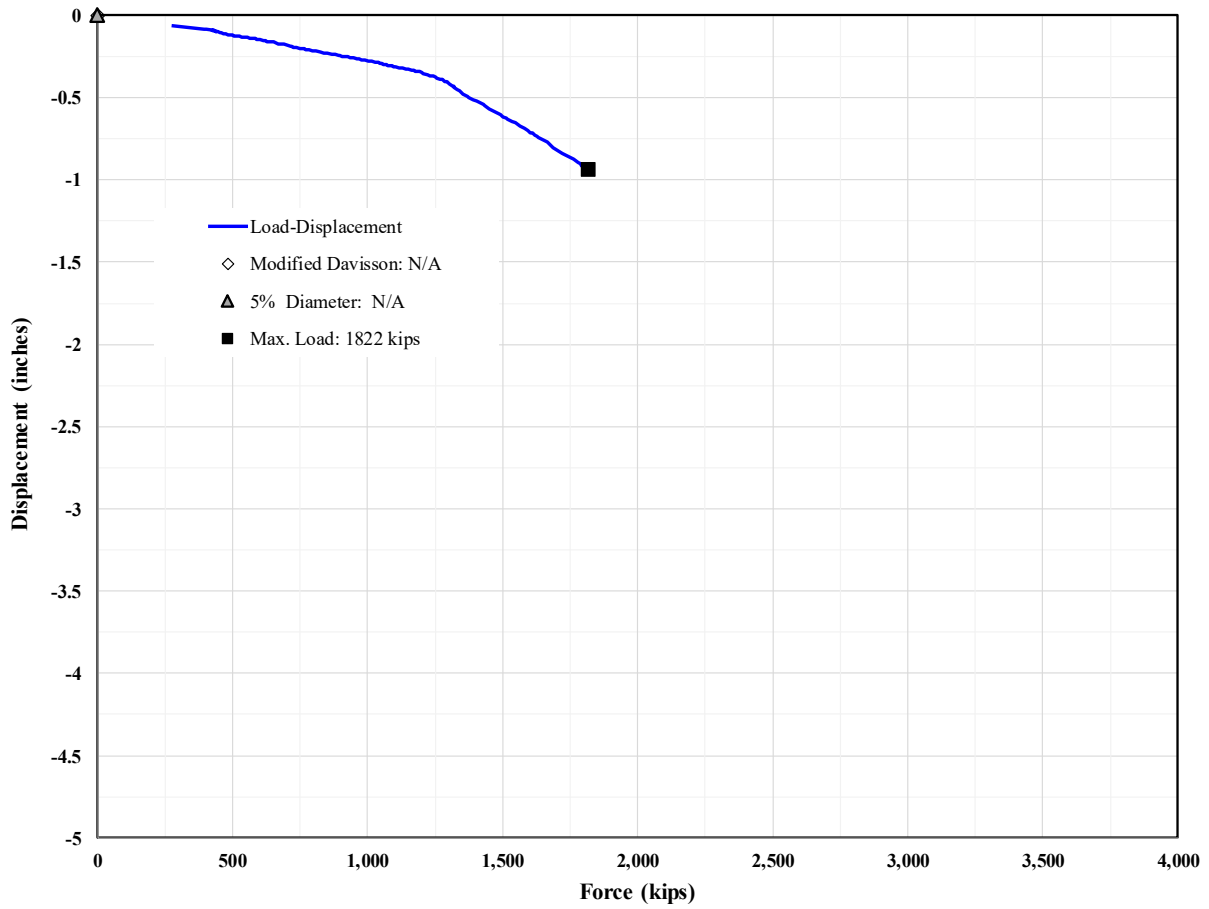
Source: FHWA.  
 1 inch = 25.4 mm; 1 kip = 4,448.2216 N.

**Figure 66. Graph. Force displacement curve. Project: Port Mann Bridge.  
 Pile designation: TestPile.**



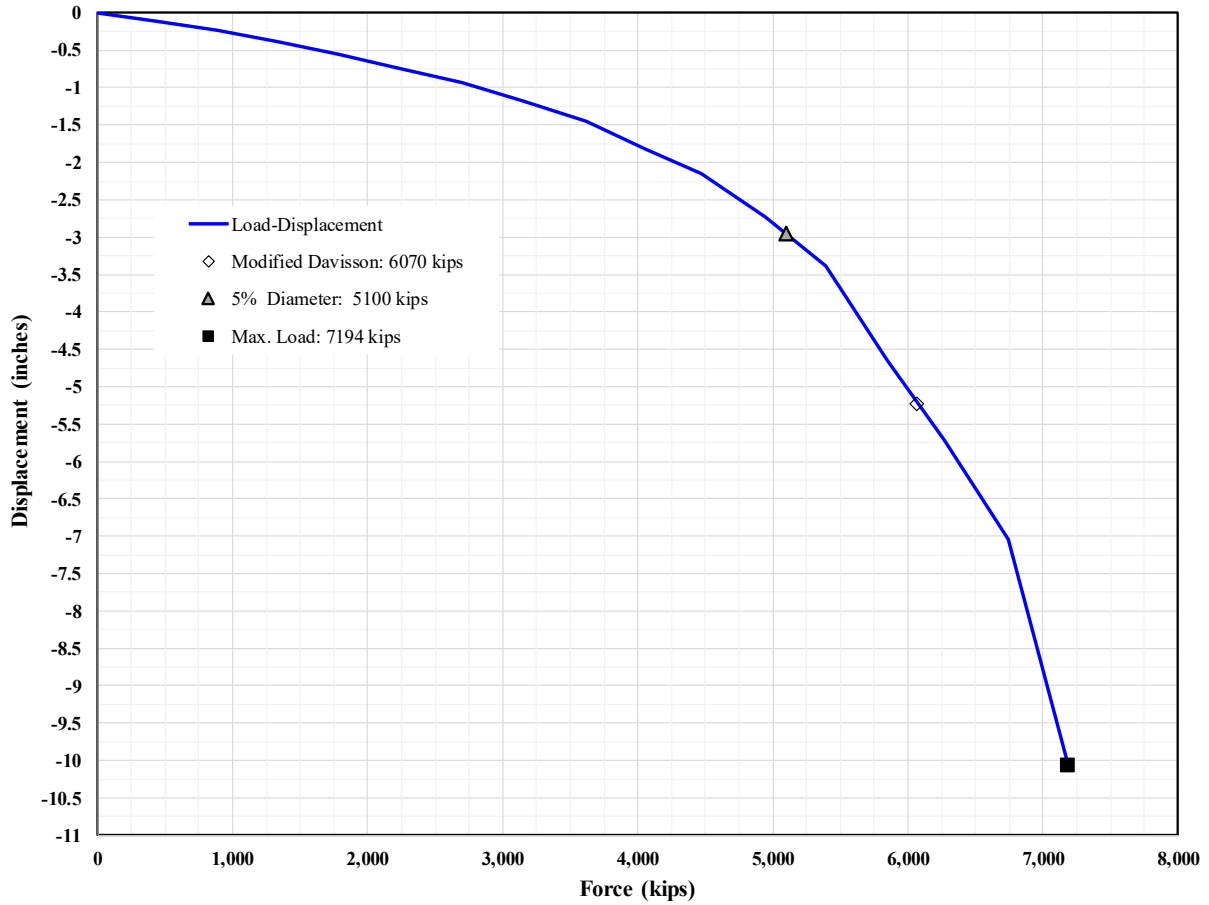
Source: FHWA.  
 1 inch = 25.4 mm; 1 kip = 4,448.2216 N.

**Figure 67. Graph. Force displacement curve. Project: Woodrow Wilson Bridge over Potomac River, VA and MD, USA. Pile designation: PL-1.**



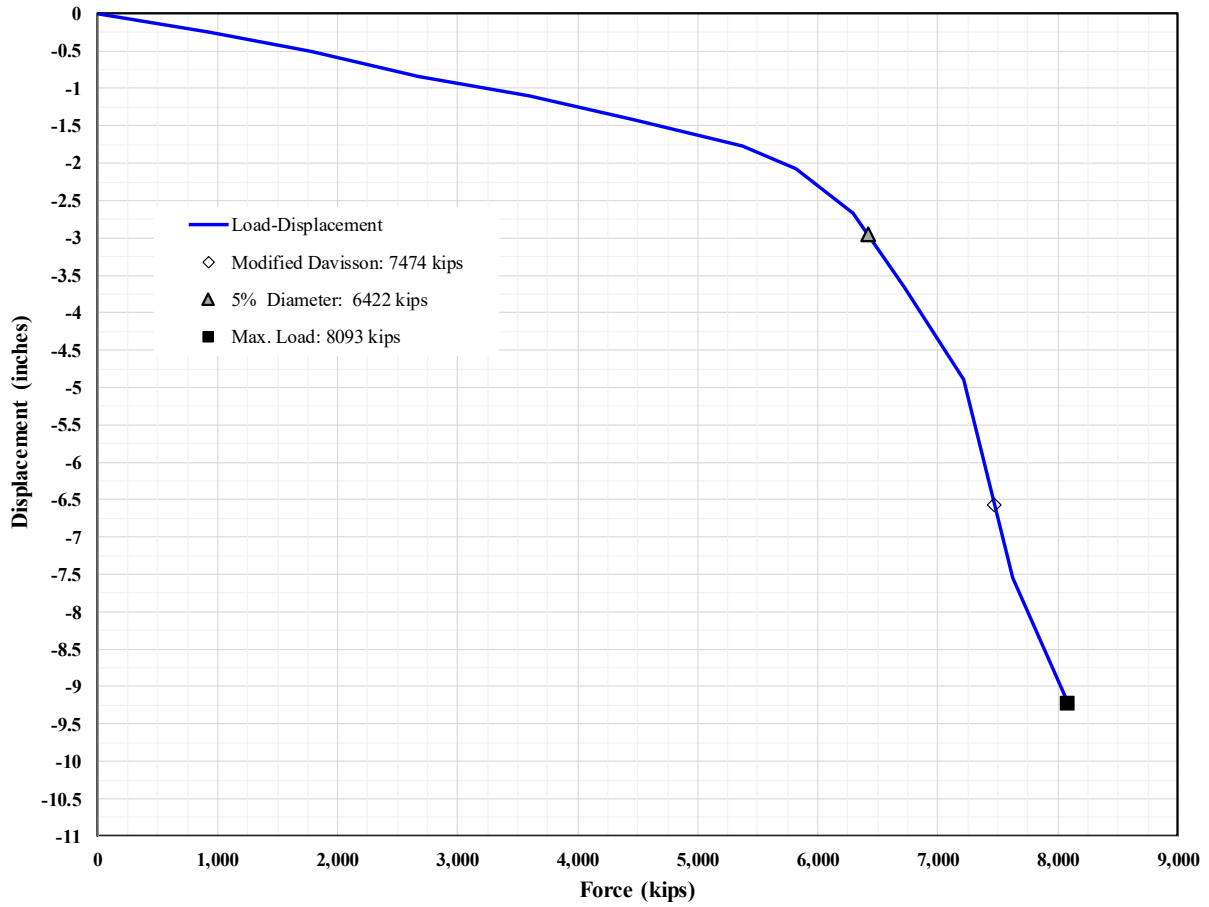
Source: FHWA.  
 1 inch = 25.4 mm; 1 kip = 4,448.2216 N.

**Figure 68. Graph. Force displacement curve. Project: Nippon Steel Corporation/Blast Furnace Foundations in Japan. Pile designation: HS-97.**



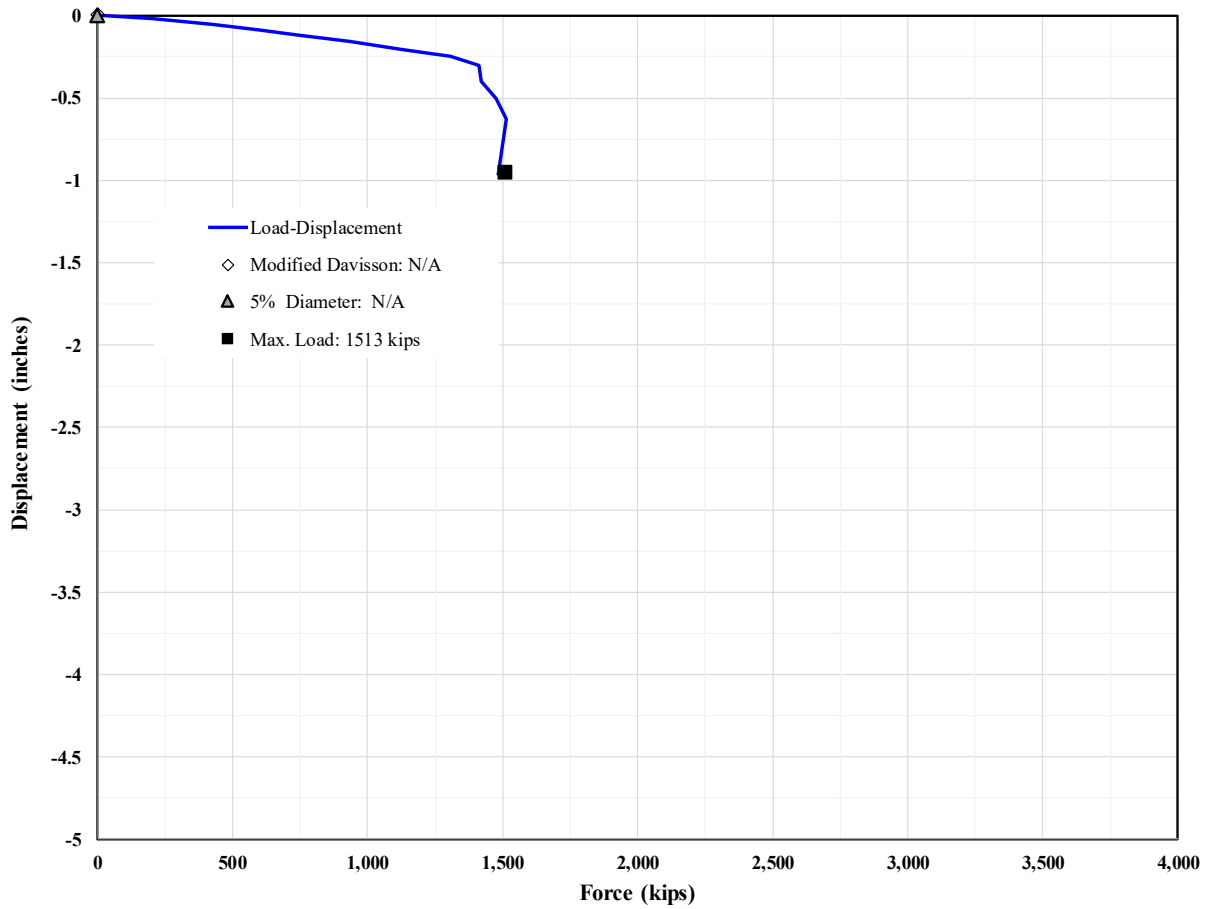
Source: FHWA.  
 1 inch = 25.4 mm; 1 kip = 4,448.2216 N.

**Figure 69. Graph. Force displacement curve. Project: Tokyo Port Bay Bridge. Pile designation: TP-4.**



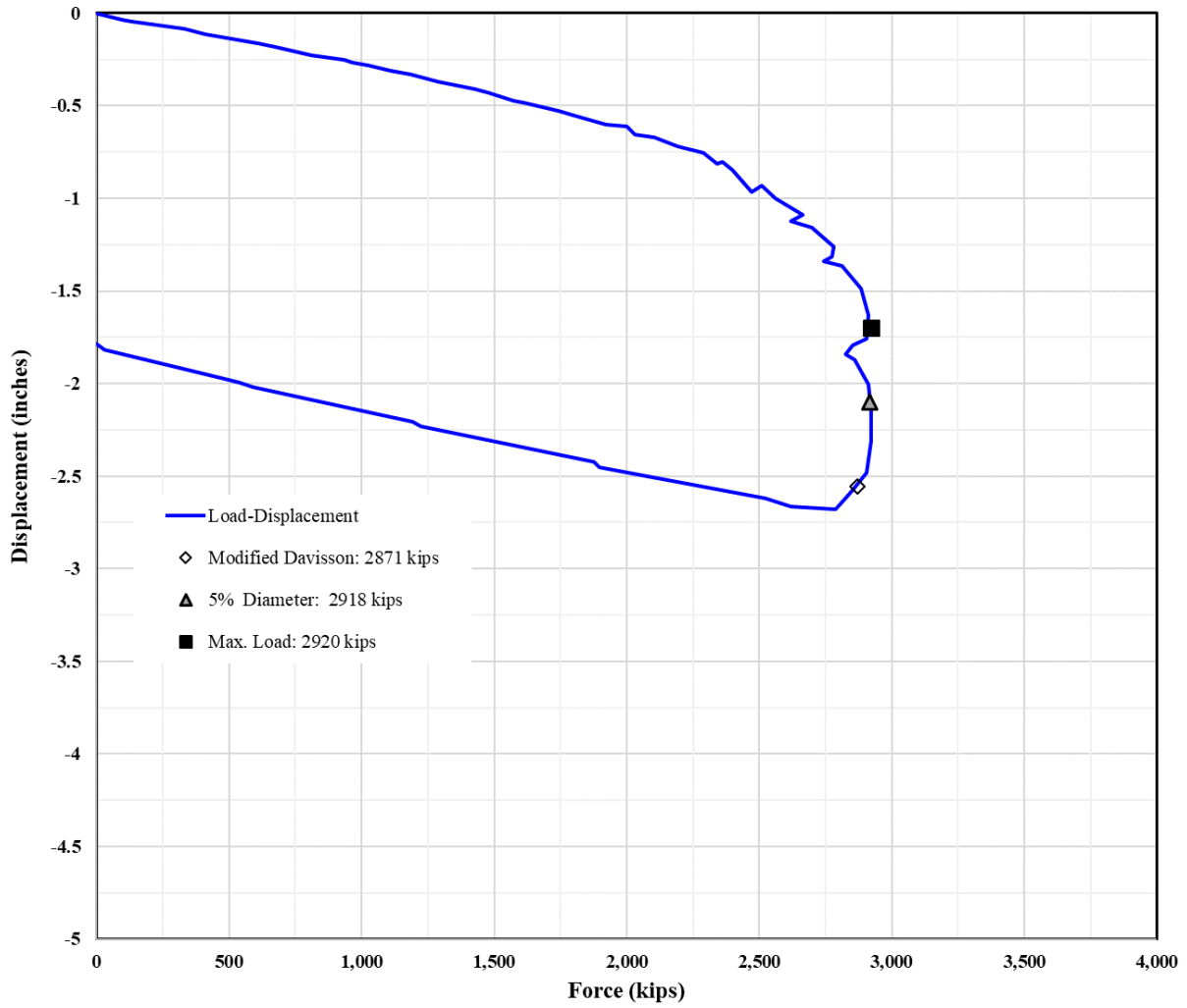
Source: FHWA.  
 1 inch = 25.4 mm; 1 kip = 4,448.2216 N.

**Figure 70. Graph. Force displacement curve. Project: Tokyo Port Bay Bridge.  
 Pile designation: TP-5.**



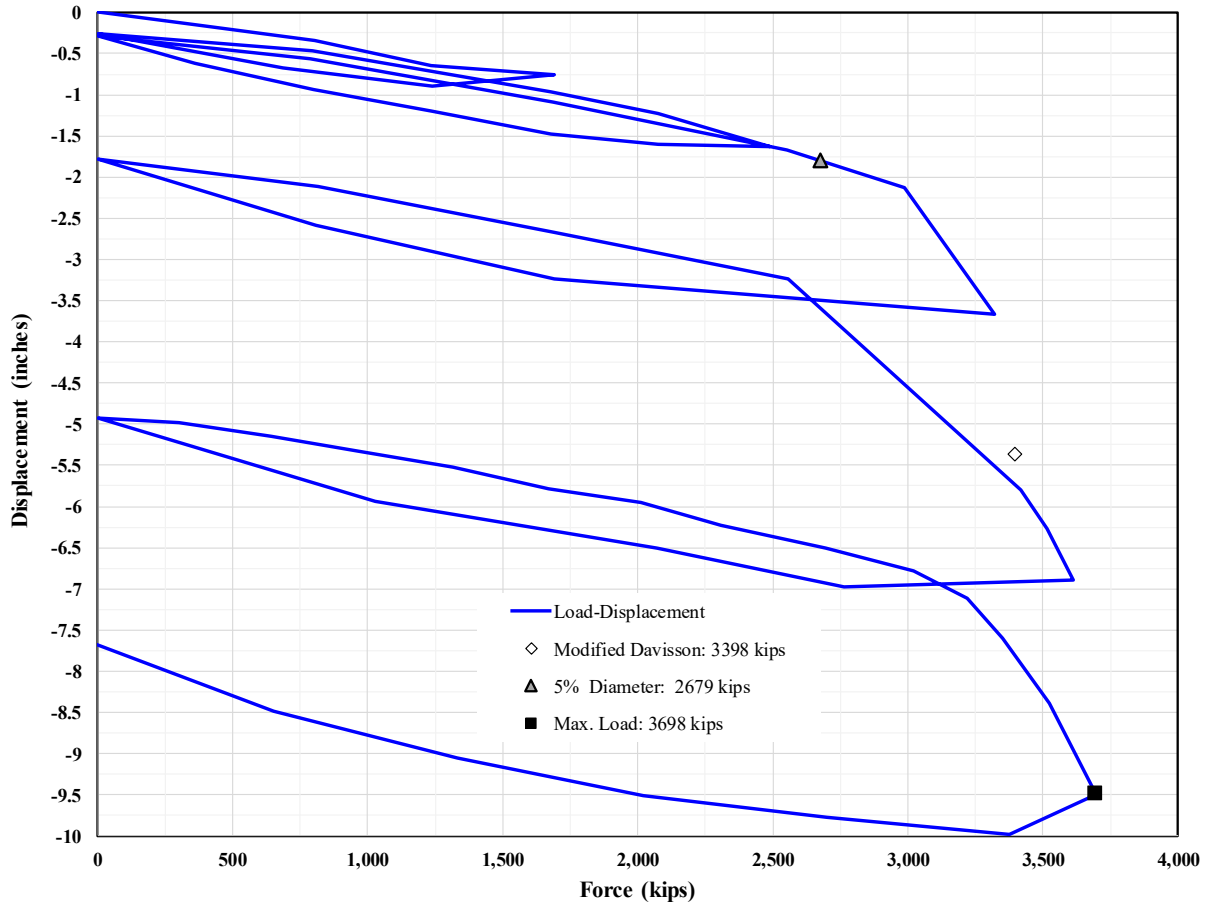
Source: FHWA.  
 1 inch = 25.4 mm; 1 kip = 4,448.2216 N.

**Figure 71. Graph. Force displacement curve. Project: Salinas River Bridge (Caltrans Bridge No. 44-216R/L). Pile designation: TestPile.**



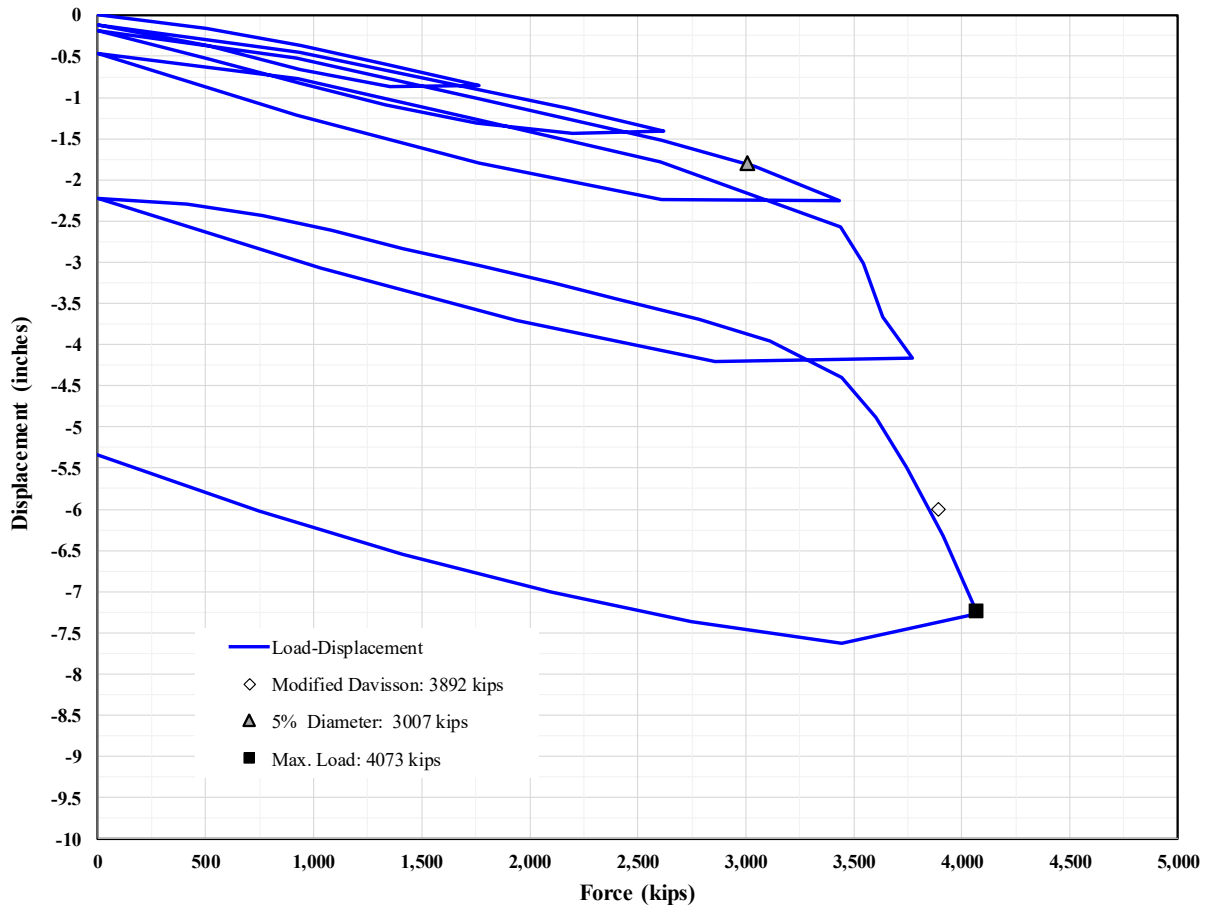
Source: FHWA.  
 1 inch = 25.4 mm; 1 kip = 4,448.2216 N.

**Figure 72. Graph. Force displacement curve. Project: Woodrow Wilson Bridge over Potomac River, VA and MD, USA. Pile designation: PL-2.**



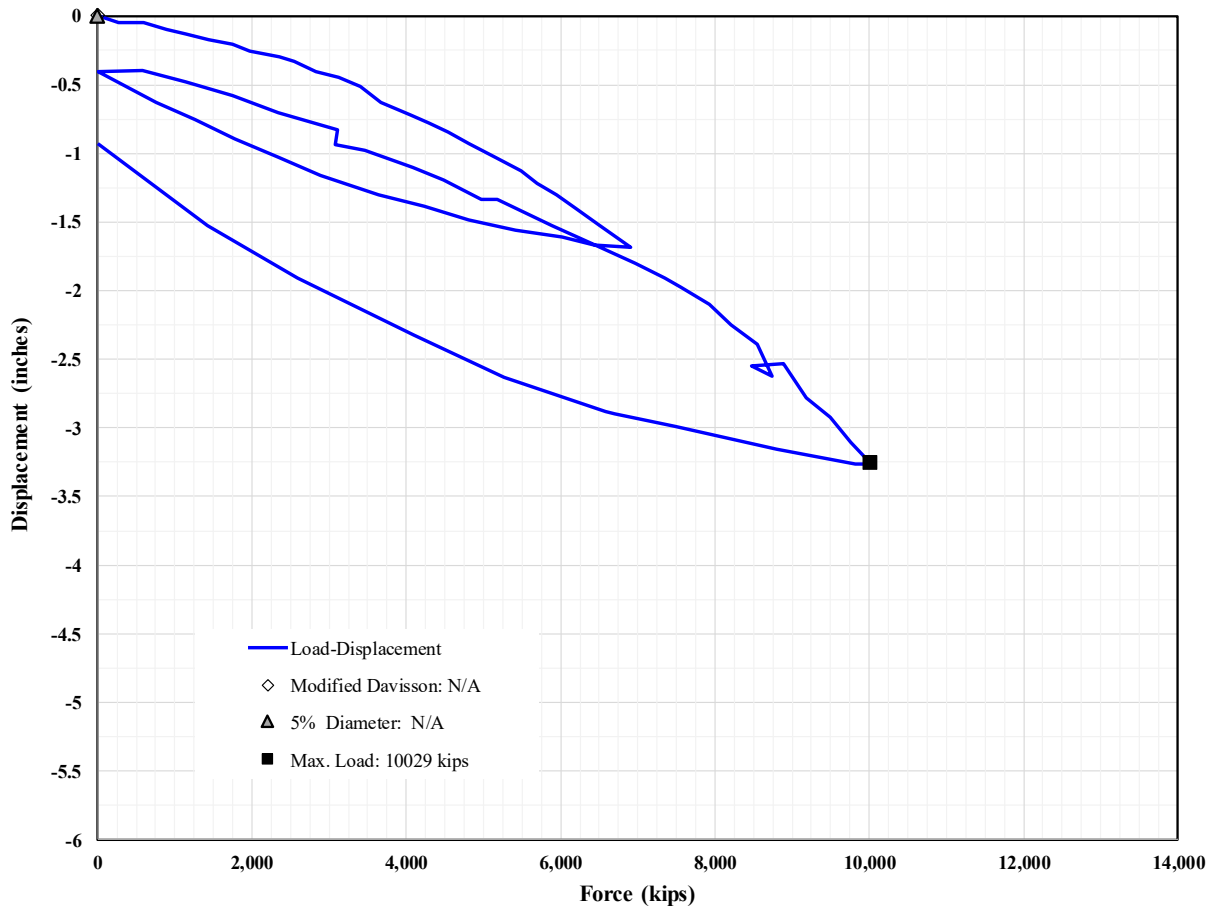
Source: FHWA.  
 1 inch = 25.4 mm; 1 kip = 4,448.2216 N.

**Figure 73. Graph. Force displacement curve. Project: Jin Mao Building.  
 Pile designation: ST-1.**



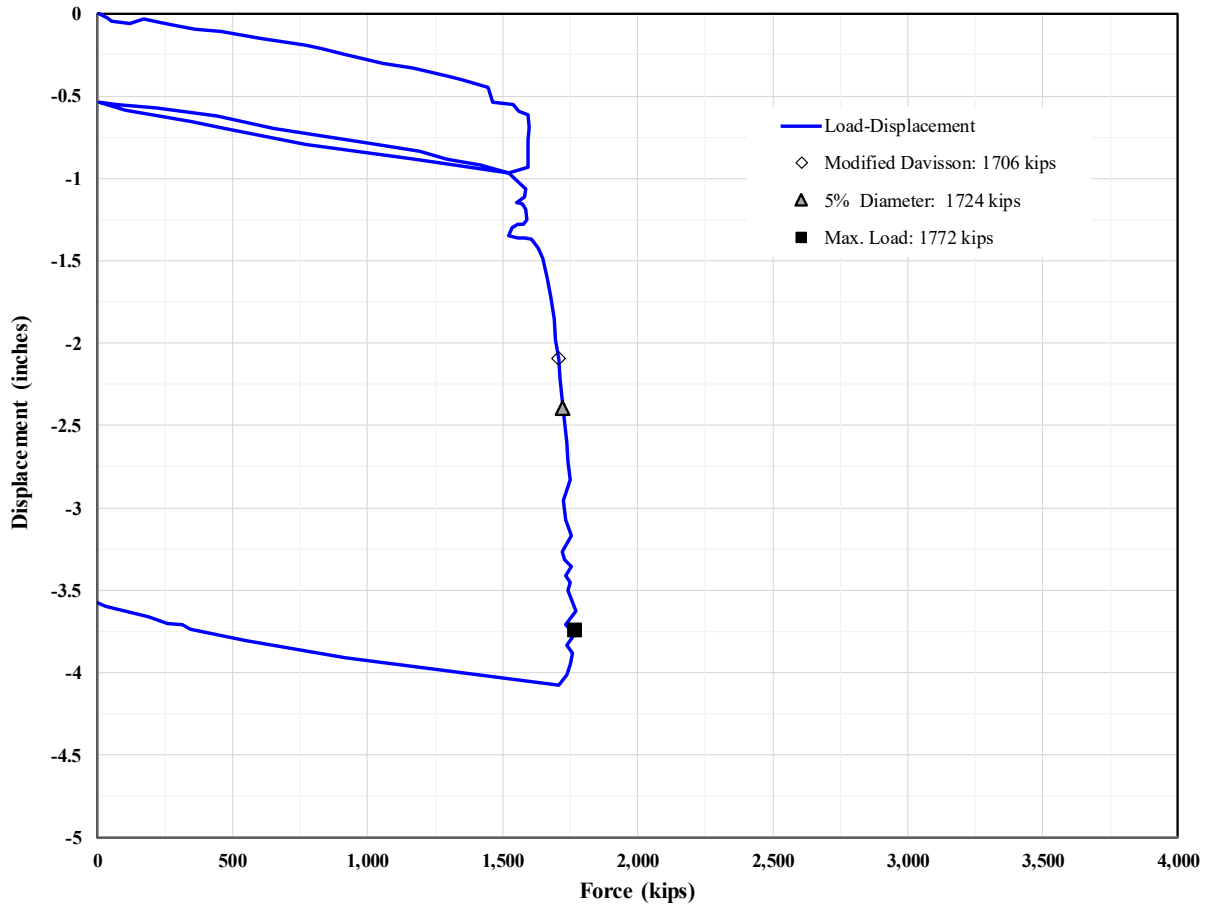
Source: FHWA.  
 1 inch = 25.4 mm; 1 kip = 4,448.2216 N.

**Figure 74. Graph. Force displacement curve. Project: Jin Mao Building.  
 Pile designation: ST-2.**



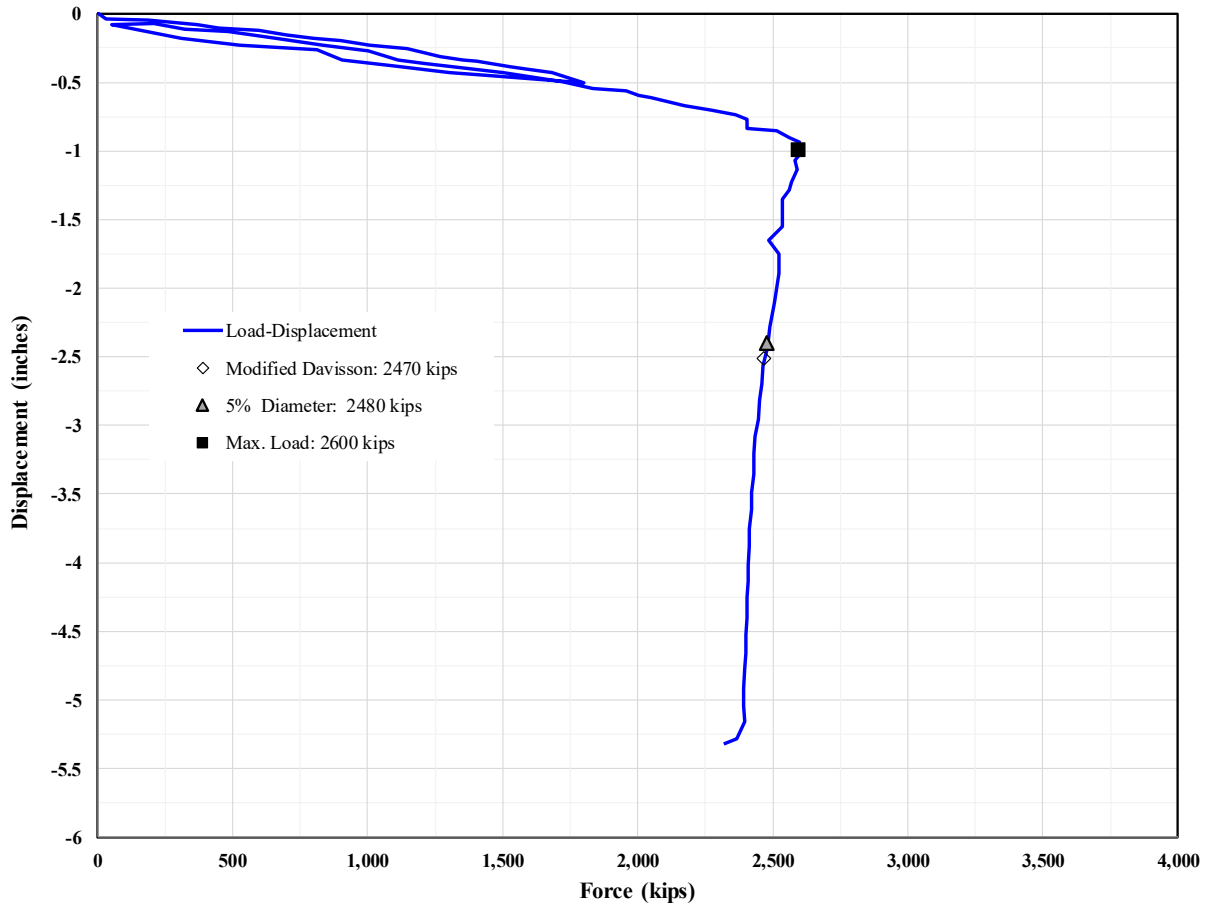
Source: FHWA.  
 1 inch = 25.4 mm; 1 kip = 4,448.2216 N.

**Figure 75. Graph. Force displacement curve. Project: Pitt River Bridge.  
 Pile designation: Pile-P5.**



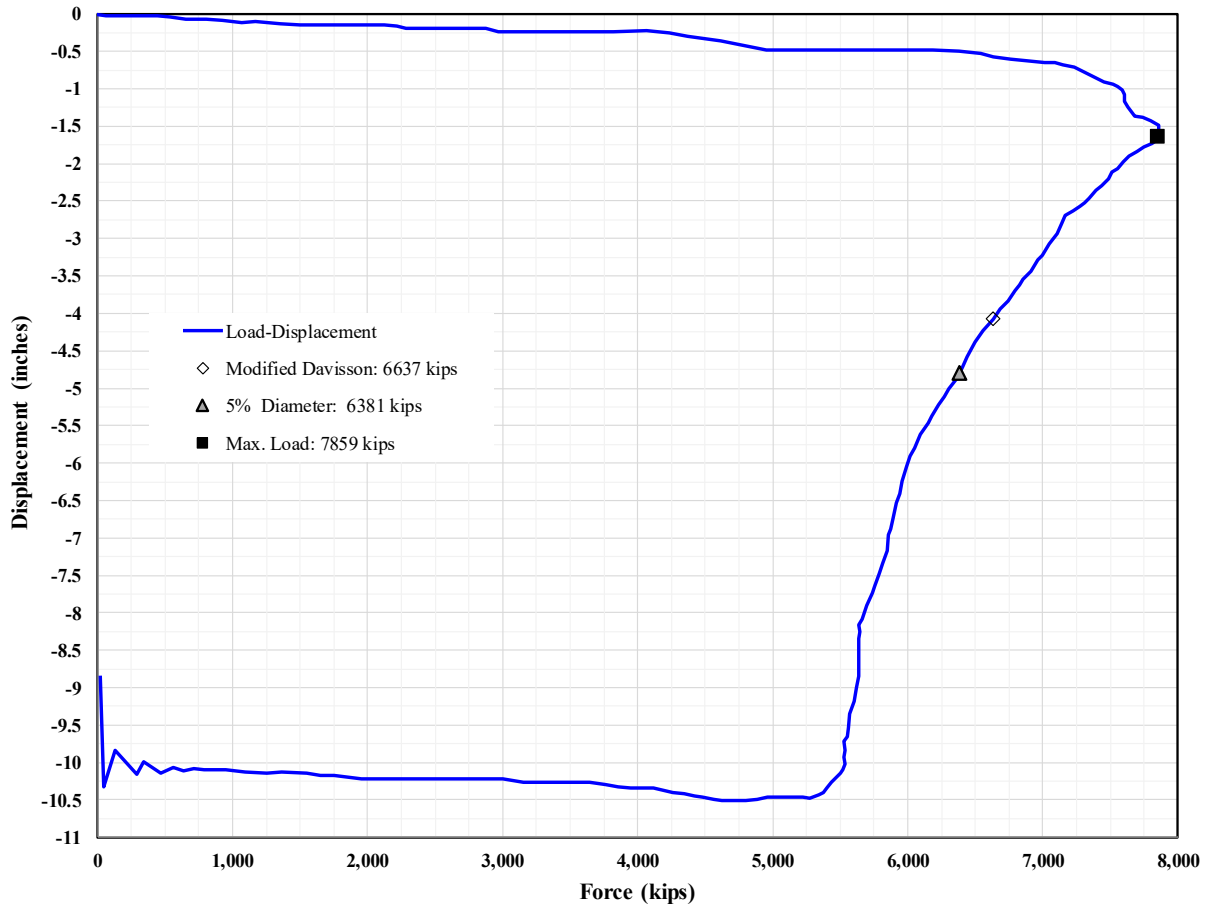
Source: FHWA.  
 1 inch = 25.4 mm; 1 kip = 4,448.2216 N.

**Figure 76. Graph. Force displacement curve. Project: I-405 and SR-22 HOV Connector Separation Bridge (Caltrans Bridge No. 55-1103E). Pile designation: TP-9.**



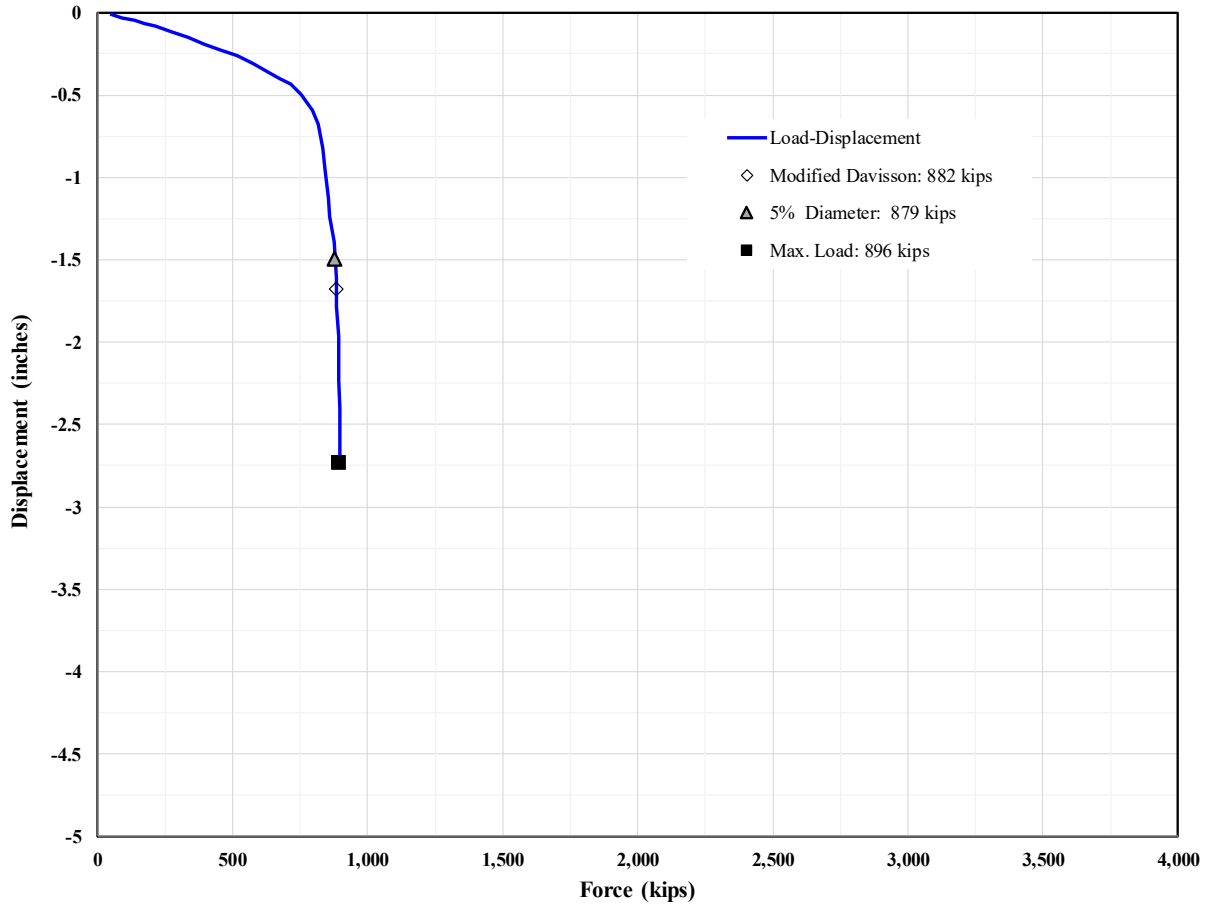
Source: FHWA.  
 1 inch = 25.4 mm; 1 kip = 4,448.2216 N.

**Figure 77. Graph. Force displacement curve. Project: I-405 and SR-22 HOV Connector Separation Bridge (Caltrans Bridge No. 55-1103E). Pile designation: TP-10.**



Source: FHWA.  
 1 inch = 25.4 mm; 1 kip = 4,448.2216 N.

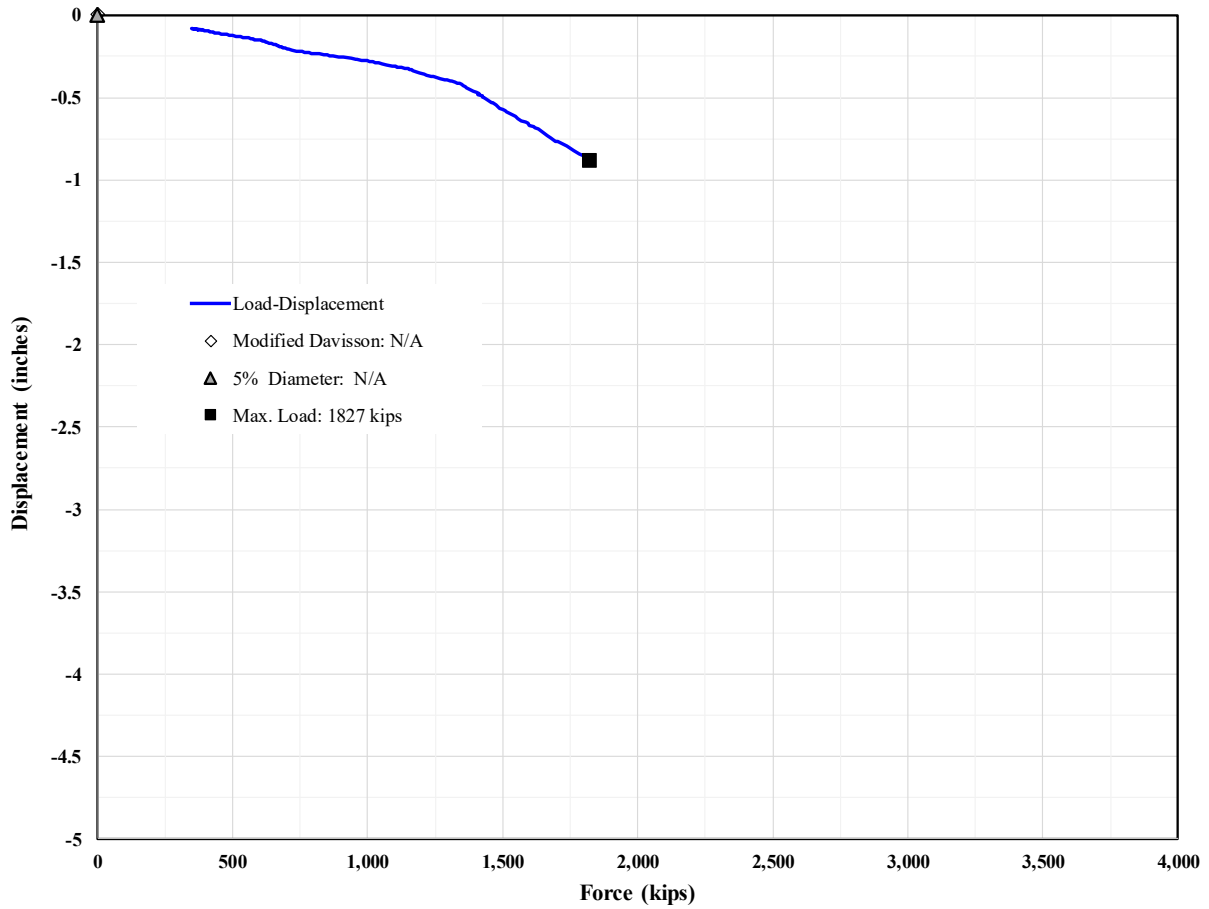
**Figure 78. Graph. Force displacement curve. Project: Highway 32 Stony Creek Bridge (Caltrans Bridge No. 11-0029). Pile designation: TP-6.**



Source: FHWA.

1 inch = 25.4 mm; 1 kip = 4,448.2216 N.

**Figure 79. Graph. Force displacement curve. Project: Legislative Route 795 Section B-6 Philadelphia, PA. Pile designation: TP-D.**



Source: FHWA.  
 1 inch = 25.4 mm; 1 kip = 4,448.2216 N.

**Figure 80. Graph. Force displacement curve. Project: Nippon Steel Corporation/Blast Furnace Foundations in Japan. Pile designation: BF-47.**



## **APPENDIX B. MEASURED AND PREDICTED NOMINAL RESISTANCE SCATTER PLOTS**

Supplementary information is available as a hardcopy draft of the measured and predicted nominal resistance scatter plots by contacting Jennifer Nicks at [Jennifer.Nicks@dot.gov](mailto:Jennifer.Nicks@dot.gov). The draft provides a graphical overview of the measured versus predicted resistances for the numerous analysis combinations considered in the resistance factor calibration. Each matrix includes an array of 16 scatter plots that reflect a single side resistance design method with multiple base resistance design methods for the side and base resistance combinations under a specified failure criterion. A 1:1 line is shown on the scatter plots to reflect equal measured and predicted resistances. Proximity to the 1:1 line generally reflects the accuracy of the prediction. The computed average bias values for the unfiltered and filtered data sets are shown at the top of each plot.



## REFERENCES

- AASHTO (American Association of State and Highway Transportation Officials). (2017). *AASHTO LRFD Bridge Design Specifications: U.S. Customary Units*, 8th Ed, Washington, DC.
- Abu-Hejleh, N., DiMaggio, J.A., Kramer, W.M., Anderson, S., and Nichols, S. (2011). *Implementation of LRFD Geotechnical Design for Bridge Foundations*, Report No. FHWA-NHI-10-039, Federal Highway Administration, Washington, DC.
- Allen, T.M. (2005). *Development of Geotechnical Resistance Factors and Downdrag Load Factors for LRFD Foundation Strength Limit State Design*, Report No. FHWA-NHI-05-052, Federal Highway Administration, Washington, DC.
- Allen, T.M., Nowak, A.S., and Bathhurst, R.J. (2005). *Calibration to Determine Load and Resistance Factors for Geotechnical and Structural Design*, Transportation Research Circular E-C079, Transportation Research Board, Washington, DC.
- API (American Petroleum Institute). (2011). *Geotechnical and Foundation Design Considerations, API RP 2GEO*, Washington, DC.
- Axelsson, G. (2000). *Long-Term Set-Up of Driven Piles in Sand*, unpublished doctoral thesis, Department of Civil and Environmental Engineering at the Royal Institute of Technology, Stockholm, Sweden.
- Bowles, J.E. (1988). *Foundation Analysis and Design*, 4th Ed., McGraw-Hill, San Francisco, CA.
- Briaud, J.L., Coyle, H.M., and Tucker, L.M. (1990). "Axial Response of Three Vibratory- and Three Impact-Driven H Piles in Sand." *Presented at the 69th Annual Meeting of the Transportation Research Board*, Washington, DC.
- Brown, D.A. and Thompson III, W.R. (2015). *Design and Load Testing of Large Diameter Open-Ended Driven Piles*, NCHRP Synthesis 478, National Academies of Sciences, Engineering, and Medicine, Washington, DC.
- Brown, R.P. (2001). *Predicting the Ultimate Axial Resistance of Single Driven Piles*, unpublished doctoral dissertation, University of Texas at Austin.
- Carnivan, G.J. and Camp III, W.M. (2002). "Three Case Histories Comparing Impact and Vibratory Driven Pile Resistances in Marl." *Presented at the 27th Annual Conference of the Deep Foundation Institute*, San Diego, CA, 53–65.
- Clausen, C.J.F., Aas, P.M., and Karlsrud, K. (2005). "Bearing Capacity of Driven Piles in Sand, the NGI Approach." *Presented at the First International Symposium on Frontiers in Offshore Geomechanics (ISFOG)*, Perth, Australia, 677–681.

- Dickenson, S.E. (2012). *CAPWAP-Based Correlations for Estimating the Static Axial Capacity of Open-Ended Steel Pipe Piles in Alaska*, Report No. FHWA-AK-RD-12-07, Alaska Department of Transportation and Public Facilities, Fairbanks, AK.
- Doherty, P., Gavin, K., and Gallagher, D. (2010). “Field Investigation of the Undrained Base Resistance of Pipe Piles in Clay.” *Proceedings of the Institution of Civil Engineers – Geotechnical Engineering*, 163(GE1), pp. 13–22.
- Gudavalli, S.R., Safaqah, O., and Seo, H. (2013). “Effect of Soil Plugging on Axial Capacity of Open-Ended Pipe Piles in Sands.” *Presented at the 18th International Conference on Soil Mechanics and Geotechnical Engineering*, Paris, France, 1487–1490.
- Hannigan, P.J., Rausche, F., Likins, G.E., Robinson, B.R., and Becker, M.L. (2016), *Design and Construction of Driven Pile Foundations*, Report nos. FHWA-NHI-16-009 and FHWA-NHI-16-010, Federal Highway Administration, Washington, DC.
- Hasofer, A.M. and Lind, N.C. (1974). “An Exact and Invariant First Order Reliability Format.” *Journal of Engineering Mechanics*, 100(1), pp. 111–121.
- Hatanaka, M. and Uchida, A. (1996). “Empirical Correlation between Penetration Resistance and Effective Friction of Sandy Soil.” *Soils and Foundations*, 36(4), pp. 1–9.
- HCN, A Terracon Company. (2014). *Pile Load Test Program Summary Report, Kentucky Lake Bridge Pile Load Test Program, US 68/KY 80 Bridge over Kentucky Lake – Advance Contract CID 131305, Lake Bridges Project, Marshall and Trigg Counties, Kentucky*, Project No. N1115097, Terracon, Cincinnati, OH.
- Hussein, M.H., Sharp, M.R., and Knight, W.F. (2002). “The Use of Superposition for Evaluating Pile Capacity.” *Presented at the International Deep Foundations Congress 2002, An International Perspective on Theory, Design, Construction, and Performance*, American Society of Civil Engineers, Reston, VA, 6–21.
- Jamiolkowski, M., LoPresti, D.C.F., and Manassero, M. (2001). “Evaluation of Relative Density and Shear Strength of Sands from Cone Penetration Test and Flat Dilatometer Test.” *Soil Behavior and Soft Ground Construction, GSP 119*, pp. 201–238, American Society of Civil Engineers, Reston, VA.
- Jardine, R., Chow, F., Overy, R., and Standing, J. (2005). *ICP Design Methods for Driven Piles in Sands and Clays*, Thomas Telford, London, England.
- Kindel, C.E. (1977). “Mechanism of Soil Resistance for Driven Pipe Piles.” *Presented at Ports '77, the 4th Annual Symposium of the Waterway, Port, Coastal, and Ocean Division of American Society of Civil Engineering*, v. 2, Long Beach, CA, 251–268.
- Ko, J. and Jeong, S. (2015). “Plugging Effect of Open-Ended Piles in Sandy Soil.” *Canadian Geotechnical Journal*, 52(5), pp. 535–547.

- Kulhawy, F.H. and Mayne, P.W. (1990). *Manual on Estimating Soil Properties for Foundation Design*, Report No. EL-6800, Electric Power Research Institute, Palo Alto, CA.
- Ladd, C.C. and Foott, R. (1974). “New Design Procedure for Stability of Soft Clays.” *Journal of the Geotechnical Engineering Division*, 100(7), pp. 763–786.
- Lee, J., Salgado, R., and Paik, K. (2003). “Estimation of Load Capacity of Pipe Piles in Sand Based on Cone Penetration Test Results.” *Journal of Geotechnical and Geoenvironmental Engineering*, 129(5), pp. 391–403.
- Lehane, B.M. and Gavin, K.G. (2001). “Base Resistance of Jacked Pipe Piles in Sand.” *Journal of Geotechnical and Geoenvironmental Engineering*, 127(6), pp. 473–480.
- Lehane, B.M. and Jardine, R.J. (1994). “Displacement-Pile Behaviour in Soft Marine Clay.” *Canadian Geotechnical Journal*, 31(2), pp. 181–191.
- Lehane, B.M. and Randolph, M.F. (2002). “Evaluation of a Minimum Base Resistance for Driven Pipe Piles in Siliceous Sand.” *Journal of Geotechnical and Geoenvironmental Engineering*, 128(3), pp. 198–205.
- Lehane, B.M., Schneider, J., and Xu, X. (2005). *A Review of Design Methods for Offshore Driven Piles in Siliceous Sand*, Report No. GEO 05358, University of Western Australia, Perth, Australia.
- Liu, J., Zhang, Z., Yu, F., and Xie, Z. (2012). “Case History of Installing Instrumented Jacked Open-Ended Piles.” *Journal of Geotechnical and Geoenvironmental Engineering*, 138(7), pp. 810–820.
- Mayne, P.W. and Kemper, J.B., Jr. (1988). “Profiling OCR in Stiff Clays by CPT and SPT.” *Geotechnical Testing Journal*, 11(2), pp. 139–147.
- McVay, M.C., Badri, D., and Hu, Z.Y. (2004). *Determination of Axial Pile Capacity of Prestressed Concrete Cylinder Piles*, Final Report No. UF Project 4910-4504-877-12, University of Florida, Gainesville, FL.
- McVay, M.C., Birgisson, B., Nguyen, T., and Kuo, C., (2002). “Uncertainty in Load and Resistance Factor Design Phi Factors for Driven Prestressed Concrete Piles.” *Transportation Research Record*, 1808, pp. 99–107, Transportation Research Board, Washington, DC.
- Meyerhof, G.G. (1957). “Discussion of Research on Determining the Density of Sands by Spoon Penetration Testing, by Gibbs, H.J. and Holtz, W.G.” *Contributed to the Fourth International Conference on Soil Mechanics and Foundation Engineering*, London, England.
- Mizutani, T., Kikuchi, Y., and Taguchi, H. (2003). “Cone Penetration Tests for the Examination of Plugging Effect of Open-Ended Piles.” *Presented at the BGA International Conference on Foundations*, Dundee, Scotland, pp. 655–664.

- Mosher, R.L. (1990). "Axial Capacity of Vibratory-Driven Piles Versus Impact-Driven Piles." *Transportation Research Record*, 1277, pp. 128–135.
- NAVFAC. (1982). *Soil Mechanics*, NAVFAC DM 7.1, U.S. Naval Facilities Engineering Command, Alexandria, VA.
- Nordlund, R.L. (1979). "Point Bearing and Shaft Friction of Piles in Sand." *Presented at the 5th Annual Conference on Fundamentals of Deep Foundation Design*, St. Louis, MO.
- Paik, K., and Salgado, R. (2003). "Determination of Bearing Capacity of Open-Ended Piles in Sand." *Journal of Geotechnical and Geoenvironmental Engineering*, 129(1), pp. 46–57.
- Paikowsky, S.G. (2004). *Load and Resistance Factor Design (LRFD) for Deep Foundations*, NCHRP Report 507, Transportation Research Board, Washington, DC.
- Paikowsky, S.G. and Whitman, R.V. (1990). "The Effects of Plugging on Pile Performance and Design." *Canadian Geotechnical Journal*, 27(4), pp. 429–440.
- Paikowsky, S.G., Whitman, R.V., and Baligh, M.M. (1989). "A New Look at the Phenomenon of Offshore Pile Plugging." *Marine Geotechnology*, 8(3), pp. 213–230.
- Peck, R.B., Hanson, W.E., and Thornburn, T.H. (1974). *Foundation Engineering*, 2nd Ed., Wiley, New York.
- Petek, K.A., Mitchell, R.A., and Ellis, H. (2016). "FHWA Deep Foundation Load Test Database (DFLTD) - Version 2.0." Available online: <https://www.fhwa.dot.gov/software/research/infrastructure/structures/bridges/dfltd/index.cfm>.
- Petek, K.A., Mitchell, R.A., Buechel, G.J., and Goodyear, D. (2012). "Full Scale Instrumented Pile Load Test for the Port Mann Bridge, Surrey, British Columbia, Canada." *Full-Scale Testing and Foundation Design: Honoring Bengt Fellenius*, GSP 227, pp. 362–375, American Society of Civil Engineers, Reston, VA.
- Randolph, M.F. and Puzrin, A.M. (2003). "Upper Bound Limit Analysis of Circular Foundations on Clay under General Loading." *Géotechnique*, 53(9), pp. 785–796.
- Randolph, M.F., Leong, E.C., and Houlsby, G.T. (1991). "One-Dimensional Analysis of Soil Plugs in Pipe Piles." *Géotechnique*, 41(4), pp. 587–598.
- Rausche, F. and Webster, S. (2007). "Behavior of Cylinder Piles during Pile Installation." *Presented at Geo-Denver 2007, Contemporary Issues in Deep Foundations*, Denver, CO.
- Rausche, F., Likins, G., Liang, L., and Hussein, M. (2010). "Static and Dynamic Models for CAPWAP Signal Matching." *Presented at Geo-Florida 2010, Art of Foundation Engineering Practice*, West Palm Beach, FL, 534–553.

- Robertson, P.K. and Cabal, K.L. (2010). “Estimating Unit Weight from CPT.” *Presented at the 2nd International Symposium on Cone Penetration Testing, CPT '10*, v. 3, Huntington Beach, CA.
- Saye, S.R., Brown, D.A., and Lutenege, A.J. (2013). “Assessing Adhesion of Driven Pipe Piles in Clay Using Adaptation of Stress History and Normalized Soil Engineering Parameter Concept.” *Journal of Geotechnical and Geoenvironmental Engineering*, 139(7), pp. 1062-1074.
- Schmertmann, J.H. (1975). “Measurement of In Situ Shear Strength.” *Proceedings of the Conference on In Situ Measurement of Soil Properties*, Raleigh, NC, v. 2, 57–138.
- Sowers, G.F. (1979). *Introductory Soil Mechanics and Foundations: Geotechnical Engineering*, 4th Ed., MacMillan, New York.
- Styler, M.A. (2006). *Development and Implementation of the DIGGS Format to Perform LRFD Resistance Factor Calibration of Driven Concrete Piles in Florida*, Master’s thesis, University of Florida, Gainesville, FL.
- Terzaghi, K. and Peck, R.B. (1967). *Soil Mechanics in Engineering Practice*, 2nd Ed., Wiley, New York.
- Tomlinson, M.J. (1980). *Foundation Design and Construction*, 4th Ed., Pitman Publishing, Boston, MA.
- Yu, F. and Yang, J. (2012). “Base Capacity of Open-Ended Steel Pipe Piles in Sand.” *Journal of Geotechnical and Geoenvironmental Engineering*, 138(9), pp. 116–128.

